Molecular genetics of hearing impairment

Celia Zazo Seco

Molecular genetics of hearing impairment

Celia Zazo Seco

Celia Zazo Seco, 2015
Molecular genetics of hearing impairment

The research described in this thesis was financially supported by ZonMW.
Publication of this thesis was financially supported by the Radboud University.

Design: Proefschrift-aio.nl
Printed by: Proefschrift-aio.nl

ISBN: 978-90-9029350-9

Molecular genetics of hearing impairment

PROEFSCHRIFT
ter verkrijging van de graad van doctor
aan de Radboud Universiteit Nijmegen
op gezag van de rector magnificus,
volgens besluit van het college van decanen
in het openbaar te verdedigen op vrijdag 4 december 2015
om 10.30 uur precies

door
Celia Zazo Seco
geboren op 13 oktober 1986
te Salamanca, Spanje

PROMOTOR
Prof. dr. Hannie Kremer

COPROMOTORES
Dr. Margit Schraders
Dr. Erwin van Wijk

MANUSCRIPTCOMMISSIE
Prof. dr. Anneke den Hollander (Voorzitter)
Prof. dr. Peter Deen
Dr. Ignacio Del Castillo (Hospital Universitario Ramon y Cajal, Spanje)

PARANIMFEN
Anna Castells Nobau
Sarah Merkling

Table of contents

ABBREVIATIONS

ABR	Auditory-evoked Brainstem Response
adNSHI	autosomal dominant Non-Syndromic Hearing Impairment
arNSHI	autosomal recessive Syndromic Hearing Impairment
arNSHL	Non-Syndromic Hearing Loss
BDSC	*Drosophila* Bloomington Stock Center
BERA	Brainstem Evoked Response Audiometry
bp	base pairs
CAP	Compound Action Potential
CH	CycloHeximide
CIBERER	Centro de Investigación Biomédica en Red de Enfermedades Raras"
Cld	Claudius cells
cM	centiMorgans
CMAP	Compound Muscle Action Potentials
CNV	Copy Number Variant
Cor	Cortex
CPK	Creatine PhosphoKinase
CT	Computed Tomography
da	dendritic arborization
dB	deciBels
DC	Deiters Cells
ddaC	dorsal class IV dendritic arborization C
EBV	Epstein-Barr-virus
ELISA	Enzyme-Linked Immunosorbent Assay
ENG	ElectroNystagmoGraphy
ENT	Ear, Nose and Throat
EP	Endocochlear Potential
ER	Endoplasmic Reticulum
ERM	Ezrin, Radixin and Moesin)
EVS	Exome Variant Server
ExAC	Exome Aggregation Consortium database
HC	Hair Cells
HI	Hearing impairment
Hip	Hippocampus
Hz	Hertz
IP	Inositol triPhosphate

ISO	International Organization for Standardization
jbg	jitterbug
LD	Lipid Droplet
LDH	Lactate DeHydrogenase
LDV	Laser Doppler Vibrometer
LOVD	Leiden Open Variation Database
Mb	Mega base
MCHC	Mean Corpuscular Haemoglobin Concentration
MCV	Mean Corpuscular Volume
MGI	Mouse Genome Informatics
MO	MOrpholino
MRI	Magnetic Resonance Imaging
MRS	Magnetic Resonance Spectroscopy
NGS	Next Generation Sequencing
NMD	Nonsense-Mediated mRNA decay
NMJ	NeuroMuscular Junction
NSHI	Non-Syndromic Hearing Impairment
NS-UHI/AHI	non- syndromic unilateral and asymmetric hearing impairment
NS-UHL/AHL	Unilateral and Asymmetric Hearing Loss
OAE	OtoAcoustic Emission
OHC	Outer Hair Cells
OMIM	Online Mendelian Inheritance in Man
PC	Pillar Cells
PDB	Protein Data Bank
Polyphen2	Polymorphism phenotyping version 2
qPCR	quantitative Polymerase Chain Reaction
RDW	Red blood cell count Distribution Width
RNAi	RNA-mediated interference
SAT	Subcutaneous Adipose Tissue
SCV	Slow Component Velocity
SGOT	Serum levels of Glutamic Oxaloacetic Transaminase
SHI	Syndromic Hearing Impairment
SIFT	Sorting Intolerant From Tolerant
SMART	Simple Modular Architectural Research Tool
SNP	Single Nucleotide Polymorphism
SP	Spiral Prominence
SR	Saccular Roof
STR	Short Tandem Repeat

TIL	Trypsin Inhibitor Like
TM	Tectorial Membrane
TSP	Threonine/Serine/Proline-rich
VAT	Visceral Adipose Tissue
VDRC	Vienna *Drosophila* RNAi Centre
VNG	VidoeoNystagmoGraphy
VNTR	Variable Number of Tandem Repeat
VOR	Vestibulo-ocular reflexes
VRA	Visual Reinforcement Audiometry
vWF	von Willebrand Factor
WES	Whole Exome Sequencing
WGA	Wheat Germ Agglutinin
WGS	Whole Genome Sequencing
WS	Waardenburg syndrome
ZFIN	ZebraFish Information Network
ZP	Zona Pellucida

Chapter 1

General introduction

PREVALENCE OF HEARING IMPAIRMENT AND IMPACT ON SOCIETY

Sooner or later many of us will experience a certain degree of hearing impairment (HI). HI is the most frequent sensory disorder with 360 millions of affected individuals in the world.[1] HI refers to a loss in the ability of hearing of more than 26 decibels (dB) for the average of four frequencies (0.5, 1, 2 and 4 kHz) in the better hearing ear.[1] Some consequences of suffering from HI in childhood are delayed development of speech, language and cognitive skills. Besides that, having HI later in life can result in economic and educational disadvantages, social isolation and/or even exclusion. Overall, all these negative consequences make HI the 10th disease burden worldwide.[1]

In developed countries, one in 750 newborns presents with bilateral permanent HI of more than 40 dB.[2,3] About half of the cases is assumed to be caused by genetic defects whereas the other half is attributed to environmental factors, *e.g.* exposure to ototoxic drugs and/or viral infections. HI can be classified as non-syndromic (NSHI) or syndromic (SHI) depending on the absence or presence of additional clinical manifestations, respectively. NSHI accounts for 70% of childhood hereditary prelingual HI, whereas the other 30% is SHI with more than 400 syndromes with HI known to date.[4] Autosomal recessively inherited NSHI (arNSHI) is the most common form accounting for about 77% of the cases with 97 loci and 63 genes known to date. Autosomal dominant NSHI (adNSHI) accounts for 22% of the cases with 67 loci and 33 genes known. X- and Y-linked and mitochondrial NSHI are uncommon, accounting for the remaining 1% of the cases (Figure 1).[5]

In developing countries, the prevalence of prelingual HI is higher as compared to that in developed countries, being inversely proportional to the gross income.[1,3] Among the leading causative factors we find maternal infections (*e.g.* rubeola), meningitis, birth anoxia, chronic ear infections, use of ototoxic drugs and also consanguinity. Siblings of consanguineous marriages display a significantly higher incidence of autosomal recessive disorders such as arHI.[6]

THE EAR AND HEARING PROCESS

Anatomy and physiology of the ear

The ear is an organ that captures the sound waves and converts them into electrical signals resulting in sound perception in the central auditory system.

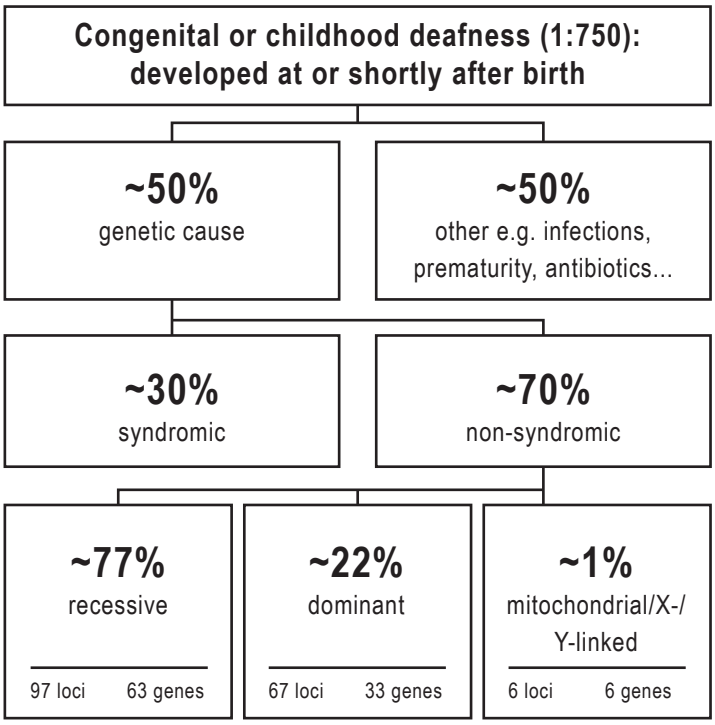

Figure 1: Diagram showing the different types of childhood HI, the attributed causes in developed countries and the patterns of inheritance.

Three parts of the ear can be distinguished: the outer ear with the pinna and the external ear canal, the middle ear with the auditory ossicles and the inner ear with the cochlea and vestibular system (Figure 2). The sound waves are captured by the pinna and travel to the middle ear through the external ear canal. The outer and middle ear sections are separated by the tympanic membrane (ear drum) that starts vibrating upon capture of sound waves. This vibration is transmitted by three auditory ossicles, the malleus, the incus and the stapes, to the oval window by the stapes footplate movement. The pressure created in the middle ear is then relieved by the Eustachian tube that connects the inner ear with the nasopharynx, the upper part of the pharynx (Figure 2).[7] The oval window separates the middle and the inner ear. The inner ear consists of bony labyrinths that reside within the temporal bone, the hardest bone of the human body. Within these bony labyrinths, the cochlea and the vestibular system are located (Figure 2).

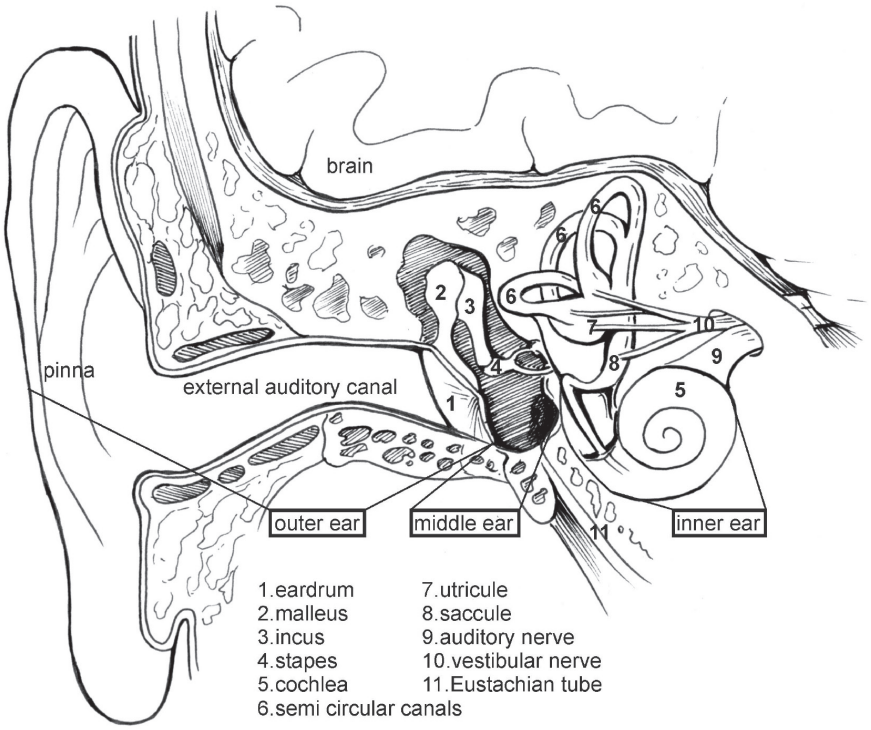

Figure 2: Schematic illustration of the outer, middle and inner ear parts (Figure published with permission of M.W.J. Luijendijk).

Inner ear

The inner ear is formed from the otic placode, a thickening of the ectoderm, during embryonic development. This placode invaginates and closes to form the otic vesicle (also called "auditory vesicle" or "otocyst").[8] After multiple rounds of cell division, rearrangements, differentiation and apoptotic events, the otic vesicle gives rise to the inner ear and cochleovestibular ganglion.[9,10]

Cochlea

The cochlea spirals around a conical bony structure called the modiolus. The cochlea is divided into three parallel chambers, the scala vestibuli, the scala media and the scala tympani, by the Reissner and basilar membranes (Figure 3). The scala vestibuli is the upper chamber with the oval window at its basal part and the helicotrema at its apex.[11] The helicotrema is a connection between the scala vestibuli and the lowermost chamber, the scala tympani (Figure 3). Therefore, both are filled with the same type of fluid, the perilymph. At the

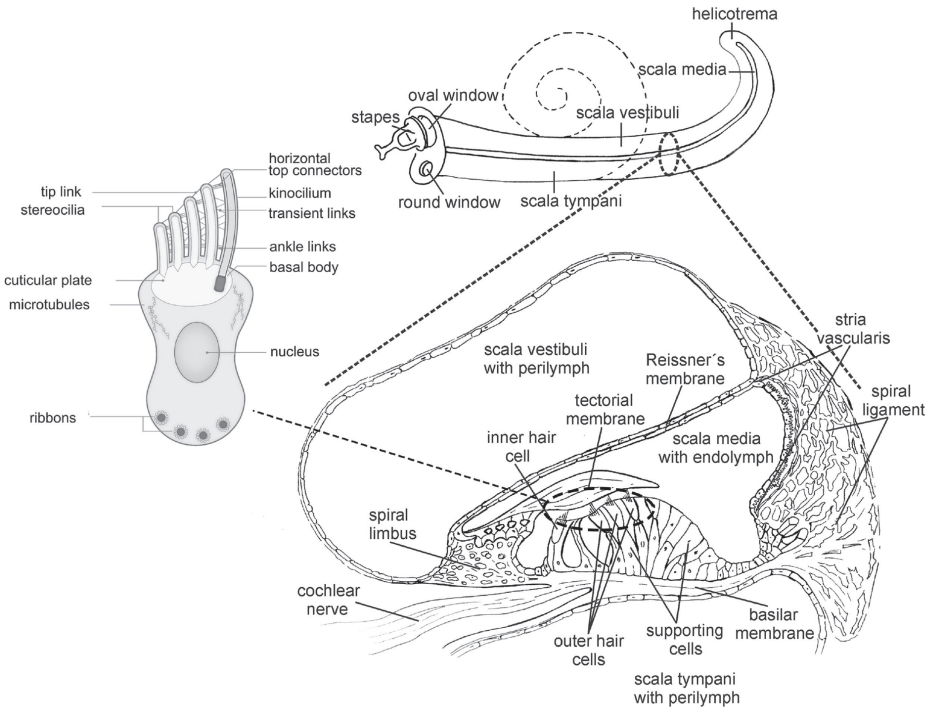

Figure 3: Schematic representation of the vertebrate cochlea, the organ of Corti and the inner ear hair cell (Figure adapted and published with permission of M.W.J. Luijendijk and [16]).

basal part of the scala tympani the round window is located. This round window is covered by an elastic membrane and bounces in and out in order to equilibrate the pressure created by the sound waves. The scala media contains the actual sensory epithelium, the organ of Corti (Figure 3). The scala media is filled with endolymph, a unique body fluid rich in potassium. In contrast, the perilymph is rich in sodium. The difference in ion concentrations between both scalae creates an electric potential ("endocochlear potential") that is the driving force for hair cell depolarization ultimately triggering neurotransmitter release at hair cell afferent synapse.

The organ of Corti in mammals consists of one row of inner hair cells, three (sometimes four[12,13]) rows of outer hairs cells and supporting cells (Figure 3). The human organ of Corti is less well organized with one or two rows of inner hair cells and less defined ranks of outer hair cells.[12] The outer hair cells enhance the sound sensitivity and selectivity. The inner hair cells perform the transduction and initiate the depolarization of the spiral ganglion.[14] The spiral

ganglion is the group of afferent and efferent nerves that send the hearing-evoked signals from the inner ear to the central nervous system and back. Supporting cells are involved in many different processes, such as the development of sensory epithelia and in preserving the structural integrity and homeostasis of the sensory organ.[15]

The apical part of the hair cells contains an actin-rich cuticular plate from which microvilli extend, the stereocilia (Figure 3). Stereocilia are typically arranged in a "V" shape staircase-like pattern. During development of the hair bundle, one true microtubule-based primary cilium (the kinocilium) is located at the vertex of the V-shape and determines the orientation of the hair bundle (Figure 3). The hair bundle on top of the hair cells is embedded in the tectorial membrane, a collagen rich extracellular matrix. Sound induces vibration of the basilar membrane with the hair cells against the tectorial membrane (Figure 3). Therefore, stereocilia bend and potassium and calcium from the endolymph enter the cell through the apical cation channels that are mechanically opened, this process is called mechanotransduction. As a consequence, the hair cells are depolarized and neurotransmitter release is triggered at their synaptic end. The potassium ions are recycled back to the endolymph via gap junctions and pumps located in the stria vascularis, at the lateral wall of the scala media, and in supporting cells (Figure 3) with two different purposes: 1) potassium efflux from hair cells leads to their repolarization; 2) potassium efflux prevents the cytotoxic accumulation of potassium ions inside the hair cells. Therefore, the supporting cells and the stria vascularis play an important role in the maintenance of the endolymph composition and therefore the endocochlear potential.

As presented, the hearing system and process is highly specialized and complex. Therefore, any defect in diverse biological processes such as gene regulation, ion homeostasis and hair bundle morphogenesis can lead to HI (Table 1).

Vestibular system

The vestibular system is the balance organ. It detects both rotational and linear accelerations by the semicircular canals and the two otolith organs (the utricle and the saccule), respectively (Figure 2).[17] As in the cochlea, the stereocilia of hair cells in the vestibular system deflect upon a stimulus, resulting in depolarisation of the cell and neurotransmitter release to the vestibular nerve. The clusters of hair cells in the saccule and utricle are embedded in gelatinous (otolith) membranes with small, calcium carbonate crystals called otoconia. The saccule and utricle are positioned at an angle of 90 degrees from each other. Therefore, any change in head position will lead to the deflection of stereocilia

by gravity due to the pushing weight of the otoconia.[18] In the semicircular canals, the hair cells are embedded in a gelatineous cupula. Rotation of the head results in the flow of endolymph within the semicircular canals eventually leading to bending of the stereocilia and as a consequence hair cell depolarization.[18] The balance information from the vestibular system converge with signals from other sensory and motor organs making central vestibular processing highly convergent and strongly multimodal.[17]

Table 1: Genes involved in HI, Usher syndrome and Waardenburg syndrome (WS) and the function of their encoded proteins in the auditory system.

Protein function in auditory system		Protein coding genes
Hair bundle morphogenesis	Cytoskeleton proteins	*ACTG1, DIAPH1, ESPN, RDX, TRIOBP, CCDC50, CLIC5*[19-22], *FAM65B*[23], *GRXCR1*[24], *SYNE4*[25], *DCDC2*[26], *EPS* [27]
	Adhesion proteins	*CDH23, GPR98, USH2A, PTPRQ*[28], *PCDH15*[29]
	Motor proteins	*MYO6, MYO7A, MYH9, MYO15A, MYO3A*
	Scaffolding proteins	*DFNB31, USH1C, USH1G, PDZD7*[30]
	METCC*	*PCDH15*[29], *LHFPL5*[31],*TMIE*[32], *TMC1*[33], *TRPN*[34]
	Others	*LOXHD1*[35], *miR-96*[36],
Extracellular matrix		*TECTA, COL11A2, STRC, OTOA, COCH, OTOG*[37], *OTOGL*[38], *CEACAM16*[39], *COL4A6*[40],
Ion homeostasis	Connexins	GJB2, GJB3, GJB6
	Ion channels	KCNQ4, SLC26A4, SLC26A5, P2RX2[41], SLC17A8[42]
	Tight junctions	CLDN14, ILDR1[43], MARVELD2[44], TJP2[45]
	Others	CRYM, WFS1, ADCY1[46], CaBP2[47], CIB2[48],
Transcription factors		*EYA4, POU4F3, POU3F4, ESRRB, GRHL2*[49]
Mitochondrial function		*MTTS1, MTRNR1, DIABLO*[50], *PNPT1*[51]
Sensory synapse structure/ function		*CLRN1*[52],*OTOF*[53]
Transcription initiation		*BDP1*[54]
Cytotoxic protection		*SERPINB6*[55]
Melanocyte development		*PAX3, MITF, SNAI2, EDN, EDNR, SOX10, KITLG*[30]
Unknown function		*TMPRSS3, MYH14, DFNA5, PJVK, ELMOD3*[56], *GPSM2*[57], *GRXCR2*[58], *HGF*[59], *KARS*[43], *LRTOMT*[60], *MSRB3*[61], *PRPS1*[62], *SMPX*[63], *TBC1D24*[64], *TSPEAR*[65], *OSBPL2*[66], *TMEM132E*[67], *GIPC3*[68]

*METCC stands for mechanoelectrical transduction channel complex of hair cells. Adapted and completed from [69].

CLINICAL EVALUATION AND DESCRIPTION OF HEARING IMPAIRMENT

Hearing of an individual is characterized by two important characteristics of the detected sounds, the pitch and the loudness. Pitch is discriminated by the location of the sound-elicited vibration in the basilar membrane and it is expressed in Hertz (Hz). The proximal end of this membrane near the oval window is relatively narrow and stiff and resonates at higher frequencies, whereas the apical end is wider and more flexible resonating at lower frequencies. The loudness depends on the sound pressure and it is expressed in decibels (dB). The higher the loudness, the higher the amplitude, the more vigorously the basilar membrane vibrates and thus the further the stereocilia bend leading to a larger action potential.[70]

There are different tests and steps to evaluate hearing:

1. Otoscopic examination is used to evaluate the ear canal and tympanic membrane as well as the nose, nasopharynx and upper respiratory tract.
2. Pure tone audiometry means the determination of the hearing thresholds in dB for a subset of pure tone frequencies based on two types of tests:
   a. Air conduction tests evaluate the external auditory canal, the middle ear, the functional integrity of the inner ear, eighth cranial nerve and central auditory pathways by using an air injection.
   b. Bone conduction tests use vibrating tuning forks which are placed against the skull. These vibrations bypass both the external and middle ear sections and therefore it is possible to distinguish between problems in those and in the inner ear.
3. Acoustic reflex testing measures the contraction of a tiny ear muscle, the stapedius muscle, that responds to stimuli. The acoustic reflex absence means that there is a defect but it does not give a hint of the source of the problem.
4. Tympanometry tests the condition of the middle ear and the ear drum.
5. Otoacoustic emissions are sounds generated by the outer hair cells. Therefore they can indicate an outer hair cell dysfunction. They are especially robust in infants.
6. The auditory brainstem response test is a method to pinpoint the site of sensorineural HI. Electrodes are placed on the scalp and sounds are presented resulting in different wave forms. The wave pattern can reflect different conditions such as lesions in the eighth cranial nerve or brainstem.

By using these tests, HI can be well characterized as seen in Table 2.

Table 2: Characteristics of the clinical description of HI (http://hereditaryhearingloss.org/).

Classification of HI		Explanation
Type	Conductive	Defects in the external and/or middle ear. Characterized by an air-bone gap >15 dB HI averaged over 0.5, 1 and 2 kHz, with normal bone conduction thresholds
	Sensorineural	Defects in the inner ear structures or cochlear nerve. Characterized by bone conduction thresholds > 20 dB HI with an absent or <15 dB HI air-bone gap, averaged over 0.5,1 and 2 kHz
	Mixed	Conductive and sensorineural. Characterized by bone conduction thresholds >20 dB HI and air-bone gap > 15 dB HI averaged over 0.5, 1 and 2 kHz
Severity of HI in the better hearing ear, averaged over 0.5, 1, 2 and 4 kHz	Mild	20-40 dB HI
	Moderate	41-70 dB HI
	Severe	71-95 dB HI
	Profound	>95 dB HI
Frequency ranges	Low	≤ 0.5 kHz
	Mid	>0.5 kHz and ≤ 2 kHz
	High	>2 kHz and ≤ 8 kHz
Symmetry of HI	Bilateral	The average of 0.5, 1 and 2 kHz of both ears > 20 dB HI
	Asymmetrical	>10 dB HI difference between the ears in at least two frequencies
Age of onset	Prelingual	HI presents before speech develops
	Postlingual	HI presents after the normal speech has developed

Table adapted and published with permission of E. Van Beelen.

NON-SYNDROMIC HEARING IMPAIRMENT

HI is called non-syndromic when it is not associated with additional symptoms other than vestibular problems.[71] NSHI accounts for around 70% of the inherited childhood cases. It is mostly sensorineural and shows different modes of inheritance as shown in Figure 1. Loci are designated with a DFN (DeaFNess) number which indicates the order of discovery. DFN is followed by an "A" for autosomal dominant, "B" for autosomal recessive, "X" for X-linked, and "Y" for Y-linked inheritance. "DFN" only is employed for mitochondrial inheritance. As shown in Figure 1, NSHI is genetically very heterogeneous which can be explained by the complexity of the auditory system (Table 1 and Figure 2).

ArNSHI is the most common form of HI accounting for 77% of the inherited non-syndromic cases. ArNSHI is typically congenital/prelingual, non-progressive, and mild to profound. Therefore, except for some specific phenotypes such as the downsloping progressive audiogram associated with *TMPRSS3* mutations,[71,72] the flat stable audiogram configuration caused by mutations in *TECTA*[71] and the late-onset HI with a progressive component in some cases,[71] it is very difficult to pinpoint a causative gene based on audiogram configuration. To date, there are 62 genes known to be associated with arNSHI, eight of which can be also associated with adNSHI by allelic variants. Mutations in GJB2 are the major cause for arNSHI worldwide.[73] The c.35delG mutation homozygously accounts for half of the arNSHI cases with southern European ancestry.[74] As it is reported in chapter 7, mutations in *MYO15A* and *STRC* are a frequent cause of arNSHI in the Netherlands. Also, mutations in *USH2A* frequently explain the congenital HI of Dutch cases who later in life develop retinitis pigmentosa. The involvement of these three genes worldwide might be underestimated due to the following reasons: 1) MYO15A (NM_016239, 65 exons) and *USH2A* (NM_206933, 72 exons) are very large genes and therefore not routinely analysed in non-syndromic early onset cases; 2) Sequencing of *STRC* can be hampered due to the close proximity of a pseudogene of more than 99% identity.

AdNSHI accounts for the remaining 22% of the non-syndromic cases. Clinically, adNSHI is usually progressive except for mutations in DFNA6/14/38,[75-78] part of DFNA8/12 cases,[79] DFNA23,[80,81] DFNA 24[82] and DFNA59[83] which result in a prelingual phenotype. DFNX, DFNY[84] and DFN types are very rare and account for around 1%.

SYNDROMIC HEARING IMPAIRMENT

SHI accounts for about 30% of the cases of congenital inherited HI with more than 400 syndromes characterized to date.[4] In this thesis, the most prevalent autosomal dominant and recessive syndromes, Waardenburg and Usher syndromes, respectively, are discussed.

Usher syndrome

Usher syndrome is a dual sensory impairment since affected individuals are born with sensorineural HI and develop retinitis pigmentosa later in life, which is often not apparent till adolescence. Visual symptoms are initially night blindness and loss of peripheral vision. Three clinical types of Usher syndrome are distinguished based on the severity of the HI and on the presence or absence of vestibular dysfunction. Type 1 is characterized by congenital severe to profound HI with vestibular areflexia; type 2 presents with congenital moderate to severe HI and normal vestibular function; and type 3 is characterized by progressive HI as well as, occasionally, progressive deterioration of the vestibular system.[85] Usher syndrome is genetically very heterogeneous as well with 13 loci known for which 10 genes have been identified to be involved in the three clinical types of the syndrome.[86] Mutations in six of these genes, *MYO7A*,[87-90] *CDH23*,[91,92] *PCDH15*,[93,94] *DFNB31*,[95,96] *USH1G*[97] and *CIB2*,[48] can lead to either Usher syndrome or NSHI. Mutations in *USH2A* can lead to either Usher syndrome or non-syndromic retinitis pigmentosa.[98,99]

Waardenburg syndrome

Waardenburg syndrome (WS) is a dominantly inherited auditory-pigmentary syndrome caused by partial absence of melanocytes in the skin, hair, eyes and stria vascularis of the cochlea.[100] Four clinical types are recognized based on the presence of specific features in addition to pigmentary abnormalities of hair, skin, eyes and congenital HL as in WS II. WS I is characterized by the presence of dystopia canthorum. WS I and II account for the majority of the cases, with an estimated prevalence of 5-10:100,000. Whereas 90% of WS I cases are explained by mutations in *PAX3*,[101] only 15% of WS II cases are explained by mutations in *MITF, SOX10* and *SNAI2*. 100,[102-104] Rarely, upper limb abnormalities and Hirschsprung disease can be part of the syndrome for WS III and IV, respectively. So far, mutations in PAX3 can explain WS III[105] whereas mutations in EDN, EDNR and SOX10 can be causative of WS IV.[106-108] All WS genes are involved in neural crest stem cell-derived melanocyte development.[109]

STRATEGIES FOR DISEASE GENE IDENTIFICATION

HI is a genetically very heterogeneous disorder. Before the era of Next Generation Sequencing (NGS) technologies, a popular gene identification approach was to combine linkage analysis or homozygosity mapping with Sanger sequencing of the most promising candidate genes in the linkage interval. This approach has been successfully followed in chapters 2, 3 and 4. However, the size of the linkage region can hamper disease gene identification by this approach (as we see in chapters 5 and 6) and, therefore, we combined linkage analysis with Whole Exome Sequencing (WES).

In the following paragraphs the strategies for disease gene identification that were employed for the research described in this thesis will be discussed.

Single Nucleotide Polymorphism (SNP) arrays

SNP arrays are powerful tools to identify regions in the genome that segregate with the disease according to a certain mode of inheritance.[110] Therefore, with SNP genotyping the chromosomal region which contains the genetic defect and co-segregates with the disease in the family relative to a SNP, whose the genomic position is already known, will be identified. SNPs are genomic variations presenting in two distinct alleles, each being common in the population (> 1%). After the disease haplotypes are determined, evaluation and sequencing of the plausible candidate genes within the candidate genomic regions will be performed in order to find the genetic cause underlying the disease.[111] The size of these candidate regions is inversely proportional to the number of meiosis available (Figure 4).

Homozygosity mapping and shared genotype determination

In autosomal recessive disorders, an affected individual carries mutations in both alleles of a single gene located on an autosome in order to be affected. If these mutations are identical, they are called homozygous.[111] When they are different, they are called compound heterozygous.[38] Homozygosity mapping and shared genotype calculations are based on the same principle: identification of shared genotypes in affected individuals, which are different in unaffected individuals within the same family. Therefore, the higher the resolution of the SNP array is, the more precise the determination of the disease haplotype will be.

When a homozygosity mapping strategy is used, the assumption is that the disease haplotypes are homozygous. This strategy has been proven to be successful in more than 50% of the cases in a population with high consanguinity

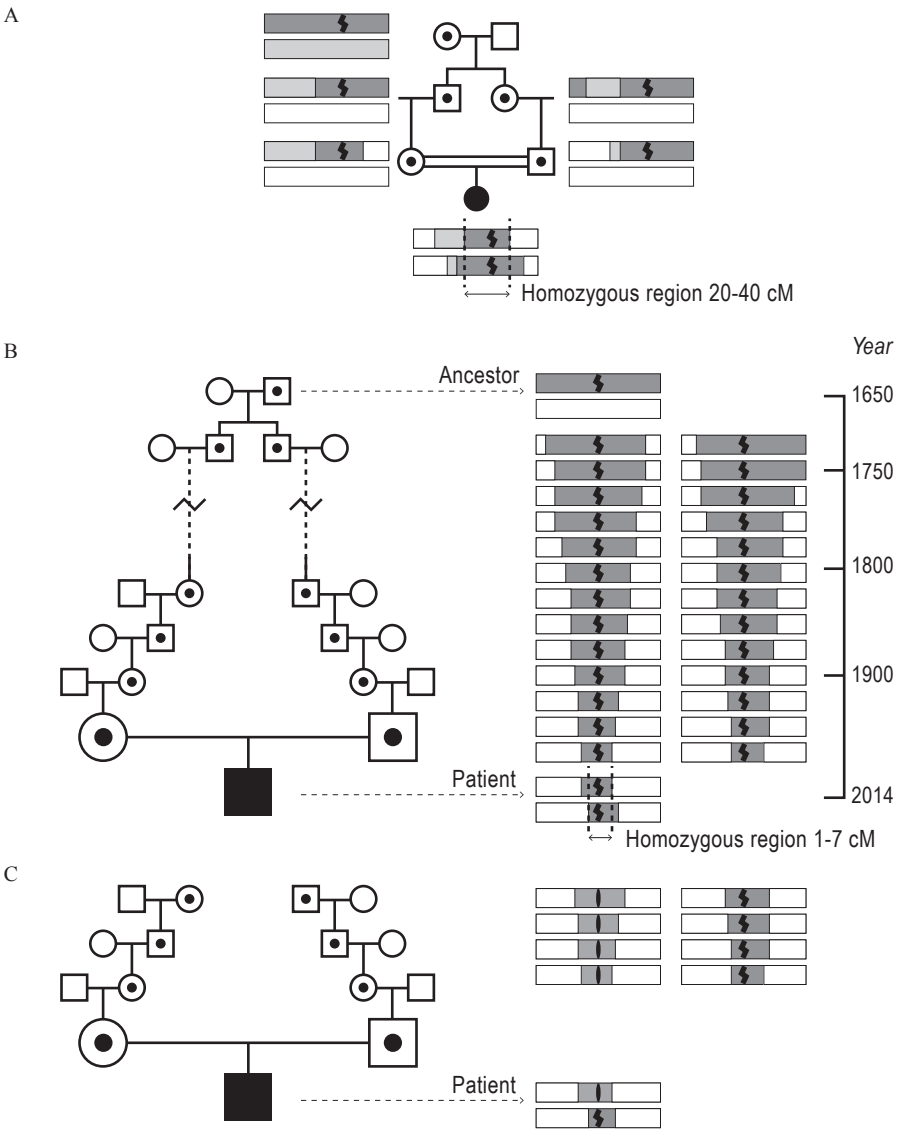

Figure 4: Schematic representation of the inheritance of recessive mutations. **A.** In consanguineous families, a recent common ancestor likely spreads the mutation. Due to the limited number of generations between the ancestor and the affected individual, a large fraction of the ancestral haplotype is inherited. **B.** When the number of generations between the ancestor and the affected individual, and thus the number of meiosis and recombination events, increases, a smaller fraction of this haplotype is inherited. **C.** In mixed populations, the patient often inherits two different heterozygous recessive alleles at a particular locus. The "cM" abbreviation stands for centiMorgans (Figure adapted and published with permission of K.L. Littink).

rates (Figure 4).[112] In presumably mixed populations, *e.g.* in the Netherlands, homozygosity mapping can also determine disease haplotypes inherited from a (distant) common ancestor (Figure 4).[113]

Determination of shared genotypes should be especially considered in mixed populations where individuals can move easily or choose a partner freely. In this case, the assumption is that the disease haplotypes segregating with the recessive disease are not necessarily homozygous, but it could also be heterozygous (Figure 4).

Linkage analysis

Linkage analysis has been very successful in localization of (novel) disease genes in autosomal dominant (chapter 5), recessive (chapter 6) and X-linked disorders.[114] In autosomal dominant disorders, an affected individual carries a mutation in one of the two alleles of the disease gene. This mutation can show full or reduced penetrance. Linkage analysis is a statistical method for identification of haplotypes segregating with the disease in a family. In contrast to homozygosity mapping and 'shared genotyping', linkage analysis does not require high density SNP arrays, but it requires SNPs that are in linkage disequilibrium. Linkage analysis also requires the availability of accurate pedigrees and SNP allele frequencies, which can be difficult to infer from the general population. Besides, linkage analysis can also be handicapped by the size of the families. When the family is small, the chromosomal regions that segregate with the disease are usually numerous and they will not reach genome-wide significance. When the family is large, the linkage region is likely to reach genome-wide significance however powerful computers are essential for the LOD score calculations. In order to circumvent these problems, several methods such as approximate linkage and haplotyping have been developed and shown to be successful as well as more user-friendly.[115,116]

Next generation sequencing technologies

DNA sequencing has evolved tremendously since 1977, when the enzymatic dideoxy Sanger sequencing technique was introduced.[117] Sanger sequencing technology provides the ultimate resolution for detecting genetic variation, however, it is difficult to scale-up, generally allowing only 96 or 384 analyses in parallel. This makes the technique time-consuming as well as expensive, at a cost of roughly $500 per Mega base (Mb).[118,119] In 2010, NGS or massive parallel sequencing revolutionized the genetics field allowing the detection of any kind of genetic variation by sequencing millions of DNA fragments in a

single experiment.[120-122] One NGS application is WES. The exome comprises only 1% of the human genome. Despite this, the exome harbours 85% of the disease causing mutations known to date.[123] Therefore, WES has the potential to unravel the causes in large numbers of rare as well as common genetic disorders.[124] As previously described, HI is genetically very heterogeneous and complex, not only because numerous genes and loci are described but also due to the presence of modifier alleles.[125,126] In the past years, research towards HI gene identification has benefited significantly from WES; however, for about 40% of the known loci, the causative gene is still elusive. On the other hand, WES does not cover non-coding parts of the genome and parts of the exome that are not targeted by the enrichment kits. WES also fails to define the boundaries of complex insertions, deletions, translocations and inversions. With whole genome sequencing (WGS) technologies, these drawbacks are expected to be relieved. Thus, WGS is considered to be the most accurate method to date.[123,127]

SCOPE AND OUTLINE OF THIS THESIS

HI is the most common sensory disorder that has a very negative impact on the quality of life of patients in our current society that relies on rapid communication. To date, many different genetic factors have been associated with HI, however, for a significant proportion of cases the genetic defects are still elusive. Therefore, the goal of my thesis was to contribute to the genetics of HI by the identification of mutations in known and novel genes involved in HI by using SNP array genotyping, WES and Sanger sequencing. Results are presented in the following chapters:

- **Chapter 2** describes the identification of a novel arNSHI gene, *OTOGL*, which is involved in congenital mid frequency HI.
- **Chapter 3** describes a homozygous nonsense mutation in *CLIC5* as a novel cause of congenital and progressive arNSHI accompanied by vestibular dysfunction.
- **Chapter 4** reports on novel and known mutations in *CIB2* causative of arNSHI and addresses their functional effects.
- **Chapter 5** describes the first gene involved in familial NS-unilateral and asymmetric HI (NS-UHI/AHI) and establishes a new phenotype-genotype correlation for mutations in *KITLG* in NS-UHI/AHI and WS II.
- **Chapter 6** describes a new syndrome characterized by HI, dystonia and sensory neuropathy caused by a homozygous nonsense mutation in *FITM2*. Besides, it provides the results of modeling the disease in *Drosophila melanogaster* by using the UAS-Gal4 system which recapitulated the human phenotype.
- **Chapter 7** reports on the clinical characterization and results of WES of 200 cases with HI.
- **Chapter 8** presents the general discussion of this thesis.

REFERENCES

1. www.who.int
2. Morton CC, Nance WE: Newborn hearing screening--a silent revolution. N Engl J Med 2006; 354: 2151-2164.
3. Stevens G, Flaxman S, Brunskill E, et al.: Global and regional hearing impairment prevalence: an analysis of 42 studies in 29 countries. Eur J Public Health 2013; 23: 146-152.
4. Toriello HR, W.; Gorlin, RJ.: Hereditary Hearing Loss and its Syndromes. Oxford UniversityPress, Inc; Oxford.
5. Smith R.J.H., Shearer A. E., Hildebrand M.S., Van Camp,G. Deafness and Hereditary Hearing Loss Overview. Gene Reviews (http://www.ncbi.nlm.nih.gov/books/NBK1434/), 2014.
6. Zakzouk S: Consanguinity and hearing impairment in developing countries: a custom to be discouraged. J Laryngol Otol 2002; 116: 811-816.
7. Heine PA: Anatomy of the ear. Vet Clin North Am Small Anim Pract 2004; 34: 379-395.
8. Morsli H, Choo D, Ryan A, Johnson R, Wu DK: Development of the mouse inner ear and origin of its sensory organs. J Neurosci 1998; 18: 3327-3335.
9. Magarinos M, Contreras J, Aburto MR, Varela-Nieto I: Early development of the vertebrate inner ear. Anat Rec (Hoboken) 2012; 295: 1775-1790.
10. Whitfield TT: Development of the inner ear. Curr Opin Genet Dev 2015; 32: 112-118.
11. http://labspace.open.ac.uk/mod/resource/view.php?id=415641#.
12. Forge A, Wright T: The molecular architecture of the inner ear. Br Med Bull 2002; 63: 5-24.
13. Wright A: Scanning electron microscopy of the human organ of Corti. J R Soc Med 1983; 76: 269-278.
14. Raphael Y, Altschuler RA: Structure and innervation of the cochlea. Brain Res Bull 2003; 60: 397-422.
15. Wan G, Corfas G, Stone JS: Inner ear supporting cells: rethinking the silent majority. Semin Cell Dev Biol 2013; 24: 448-459.
16. Kremer H, van Wijk E, Marker T, Wolfrum U, Roepman R: Usher syndrome: molecular links of pathogenesis, proteins and pathways. Hum Mol Genet 2006; 15 Spec No 2: R262-270.
17. Angelaki DE, Cullen KE: Vestibular system: the many facets of a multimodal sense. Annu Rev Neurosci 2008; 31: 125-150.
18. http://neuroscience.uth.tmc.edu/s2/chapter10.html.
19. Gagnon LH, Longo-Guess CM, Berryman M, et al.: The chloride intracellular channel protein CLIC5 is expressed at high levels in hair cell stereocilia and is essential for normal inner ear function. J Neurosci 2006; 26: 10188-10198.
20. Pierchala BA, Munoz MR, Tsui CC: Proteomic analysis of the slit diaphragm complex: CLIC5 is a protein critical for podocyte morphology and function. Kidney Int 2010; 78: 868-882.

21. Wegner B, Al-Momany A, Kulak SC, et al.: CLIC5A, a component of the ezrin-podocalyxin complex in glomeruli, is a determinant of podocyte integrity. Am J Physiol Renal Physiol 2010; 298: F1492-1503.
22. Salles FT, Andrade LR, Tanda S, et al.: CLIC5 stabilizes membrane-actin filament linkages at the base of hair cell stereocilia in a molecular complex with radixin, taperin, and myosin VI. Cytoskeleton (Hoboken) 2014; 71: 61-78.
23. Diaz-Horta O, Subasioglu-Uzak A, Grati M, et al.: FAM65B is a membrane-associated protein of hair cell stereocilia required for hearing. Proc Natl Acad Sci U S A 2014; 111: 9864-9868.
24. Odeh H, Hunker KL, Belyantseva IA, et al.: Mutations in Grxcr1 are the basis for inner ear dysfunction in the pirouette mouse. Am J Hum Genet 2010; 86: 148-160.
25. Worman HJ, Segil N: Nucleocytoplasmic connections and deafness. J Clin Invest 2013; 123: 553-555.
26. Grati M, Chakchouk I, Ma Q, et al.: A missense mutation in DCDC2 causes human recessive deafness DFNB66, likely by interfering with sensory hair cell and supporting cell cilia length regulation. Hum Mol Genet 2015.
27. Taylor R, Bullen A, Johnson SL, et al.: Absence of plastin 1 causes abnormal maintenance of hair cell stereocilia and a moderate form of hearing loss in mice. Hum Mol Genet 2015; 24: 37-49.
28. Goodyear RJ, Legan PK, Wright MB, et al.: A receptor-like inositol lipid phosphatase is required for the maturation of developing cochlear hair bundles. J Neurosci 2003; 23: 9208-9219.
29. Pepermans E, Michel V, Goodyear R, et al.: The CD2 isoform of protocadherin-15 is an essential component of the tip-link complex in mature auditory hair cells. EMBO Mol Med 2014; 6: 984-992.
30. Zou J, Zheng T, Ren C, et al.: Deletion of PDZD7 disrupts the Usher syndrome type 2 protein complex in cochlear hair cells and causes hearing loss in mice. Hum Mol Genet 2014; 23: 2374-2390.
31. Beurg M, Xiong W, Zhao B, Muller U, Fettiplace R: Subunit determination of the conductance of hair-cell mechanotransducer channels. Proc Natl Acad Sci U S A 2014.
32. Zhao B, Wu Z, Grillet N, et al.: TMIE is an essential component of the mechanotransduction machinery of cochlear hair cells. Neuron 2014; 84: 954-967.
33. Pan B, Geleoc GS, Asai Y, et al.: TMC1 and TMC2 are components of the mechanotransduction channel in hair cells of the mammalian inner ear. Neuron 2013; 79: 504-515.
34. Lee J, Moon S, Cha Y, Chung YD: Drosophila TRPN(=NOMPC) channel localizes to the distal end of mechanosensory cilia. PLoS One 2010; 5: e11012.
35. Grillet N, Schwander M, Hildebrand MS, et al.: Mutations in LOXHD1, an evolutionarily conserved stereociliary protein, disrupt hair cell function in mice and cause progressive hearing loss in humans. Am J Hum Genet 2009; 85: 328-337.

36. Kuhn S, Johnson SL, Furness DN, et al.: miR-96 regulates the progression of differentiation in mammalian cochlear inner and outer hair cells. Proc Natl Acad Sci U S A 2011; 108: 2355-2360.
37. Schraders M, Ruiz-Palmero L, Kalay E, et al.: Mutations of the gene encoding otogelin are a cause of autosomal-recessive nonsyndromic moderate hearing impairment. Am J Hum Genet 2012; 91: 883-889.
38. Yariz KO, Duman D, Seco CZ, et al.: Mutations in OTOGL, encoding the inner ear protein otogelin-like, cause moderate sensorineural hearing loss. Am J Hum Genet 2012; 91: 872-882.
39. Zheng J, Miller KK, Yang T, et al.: Carcinoembryonic antigen-related cell adhesion molecule 16 interacts with alpha-tectorin and is mutated in autosomal dominant hearing loss (DFNA4). Proc Natl Acad Sci U S A 2011; 108: 4218-4223.
40. Rost S, Bach E, Neuner C, et al.: Novel form of X-linked nonsyndromic hearing loss with cochlear malformation caused by a mutation in the type IV collagen gene COL4A6. Eur J Hum Genet 2014; 22: 208-215.
41. Telang RS, Paramananthasivam V, Vlajkovic SM, et al.: Reduced P2x(2) receptor-mediated regulation of endocochlear potential in the ageing mouse cochlea. Purinergic Signal 2010; 6: 263-272.
42. Ruel J, Emery S, Nouvian R, et al.: Impairment of SLC17A8 encoding vesicular glutamate transporter-3, VGLUT3, underlies nonsyndromic deafness DFNA25 and inner hair cell dysfunction in null mice. Am J Hum Genet 2008; 83: 278-292.
43. Morozko EL, Nishio A, Ingham NJ, et al.: ILDR1 null mice, a model of human deafness DFNB42, show structural aberrations of tricellular tight junctions and degeneration of auditory hair cells. Hum Mol Genet 2014.
44. Nayak G, Lee SI, Yousaf R, et al.: Tricellulin deficiency affects tight junction architecture and cochlear hair cells. J Clin Invest 2013; 123: 4036-4049.
45. Lenz DR, Avraham KB: Hereditary hearing loss: from human mutation to mechanism. Hear Res 2011; 281: 3-10.
46. Santos-Cortez RL, Lee K, Giese AP, et al.: Adenylate cyclase 1 (ADCY1) mutations cause recessive hearing impairment in humans and defects in hair cell function and hearing in zebrafish. Hum Mol Genet 2014; 23: 3289-3298.
47. Schrauwen I, Helfmann S, Inagaki A, et al.: A mutation in CABP2, expressed in cochlear hair cells, causes autosomal-recessive hearing impairment. Am J Hum Genet 2012; 91: 636-645.
48. Riazuddin S, Belyantseva IA, Giese AP, et al.: Alterations of the CIB2 calcium- and integrin-binding protein cause Usher syndrome type 1J and nonsyndromic deafness DFNB48. Nat Genet 2012; 44: 1265-1271.
49. Han Y, Mu Y, Li X, et al.: Grhl2 deficiency impairs otic development and hearing ability in a zebrafish model of the progressive dominant hearing loss DFNA28. Hum Mol Genet 2011; 20: 3213-3226.

50. Cheng J, Zhu Y, He S, et al.: Functional mutation of SMAC/DIABLO, encoding a mitochondrial proapoptotic protein, causes human progressive hearing loss DFNA64. Am J Hum Genet 2011; 89: 56-66.
51. von Ameln S, Wang G, Boulouiz R, et al.: A mutation in PNPT1, encoding mitochondrial-RNA-import protein PNPase, causes hereditary hearing loss. Am J Hum Genet 2012; 91: 919-927.
52. Adato A, Vreugde S, Joensuu T, et al.: USH3A transcripts encode clarin-1, a four-transmembrane-domain protein with a possible role in sensory synapses. Eur J Hum Genet 2002; 10: 339-350.
53. Pangrsic T, Reisinger E, Moser T: Otoferlin: a multi-C2 domain protein essential for hearing. Trends Neurosci 2012; 35: 671-680.
54. Kassavetis GA, Han S, Naji S, Geiduschek EP: The role of transcription initiation factor IIIB subunits in promoter opening probed by photochemical cross-linking. J Biol Chem 2003; 278: 17912-17917.
55. Sirmaci A, Erbek S, Price J, et al.: A truncating mutation in SERPINB6 is associated with autosomal-recessive nonsyndromic sensorineural hearing loss. Am J Hum Genet 2010; 86: 797-804.
56. Jaworek TJ, Richard EM, Ivanova AA, et al.: An alteration in ELMOD3, an Arl2 GTPase-activating protein, is associated with hearing impairment in humans. PLoS Genet 2013; 9: e1003774.
57. Walsh T, Shahin H, Elkan-Miller T, et al.: Whole exome sequencing and homozygosity mapping identify mutation in the cell polarity protein GPSM2 as the cause of nonsyndromic hearing loss DFNB82. Am J Hum Genet 2010; 87: 90-94.
58. Imtiaz A, Kohrman DC, Naz S: A frameshift mutation in GRXCR2 causes recessively inherited hearing loss. Hum Mutat 2014; 35: 618-624.
59. Schultz JM, Khan SN, Ahmed ZM, et al.: Noncoding mutations of HGF are associated with nonsyndromic hearing loss, DFNB39. Am J Hum Genet 2009; 85: 25-39.
60. Ahmed ZM, Masmoudi S, Kalay E, et al.: Mutations of LRTOMT, a fusion gene with alternative reading frames, cause nonsyndromic deafness in humans. Nat Genet 2008; 40: 1335-1340.
61. Ahmed ZM, Yousaf R, Lee BC, et al.: Functional null mutations of MSRB3 encoding methionine sulfoxide reductase are associated with human deafness DFNB74. Am J Hum Genet 2011; 88: 19-29.
62. Liu X, Han D, Li J, et al.: Loss-of-function mutations in the PRPS1 gene cause a type of nonsyndromic X-linked sensorineural deafness, DFN2. Am J Hum Genet 2010; 86: 65-71.
63. Schraders M, Haas SA, Weegerink NJ, et al.: Next-generation sequencing identifies mutations of SMPX, which encodes the small muscle protein, X-linked, as a cause of progressive hearing impairment. Am J Hum Genet 2011; 88: 628-634.

64. Azaiez H, Booth KT, Bu F, et al.: TBC1D24 mutation causes autosomal-dominant nonsyndromic hearing loss. Hum Mutat 2014; 35: 819-823.
65. Delmaghani S, Aghaie A, Michalski N, et al.: Defect in the gene encoding the EAR/EPTP domain-containing protein TSPEAR causes DFNB98 profound deafness. Hum Mol Genet 2012; 21: 3835-3844.
66. Xing G, Yao J, Wu B, et al.: Identification of OSBPL2 as a novel candidate gene for progressive nonsyndromic hearing loss by whole-exome sequencing. Genet Med 2014.
67. Li J, Zhao X, Xin Q, et al.: Whole-Exome Sequencing Identifies a Variant in TMEM132E Causing Autosomal-Recessive Nonsyndromic Hearing Loss DFNB99. Hum Mutat 2015; 36: 98-105.
68. Charizopoulou N, Lelli A, Schraders M, et al.: Gipc3 mutations associated with audiogenic seizures and sensorineural hearing loss in mouse and human. Nat Commun 2011; 2: 201.
69. Hilgert N, Smith RJ, Van Camp G: Function and expression pattern of nonsyndromic deafness genes. Curr Mol Med 2009; 9: 546-564.
70. Oghalai JS: The cochlear amplifier: augmentation of the traveling wave within the inner ear. Curr Opin Otolaryngol Head Neck Surg 2004; 12: 431-438.
71. Hoefsloot LH, Feenstra I, Kunst HP, Kremer H: Genotype phenotype correlations for hearing impairment: approaches to management. Clin Genet 2014; 85: 514-523.
72. Weegerink NJ, Schraders M, Oostrik J, et al.: Genotype-phenotype correlation in DFNB8/10 families with TMPRSS3 mutations. J Assoc Res Otolaryngol 2011; 12: 753-766.
73. Kenneson A, Van Naarden Braun K, Boyle C: GJB2 (connexin 26) variants and nonsyndromic sensorineural hearing loss: a HuGE review. Genet Med 2002; 4: 258-274.
74. Snoeckx RL, Huygen PL, Feldmann D, et al.: GJB2 mutations and degree of hearing loss: a multicenter study. Am J Hum Genet 2005; 77: 945-957.
75. Bespalova IN, Van Camp G, Bom SJ, et al.: Mutations in the Wolfram syndrome 1 gene (WFS1) are a common cause of low frequency sensorineural hearing loss. Hum Mol Genet 2001; 10: 2501-2508.
76. Cryns K, Pfister M, Pennings RJ, et al.: Mutations in the WFS1 gene that cause low-frequency sensorineural hearing loss are small non-inactivating mutations. Hum Genet 2002; 110: 389-394.
77. Sun Y, Cheng J, Lu Y, et al.: Identification of two novel missense WFS1 mutations, H696Y and R703H, in patients with non-syndromic low-frequency sensorineural hearing loss. J Genet Genomics 2011; 38: 71-76.
78. Pennings RJ, Bom SJ, Cryns K, et al.: Progression of low-frequency sensorineural hearing loss (DFNA6/14-WFS1). Arch Otolaryngol Head Neck Surg 2003; 129: 421-426.
79. Li Z, Guo Y, Lu Y, et al.: Identification of a Novel TECTA mutation in a Chinese DFNA8/12 family with prelingual progressive sensorineural hearing impairment. PLoS One 2013; 8: e70134.

80. Ruf RG, Xu PX, Silvius D, et al.: SIX1 mutations cause branchio-oto-renal syndrome by disruption of EYA1-SIX1-DNA complexes. Proc Natl Acad Sci U S A 2004; 101: 8090-8095.
81. Salam AA, Hafner FM, Linder TE, et al.: A novel locus (DFNA23) for prelingual autosomal dominant nonsyndromic hearing loss maps to 14q21-q22 in a Swiss German kindred. Am J Hum Genet 2000; 66: 1984-1988.
82. Hafner FM, Salam AA, Linder TE, et al.: A novel locus (DFNA24) for prelingual nonprogressive autosomal dominant nonsyndromic hearing loss maps to 4q35-qter in a large Swiss German kindred. Am J Hum Genet 2000; 66: 1437-1442.
83. Chatterjee A, Jalvi R, Pandey N, Rangasayee R, Anand A: A novel locus DFNA59 for autosomal dominant nonsyndromic hearing loss maps at chromosome 11p14.2-q12.3. Hum Genet 2009; 124: 669-675.
84. Wang Q, Xue Y, Zhang Y, et al.: Genetic basis of Y-linked hearing impairment. Am J Hum Genet 2013; 92: 301-306.
85. Smith RJ, Berlin CI, Hejtmancik JF, et al.: Clinical diagnosis of the Usher syndromes. Usher Syndrome Consortium. Am J Med Genet 1994; 50: 32-38.
86. Cosgrove D, Zallocchi M: Usher protein functions in hair cells and photoreceptors. Int J Biochem Cell Biol 2014; 46: 80-89.
87. Weil D, Blanchard S, Kaplan J, et al.: Defective myosin VIIA gene responsible for Usher syndrome type 1B. Nature 1995; 374: 60-61.
88. Liu XZ, Walsh J, Mburu P, et al.: Mutations in the myosin VIIA gene cause non-syndromic recessive deafness. Nat Genet 1997; 16: 188-190.
89. Weil D, Kussel P, Blanchard S, et al.: The autosomal recessive isolated deafness, DFNB2, and the Usher 1B syndrome are allelic defects of the myosin-VIIA gene. Nat Genet 1997; 16: 191-193.
0. Liu XZ, Walsh J, Tamagawa Y, et al.: Autosomal dominant non-syndromic deafness caused by a mutation in the myosin VIIA gene. Nat Genet 1997; 17: 268-269.
91. Wayne S, Der Kaloustian VM, Schloss M, et al.: Localization of the Usher syndrome type ID gene (Ush1D) to chromosome 10. Hum Mol Genet 1996; 5: 1689-1692.
92. Bork JM, Peters LM, Riazuddin S, et al.: Usher syndrome 1D and nonsyndromic autosomal recessive deafness DFNB12 are caused by allelic mutations of the novel cadherin-like gene CDH23. Am J Hum Genet 2001; 68: 26-37.
93. Ahmed ZM, Riazuddin S, Bernstein SL, et al.: Mutations of the protocadherin gene PCDH15 cause Usher syndrome type 1F. Am J Hum Genet 2001; 69: 25-34.
94. Ahmed ZM, Riazuddin S, Ahmad J, et al.: PCDH15 is expressed in the neurosensory epithelium of the eye and ear and mutant alleles are responsible for both USH1F and DFNB23. Hum Mol Genet 2003; 12: 3215-3223.

95. Mburu P, Mustapha M, Varela A, et al.: Defects in whirlin, a PDZ domain molecule involved in stereocilia elongation, cause deafness in the whirler mouse and families with DFNB31. Nat Genet 2003; 34: 421-428.
96. Ebermann I, Scholl HP, Charbel Issa P, et al.: A novel gene for Usher syndrome type 2: mutations in the long isoform of whirlin are associated with retinitis pigmentosa and sensorineural hearing loss. Hum Genet 2007; 121: 203-211.
97. Oonk AM, van Huet RA, Leijendeckers JM, et al.: Nonsyndromic Hearing Loss Caused by USH1G Mutations: Widening the USH1G Disease Spectrum. Ear Hear 2014.
98. Eudy JD, Weston MD, Yao S, et al.: Mutation of a gene encoding a protein with extracellular matrix motifs in Usher syndrome type IIa. Science 1998; 280: 1753-1757.
99. Rivolta C, Sweklo EA, Berson EL, Dryja TP: Missense mutation in the USH2A gene: association with recessive retinitis pigmentosa without hearing loss. Am J Hum Genet 2000; 66: 1975-1978.
100. Read AP, Newton VE: Waardenburg syndrome. J Med Genet 1997; 34: 656-665.
101. Tassabehji M, Read AP, Newton VE, et al.: Waardenburg's syndrome patients have mutations in the human homologue of the Pax-3 paired box gene. Nature 1992; 355: 635-636.
102. Tassabehji M, Newton VE, Read AP: Waardenburg syndrome type 2 caused by mutations in the human microphthalmia (MITF) gene. Nat Genet 1994; 8: 251-255.
103. Sanchez-Martin M, Rodriguez-Garcia A, Perez-Losada J, et al.: SLUG (SNAI2) deletions in patients with Waardenburg disease. Hum Mol Genet 2002; 11: 3231-3236.
104. Bondurand N, Dastot-Le Moal F, Stanchina L, et al.: Deletions at the SOX10 gene locus cause Waardenburg syndrome types 2 and 4. Am J Hum Genet 2007; 81: 1169-1185.
105. Hoth CF, Milunsky A, Lipsky N, et al.: Mutations in the paired domain of the human PAX3 gene cause Klein-Waardenburg syndrome (WS-III) as well as Waardenburg syndrome type I (WS-I). Am J Hum Genet 1993; 52: 455-462.
106. Edery P, Attie T, Amiel J, et al.: Mutation of the endothelin-3 gene in the Waardenburg-Hirschsprung disease (Shah-Waardenburg syndrome). Nat Genet 1996; 12: 442-444.
107. Pingault V, Bondurand N, Kuhlbrodt K, et al.: SOX10 mutations in patients with Waardenburg-Hirschsprung disease. Nat Genet 1998; 18: 171-173.
108. Attie T, Till M, Pelet A, et al.: Mutation of the endothelin-receptor B gene in Waardenburg-Hirschsprung disease. Hum Mol Genet 1995; 4: 2407-2409.
109. Hou L, Pavan WJ: Transcriptional and signaling regulation in neural crest stem cell-derived melanocyte development: do all roads lead to Mitf? Cell Res 2008; 18: 1163-1176.
110. LaFramboise T: Single nucleotide polymorphism arrays: a decade of biological, computational and technological advances. Nucleic Acids Res 2009; 37: 4181-4193.
111. Seco CZ, Oonk AM, Dominguez-Ruiz M, et al.: Progressive hearing loss and vestibular dysfunction caused by a homozygous nonsense mutation in CLIC5. Eur J Hum Genet 2014.

112. Duman D, Tekin M: Autosomal recessive nonsyndromic deafness genes: a review. Front Biosci (Landmark Ed) 2012; 17: 2213-2236.
113. Schraders M, Oostrik J, Huygen PL, et al.: Mutations in PTPRQ are a cause of autosomal-recessive nonsyndromic hearing impairment DFNB84 and associated with vestibular dysfunction. Am J Hum Genet 2010; 86: 604-610.
114. Huebner AK, Gandia M, Frommolt P, et al.: Nonsense mutations in SMPX, encoding a protein responsive to physical force, result in X-chromosomal hearing loss. Am J Hum Genet 2011; 88: 621-627.
115. Carr IM, Johnson CA, Markham AF, et al.: DominantMapper: rule-based analysis of SNP data for rapid mapping of dominant diseases in related nuclear families. Hum Mutat 2011; 32: 1359-1366.
116. Silberstein M, Weissbrod O, Otten L, et al.: A system for exact and approximate genetic linkage analysis of SNP data in large pedigrees. Bioinformatics 2013; 29: 197-205.
117. Sanger F, Air GM, Barrell BG, et al.: Nucleotide sequence of bacteriophage phi X174 DNA. Nature 1977; 265: 687-695.
118. Metzker ML: Emerging technologies in DNA sequencing. Genome Res 2005; 15: 1767-1776.
119. Tucker T, Marra M, Friedman JM: Massively parallel sequencing: the next big thing in genetic medicine. Am J Hum Genet 2009; 85: 142-154.
120. Metzker ML: Sequencing technologies - the next generation. Nat Rev Genet 2010; 11: 31-46.
121. Ng SB, Bigham AW, Buckingham KJ, et al.: Exome sequencing identifies MLL2 mutations as a cause of Kabuki syndrome. Nat Genet 2010; 42: 790-793.
122. Ng SB, Buckingham KJ, Lee C, et al.: Exome sequencing identifies the cause of a mendelian disorder. Nat Genet 2010; 42: 30-35.
123. Majewski J, Schwartzentruber J, Lalonde E, Montpetit A, Jabado N: What can exome sequencing do for you? J Med Genet 2011; 48: 580-589.
124. Rabbani B, Tekin M, Mahdieh N: The promise of whole-exome sequencing in medical genetics. J Hum Genet 2014; 59: 5-15.
125. Yan D, Liu XZ: Modifiers of hearing impairment in humans and mice. Curr Genomics 2010; 11: 269-278.
126. Cohn ES, Kelley PM, Fowler TW, et al.: Clinical studies of families with hearing loss attributable to mutations in the connexin 26 gene (GJB2/DFNB1). Pediatrics 1999; 103: 546-550.
127. Gilissen C, Hehir-Kwa JY, Thung DT, et al.: Genome sequencing identifies major causes of severe intellectual disability. Nature 2014; 511: 344-347.

[1]John P. Hussman Institute for Human Genomics, University of Miami Miller School of Medicine, Miami, FL 33136, USA; [2]Dr. John T. Macdonald Department of Human Genetics, University of Miami Miller School of Medicine, Miami, FL 33136, USA; [3]Division of Pediatric Genetics, Ankara University School of Medicine, 06100, Ankara, Turkey; [4]Department of Otorhinolaryngology, Radboud University Nijmegen Medical Centre, 6500 HB Nijmegen, The Netherlands; [5]Donders Institute for Brain, Cognition and Behavior, Radboud University Nijmegen Medical Centre, 6500 HB Nijmegen, The Netherlands; [6]Nijmegen Centre for Molecular Life Sciences, Radboud University Nijmegen Medical Centre, 6500 HB Nijmegen, The Netherlands; [7]Department of Biology, University of Miami, Miami, FL 33146, USA; [8]Eaton-Peabody Laboratory, Department of Otology and Laryngology, Massachusetts Eye and Ear Infirmary, Harvard Medical School, Boston 02114, USA; [9]Department of Otology & Skull Base Surgery, Affiliated Eye and ENT Hospital of Fudan University, 83 Fenyang Road, Shanghai, 200031, China; [10]Hearing and Balance Disorders Diagnosis and Rehabilitation Center, Ataturk Research and Training Hospital, 06800, Ankara, Turkey; [11]Department of Life Sciences, Bethlehem University, Bethlehem, Palestine; [12]Department of Otolaryngology, University of Miami Miller School of Medicine, Miami, FL 33136, USA; [13]Department of Human Genetics, Radboud University Nijmegen Medical Centre, 6500 HB Nijmegen, The Netherlands.

Chapter 2

Mutations in *OTOGL*, encoding the inner ear protein Otogelin-like, cause moderate sensorineural hearing loss

Kemal Yariz[1,2,*], Duygu Duman[3,*], **Celia Zazo Seco**[4,5,6], Julia Dallman[7], Mingqian Huang[8], Theo Peters[4,5,6], Asli Sirmaci[1,2], Na Lu[8,9], Margit Schraders[4,5,6], Isaac Skromne[7], Jaap Oostrik[4,5,6], Oscar Diaz-Horta[1,2], Juan I. Young[1,2], Suna Tokgoz-Yilmaz[3], Ozlem Konukseven[10], Hashem Shahin[11], Lisette Hetterschijt[6,13], Moien Kanaan[11], Anne M.M. Oonk[4,5], Yvonne J.K. Edwards[1,2], Huawei Li[9], Semra Atalay[3], Susan Blanton[1,2], Alexandra A. DeSmidt[7], Xue-Zhong Liu[1,12], Ronald J. E. Pennings[4,5], Zhongmin Lu[7], Zheng-Yi Chen[8], Hannie Kremer[4,5,6,13], Mustafa Tekin[1,2,3]

* Authors contributed equally

American journal of human genetics 2012 Nov 2;91(5):872-82

ABSTRACT

Hereditary hearing loss is characterized by a high degree of genetic heterogeneity. Here we present *OTOGL* mutations, a homozygous one base pair deletion (c.1430delT) causing a frameshift (p.Val477Glufs*25) in a large consanguineous family and two compound heterozygous mutations, c.547C>T (p.Arg183*) and c.5238+5G>A, in a non-consanguineous family with moderate non-syndromic sensorineural hearing loss. *OTOGL* maps to the DFNB84 locus at 12q21.31 and encodes otogelin-like, which has structural similarities to the epithelial-secreted mucin protein family. We demonstrate that *Otogl* is expressed in the inner ear of vertebrates with a transcription level that is high in embryonic, lower in neonatal and much lower in adult stages. Otogelin-like is localized to the acellular membranes of the cochlea and the vestibular system and to a variety of inner ear cells located underneath these membranes. Knocking down of *otogl* with morpholinos in zebrafish leads to sensorineural hearing loss and anatomical changes in the inner ear, supporting that otogelin-like is essential for normal inner ear function. We propose that *OTOGL* mutations affect the production and/or function of acellular structures of the inner ear, which ultimately leads to sensorineural hearing loss.

INTRODUCTION

Hereditary hearing loss is characterized by genetic heterogeneity with mutations in several hundreds of genes encoding a variety of proteins[1-3]. Mutations in these genes lead to various clinical scenarios ranging from non-syndromic hearing loss to one of the more than 400 syndromes that include hearing loss and from mild adult onset hearing loss to profound congenital deafness spanning a full-spectrum of Mendelian inheritance[1,2]. The autosomal recessive pattern of inheritance occurs in the majority of families with Non-Syndromic Hearing Loss (arNSHL) and is typically congenital or prelingual-onset[2]. Mutations in 40 genes have thus far been shown to cause arNSHL, which can account for more than 60% of families with this type of inheritance pattern[3]. Hearing loss is usually severe or profound in cases with arNSHL, although varying degrees of residual hearing are observed in some families. Individuals with mutations in *STRC* (MIM 606440), for example, essentially present with moderate hearing loss[4] and 22% of the persons with mutations in the DFNB[1] locus have moderate deafness[5].

In this study we report mutations in *OTOGL*, encoding otogelin-like, that are associated with moderate arNSHL. We demonstrate that *OTOGL* is expressed in the inner ears of humans, mouse, rat, and zebrafish, and its disruption in zebrafish leads to hearing loss.

MATERIALS AND METHODS

Studied Families

The study on hereditary deafness was approved by the Ethics Committees of Ankara University (Turkey) and the Radboud University Nijmegen Medical Centre (the Netherlands), and by the IRB at the University of Miami (U.S.A.). Informed consents were obtained from all participants, or in the case of minors, from the parents. Diagnosis of sensorineural hearing loss was established via standard audiometry in a sound-proofed room according to current clinical standards. Hearing loss was classified according to the GENDEAF guidelines (hereditary hearing loss home page). Evaluation for vestibular function included Unterberger, Romberg, head thrust, and head shake tests, oculomotor examination, spontaneous nystagmus and positioning tests, and bithermal caloric tests via vidoeonystagmography (VNG, Micromedical Technologies, Illinois U.S.A.). Slow Component Velocity (SCV) of the nystagmus was measured

with a threshold of 6 degree per second. Clinical evaluation of all affected individuals by a geneticist and an ENT surgeon included a thorough physical examination and otoscopy. A high resolution CT scan of the temporal bone was obtained in one affected person in each family. The studies presented here were performed in two families: Family 1, a consanguineous Turkish family with four children (Figure 1A) and Family 2, a non-consanguineous Dutch family with three children having sensorineural hearing loss (Figure 1D). DNA was extracted from blood via standard methods. One affected individual from each family was prescreened and found not to have common causes of non-syndromic deafness including mutations in *GJB2* (MIM 121011) and for the m.1555A>G mutation in *MTRNR1* (MIM 561000).

Autozygosity Mapping

Genome-wide SNP genotyping was performed via Affymetrix 6.0 and Illumina Human Omni Express 700K arrays in Families 1 and 2, respectively. Autozygosity mapping was performed as reported previously[6,7]. The co-segregation of the genotypes for each previously reported deafness gene was visually evaluated. Multipoint linkage analysis of an autozygous segment was conducted with GeneHunter[8], assuming a fully penetrant autosomal recessive phenotype with population frequency for the hearing loss allele of 0.0001. SNPs spanning the autozygous region were chosen for linkage analysis based on tagging and heterozygosity in the parents. Copy number variants (CNVs) were assessed by determining the relative loss or gain of fluorescent signal intensity from SNP or CNV probes on the array as previously described[6].

Whole Exome and Sanger Sequencing

The Agilent SureSelect Human All Exon 50 MB kit was used with an Illumina HiSeq 2000 instrument. Adapter sequences for the Illumina HiSeq2000 were ligated and the enriched DNA samples were subjected to standard sample preparation for the HiSeq2000 instrument (Illumina). Paired-end reads of 100 bases length were produced. The Illumina CASAVA v1.8 pipeline was used to produce 99 bp sequence reads. BWA[9] was used to align sequence reads to the human reference genome (hg19) and variants were called using the GATK software package[10]. All variants were submitted to SeattleSeq135 for further characterization.

All 58 exons and exon-intron boundaries of *OTOGL* (NM_173591.3) were screened via Sanger-sequencing (detailed in Supplemental Table S1). To screen additional families for linkage to the *OTOGL* locus, eight SNPs within the gene

were chosen, custom TaqMan probes were developed, and assayed according to the manufacturer`s protocol Data were analyzed via SDS 2.3 (Applied Biosystems) software.

Minigene Construction and Splicing Assay

For prediction of the effect of the c.5238+5G>A transition on splicing efficiency, the following software tools were used: NetGene[11], BDGP Splice prediction site[12] and Human Splice Finder (Alamut; Interactive Biosoftware).

The splicing assay for the c.5238+5G>A mutation was performed using the pCIneo vector described by Gamundi et al. containing exons 3-5 of *RHO*[13], which was adapted for the Gateway cloning system by replacing exon 4 and flanking sequences by a Gateway cassette using the EcoNI and PflMI sites of the vector. A fragment containing exon 43 and 225 and 126 bp respectively of 5'and 3'flanking sequences of *OTOGL* was amplified from genomic DNA of one of the parents of Family 2 and clones for the wild type and the mutant alleles were selected after sequencing. Primers used for amplification of the fragment are provided in Supplemental Table S2. Transfection of HEK293T cells with the plasmids, isolation of RNA, and RT-PCR were performed as described[14]. The *RHO* and *OTOGL* exons were amplified from the cDNA with forward primer 5'-cggaggtcaacaacgagtct-3' and reverse primer 5'-aggtgtaggggatgggagac-3', which are located in *RHO* exon 3 and exon 5, respectively. The assay was performed in triplo in two independent experiments. The RT-PCR fragments were sequenced to verify normal splicing and exon skipping.

OTOGL Expression Profile by Quantitative PCR in Humans

RNA derived from various adult tissues as well as from fetal liver was purchased from Clontech. In addition, RNA was isolated from fetal inner ear, heart, skeletal muscle, and lung as described previously[15]. cDNA was synthesized as previously described[15] and purified with NucleoSpin Extract II columns (Macherey-Nagel) in accordance with the manufacturer's protocol. For PCR, specific primers (Supplemental Table S2) were designed with Primer3 Plus and reference sequence NM_173591.3. Amplifications were performed with the Applied Biosystem Fast 7900 System in accordance with the manufacturer's protocol. The human beta glucuronidase gene (*GUSB*; MIM 611499) was employed as an internal reference. PCR reaction mixtures were prepared with the Power SYBR® Green Master Mix (Applied Biosystems) in accordance with the manufacturer's protocol. Temperatures and reaction times for PCR were as follows: 10 min at 95°C, followed by 40 cycles of

15 sec at 95°C and 30 sec at 60°C. All reactions were performed in duplicate. Relative gene expression levels were determined with the delta delta Ct method as described previously[16].

Otogl Expression by Semi-Quantitative RT-PCR in Mice

Otogl transcript levels in different developmental stages of mouse inner ear were evaluated by semi-quantitative RT-PCR. All the procedures were approved by the Institutional Animal Care and Use Committee of the Massachusetts Eye and Ear Infirmary. Mouse cochleae were dissected from CD1 mice at different stages. RNA extractions were performed using Trizol reagent (Life Technologies). Reverse transcriptase reactions were performed using SuperScript II (Life Technologies), and PCR reactions using Taq polymerase (Life Technologies). The PCR primers are given in Supplemental Table S2. PCR conditions were: 94°C, 2 min; 94°C, 30 sec; 62°C, 1 min; 72°C, 1 min 30 sec for 40 cycles; 72°C, 10 min. Gene expression was normalized to *GAPDH* expression.

Rodent Immunohistochemistry and *in situ* Hybridization

CD1 mouse inner ear tissues from timed pregnancy were collected following an established procedure. The procedure in the use of animals and tissue preparation were approved by the Institutional Animal Care and Use Committee of the Massachusetts Eye and Ear Infirmary and of the Radboud University Nijmegen. Standard immunohistochemical procedures were used for the labeling of cryosectioned mouse cochlear slides, with the antibodies against the following antigens: OTOGL (1:150, Atlas Antibodies, HPA040364), SOX2 (1:200, Santa Cruz, sc-17320), MYO7A (1:1000, Developmental Studies Hybridoma Bank, MYO7A 138-1). The nuclei were labeled with DAPI (1X , Molecular Probe).

For the preadsorption control experiment, the OTOGL antibody was incubated with 10-fold excess (relative to antibody concentration) of OTOGL antigen (Atlas Antibodies, HPA040364, dissolved in 1M urea and 1x PBS) at room temperature for 2 hours. The mixture was spun at 16,000 g for 20', and the supernatant was used for immunofluorescence. The MYO7A antibody was also mixed with OTOGL antigen/antibody on the same condition and the MYO7A staining was not different from the pattern using the non-treated MYO7A antibody. The image acquisition conditions were identical for all immunolabeling results.

Temporal bones of P10, P20, and P30 Wistar rats were fixed in 2% buffered paraformaldehyde, before dissection of the cochlea and vestibular structures. For these cryosections, the OTOGL antibody was 1:50 diluted and Alexa Fluor

568 labeled phalloidin (1:400; Life Technologies) was added for actin staining. The nuclei were labeled with DAPI (1X , Molecular Probe) and for controls, the primary antibody was omitted. Sections were examined with a fluorescence microscope. In addition, 2% paraformaldehyde fixed whole mount organs of Corti of P12 rats were incubated with anti-otogl (1:50), phalloidin (1:400) and DAPI (1:8000) as previously described17 and analyzed with a confocal microscope.

For *in situ* hybridization the same sample preparation for mouse inner ear tissue was used as in immunohistochemistry. The protocol used was identical to the one described previously[18].

Zebrafish *otogl* Identification, Cloning, *in situ* Hybridization and Immunohistochemistry

Zebrafish (*Danio rerio*) were raised and handled following standard techniques[19] approved by the Institutional Animal Care and Use Committee of the University of Miami. Embryos from wild-type AB stock were used for gene cloning, and enhancer trap transgenic line SqET4[20] expressing GFP in hair cells for expression analysis and physiology. We identified the zebrafish homolog of the human *OTOGL* by sequence similarity and synteny analysis. The human *OTOGL* protein sequence NP_775862.3 was used to query the zebrafish genome version-9 by BLAT using VEGA Genome Browser (release 46), the manually curated zebrafish genomic database. Two high-scoring genomic loci were recovered, *dkeyp-27b10.2*, a predicted *otogl* gene (BX321877.7) on chromosome 18 and (BX842701.1-201) on chromosome 7 that encodes zebrafish *otog*. Separately, linkage analysis of the zebrafish genes to ptprq, a deafness gene that in humans is closely linked to *OTOGL*[7,21], showed that only *dkeyp-27b10.2* is closely associated to the zebrafish *ptprq*. Based on sequence and synteny evidence we established the zebrafish gene on chromosome 7 as the ortholog of human *OTOG* on chromosome 11, and *dkeyp-27b10.2* on chromosome 18 as the ortholog of human *OTOGL* on chromosome 12. The zebrafish nomenclature committee reviewed and approved these name designations, assigning the Zebrafish Information Network (ZFIN) number ZDB-GENE-120228-1 to *otogelin* (*otog*) and ZDB-GENE-050419-93 to *otogelin-like* (*otogl*).

An 800 base pair region of zebrafish *otogl* near the center of the gene that was devoid of repetitive protein domains was cloned using an RT-PCR strategy. Nested primers were designed using the zebrafish genome assembly version-9. cDNA from 48 hpf embryos was PCR-amplified with Taq polymerase (Promega) and primer set 5out-otogl, TGGAGGAAGGAGTCTGCT and

3out-otogl, CACGGTCACAGGTGCATT. A second round of amplification used inner primers 5in-otogl, GAGTCTGCTGTCCCAAGA and 3in-otogl, CAACCGCAGTCTCCATAC. The PCR cycling parameters used for both reactions was: 94°C, 2 min, 1 time; 94°C, 30 sec, 60°C, 1 min, 72°C, 2 min, 35 times; 72°C, 10 min, 4°C, hold, 1 time. PCR product was gel purified, and ligated to pGEM-T Easy (Promega) using manufacturer's instructions. Eight clones were sequenced to verify identity of inserts. One plasmid containing the correct insert was linearized and *in vitro* transcribed to generate DIG-labeled RNA to use as a probe. Whole mount *in situ* hybridization was carried out as previously described[22], with the following modification: prior to developing the chromogenic reaction with Fast Red substrate (Roche), embryos were immunostained to detect GFP expression in ear hair cells.

Immunodetection of GFP and acetylated-tubulin in zebrafish embryos was done following a previously described protocol[23]. Anti-GFP (Anaspec) and Anti-acetylated tubulin (Santa Cruz Biotechnology) were used as primary antibodies and an Anti-rabbit Alexa488-conjugated antibody as a secondary antibody (Life Technologies). Actin was detected using Alexa568-conjugated phalloidin (Life Technologies). Immunostaining and *in situ* hybridization were performed via standard methods[23].

Zebrafish *otogl* Morpholino Knock-down

To generate zebrafish larvae lacking *otogl* function, we first identified the gene's intron/exon junctions by comparing *Otogl* protein sequence XP_683212 to the *otogl* genomic region of VEGA. We designed two splice-blocking morpholinos against exon/intron junctions 36 and 37 found at the 3' half of the gene because the gene's 5' end is poorly annotated. Missplicing events at these locations were predicted to generate truncated proteins lacking the last von Willebrand Factor (vWF)/cytokine rich paired domains and C-terminal cysteine knot domain. The two splice-blocking morpholinos (GeneTools, LLC) are MO1 GATGCACACACACACTGACCGCAGA against exon/intron junction 36 and MO2 CATCCTGAGGAAAGGAGGGTAACAC against exon/intron junctions 37. The efficacy of *otogl* knockdown by each morpholino was assessed by RT-PCR analysis of morpholino-induced intron retention. Total RNA was extracted from 3-day old embryos using Trizol (Life Technologies), and treated with Turbo DNase (Ambion). 500 ng of purified RNA was reverse transcribed to cDNA using an anchored oligodT primer and Superscript III (Life Technologies). 1 µL of cDNA was then used as template for a PCR reaction with diagnostic primers TACCACAGCACTGGCATCAT and TTCCTCCAGCTGAAGCAGAT

that span the exon/intron junctions targeted by the morpholinos. Primers against an unrelated gene, the glycine receptor β sub-unit (*glrbb*) serves as a loading control. Morpholinos were titrated to determine the lowest dose that induced missplicing events. Physiology and molecular biology were carried out on embryos injected with 2-5 nL of 0.25 mM *otogl*MO1 or 2. For phenotypic assessment, *otogl* MO-injected larvae were compared to stage-matched larvae injected with the same concentration of a standard control morpholino CCTCTTACCTCAGTTACAATTTATA (GeneTools, LLC). Both *otogl* morpholinos produced similar phenotypes that include severe cardiac edema and, at higher doses, curvature to the body axis.

Microphonic Potential Recording in Zebrafish

The microphonic potential recording from larval zebrafish was modified from previously described protocols[24,25]. Morpholino-injected zebrafish at 2 or 3 dpf were anaesthetized in 0.01% buffered MS-222 solution and embedded dorsal up in 1.8% agarose with 0.01% buffered MS-222 in a low profile 35-mm MatTek dish. The MatTek dish was then placed in a QE-1 platform (Warner Instruments, Hamden, CT) that was temperature controlled at about 28.5 oC on a Gibraltar stage of Zeiss Axioskop 2 FS plus microscope. The Zeiss microscope setup rested on an anti-vibration table and enclosed in a Faraday cage (Technical Manufacturing Co., Peabody, MA).

A stimulus probe with the tip size of 20 μm in diameter was made from a glass capillary (OD = 1.50 mm, ID = 0.84 mm, World Precision Instruments, Sarasota, FL) using a micropipette puller (P97, Sutter Instrument Co., Novato, CA) and a microforge (MF-900, Narishige International USA, East Meadow, NY). The stimulus probe was driven by a piezoelectric actuator and calibrated using a high-speed camera. The probe tip was placed against the posterior edge of the inner ear (pointing to the saccular otolith) and provided linear oscillatory motion at 200 Hz along an axis parallel to the longitudinal axis of fish body.

The recording electrodes were made from glass capillaries (OD = 1.5, ID = 1.12 mm, WPI), filled with standard fish saline solution (pH = 7.2) and then sharpened with a Sutter BV-10-E micropipette beveler until the electrode resistance dropped to about 6 MΩ. The recording electrode tip was advanced to penetrate the wall of the inner ear of larval zebrafish using a Narishige MHW-3 three-dimensional hydraulic micromanipulator. Microphonic responses were amplified 1,000x, bandpass filtered between 0.1 and 3000 Hz, averaged up to 200 times, and recorded at a sampling rate of 25 kHz. The amplitude of microphonic responses (RMS) was measured at twice the stimulus frequency in FFT plots.

Student's t-test was performed to determine the significance of differences in microphonic amplitude between *otogl* morphants and larvae injected with a control morpholino.

RESULTS

OTOGL Mutations Cause Moderate Sensorineural Hearing Loss in Humans

In Family 1, all four affected individuals had symmetric moderate sensorineural hearing loss. Available audiograms did not show progression (Figure 1B). Clinical examinations did not reveal additional findings. CT scan of the temporal bone of one affected family member was normal as well. Detailed vestibular analyses were performed in one individual, II:7, who complained about one episode of dizziness lasting for 3 months at age 17. He described it as a blurry vision caused by turning his head abruptly to the left and lasting for only a few seconds. There were no other symptoms such as vertigo. Vestibular tests revealed vestibular hypofunction on the left side via caloric tests. All positional tests produced persistent up-left non-torsional nystagmus with the average of 7 degrees per second without vertigo sensation.

Only one autozygous genomic region larger than 1 Mb was shared by all four affected members of Family 1. The length of this autozygous region was 15 Mb on chromosome 12 (68,804,480 bp-83,923,162 bp) and included the DFNB84 locus (Figure 1A). The autozygous region contains 51 RefSeq genes including *PTPRQ* (MIM 603317), which was recently found to be associated with arNSHL[7,21]. A multipoint LOD score of 3.36 was obtained for this region. Sanger-sequencing of the exons and intron-exon boundaries of *PTPRQ* (NM_001145026.1) in one affected member did not show a mutation. None of the other previously identified deafness genes mapped to an autozygous region suggesting that a previously unrecognized human deafness gene was involved in this family.

We then performed whole exome sequencing in individual II:7, which generated 177,257,596 reads. Using a minimum depth of 4x, 84% of the targeted regions were covered with an average read depth of 100x. The longest autozygous region on chromosome 12 was fully covered by SureSelect Human All Exon 50 Mb kit except for *PTPRQ* which was Sanger-sequenced in Family 1. After multiple filters were employed (Table 1), whole exome data revealed two novel homozygous variants both located in *OTOGL* (hg19): a one base pair deletion at 80,648,835, c.1430delT (NM_173591.3) predicted to

cause a reading frame shift and a premature termination of protein synthesis, p.Val477Glufs*25 (NP_775862.3) and 80,717,580T>C corresponding to c.4132T>C (NM_173591.3) predicted to lead to the substitution of an Arginine for a Cysteine, p.Cys1378Arg (NP_775862.3). Both variants were confirmed via Sanger-sequencing (Figure 1C). They both co-segregated with the phenotype in the family as an autosomal recessive trait and were absent in 373 ethnicity-matched control samples. Neither variant has been found in the NHLBI Exome Sequencing Project (Exome Variant Server), or in dbSNP databases. The p.Cys1378Arg variant affected a highly conserved residue in *OTOGL*. However, since p.Cys1378Arg is located at the C-terminal relative to p.Val477Glufs*25, it is unlikely to contribute to the phenotype. Screening for additional mutations in *OTOGL* via linkage analysis followed by Sanger-sequencing in additional 195 families with severe or profound arNSHL failed to detect a mutation.

Family 2, presented with three brothers with moderate and stable hearing loss. Physical examination and otoscopy revealed no abnormalities. Diagnosis of hearing loss was at the neonatal hearing screening for II.3 and can therefore be assumed to be congenital. Subsequently, the older brothers where diagnosed at the ages of 3 (II.1) and 2 (II.2) years. All three boys performed normally in the Unterberger, Romberg, head thrust, and head shake tests and in addition the eye tracking movements although a delay in gross motor development was reported. A high resolution CT scan in II.3 did not reveal abnormalities. Autozygosity mapping in family 2 did not reveal any significant homozygous regions (> 1 Mb) shared by all three affected children. As a next step, the data were analyzed for the presence of shared genotypes (>3 Mb) in the 3 affected children for the previously described autosomal recessive deafness loci; a shared region of 10.9 Mb on chromosomal region 12q21.2-q21.32 was identified encompassing the DFNB84 locus. Because of the moderate, stable nature of the hearing impairment that was also noted in Family 1, we initiated mutation analysis of *OTOGL*. Two variants, which were not present in the NCBI dbSNP134 or 135 database, NHLBI Exome Sequencing Project (Exome Variant Server) nor in the 1000 Genomes Project, were identified; a nonsense mutation c.547C>T (p.Arg183*) and a splice site mutation c.5238+5G>A. All three affected children were compound heterozygous for these mutations; father and mother were heterozygous for p.Arg183* and c.5238+5G>A, respectively. The splice site mutation is predicted to reduce splicing efficiency by ~50% (0.47 vs 0.98 for the wild-type sequence; BDGP Splice Prediction). Two other prediction tools, NetGene Splice site predictions and Human Splice Finder, do not predict a splice donor site for the sequence with the G to A transition. A minigene assay

A

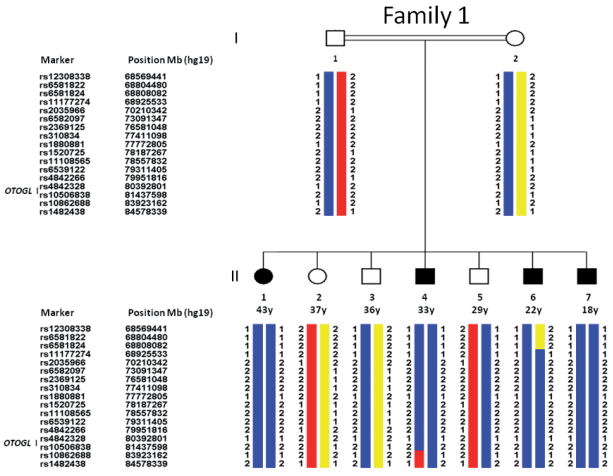

B

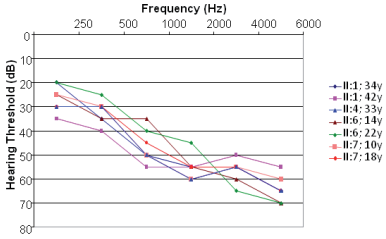

C

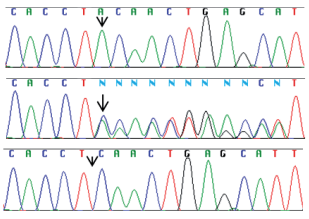

c.1430delT
(p.Val477Glufs*25)
wild type

c.1430delT (p.Val477Glufs*25)
heterozygous

c.1430delT (p.Val477GlufsX*5)
homozygous

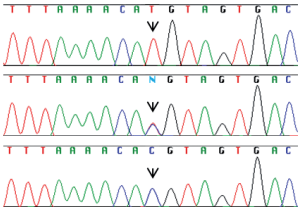

c.4132T>C
(p.Cys1378Arg) wild type

c.4132T>C
(p.Cys1378Arg) heterozygous

c.4132T>C
(p.Cys1378Arg) homozygous

D

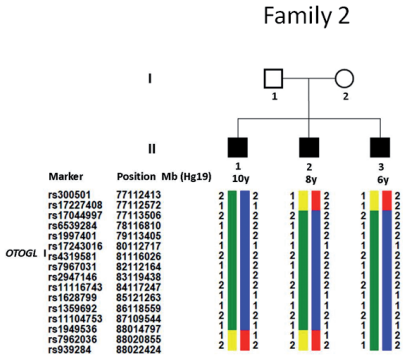

E

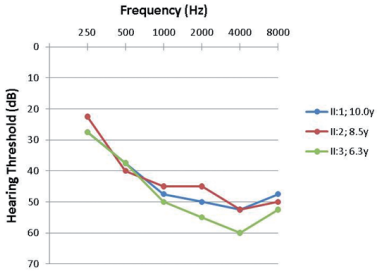

F

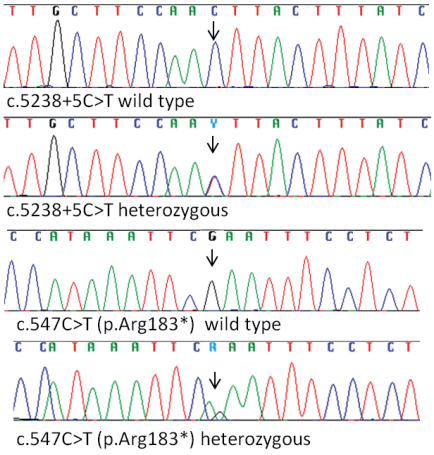

Figure 1. Studied Families, Audiograms, and *OTOGL* Mutations

A) Family 1 and the longest autozygous region on chromosome 12. Parents are first cousins; B) Audiograms show moderate sensorineural hearing loss in Family 1; C) Electropherograms showing identified mutations in *OTOGL* in Family 1; D) Pedigree and SNP genotypes in Family 2; E) Audiograms of affected subjects in Family 2 show moderate hearing loss; F) Electropherograms of the *OTOGL* mutations identified in Family 2.

was performed to test the effect of the mutation on splicing in HEK293T cells which demonstrated skipping of exon 43 (Supplemental Figure S1).

Otogelin-like, the predicted product of *Otogl*, was recently identified in mouse by amplification and sequencing of the transcript. The gene was annotated and named because of its structural similarity to otogelin[21]. Otogelin encoded by *Otog* was first discovered as an extracellular glycoprotein specific to the acellular membranes of inner ear[26]. Otogelin shows structural similarities to the epithelial-secreted mucin protein family since it is comprised of an N-terminal signal peptide, a central threonine/serine/proline-rich (TSP) region flanked by vWF-like cysteine-rich domains and a C-terminal knot motif domain[26]. Otogelin-like similarly contains an N-terminal signal peptide of 22 amino acids in the N-terminal (predicted by the SignalP software) as well as vWF and knot domains in the mature peptide (Figure 5B). Otogelin and otogelin-like have an amino acid identity of 33.3% (56.0% similarity).

Expression Profile of *OTOGL*

The expression of *OTOGL* relative to *GUSB* standard internal control was studied via quantitative PCR (qPCR) in 10 adult and 10 fetal-stage human tissues including human fetal inner ear (Figure 2). Because this was performed for adult and fetal tissues in two separate experiments, fetal inner ear was included in both for comparison. In adult tissues, relatively low *OTOGL* transcript levels as compared to fetal inner ear were seen in lung, spleen, and duodenum, and relatively moderate levels in heart, kidney, brain, and retina. In three of the adult tissues - skeletal muscle, liver and testis - expression of *OTOGL* was below the detection level. Among the fetal tissues that were tested, the transcript level was highest in the inner ear. However, since these tissues were not derived from fetuses of the same gestational stage a direct comparison of the transcript levels cannot be made. The inner ear was derived from a fetus at 8 weeks of gestation and all other fetal tissues from fetuses at 20-21 weeks gestation. At the latter stage, *OTOGL* transcript levels were highest in fetal heart. A low relative *OTOGL* transcript level was observed in skeletal muscle, kidney, spleen and colon. In the fetal liver, lung, brain and stomach, expression was below the detection level.

Otogelin-like is Present in Several Cell Types and the Acellular Membranes of the Inner Ear

The localization of otogelin-like (*OTOGL*) in the inner ear was studied by immunostaining with an anti-*OTOGL* antibody in the mouse and rat.

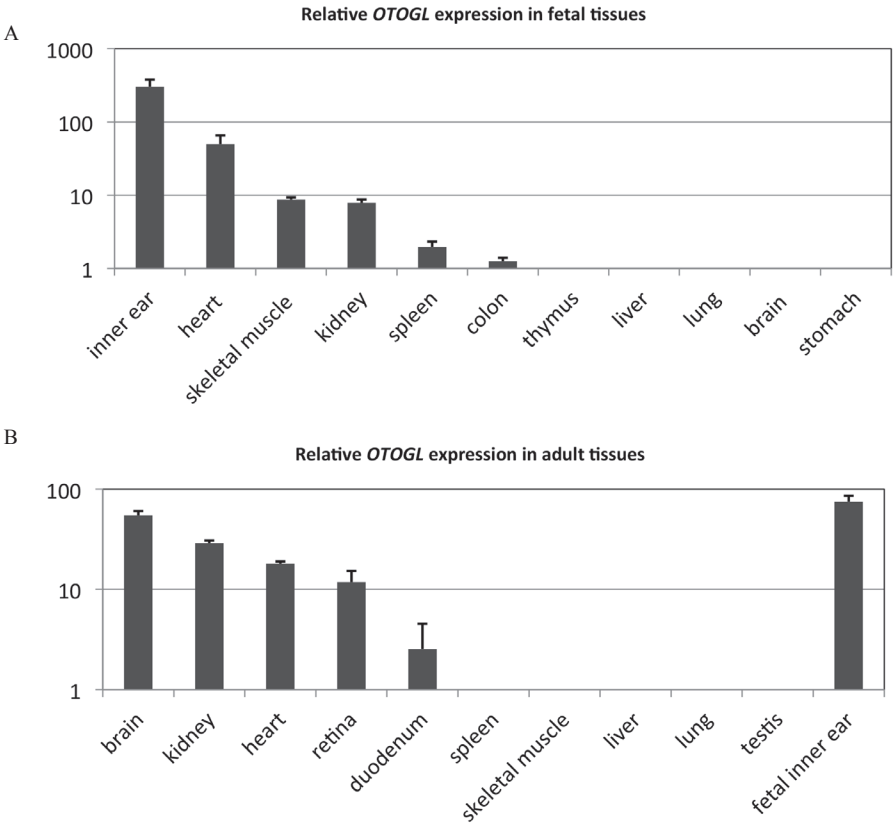

Figure 2. *OTOGL* Expression Profile in Human Tissues

Relative *OTOGL* mRNA levels as determined by qPCR in human fetal (A) and adult (B) tissues. The relative expression values were determined by using the delta delta Ct method. Relative *OTOGL* transcript levels were highest in fetal inner ear.

Table 1. The number of variants (SNPs and indels) identified by whole exome sequencing of individual II:7 in family 1compared to the reference genome (hg19)

Region	Total Variants	Novel Variants
Whole Exome	221,686	77,655
+Homozygous Variants	64,180	2,828
+Chr12:68,804,480-83,923,162	407	38
+Missense, nonsense, splice, frame-shift	16	2
Sanger confirmed	NA	2 in *OTOGL*

The different filters and annotation categories are shown.

NA: not available

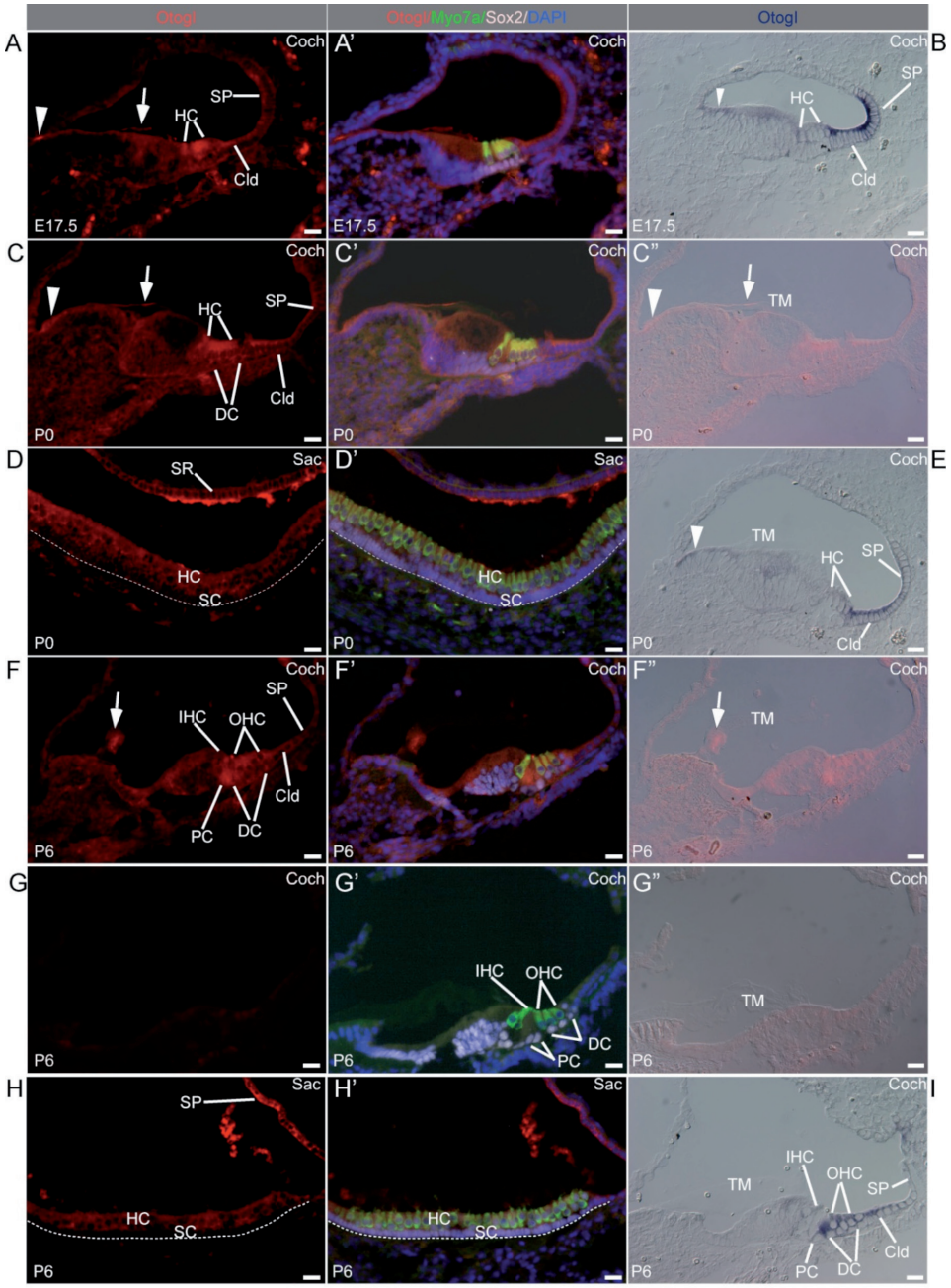
Otogl
Otogl/Myo7a/Sox2/DAPI
Otogl
A
A'
B
C
C'
C"
D
D'
E
F
F'
F"
G
G'
G"
H
H'
I
Coch
Sac
SP
HC
Cld
DC
SR
SC
IHC
OHC
PC
TM
E17.5
P0
P6
J
P6
P13
1 M
Cor
Hip
Otogl
Gapdh

Figure 3. *Otogl* Expression and Distribution in the Mouse Inner Ear

A-A') In E17.5 cochlea, OTOGL was detected by immunohistochemistry on the lumen surface of interdental cells close to the Reissner's membrane (arrowhead), the base of tectorial membrane (arrow), hair cells (HC), Claudius cells (Cld) and spiral prominence (SP). Figures in the middle column (A'-G') are merged images that include the 1st column; B) By *in situ* hybridization, *Otogl* mRNA was detected in the same cell types as shown by immunostaining, with the difference that immunolabeling also detected staining on the surface (A, arrowhead and arrow). Scale bars represent 20 μm; C) in P0 cochlea, a similar OTOGL distribution pattern was detected by immunostaining, with clear presence in the Deiters cells (DC). The figure on the 3rd column (C'') is a merged picture from Otogl labeling with a DIC image, to show the tectorial membrane (TM); D) In P0 saccule, OTOGL was weakly detected in hair cells, but prominently detected in the saccular roof (SR). The strong labeling on the surface of the SR was likely the otolithic membrane. The dashed line represents the base of the basilar membrane; E) *In situ* hybridization showed *Otogl* expression in the cochlea that was consistent with immunolabeling results; F) In P6 cochlea, OTOGL distribution was restricted to outer hair cells (OHC), Pillar cells (PC), Deiters cells (DC), and Claudius cells (Cld). In the tectorial membrane, it was limited to the base (arrow); G) Preadsorption with a synthetic OTOGL antigen eliminated the signals reveled by the OTOGL antibody including TM staining; H) In the P6 saccule, OTOGL distribution was similar to that at P0, however with a higher level in the saccular roof; I) the level of *Otogl* mRNA was enhanced in the OHC, Deiters, and Pillar cells; J) Semi-quantitative RT-PCR of whole cochlea showed that *Otogl* transcripts were most abundant at P13, and decreased in towards young adulthood. Otogl was also detected in the Cortex (Cor) but not in the Hippocampus (Hip). *Gapdh* transcript levels were used as a control.

Furthermore, we analyzed the transcription of *otogl* by in situ hybridization in the mouse and zebrafish, and by semi-quantitative RT-PCR in the mouse. Overall *OTOGL* showed a dynamic expression pattern throughout development, and immunostaining and in situ results were consistent with each other. At E17.5, *OTOGL* was primarily detected in the spiral prominence and the Claudius cells, weakly in hair cells (Figure 3A,B). It was detected in the lumen surface of interdental cells in the proximity of Reissner's membrane (Figure3A, arrowhead) and in the base of nascent tectorial membrane (Figure 3A, arrow). A similar *OTOGL* distribution was detected in P0 cochlea (Figure 3C,D), with additional detection in some supporting cells. In saccule, *OTOGL* was detected weakly in hair cells and more prominently in the saccular roof (Figure 3E). By P6, *OTOGL* distribution became more restricted. It was detected mainly in the outer hair cells, Deiters cells and Claudius cells (Figure 3F). In the tectorial membrane, it was localized to the base (Figure 3F, arrow). In the saccule, elevated level was detected in the saccule roof with little change in the hair cells (Figure 3H). To

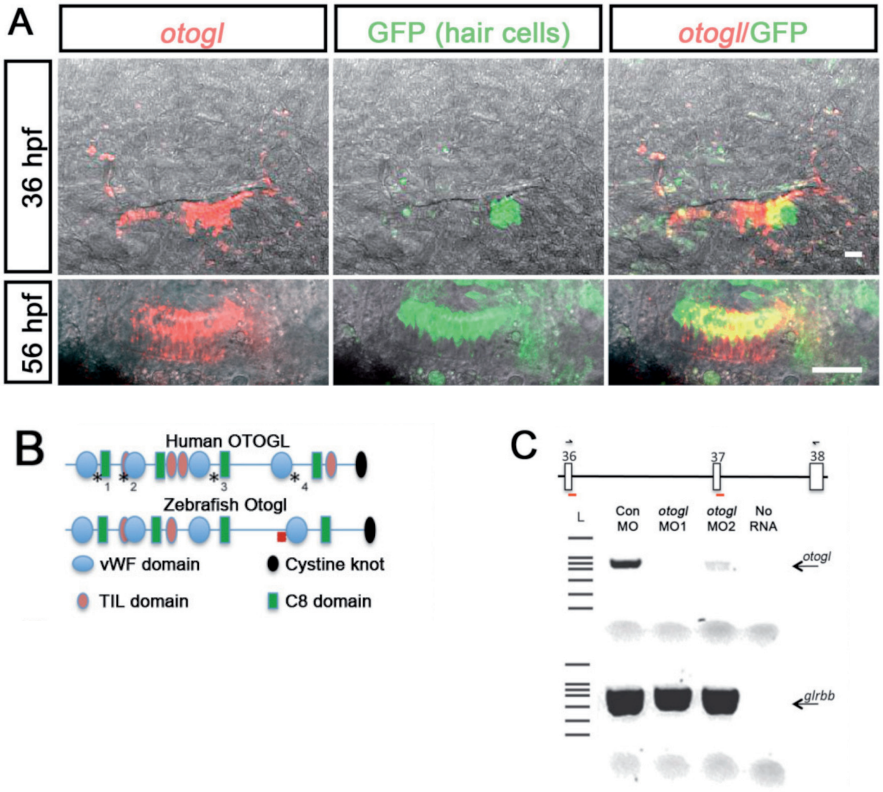

Figure 4. *otogl* Expression and Loss of Function Analysis in Zebrafish

A) Expression of *otogl* (red, *in situ* hybridization) in ear epithelial cells and its relation to hair cell development (green, GPF immunostaining). Sagittal confocal images of developing otocysts showing, at 36 hours post fertilization (hpf), initial *otogl* expression in the forming macula communis and, at 56 hpf, in the macula of the utricle. Throughout larval stages, most hair cells in all maculae express *otogl*, but some *otogl*-negative hair cells can also be seen (not shown). Many basal ear epithelial cells directly below hair cells also express *otogl*. Scale bars 25 µm, embryos mounted anterior to the left; B) Diagrams comparing the structural organization of human OTOGL and zebrafish Otogl four vWF/C8 domains (von Willebrand Factor (blue ovals)/cysteine rich (green rectangles) domains), four Trypsin Inhibitor Like domains (TIL domains, pink ovals) and one C-terminal cystine knot domain (black oval). These diagrams are adapted from the output of SMART. The location of human mutations (1.p.Arg183*; 2.p.Val477Glufs*25; 3.p.Cys1378Arg; 4.c.5238+5G>A) are indicated by asterisks and the location of the zebrafish mis-splicing site targeted by the morpholinos is indicated by a red box; C) Diagram of zebrafish *otogl* exons 36, 37, and 38 showing the targeting site of MO1 at exon/intron junction 36 and the targeting site of MO2 at intron/exon-junction 37 (red bars). Position of diagnostic PCR primers is indicated in exons 36 and 37 (back arrows). Below the diagram, a DNA gel

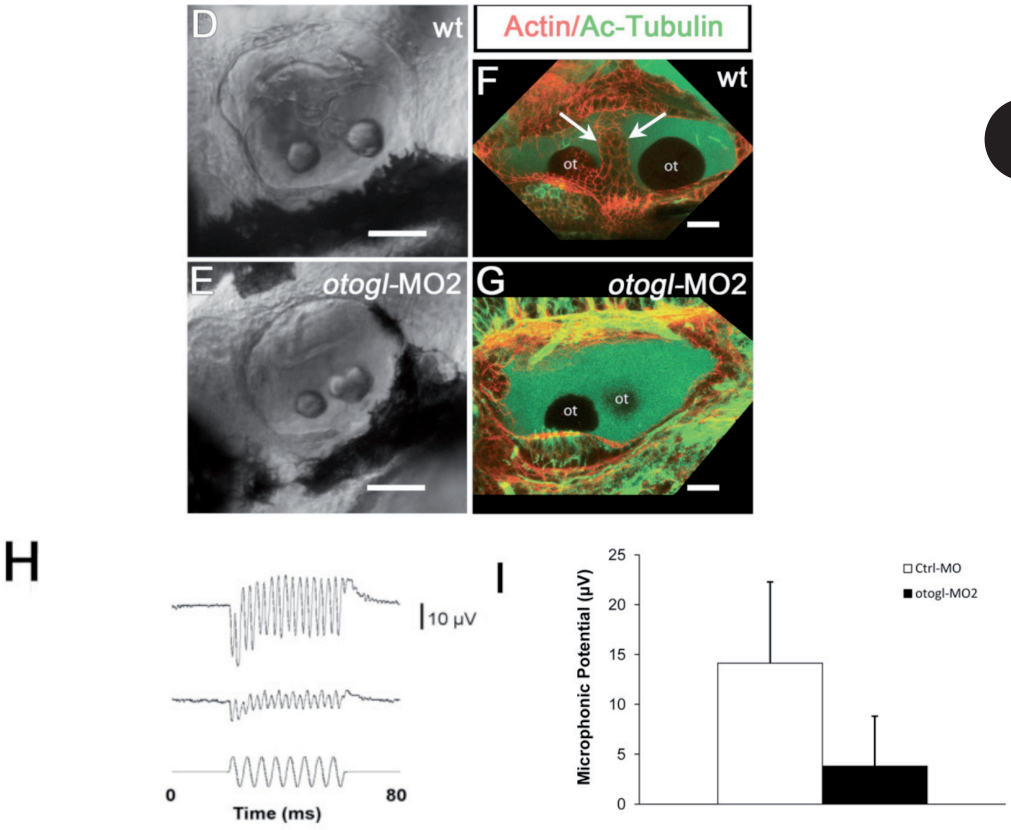

demonstrates efficacy and specificity of *otogl* morpholinos. The gel shows RT-PCR products generated from 500 ng RNA harvested from 56 hpf embryos injected at the one-cell stage either with control morpholino (Con MO), *otogl*MO1, or *otogl*MO2. Two primer sets amplify either *otogl* (top row) or *glrbb* (bottom row; internal control) from cDNA synthesized using anchored oligodT primers. L indicates the DNA ladder. A sample without RNA was used as a negative control (no RNA). The faint bands at the bottom of the gel are unincorporated primers; D-E) Loss of *otogl* function by *otogl*MO2 causes inner ear and saccular otolith malformations (E, n=3) compared to stage matched, 56 hpf, wild type embryos (D, n=5). Bar is 50 µm. Embryos mounted anterior to the left; F-G) Confocal microscope images of 56 hpf control (F, n=5) and *otogl*MO2 (G, n=3) embryos show that inner ear malformations are due to defects in the development of the tissue pillars that form the semicircular canals (arrows in F). Bars are 20 µm. Embryos were mounted anterior to the left; H) Microphonic responses from the inner ear of control (top trace) and *otogl*MO2 morphants (middle trace) at 56 hpf. The bottom trace is the stimulus waveform at 200 Hz and ± 3 µm displacement. I) Histograms showing the means ± SD of microphonic responses that were averaged 200 times for control morphants and *otogl*MO2 morphants.

study the specificity of the antibody staining, we performed preadsorption with a synthesized peptide containing the *OTOGL* antigen as control. Preadsorption abolished the signals revealed by the *OTOGL* antibody but did not affect Myo7a (Figure 3G), demonstrating the specificity of the *OTOGL* antibody.

By semi-quantitative RT-PCR, *Otogl* was upregulated up to P13 in the cochlea, and downregulated in the adult. In addition to the inner ear, *Otogl* transcript was detected weakly in the cortex, but not in the hippocampus (Figure 3J).

In the rat, *OTOGL* continued to be present in various inner ear cells, particularly in Hensen's cells in the postnatal period and was present in the acellular membranes and basilar membrane (Supplemental Figures S2 and S3).

In zebrafish, *otogl* transcription during the first 5 days of larval development was confined to the otic vesicle (Figure 4A, data not shown). Using fluorescent *in situ* hybridization, we first detected *otogl* transcripts at 36 hours post fertilization in the developing macula communis (Figure 4A)[22]. At later developmental stages *otogl* expression was also detected in the other maculae (Figure 4A and not shown). Within the maculae, two different apical epithelial cell populations were found to express *otogl*, hair and non-hair cells (Figure 4A and data not shown). In older larvae, *otogl* transcription was also seen in many basal epithelial cells directly below hair cells (Figure 4A). Thus, different populations of basal and apical cells associated with the maculae express *otogl*.

Knocking-down *otogl* in Zebrafish Causes Sensorineural Hearing Loss and Anatomical Changes in the Inner Ear

To determine the function of *otogl*, we knocked down the expression of the highly conserved *Otogl* protein (XP_683212; 73.1% identity over a stretch of 746 amino acids) in zebrafish by injecting splice-junction blocking morpholinos (MOs) into fertilized eggs. Both human and predicted zebrafish *Otogl* are large proteins, 2343 and 2454 aa respectively, consisting of 4 repeats of paired vWF /C8 (von Willebrand Factor /cysteine rich) domains with a C-terminal cystine knot domain (Figure 5B). Other proteins with this domain structure are mucin and otogelin[26]. We designed two splice-junction blocking morpholinos against exon/inton 36 and 37 of the zebrafish gene that result in protein truncations (Figure 4B, C). Both *otogl*MO1 and MO2 morphants significantly knocked down the expression of *otogl* at day 2 (Figure 4C). *Otogl*MO2 morphants were used for inner ear morphological analysis and physiological recordings because MO1 caused severe cardiac edema. MO2 morphant phenotypes were characterized by mild cardiac edema, slight reduction in larvae length (t-test, $P = 0.007$), failure to escape in response to vibration stimuli, a smaller inner ear ($P = 0.002$) and

smaller saccular otolith (P = 0.001) (Figure 5D, E). There was no significant difference in size of utricular otolith between the control and morphants (P = 0.41). Furthermore, loss of *otogl* function also caused defects in the development of the tissue pillars that shape the semicircular canals (Figure 4F,G). It is unclear if these misshapen semicircular canals impacted vestibular function, as the severe cardiac edema precluded the analysis of circling behaviors at day 5 post fertilization that are characteristic of vestibular deficits[27]. Microphonic potentials were recorded from controls and *otogl*MO2 morphants in response to oscillatory stimulation at 200 Hz and ± 3 μm in displacement. The microphonic waveforms recorded had a characteristic feature of doubling of the stimulus frequency (Figure 5H). The average amplitude of microphonic responses that were measured at 400 Hz in FFT plots ranged from 14 ± 8 μV (N = 11) for control morphlino-injected larvae and 4 ± 5 μV (N = 12) for *otogl* morphants (Figure 4I). Microphonic responses of *otogl* morphants are significantly smaller than those of controls (P = 0.0008).

DISCUSSION

We present mutations in *OTOGL* as a cause of non-syndromic deafness at the DFNB84 locus where mutations in *PTPRQ* were previously discovered[7,21]. We focused on this genomic region since statistically significant linkage was obtained in a genome scan and we found a truncating mutation in *OTOGL* via whole exome sequencing. A second multiplex family was independently identified with two compound heterozygous mutations, which provided further genetic support for the causative role of *OTOGL* mutations in hearing loss. We subsequently showed that *OTOGL* is preferentially expressed in the inner ear in various species and that knocking-down *otogl* leads to sensorineural hearing loss in zebrafish. We thus present mutations in *OTOGL* as a cause of hereditary deafness. The clinical phenotype is quite similar in the two families with *OTOGL* mutations and is characterized by a stable, moderate sensorineural hearing loss. One affected person tested demonstrated vestibular abnormalities, indicating that mutations in *OTOGL* may cause vestibular dysfunction.

Sensory epithelia of the vertebrate inner ear consist of highly organized arrays of sensory hair cells and supporting cells. The acellular membranes of the inner ear form intimate contact with the stereocilia bundles of the hair cells. Each neuroepithelium of the inner ear is covered by an acellular gelatinous membrane: a voluminous gelatinous substance forming a dome-shaped cupula

sits on top of each crista in the ampullae of the semicircular canals. In the utricle and saccule, an otoconial membrane loaded with crystal-like structures, the otoconia, covers the surface of the macula. In the cochlea, a tectorial membrane overlies the auditory epithelia[28]. These extracellular matrices generally serve to either transmit the primary stimulus to the stereocilia bundle, or act as structures against which the stereocilia bundles can react. They also serve to load the bundles and change their resonance frequency[29]. Acellular membranes of the inner ear contain various collagens and noncollagenous proteins that include α-tectorin (TECTA), β-tectorin (TECTB) and otogelin (OTOG)[28]. In this study we show that otogelin-like is an additional component of the inner ear acellular membranes that plays important functional roles in hearing.

In the mammalian inner ear, the cupula, the otoconial membrane, and the tectorial membrane exhibit a progressive increase in molecular and structural complexity, with the cupula appearing the least complex and the tectorial membrane the most complex[28]. This increase of complexity may reflect changes that occurred in the acellular membranes of the inner ear as a mammalian hearing organ arose during evolution from a simple equilibrium receptor[28]. Otogelin was shown to be present in all three membranes suggesting a fundamental and ancient role for this protein[28]. Our study shows that the expression pattern of otogelin-like is similar to that of otogelin by its presence in all three acellular membranes of the inner ear and in all four species analyzed; zebrafish, mouse, rat, and human.

Our data show that *Otogl* is mainly expressed in Claudius cells, Hensen's cells and outer hair cells with a transcription level that is high in embryonic, lower in neonatal and much lower in adult stages. The protein product, however, is also prominently present in the acellular structures. High levels of transcription of *Otogl* in early and downregulation of the gene in later development strongly suggests that otogelin-like, similarly to other acellular structure components such as otogelin, is normally involved in the production of the structure, which may require relatively low of gene activity for the maintenance on the continuous basis[30].

Although a human phenotype of OTOG mutations has not been reported yet, targeted disruption of Otog resulted in deafness and severe imbalance in mice[31]. Histological analysis of these mutants demonstrated that in the vestibule, otogelin was required for the anchoring of the otoconial membranes and cupulae to the neuroepithelia. In the cochlea, ultrastructural analysis of the tectorial membrane indicated that otogelin was involved in the organization of its fibrillar network. Thus, otogelin is likely to have a role in the resistance of this membrane to

sound stimulation[31]. Because of structural and expressional similarities, it is possible that otogelin-like plays a similar role in the inner ear. The clinical phenotype in humans with a stable hearing loss and vestibular findings further supports this possibility. On the other hand, the functions of otogelin-like and otogelin are highly likely to be at least partially non-compensatory, as mutations in each of the corresponding genes can cause hearing loss.

Acknowledgements

We want to acknowledge the families for their participation in the study. This work was supported by National Institutes of Health grants R01DC009645 to M.T. , R01 DC006908 to Z.Y.C, R21 DC009879 to Z. L., RO1DC05575 to X.L., the Fredrick and Ines Yeatts Inner Ear Hair Cell Regeneration Fellowship to M.H and N.L., the Heinsius Houbolt Foundation to H.K., the Oticon Foundation (09-3742) to H.K., ZonMW (40-00812-98-09047 to H.K. and 90700388 to R.P.) and the RNID (GR36) to H.K.. N.L. was supported by a grant from the China Scholarship Council, P.R. China. Z.L. was supported by the University of Miami Provost Research Award and College of Arts and Sciences Gabelli Fellowship. We are grateful to Atlas Antibodies for providing the *OTOGL* immunogenic peptide.

WEB RESOURCES

Ensembl: http://www.ensembl.org
Exome Variant Server, NHLBI Exome Sequencing Project (ESP): http://evs.gs.washington.edu/EVS/
ExonPrimer: http://ihg2.helmholtz-muenchen.de/ihg/ExonPrimer.html
Hereditary hearing loss homepage: http://hereditaryhearingloss.org/
Online Mendelian Inheritance in Man: http://www.omim.org
Polyphen-2: http://genetics.bwh.harvard.edu/pph2/
Primer3plus: http://www.bioinformatics.nl/cgi-bin/primer3plus/primer3plus.cgi
SIFT: http://sift.jcvi.org/
SignalP: http://www.cbs.dtu.dk/services/SignalP-4.0/
Simple Modular Architectural Research Tool (SMART): http://smart.embl-heidelberg.de/.
The 1000 genomes project: http://www.1000genomes.org/
The SeattleSeq annotation: http://snp.gs.washington.edu/SeattleSeqAnnotation
Zebrafish VEGA genome browser: http://vega.sanger.ac.uk/Danio_rerio/Info/Index

REFERENCES

1. Lenz, D.R., Avraham, K.B. (2011). Hereditary hearing loss: from human mutation to mechanism. Hear. Res. 281, 3-10.
2. Morton, C.C., Nance, W.E. (2006). Newborn hearing screening--a silent revolution. N. Engl. J. Med. 354, 2151-2164.
3. Duman, D., Sirmaci, A., Cengiz, F.B., Ozdag, H., Tekin, M. (2011). Screening of 38 genes identifies mutations in 62% of families with nonsyndromic deafness in Turkey. Genet. Test. Mol. Biomarkers 15, 29-33.
4. Francey, L.J., Conlin, L.K., Kadesch, H.E., Clark, D., Berrodin, D., Sun, Y., Glessner, J., Hakonarson, H., Jalas, C., Landau, C., et al. (2012). Genome-wide SNP genotyping identifies the Stereocilin (STRC) gene as a major contributor to pediatric bilateral sensorineural hearing impairment. Am. J. Med. Genet. 158A, 298-308.
5. Marlin, S., Feldmann, D., Blons, H., Loundon, N., Rouillon, I., Albert, S., Chauvin, P., Garabédian, E.N., Couderc, R., Odent, S., et al. (2005). GJB2 and GJB6 mutations: genotypic and phenotypic correlations in a large cohort of hearing-impaired patients. Arch. Otolaryngol. Head Neck Surg. 131, 481-487.
6. Sirmaci, A., Erbek, S., Price, J., Huang, M., Duman, D., Cengiz, F.B., Bademci, G., Tokgoz-Yilmaz, S., Hismi, B., Ozdag, H. et al. (2010). A truncating mutation in SERPINB6 is associated with autosomal-recessive nonsyndromic sensorineural hearing loss. Am. J. Hum. Genet. 86, 797-804.
7. Schraders, M., Oostrik, J., Huygen, P.L., Strom, T.M., van Wijk, E., Kunst, H.P., Hoefsloot, L.H., Cremers, C.W., Admiraal, R.J., Kremer, H. (2010). Mutations in PTPRQ are a cause of autosomal-recessive nonsyndromic hearing impairment DFNB84 and associated with vestibular dysfunction. Am. J. Hum. Genet. 86, 604-610.
8. Kruglyak, L., Daly, M.J., Reeve-Daly, M.P., Lander, E.S. (1996). Parametric and nonparametric linkage analysis: a unified multipoint approach. Am. J. Hum. Genet. 58, 1347-1363.
9. Li, H., Durbin, R. (2009). Fast and accurate short read alignment with Burrows-Wheeler transform. Bioinformatics 25, 1754-1760.
10. McKenna, A., Hanna, M., Banks, E., Sivachenko, A., Cibulskis, K., Kernytsky, A., Garimella, K., Altshuler, D., Gabriel, S., Daly, M. et al. (2010). The Genome Analysis Toolkit: a MapReduce framework for analyzing next-generation DNA sequencing data. Genome Res. 20, 1297-1303.
11. Bohr, H., Bohr, J., Brunak, S., Cotterill, R.M., Lautrup, B., Norskov, L., Olsen, O.H., Petersen, S.B. (1988). Protein secondary structure and homology by neural networks. The alpha-helices in rhodopsin. FEBS Lett. 241, 223-228.
12. Reese, M.G., Eeckman, F.H., Kulp, D., Haussler, D. (1997). Improved splice site detection in Genie. J. Comput. Biol. 4, 311-323.

13. Gamundi, M.J., Hernan, I., Muntanyola, M., Maseras, M., López-Romero, P., Alvarez, R., Dopazo, A., Borrego, S., Carballo, M. (2008). Transcriptional expression of cis-acting and trans-acting splicing mutations cause autosomal dominant retinitis pigmentosa. Hum. Mutat. 29, 869-878.
14. de Heer, A.R., Collin, R.W.J., Huygen, P.L.M., Schraders, M., Oostrik, J., Rouwette, M., Kunst, H.P.M., Cremers, C.W.R.J. (2011). Progressive Sensorineural Hearing Loss and Normal Vestibular Function in a Dutch DFNB7/11 Family with a Novel Mutation in TMC1. Audiol. Neurotol. 16, 93–105.
15. Luijendijk, M.W., van de Pol, T.J., van Duijnhoven, G., den Hollander, A.I., ten Caat, J., van Limpt, V., Brunner, H.G., Kremer, H., Cremers, F.P. (2003). Cloning, characterization, and mRNA expression analysis of novel human fetal cochlear cDNAs. Genomics 82, 480-490.
16. Livak, K.J., Schmittgen, T.D. (2001). Analysis of relative gene expression data using real-time quantitative PCR and the 2(-Delta Delta C(T)) Method. Methods 25, 402-408.
17. Stapelbroek, J.M., Peters, T.A., van Beurden, D.H., Curfs, J.H., Joosten, A., Beynon, A.J., van Leeuwen, B.M., van der Velden, L.M., Bull, L., Oude Elferink, R.P., et al. (2009). ATP8B1 is essential for maintaining normal hearing. Proc. Natl. Acad. Sci. U S A. 106, 9709-9714.
18. Huang, M., Sage, C., Li, H., Xiang, M., Heller, S., Chen, Z.Y. (2008). Diverse expression patterns of LIM-homeodomain transcription factors (LIM-HDs) in mammalian inner ear development. Dev. Dyn. 237, 3305-3312.
19. Westerfield, M. (2000). The Zebrafish Book. A Guide for the Laboratory use of Zebrafish (Danio Rerio). (Eugene, OR: Univ. of Oregon Press).
20. Go, W., Bessarab, D., Korzh, V. (2010). atp2b1a regulates Ca(2+) export during differentiation and regeneration of mechanosensory hair cells in zebrafish. Cell Calcium 48, 302-313.
21. Shahin, H., Rahil, M., Abu Rayan, A., Avraham, K.B., King, M.C., Kanaan, M., Walsh, T. (2010). Nonsense mutation of the stereociliar membrane protein gene PTPRQ in human hearing loss DFNB84. J. Med. Genet. 47, 643-645.
22. Haddon, C., Lewis, J. (1996). Early ear development in the embryo of the zebrafish, Danio rerio. J. Comp. Neurol. 365, 113-128.
23. Skromne, I., Thorsen, D., Hale, M., Prince, V.E., Ho, R.K. (2007). Repression of the hindbrain developmental program by Cdx factors is required for the specification of the vertebrate spinal cord. Development 134, 2147-2158.
24. Starr, C.J., Kappler, J.A., Chan, D.K., Kollmar, R., Hudspeth, A.J. (2004). Mutation of the zebrafish choroideremia gene encoding Rab escort protein 1 devastates hair cells. Proc. Natl. Acad. Sci. U. S. A. 101, 2572-2577.
25. Corey, D.P., Garcia-Anoveros, J., Holt, J.R., Kwan, K.Y., Lin, S.Y., Vollrath, M.A., Amalfitano, A., Cheung, E.L., Derfler, B.H., Duggan, A. et al. (2004). TRPA1 is a candidate for the mechanosensitive transduction channel of vertebrate hair cells. Nature 432, 723-730.

26. Cohen-Salmon, M., El-Amraoui, A., Leibovici, M., Petit, C. (1997). Otogelin: a glycoprotein specific to the acellular membranes of the inner ear. Proc. Natl. Acad. Sci. U. S. A. 94, 14450-14455.
27. Moorman, S.J., Cordova, R., Davies, S. A. (2002) A critical period for functional vestibular development in zebrafish. Dev. Dyn. 223:285-291.
28. Goodyear, R.J., Richardson, G.P. (2002). Extracellular matrices associated with the apical surfaces of sensory epithelia in the inner ear: molecular and structural diversity. J. Neurobiol. 53, 212-227.
29. Manley, G.A. (2000). Cochlear mechanisms from a phylogenetic viewpoint. Proc. Natl. Acad. Sci. U. S. A. 97, 11736-11743.
30. El-Amraoui, A., Cohen-Salmon, M., Petit, C., Simmler, M.C. (2001). Spatiotemporal expression of otogelin in the developing and adult mouse inner ear. Hear. Res. 158, 151-159.
31. Simmler, M.C., Cohen-Salmon, M., El-Amraoui, A., Guillaud, L., Benichou, J.C., Petit, C., Panthier, J.J. (2000). Targeted disruption of otog results in deafness and severe imbalance. Nat. Genet. 24, 139-143.

SUPPLEMENTAL FIGURES AND TABLES

A

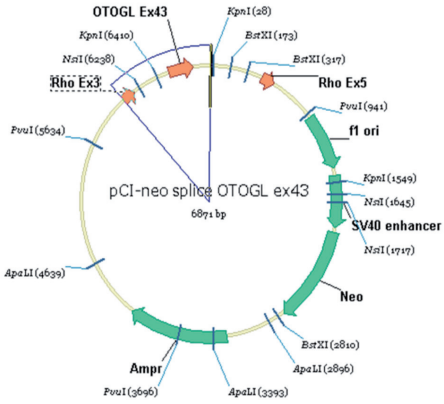

B

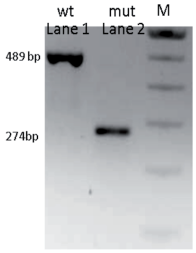

C

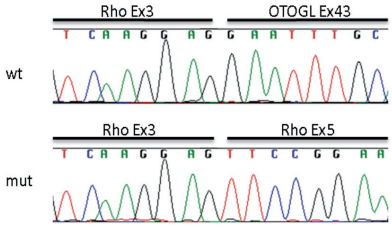

Supplemental Figure S1. Results of minigene assay for the c.5238+5G>A mutation

(**A**) Representation of the plasmid used in the minigene assay; (**B**) Lane 1, RT-PCR after transfection with wild type plasmid showing a fragment of 489 bp; lane 2, RT-PCR after transfection with mutant plasmid revealing a fragment of 274 bp; M, 100 bp ladder; (**C**) Electropherograms of wild type and mutant cDNA showing the skipping of *OTOGL* exon 43.

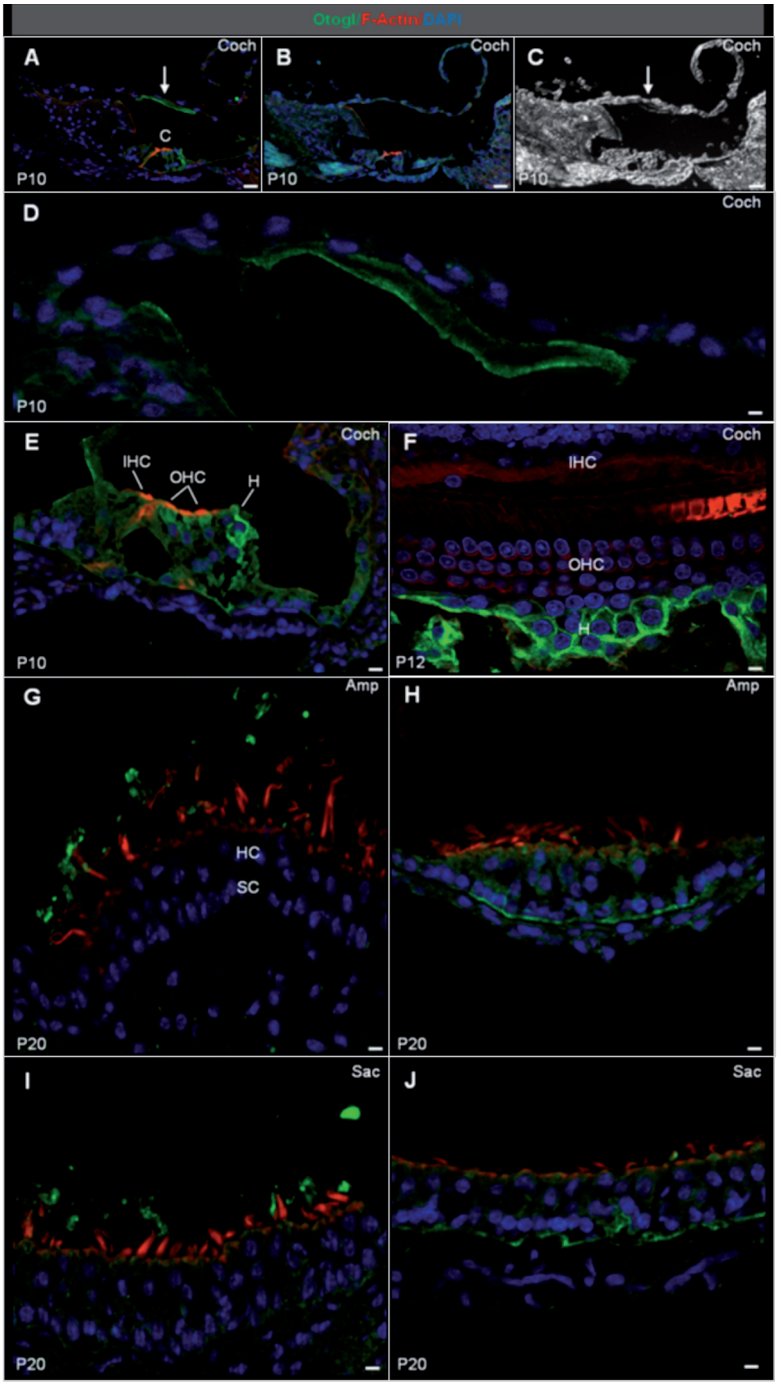
Otogl/F-Actin/DAPI
A
Coch
C
P10
B
Coch
P10
C
Coch
P10
D
Coch
P10
E
Coch
IHC
OHC
H
P10
F
Coch
IHC
OHC
H
P12
G
Amp
HC
SC
P20
H
Amp
P20
I
Sac
P20
J
Sac
P20

Supplemental Figure S2. Immunohistochemical Localization of OTOGL in the Inner Ear of the Rat

(A) In P10 rat cochlea, OTOGL distribution was restricted to the tectorial membrane (arrow) and the organ of Corti **(C); B)** In the control with omission of the first antibody, no staining was observed in these structures; **(C)** The differential interference contrast image is included to show the position of the tectorial membrane (arrow) in the negative control **(B); (D)** A higher magnification of the tectorial membrane demonstrated staining predominantly at the margin and **(E)** a higher magnification of the organ of Corti shows immunostaining in the apical part of the outer hair cells (OHC) and very pronounced in Hensen's cells **(H); (F)** A whole mount staining of a P12 organ of Corti demonstrated the distribution of OTOGL near the lateral cell membrane and/or between Hensen's cells **(H); (G)** In the P20 rat vestibulum, Otogl was observed in the cupula of the cristae, **(I)** the gelatinous layer of the maculae **(H, J)** and in the basilar membrane of these sensory patches. Amp = ampulla; Coch = cochlea; IHC = Inner Hair Cell; HC = Hair Cell; Sac = Saccule; SC = Supporting Cell. Scale bars represent 30 µm in A-C, 3 µm in D, 11 µm in E, 8 µm in F, and 5 µm in G-J.

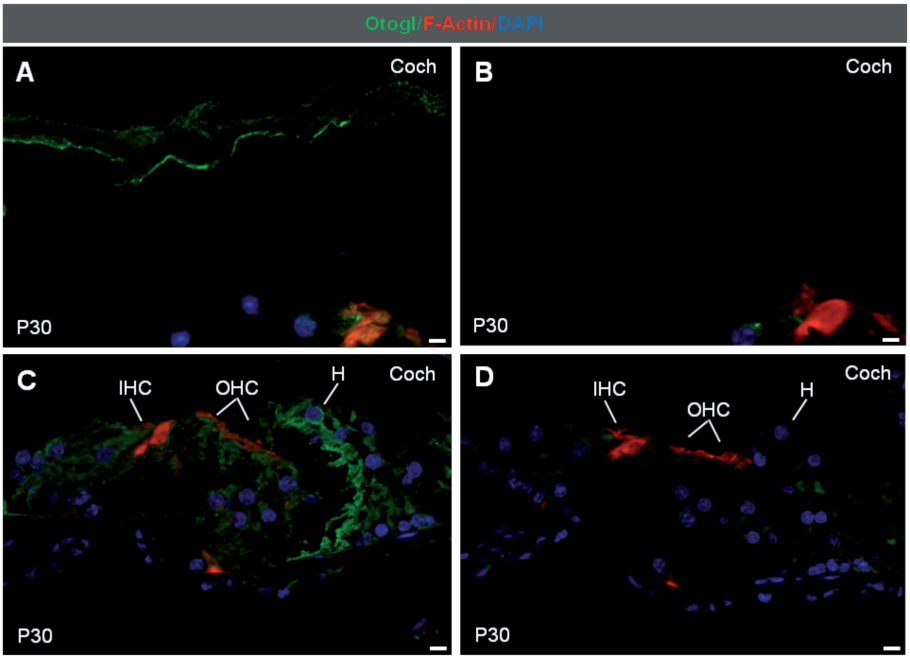

Supplemental Figure S3. Immunostaining of OTOGL in the Adult Rat

In P30 rat cochlea, immunostaining was detected in **(A)** the tectorial membrane and **(C)** Hensen's cells **(H)** of the organ of Corti. In the absence of the OTOGL antibody **(B, D)**, no staining was observed in these structures. Note the absence of staining in the outer hair cells (OHC) at this age **(C)**. IHC = Inner Hear Cell. Scale bars = 5 µm in A, B and 11 µm in C, D.

Supplemental Table S1. PCR primers for OTOGL

PCR Amplicon	Oligonucleotides (5` to 3`)		Size (bp)	Annealing Temp. (°C)	PCR Amplicon	Alternative Oligonucleotides (5` to 3`)		Size (bp)	Annealing Temp. (°C)
exon 1	Forward	tgggtgtaactaatacgggc	799	57	exon 1	Forward	caatttggttacatttcagggg	211	touchdown
	Reverse	ggttgatggcatgaagaaag				Reverse	ttcaaagtgctttataagggaaaac		
exon 2	Forward	gaaatttgctggtcaaatcc	281	55	exon 2	Forward	ttcttttaaacaactggaacatgtag	177	touchdown
	Reverse	agcagatatagttgcctgctg				Reverse	ggtttgctcattcccattaac		
exon 3	Forward	aaacaccagctctctcttgg	225	57	exon 3	Forward	cttgggaaaggcttgttcag	187	touchdown
	Reverse	cctccacaaaggtctcattg				Reverse	aagtgacagcagagtccaaaac		
exon 4	Forward	ccaatttgcatgtttggc	255	57	exon 4	Forward	caatttgcatgtttggcttg	189	touchdown
	Reverse	taccatcctggctcactttc				Reverse	ccccaaagggattttctgag		
exon 5	Forward	agtgattacaatttgtccaagc	290	57	exon 5	Forward	tgcttaaaagaacaaatggatg	215	touchdown
	Reverse	acaactcccaatggatgaac				Reverse	atgccttaatttttctccttgg		
exon 6	Forward	agaatcatttaccatgactgactg	377	57	exon 6	Forward	cctgtgttatagaccaaggaagg	422	touchdown
	Reverse	actgaacccagaccctcttc				Reverse	tcgtaactgaacccagaccc		
exon 7	Forward	aacgttgtaaagtgtcatggg	327	57	exon 7	Forward	aacgttgtaaagtgtcatggg	314	touchdown
	Reverse	ctccacagttcacttccagc				Reverse	ttccagcatgtgatgtttgg		
exon 8	Forward	ctcttgctgcacagcttattc	417	57	exon 8	Forward	tttggagctcttgctgcac	416	touchdown
	Reverse	ttctgggtacaaacaacttgg				Reverse	acaaacaacttggtcagggg		
exon 9	Forward	tgaccaggaagtttgtgttg	360	58 (AmpliTaQ 360 mix)	exon 9	Forward	ccatgtctgtttgtggaaaatg	338	touchdown
	Reverse	attgcaattacatttcctgg				Reverse	cctattgcaattacatttcctgg		
exon 10	Forward	tgtaattgcaataggaaatcacc	428	57	exon 10	Forward	gagaactgaaaatcttgcaaataga	301	touchdown
	Reverse	cagctgaaatggttaagtaacag				Reverse	tgtgaacagctgaaatggttaag		
exon 11	Forward	catcatgcactcagcatttc	318	57	exon 11	Forward	tgcactcagcatttctaggg	341	touchdown
	Reverse	tcaataacaaatccttgcaattc				Reverse	tcaaaaagtatgcaagttcatgg		
exon 12	Forward	ttgcaaggatttgttattgag	471	57	exon 12	Forward	ccatgaacttgcatacttttga	378	touchdown
	Reverse	tagccattcctccttgtcac				Reverse	ctgggaaaggacagcaaaac		
exon 13	Forward	tgcctgagagtcaggttgtc	390	57	exon 13	Forward	tgcctgagagtcaggttgtc	393	touchdown
	Reverse	ttgtgttggaatttgggaag				Reverse	tttgtgttggaatttgggaag		
exon 14	Forward	ttaccagtcaattgaacttatgc	437	57	exon 14	Forward	gccagccagctcaaaattac	447	touchdown
	Reverse	gttgcccactcaatgctatc				Reverse	agatgtcttcataaagatcagtgcta		
exon 15	Forward	aatggtatcatcctcctctctc	438	57	exon 15	Forward	tgcttttaaaggattaacctaatgg	407	touchdown
	Reverse	tcaagatgcgtcatgtaacc				Reverse	tccatattcctctggtcattttg		
exon 16	Forward	catctccaccttcctgtctc	345	57	exon 16	Forward	ccttctccctttctcccatc	304	touchdown
	Reverse	ggcctgatgacacatacaaac				Reverse	aagatcccattttgtttgcg		
exon 17	Forward	ttcagaacaccgtctatgaatg	297	57	exon 17	Forward	ggaagagagtcctggtggtg	328	touchdown
	Reverse	tgaatttatatcctttaaatgaccag				Reverse	tgaatttatatcctttaaatgaccag		
exon 18	Forward	tttcaagctgtaagatttccttg	376	57	exon 18	Forward	tttcaagctgtaagatttccttg	371	touchdown
	Reverse	aggaatggcattgattttacc				Reverse	gcattgattttaccataatggag		

exon 19	Forward	tgtggattaagtgctgttacc	585	57	exon 19	Forward	aagctgaaattgttcactcttgt	498	touchdown
	Reverse	ttggtcttatccaacatatctcc				Reverse	tttcatttgcttttcatgtttg		
exon 20	Forward	ccatggcaatctttctcaag	265	57	exon 20	Forward	cccaattccttgccttgtaa	346	touchdown
	Reverse	gcccgtaaggagaaaaagag				Reverse	gcccgtaaggagaaaaagag		
exon 21	Forward	aatggagagcacaaggtcag	186	57	exon 21	Forward	tgaccaatggagagcacaag	297	touchdown
	Reverse	aaacacaatccccatcattg				Reverse	aaacctgcacgttgtacacata		
exon 22	Forward	cctgaaattggacctaaccc	301	57	exon 22	Forward	gcttgtaaaaacttctgtgggaaa	299	touchdown
	Reverse	ggtgattgatgacttctgcc				Reverse	catgcacattgggaagaaga		
exon 23	Forward	ggaaggcagctaacattctc	388	57	exon 23	Forward	ggaaggcagctaacattctca	392	touchdown
	Reverse	gaacaacaattctggctatttc				Reverse	cagaacaacaattctggctatttc		
exon 24	Forward	aagactggattcatctcctcag	392	57	exon 24	Forward	atgtggaaaaagcgaggaga	390	touchdown
	Reverse	gcaggcctttaaattatttgc				Reverse	ggcttgatttacttttgctga		
exon 25	Forward	aactggcaatattcgtaaggg	351	57	exon 25	Forward	gaactggcaatattcgtaaggg	440	touchdown
	Reverse	gatatatcagggaccagcatac				Reverse	cagaccttcccaagtacccc		
exon 26	Forward	aatggtaaacttggctggaac	481	57	exon 26	Forward	tgcaatccattgtcaatatttaag	331	touchdown
	Reverse	tcatgaccatttacagagaggag				Reverse	gaccatttacagagaggagtagacc		
exon 27	Forward	ggtccatctgctagttcgtg	391	57	exon 27	Forward	aaaaggcatgaccatgcaac	415	touchdown
	Reverse	ctcatttggagcttaggttgac				Reverse	caagggtatgagttagtaattctgg		
exon 28	Forward	aaatgattgctgtgaaaatgc	479	57	exon 28	Forward	aattaaattggtatgagaaaatccac	513	touchdown
	Reverse	actcatttaacctccctgagc				Reverse	ccctgagcctcaatttcttc		
exon 29	Forward	aggcgcaattgtaatgagtg	302	57	exon 29	Forward	ggttactctgtttgagaaattgtcc	256	touchdown
	Reverse	ggatcacccagttacgtgtc				Reverse	tgtcgtgttcacctcagtattatag		
exon 30	Forward	gagaactctctaggtggcagtg	382	57	exon 30	Forward	agagaactctctaggtggcagtg	387	touchdown
	Reverse	tgagtctcctggcattatttc				Reverse	catgagtctcctggcattatttc		
exon 31	Forward	catatcttgcccacattcag	192	57	exon 31	Forward	gccatatcttgcccacattc	192	55 (betaine added)
	Reverse	tttgttcacagcataagttgttc				Reverse	ttcacagcataagttgttcaaaa		
exon 32	Forward	ttgcataacctacaacacgaac	540	57	exon 32	Forward	ttgctcaatttttgaagtattttg	436	touchdown
	Reverse	aaagagaaagctggctgatatg				Reverse	aagctggctgatatgccaat		
exon 33	Forward	tatgtttggcaattgtgcag	421	55	exon 33	Forward	atgtttggcaattgtgcagt	494	touchdown
	Reverse	ttctctttttggagatctcagg				Reverse	tgcttatatgcagtaagaatggtttt		
exon 34	Forward	ttcaagctatgtattaaatatgcacac	220	57	exon 34	Forward	cctgagtgacagagcgagac	243	touchdown
	Reverse	cagaatttgctaaggctggac				Reverse	cctgccacatagtaggctctc		
exon	Forward	gcttgacaagggtatatagaagc	705	57	exon 35	Forward	aacgaagtagcagatggagca	344	touchdown
35-36	Reverse	ctgggtttcctagcccatag				Reverse	gagttgattgtctgtttaaaacttctg		
exon 37	Forward	tgcattccactaatgaggattac	235	57	exon 36	Forward	ttcccaaaacattttccttga	295	touchdown
	Reverse	agcaaggctagactagagaacatatc				Reverse	gggtttcctagcccataggt		
exon	Forward	catgggcaatatgaatgtgg	758	57	exon 37	Forward	catcacaggattctaggaaggaa	288	touchdown
38-39	Reverse	gtgagaatccctgatgttgc				Reverse	gcatttggatattgacacagaaa		

exon	Forward	gggagctcaagaactcactg	585	57		exon 38	Forward	catgggcaatatgaatgtgg	362	touchdown
40-41	Reverse	ctgcagttaacctcacaggg					Reverse	aacttggctgatgaggtg		
exon 42	Forward	gaagctgtggcagcagtaag	414	57		exon	Forward	tgatttatgatttggctcacag	670	touchdown
	Reverse	aaatggcatagcgtgaatag				39-40	Reverse	agatttcctcagaggggagcc		
exon 43	Forward	ctggttaaggcagttagttc	606	57		exon 41	Forward	tttctgaaaaccttttatcaatc	400	touchdown
	Reverse	tccttcttgtgttgtaagcc					Reverse	aattttccctctattggaaataact		
exon 44	Forward	cttgctacccttttgattctcc	373	57		exon 42	Forward	aggcacagcaaaggaacaat	481	touchdown
	Reverse	tttgtcatagcttctctgtgc					Reverse	tgaaaaatgggggcaacagg		
exon 45	Forward	gccttgtttctgatttatgg	475	57		exon 43	Forward	tttcaatgtaaagttcaaggatacа	486	touchdown
	Reverse	catttccttccaacagagg					Reverse	gacagaaggttgggggtttt		
exon 46	Forward	tttagtgcccaggttttgag	396	57		exon 44	Forward	gatttgtgtagattagtgcagatgg	482	touchdown
		acaaaacttgctttgagaaaatg					Reverse	gcttcttctgtgcatttatgct		
exon	Forward	ccgtctttgagtttcctgtc	706	57		exon 45	Forward	catgatgccttgtttcttga	479	touchdown
47-48	Reverse	cagaatattgcttgccatcag					Reverse	ccttccaacagaggctgtc		
exon 49	Forward	tggccaaataaggaaatatacc	322	57		exon 46	Forward	tggtgatgaaagagaaatctgag	481	touchdown
	Reverse	agccaactaagatgcactgg					Reverse	tgacatttatggccctttttt		
exon	Forward	tgggaaatatgaatccatgc	577	57		exon47	Forward	gatgtatgaatcaagggtgaaagac	469	touchdown
50-51	Reverse	aagattagcagattctatcagcag					Reverse	aaaattagcaagacaagtcngc		
exon 52	Forward	gtctggctgtgtgataaggg	347	57		exon 48	Forward	gcngacttgtctgctaatttt	484	touchdown
	Reverse	ctcaaatactggcaaatggc					Reverse	tgttgatgggggaaggtattta		
exon 53	Forward	catcgcaatgaaaacatagactc	336	57		exon 49	Forward	gtgttctatatgtcactgtgcttgg	449	touchdown
	Reverse	actctgccatttttgaatgc					Reverse	agagtactggtgctaggatagctca		
exon 54	Forward	cagttgtctggaaagagcttg	292	55		exon	Forward	ccaacacatggcaatctgac	658	touchdown
	Reverse	gggggacatttccaaac				50-51	Reverse	caatatttgctcatttaatacagg		
exon 55	Forward	agccttgcatcttgatttg	318	57		exon 52	Forward	ttaaagtgtctggctgtgataag	355	touchdown
	Reverse	agccacaatgaaagtatgacc					Reverse	actcaaatactggcaaatggct		
exon 56	Forward	cctttacactctttccatagtacc	678	57		exon 53	Forward	gctttggaggaagttcaatca	609	touchdown
	Reverse	cttgtttaagttcagcatggttc					Reverse	gttatgcacaggaaagtgaaagtct		
exon 57	Forward	cacacacaggttgatgttagc	607	57		exon 54	Forward	ggaagcttctcatattcaaccttag	392	touchdown
	Reverse	ttgcaaccatcattcagaac					Reverse	aatgtaactgtgtctgtgtgctgt		
exon	Forward	ttgagggttggagtgatgag	619	57		exon 55	Forward	agggtcatttcagatggaac	486	touchdown
58_1	Reverse	aaataaccttccagttgatgag					Reverse	cgattgcacagtatctattcaagac		
Exon	Forward	aggcatgtggcagatttatg	726	55		exon 56	Forward	tggaagtagtttaggttatttcaagg	674	touchdown
58_2	Reverse	ctattggaataacaatgtatg					Reverse	aaatgcaaacacttcttacactc		
exon	Forward	cagaggaagctgtgtgactc	590	57		exon 57	Forward	cattatacatgtgtggaatatttctg	482	touchdown
58_3	Reverse	ataggtggcaaagaatttgg					Reverse	tgttaagcgttggcagtttg		
						exon 58	Forward	cagaagcttgagggttggag	416	touchdown
							Reverse	agcataaatctgccacatgc		

PCR reactions included 10-40 ng of genomic DNA with Taq DNA polymerase (Roche) and AmpliTaq 360 mix for exon 9 (Life Technologies). PCR products were visualized on agarose gels, cleaned over Sephadex columns or with NucleoFast 96 PCR plates (Clontech) in accordance with the manufacturers' protocols. Sequence analysis was performed with the ABI PRISM Big Dye Terminator Cycle Sequencing V3.1 Ready Reaction Kit and the ABI PRISM 3730 DNA Analyzer (Applied Biosystems). Results were visualized using the Sequencher 4.7 program (Gene Codes Corporation).

Supplemental Table S2. Primers for QPCR and Minigene Assay

Primers for qPCR Human			
	Forward Primers (5` to 3`)	**Reverse Primers (5` to 3`)**	**Size (bp)**
OTOGL exon 9-10 (for qPCR HUMAN)	gattttccaaatccgtgctc	ctcatggcagctcagaaaag	99
Primers for Mouse Semiquantitative PCR			
	Forward Primers	**Reverse Primers**	**Size (bp)**
Otogl (for RT-PCR):	ggtgctccatgttgtcagag	atttcccagctgccaataaa	547
Otogl (For *in situ*):	acccctgactattgccctct	cctgtcgaacttgaagcaca	598
GAPDH:	gatgcctgcttcaccaccttcttg	gcagaaggggcggagatgatgac	413
Primers for Minigene Assay			
OTOGL intron 42 – intron 43*	GGGGACAAGTTTGTACAA AAAAGCAGGCTTCttctttctt actgggttaaggc	GGGGACCACTTTGTACAAG AAAGCTGGGTCatactgacagaa ggttgggg	624

*the nucleotides in capitals represent the adaptors for the Gateway cloning.

[1]Department of Otorhinolaryngology, Hearing & Genes, [2]Nijmegen Centre for Molecular Life Sciences, and [3]Donders Institute for Brain, Cognition and Behaviour, Radboud university medical center, Nijmegen, the Netherlands. [4]Servicio de Genética, Hospital Universitario Ramon y Cajal, IRYCIS, Madrid, Spain. [5]Centro de Investigación Biomédica en Red de Enfermedades Raras (CIBERER), Madrid, Spain. [6]Department of Pediatrics, [7]Department of Human Genetics and 8Institute for Genetic and Metabolic Disease, Radboud university medical center, Nijmegen, the Netherlands.

Chapter 3

Progressive hearing loss and vestibular dysfunction caused by a homozygous nonsense mutation in *CLIC5*

Celia Zazo Seco[1,2,3,*], Anne M.M. Oonk[1,3,*], María Domínguez-Ruiz[4,5], Jos M.T. Draaisma[6], Marta Gandía[4,5], Jaap Oostrik[1,2,3], Kornelia Neveling[7,8], Henricus P.M. Kunst[1,3], Lies H. Hoefsloot[7], Ignacio del Castillo[4], Ronald J.E. Pennings[1,3], Hannie Kremer[1,2,3,7], Ronald J.C. Admiraal[1,3], Margit Schraders[1,2,3]

*Authors contributed equally

European journal of human genetics 2015 Feb;23(2):189-94

ABSTRACT

In a consanguineous Turkish family diagnosed with autosomal recessive nonsyndromic hearing impairment (arNSHI), a homozygous region of 47.4 Mb was shared by the two affected siblings on chromosome 6p21.1-q15. This region contains 247 genes including the known deafness gene *MYO6*. No pathogenic variants were found in *MYO6* neither with sequence analysis of the coding region and splice sites nor with mRNA analysis. Subsequent candidate gene evaluation revealed *CLIC5* as an excellent candidate gene. The orthologous mouse gene is mutated in the *jitterbug* mutant that exhibits progressive hearing impairment and vestibular dysfunction. Mutation analysis of *CLIC5* revealed a homozygous nonsense mutation c.96T>A (p.(Cys32Ter)) that segregated with the hearing loss. Further analysis of *CLIC5* in 213 arNSHI patients from mostly Dutch and Spanish origin did not reveal any additional pathogenic variants. *CLIC5* mutations are thus not a common cause of arNSHI in these populations.

The hearing loss in the present family had an onset in early childhood and progressed from mild to severe or even profound before the second decade. Impaired hearing is accompanied by vestibular areflexia and in one of the patients with mild renal dysfunction. Although we demonstrate that *CLIC5* is expressed in many other human tissues no additional symptoms were observed in these patients.

In conclusion, our results show that *CLIC5* is a novel arNSHI gene involved in progressive hearing impairment, vestibular and possibly mild renal dysfunction in a family of Turkish origin.

INTRODUCTION

Hearing impairment is the most common sensory disorder worldwide and it is clinically and genetically very heterogeneous.[1] Approximately 80% of early onset hereditary non-syndromic hearing impairment inherits in an autosomal recessive pattern. Currently, 80 loci and 49 genes have been identified for autosomal recessive non-syndromic hearing impairment (arNSHI), showing the great genetic heterogeneity (Hereditary Hearing Loss Homepage, http://hereditaryhearingloss.org/). This heterogeneity might well be explained by the complexity of the auditory system. Defects in a large variety of biological processes such as gene regulation, ion homeostasis and hair bundle morphogenesis can lead to hearing impairment.[2]

In the last decade, homozygosity mapping using genome-wide SNP genotyping has been a powerful tool in the identification of arNSHI loci and genes.[3] Lately, next generation sequencing technologies have revolutionized the genetics field and also led to the identification of novel arNSHI genes at fast pace.[4] The most powerful evidence to assign a candidate gene as a novel deafness gene is to discover pathogenic variants in several families and not in controls. However, due to the large genetic heterogeneity of hearing impairment this can be very difficult even with the current technologies. This is also evident from three recently identified arNSHI genes, *PNPT1, SERPINB6* and *TSPEAR*, for which mutations have only been described in a single family each.[5-7] Further evidence to assign a candidate gene as a deafness gene can come from animal models, especially mouse models with hearing loss. Several genes essential for hearing in humans were identified after they had already been demonstrated to be associated with deafness in mice.[8]

Using homozygosity mapping and candidate gene analysis we identified a homozygous nonsense mutation in *CLIC5* in a consanguineous Turkish family (W05-009). The orthologous mouse gene, *Clic5*, was described to be mutated in the *jitterbug (jbg)* mouse exhibiting congenital progressive hearing impairment and vestibular dysfunction due to progressive hair cell degeneration.[9]

MATERIALS AND METHODS

Subjects and clinical evaluations

This study was approved by the local medical ethics committee of the Radboud university medical center and Hospital Universitario Ramon y Cajal. Signed

informed consent was obtained from the parents, since all patients are minors. In addition, a signed form was used to retrieve relevant data from other medical centers.

For the affected individuals of family W05-009 general physical examination was performed by a pediatrician. Blood and urine samples were analyzed to evaluate renal and thyroid function. ENT examination was executed to exclude other possible causes of hearing impairment like previous ear surgery and external ear deformities. A computed tomography (CT) scan of the temporal bone was performed in order to exclude possible anatomical causes of hearing loss. Pure tone audiometry was performed according to current standards to determine hearing thresholds at 0.25, 0.5, 1, 2, 4 and 8 kHz. To exclude conductive hearing loss both air conduction and bone conduction thresholds were obtained. Classification of the hearing loss is in accordance with the GENDEAF guidelines (Hereditary Hearing Loss Homepage, http://hereditaryhearingloss.org/). In addition, otoacoustic emissions (OAEs) were measured in individual II.3. Vestibular function was evaluated by electronystagmography and rotatory tests.[10] GraphPad Prism 5.00 (GraphPad, San Diego, CA, USA) was used to perform linear regression analysis to evaluate progression of the hearing impairment.

Three panels of arNSHI patients were analyzed for involvement of *CLIC5*. *GJB2* mutations or *GJB6* deletions were excluded by routine analysis in most of these patients. The first panel consisted of 76 arNSHI index patients, mostly of Dutch origin, and these were selected based on the hearing loss phenotype. They presented either with a downsloping audiogram configuration and progression of hearing loss or early onset progressive hearing loss accompanied by vestibular areflexia or hyporeflexia. The second panel consisted of 69 unrelated arNSHI sibships of Spanish origin which were not preselected based on type or severity of their hearing impairment. The third panel contained 18 arNSHI index patients of Spanish origin selected based on the hearing loss phenotype. In most of the cases, the hearing loss was postlingual (16 in childhood, at school age; two in the second decade of life) and progressive with a downsloping audiogram configuration.

Homozygosity Mapping

Genomic DNA was isolated from peripheral-blood lymphocytes by standard procedures. Individuals II.2 and II.3 from family W05-009 were genotyped using the Affymetrix mapping 250K NspI SNP array. All SNP array experiments were performed and analyzed according to the manufacturer's protocol

(Affymetrix, Santa Clara, CA, USA). Genotype calling and calculation of the regions of homozygosity were performed with the Genotyping Console software (Affymetrix) with the default settings. The cosegregation of the genotypes for each previously reported arNSHI gene was visually evaluated.

Mutation Analysis

Primers for amplification of exons and exon-intron boundaries of *CLIC5* (NM_016929.4, *CLIC5A* and NM_001114086.1, *CLIC5B*), *ESPN* (NM_031475.2), *MYO6* (NM_004999.3) and for mRNA analysis of *MYO6* (NM_004999.3) were designed with ExonPrimer (http://ihg.gsf.de/ihg/ExonPrimer.html). Primer sequences and PCR conditions are provided in Supplemental Table S1. Amplification by PCR was performed on 40 ng of genomic DNA with Taq DNA polymerase (Roche, Mannheim, Germany). For *MYO6* mRNA analysis, total RNA was isolated from Epstein-Barr-virus (EBV)-transformed lymphoblastoid cells of affected individual II.2 using the NucleoSpin RNA II kit (Machery Nagel, Düren, Germany) according to the manufacturer's protocol. Subsequently, cDNA synthesis was performed with 1.5 µg RNA as starting material by using the iScript cDNA Synthesis Kit (Bio-Rad Laboratories, Hercules, CA, USA), according to the manufacturer's protocol. PCR reactions were performed on 2 µl cDNA with the Taq DNA polymerase (Invitrogen, Carlsbad, CA, USA).

PCR fragments were purified with the use of NucleoFast 96 PCR plates (Clontech, Mountain View, CA, USA) or ExoI/FastAP (Fermentas, Vilnius, Lithuania) in accordance with the manufacturer's protocol. Sequence analysis was performed with the ABI PRISM BigDye Terminator Cycle Sequencing V2.0 Ready Reaction kit and analyzed with the ABI PRISM 3730 DNA analyzer (Applied Biosystems Foster City, CA, USA). The presence of the CLIC5 c.96T>A transversion was investigated in 111 ethnically matched healthy controls. Exon 2 of CLIC5 was amplified and PCR products were purified as described above. Digestion of the PCR products with *HpyCH4III* (New England Biolabs, Ipswich, MA, USA) was performed in accordance with the manufacturer's protocol, and restriction fragments were analyzed on gels containing 1.5% agarose and 1% low-melting agarose. The mutation removes a restriction site.

Nonsense-mediated mRNA decay (NMD) evaluation

EBV-transformed lymphoblastoid cell lines were established from heparin blood of individuals II.2 and II.3. Cells were grown with and without cycloheximide, a protein synthesis inhibitor, which prevents the nonsense-mediated mRNA decay

process as described previously.[11] Total RNA was isolated as described above. cDNA synthesis was performed with 3 µg RNA as starting material by using the iScript cDNA Synthesis Kit (Bio-Rad Laboratories, Hercules, CA, USA), according to the manufacturer's protocol. For the quantitative PCR (qPCR), specific primers (Supplemental Table S1) were designed with Primer3Plus (http://www.bioinformatics.nl/cgi-bin/primer3plus/primer3plus.cgi) and reference sequence NM_016929.4. PCRs were performed with the Applied Biosystem Fast 7900 System in accordance with the manufacturer's protocol. The human beta glucuronidase gene (GUSB [MIM 611499]) was employed as an internal control. PCR mixtures were prepared with the Power Syber Green Master Mix (Applied Biosystems) in accordance with the manufacturer's protocol. Temperatures and reaction times for PCR were as follows: 10 min at 95°C, followed by 40 cycles of 15 s at 95°C and 30 s at 60°C. All reactions were performed in duplicate. Relative gene expression levels were determined with the delta delta Ct method as described previously.[11]

CLIC5 Expression Profile

RNA derived from adult heart, retina, brain and kidney was purchased from Clontech (Mountain View, CA, USA). RNA derived from adult skeletal muscle, liver, duodenum, testis, spleen, thymus, and placenta were purchased from Stratagene (La Jolla, CA, USA) and bone marrow from Bio-chain (Newark, CA, USA). RNA derived from fetal brain, colon, kidney, stomach, spleen, heart, skeletal muscle, lung and thymus was purchased from Stratagene. In addition, RNA was isolated from adult lung, fetal cochlea and fetal liver as described previously.[12] The inner ear was derived from a fetus at 8 weeks of gestation and the other fetal tissues from fetuses at 20 – 21 weeks of gestation. cDNA synthesis, primer design (Supplemental Table S1) and qPCR analysis were performed as described above. The forward primer was located on the boundary of exons 2 and 3, and the reverse primer in exon 3. This enabled detection of all CLIC5 isoforms affected by the nonsense mutation that is located in exon 2. Relative gene expression levels were determined with the comparative delta Ct method as described previously.[13]

RESULTS

Hearing loss and vestibular dysfunction in family W05-009

ENT examination and CT scanning did not reveal an apparent cause of hearing

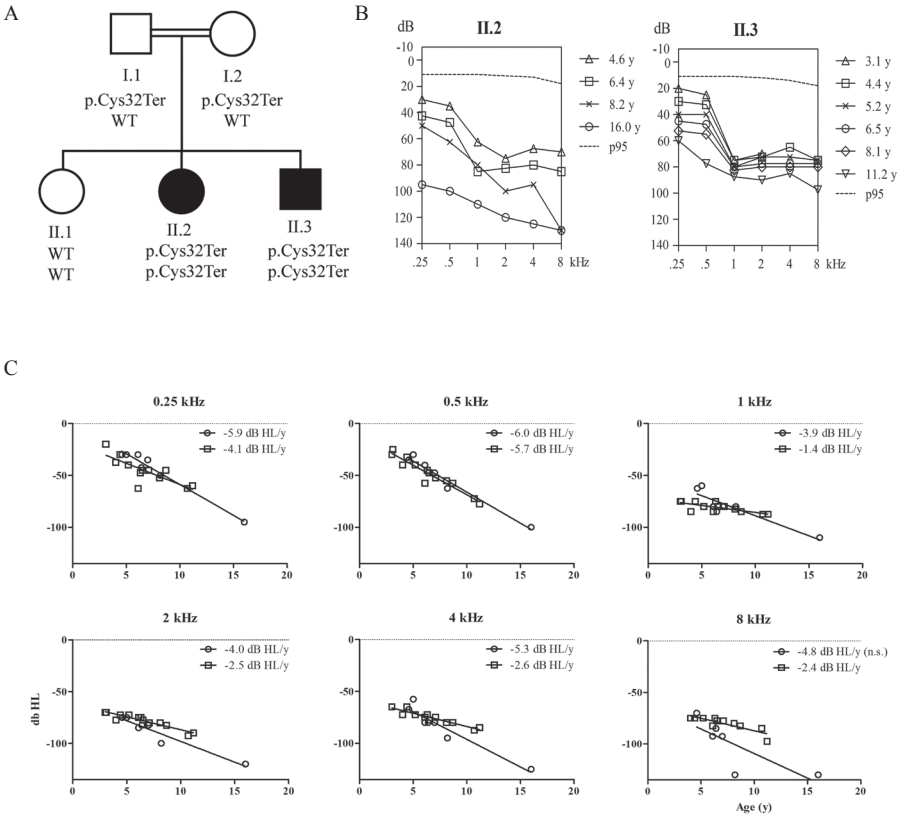

Figure 1. A) Pedigree of family W05-009 and segregation of the *CLIC5 c.96T>*A variant

B) Longitudinal binaural mean air-conduction pure tone thresholds are shown of affected members of family W05-009

Age (years) is shown with a symbol key. The p95 line, matched for age and sex, indicates that 95% of the population has thresholds lower than these.

C) Regression analysis of longitudinal binaural mean air conduction threshold data for each frequency separately

Circles indicate individual II.2, squares indicate individual II.3. Annual threshold deterioration is shown behind the symbol key for each frequency.

impairment in the two affected children of family W05-009. The parents have normal hearing and are first cousins of Turkish ancestry (Figure 1A). The patients presented with an early onset sensorineural hearing loss since the bone conduction thresholds did not differ from the air conduction thresholds. The hearing impairment probably was not congenital since individual II.2 passed a behavioural reflex audiometry test which is performed between 7 and 9 months of age (Ewing test) and individual II.3 had normal hearing at the age

of 3 months during brainstem evoked response audiometry. The hearing loss started mildly, affecting the mid and high frequencies mostly. It progressed to a severe-to-profound hearing loss with a gently to steeply downsloping audiogram configuration as is shown in Figure 1B. linear regression analysis indicated significant progression in all frequencies (Figure 1C). OAEs were not present in individual II.3 at the age of 4 months. Individual II.2 received a cochlear implant at the age of 11 years. Five years post-implantation, the speech recognition scores were 88% (using the standard Dutch phonetically balanced consonant-vocal-consonant word lists).[14] Initial motor milestones were reported to be normal, but later in life balance problems did occur e.g. difficulties with walking in the dark and cycling. Vestibular areflexia was found in both individuals during the rotatory test at the age of 16 years (II.2) and 11 years (II.3).

General physical examination showed that both children had a normal height and weight. No other abnormalities besides the hearing impairment were noted in individual II.2. On history, there were no signs of any other abnormalities in individual II.3. Thyroid function was also normal in individuals II.2 and II.3. Renal function was normal in II.2. However, in individual II.3 a blood pressure of 127/73 to 129/88 mmHg (90% value for this age and length: 120/76 mmHg) was measured and an elevated albumin/creatinine ratio was detected at the last two visits in the outpatient clinic (9.2 and 3.8 mg/mmol, respectively, normal value <2.5 mg/mmol) during urine analysis at the age of 11 years. The glomerular filtration rate, calculated with the Schwartz equation, was normal with a value of 114 ml/min/1.73 m^2 (normal > 90 ml/min/1.73 m^2). Since the elevated blood pressure and albumin/creatinine ratio were seen in repeated measurements, these might be the first signs of a nephropathy. However, no other more invasive studies were performed, since the renal function was overall only mildly affected. Subsequent renal function follow-up of patient II.3 in the future will be needed to determine whether it is indeed a nephropathy.

Homozygosity mapping confines a critical region on chromosome 6p21.1-q15

To identify genes for arNSHI, homozygosity mapping was performed in some large series of familial and isolated arNSHI patients living in the Netherlands. In family W05-009 homozygosity mapping revealed a homozygous region of 47.4 Mb on chromosome 6p21.1-q15 (Figure 2A). This was the largest homozygous region shared by the two affected individuals. This region contains the known deafness gene *MYO6*. There were 15 other shared homozygous regions larger

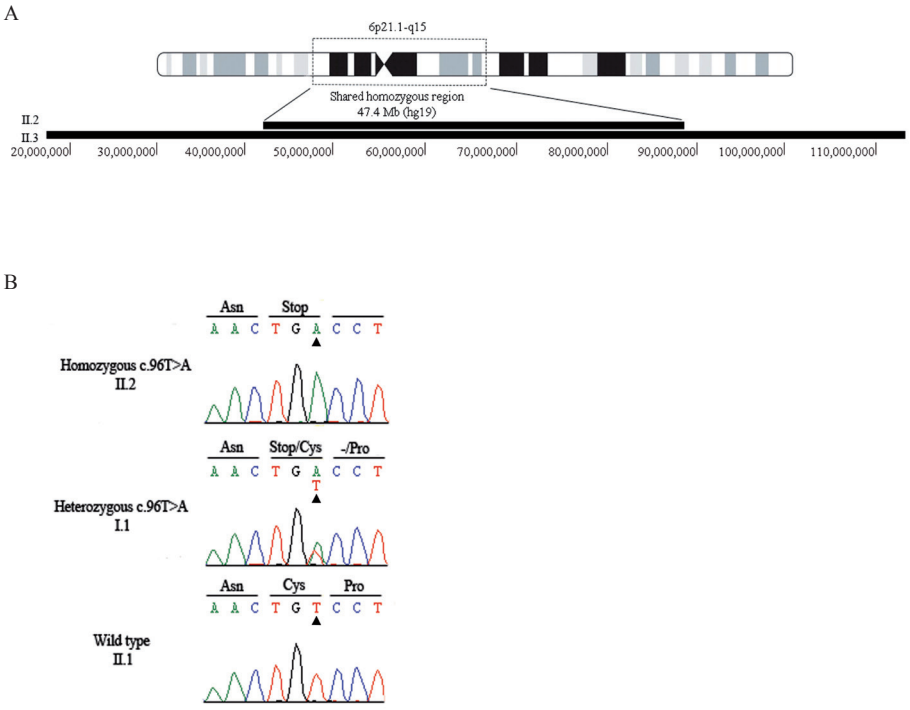

Figure 2. A) Schematic overview of the chromosomal region 6q21.1-q15 showing the homozygous regions (black bars) identified in the affected individuals of family W05-009

The homozygous region of individual II.2 delimits the region to 47.4 Mb. Mb positions and chromosome bands are according to the UCSC genome browser (GRCh37).

B) Partial sequences are shown of *CLIC5* exon 2 from an affected member, a parent and an unaffected sib of family W05-009

The predicted amino acid changes and the surrounding amino acids are indicated above the sequence. Mutated nucleotides are marked by an arrowhead. As reference sequence NM_016929.4 was employed.

than 1 Mb (Supplemental Table S2), and in one of them *ESPN* is located, which is another gene known for arNSHI. Mutation analysis was performed for all exons and exon-intron boundaries of *ESPN* and *MYO6*, which revealed no putative causative variants. Since *MYO6* was located in the largest shared homozygous region, *MYO6* mRNA was analyzed by RT-PCR. No PCR-products of an aberrant size were indentified and also sequence analysis of the PCR products did not reveal indications for aberrant splicing. To exclude compound heterozygous or allozygous mutations in the other known arNSHI genes, cosegregation of the genotypes was visually evaluated for each gene. *PNPT1, ILDR1, RDX, TECTA, OTOGL, PTPRQ* and *OTOA* were present within the genotype shared regions.

OTOA could be excluded by short tandem repeat (STR) marker analysis in the family. No putative pathogenic variants were identified in the other genes by sequence analysis of the exons and exon-intron boundaries.

A nonsense mutation in *CLIC5* causes arNSHI

Since no pathogenic variants could be identified in *MYO6* or *ESPN* we hypothesized that another gene would be underlying the hearing loss in this family. Therefore, we continued with the evaluation of the 247 annotated genes in the largest homozygous region, 6p21.1-q15 (http://genome.ucsc.edu/, RefSeq genes, hg19; assigned DFNB102). For three of the genes, mutations in the orthologous mouse gene cause deafness. *Slc17a5* (MGI:1924105)[15] and *Bmp5* (MGI:88181) are associated with mixed and conductive hearing loss in the mouse, respectively. The third gene, *Clic5*, was described to underlie progressive sensorineural hearing loss and vestibular dysfunction in the *jbg* mouse mutant.[9] Therefore, *CLIC5* represented an excellent candidate gene.

Mutation analysis of *CLIC5* revealed a homozygous nonsense variant c.96T>A (p.(Cys32Ter)) (Figure 2B), which segregated with the hearing impairment in family W05-009 (Figure 1A). This variant was not present in 222 Turkish control alleles, the Exome Variant Server (http://evs.gs.washington.edu/EVS/) and the Nijmegen in-house exome database (1302 exomes). This variant was submitted to the Leiden Open Variant Database (http://databases.lovd.nl/shared/variants/0000022995).

The homozygous *CLIC5* c.96C>T mutation is predicted to result in NMD, since it creates a premature stop codon (p.(Cys32Ter)) more than 54 bp upstream of the 3'-most intron.[16] However, we could not confirm NMD. The relative *CLIC5* mRNA expression is comparable in cycloheximide treated and untreated patient EBV-cell lines (157.24% vs 157.89%, respectively) and higher - albeit not significantly - than in controls (set at 100%) as shown in Supplemental figure 1.

For identification of other families with *CLIC5* mutations, sequence analysis of the coding region and splice sites of *CLIC5* was performed in 76 arNSHI index patients, mostly of Dutch origin, and 18 Spanish arNSHI index patients. These patients were preselected based on the hearing loss and vestibular phenotype as described in the materials and methods section. No putatively causative variants were identified in these patients. In a parallel approach, compatibility with linkage to DFNB102 was investigated in a panel of 69 unrelated arNSHI sibships of Spanish origin. These were genotyped for STR-markers D6S459, D6S1920, D6S1632 and D6S1638, which flank *CLIC5*. Haplotype analysis revealed compatibility with linkage of the disease locus to these markers in 18

A

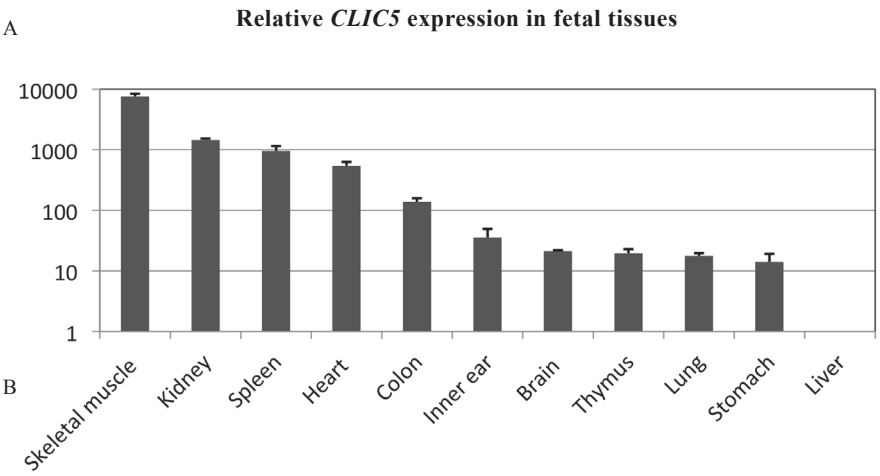

B

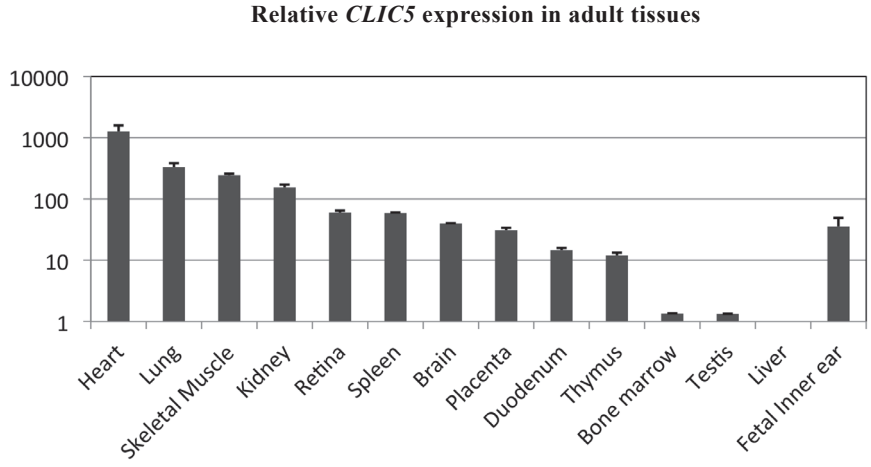

Figure 3. *CLIC5* expression profile in human tissues

Relative *CLIC5* mRNA levels as determined by qPCR in human fetal (A) and adult (B) tissues. The relative expression values were determined by using the comparative delta Ct method.[13] The expression levels are relative to those in liver, which showed the lowest *CLIC5* expression of all the tissues that were tested.

sibships. Sequence analysis of *CLIC5* in the index cases of these sibships did not reveal any putative pathogenic variants. Finally, data of 50 whole exome sequence analysis of arNSHI patients, mainly of Dutch origin were evaluated for the presence of variants in *CLIC5*. These patients were not preselected based on the type or severity of the hearing loss. No putatively pathogenic variants were identified in this cohort.

CLIC5 is expressed in the human inner ear

The expression of *CLIC5* was studied via qPCR in human fetal inner ear and compared to that in additional 13 adult and 10 fetal-stage human tissues (Figure 3). Since this was performed in two separate experiments for adult and fetal tissues, fetal inner ear was included in both for comparison. The tissues were not derived from fetuses of the same gestational stage; therefore, a direct comparison of the transcript levels cannot be made. In fetal tissues, *CLIC5* transcript levels were highest in skeletal muscle, kidney, spleen, heart and colon. A lower expression level was found in fetal brain, thymus, lung and stomach. Expression in the fetal inner ear was 26 fold higher than in fetal liver in which the expression level was the lowest. In adult tissues, the highest expression levels were found in heart, lung, skeletal muscle and kidney and there was a gradual decrease through retina, spleen, brain, placenta, duodenum and thymus. Finally, the lowest expression levels were found in bone marrow, testis and liver. We can conclude that *CLIC5* is widely expressed in both fetal and adult human tissues.

DISCUSSION

We present a homozygous nonsense mutation, c.96T>A (p.(Cys32Ter)) in *CLIC5* (DFNB102) as a cause of sensorineural hearing impairment accompanied by vestibular dysfunction. This nonsense variant will lead to an early truncation of the protein. Screening a series of arNSHI index patients did not reveal additional causative variants, suggesting that mutations in *CLIC5* are not a common cause of arNSHI neither in the Netherlands nor in Spain.

Initially, the hearing loss in the affected individuals of family W05-009 was mild, mainly affecting the mid and high frequencies, and then it progressed to severe to profound. They also showed vestibular areflexia in the second decade of life. The combination of progression to profound hearing loss and complete vestibular dysfunction in the patients of family W05-009 resembles the phenotype of the *jbg* mutants. Auditory-evoked brainstem responses (ABRs) at 1-5 months of age in *jbg* mutant mice, which are null for *Clic5*, were 40-50 dB above those of wildtype mice. By 7 months of age their hearing loss had progressed to complete deafness due to progressive hair bundle degeneration and a reduced density of spiral ganglion cells.[9] The vestibular hair cells of *jbg* mice also showed a progressive degeneration. In the crista ampullaris, the number of vestibular hair cells was reduced at 3 months and hair cells were nearly absent at 12 months of age.[9]

Besides inner ear dysfunction, the phenotype in humans and mice with *Clic5* mutations may well overlap with respect to the renal phenotype. The *jbg* mice have abnormalities in the foot processes of the kidney podocytes leading to proteinuria.[17,18] The elevated albumin/creatinine ratio and pre-hypertension in affected individual II.3 indicate mild renal dysfunction and may well be the first signs of a nephropathy. Therefore, follow-up of renal function is indicated for individual II.3 but also for his hearing impaired sister.

In addition to the inner ear and kidney phenotypes, the *jbg* mutant mice also exhibit emphysema-like lung pathology, hyperactivity and resistance to diet-induced obesity.[19] Characteristics of lung emphysema and hyperactivity were excluded in family W05-009 by history taking. The affected individuals had normal height and weight. No other gross abnormalities in the organs of the *jbg* mutants were detected and no other complaints from the affected siblings were reported so far. The lack of symptoms in organs with relatively high *CLIC5* expression (Figure 3) points towards redundancy for CLIC5 function there.

CLIC5 belongs to a family of chloride intracellular channel proteins, but its protein structure differs from other typical ion channel proteins. CLICs (CLIC1-6) show no sequence homology to any known channel family, but significant homology to glutathione S-transferases in the core region.[20] Moreover, some of the CLIC proteins, including CLIC5, are not only integral membrane proteins, but are also found as soluble proteins in the cytoplasm.[21] In the inner ear, CLIC5 localizes to stereocilia of both the cochlear and vestibular hair cells and on the surface of Kolliker's organ during cochlea development in mice.[9] Specifically, CLIC5 is predominantly present at the base of stereocilia and, to lesser extent, in the cell bodies of hair cells in the region surrounding the cuticular plate.[9] CLIC5 was initially identified in placental microvilli as a component of a multimeric complex consisting of several known cytoskeletal proteins, including actin and ezrin.[22] Although the function of CLIC5 is still elusive, there are several facts that support its role in stereocilia integrity. Firstly, radixin immunostaining is reduced in the hair bundle of *jbg* mice where it colocalizes with Clic5.[9] This suggests that Clic5 is needed for proper radixin activity, so when interacting with the ERM (ezrin, radixin and moesin) complex, Clic5 may stabilize connections between the plasma membrane and the filamentous actin core.[9] Secondly, Clic5 functions as an adapter between the plasma membrane of podocytes and the actin cytoskeleton by facilitating the interaction between ezrin and podocalyxin.[17,18,23] Thirdly, a recent study proposes that Clic5 functions as part of a multiprotein linker complex in companion with radixin, ezrin and taperin.[24] Protein tyrosine phosphatase receptor Q (Ptprq), which is mislocalized as radixin in the *jbg*

mice, and Myosin VI, key regulator of the proper localization of Ptprq[25], might well participate in this complex too. Radixin[26], Ptprq[25,27] Myosin VI28 and Clic5 deficient mice[9] show loss of stereocilia at the bundle vertex and fusion of stereocilia in postnatal stage. This suggests that this multiprotein complex is essential for stable membrane-cytoskeletal attachments at the stereocilia base.
In conclusion, we show that a homozygous nonsense mutation in *CLIC5* (p.(Cys32Ter)) underlies the progressive hearing impairment, vestibular and possibly mild renal dysfunction in a family of Turkish origin. *CLIC5* mutations do not seem to be a common cause of arNSHI in the Dutch and Spanish populations. Further screening of *CLIC5* in other populations will provide important information about the frequency of *CLIC5* mutations and may aid to further define the phenotype associated with *CLIC5* mutations.

Acknowledgements
We are grateful to the family for their participation in this study. We thank Saskia van der Velde-Visser, Marloes Steehouwer and Irene Janssen for excellent technical assistance, Ersan Kalay for providing Turkish control DNA samples, Arjan de Brouwer for his contribution to the NMD analysis and Rob Collin for SNP-array analysis. This work was financially supported by grants from the Heinsius Houbolt Foundation [to H.K.], The Oticon Foundation [09-3742, to H.K.], ZorgOnderzoek Nederland / Medische Wetenschappen [40-00812-98-09047, to H.K., 90700388 to R.P. and 016.136.088 to M.S.], the Netherlands Genomics Initiative [40-41009-98-9073, to M.S.] and Instituto de Salud Carlos III (FIS PI11/00612, to I.d.C.).

REFERENCES

1. Mehl AL, Thomson V: The Colorado newborn hearing screening project, 1992-1999: on the threshold of effective population-based universal newborn hearing screening. Pediatrics 2002; 109: E7.
2. Dror AA, Avraham KB: Hearing loss: mechanisms revealed by genetics and cell biology. Annu Rev Genet 2009; 43: 411-437.
3. Schraders M, Lee K, Oostrik J et al: Homozygosity mapping reveals mutations of GRXCR1 as a cause of autosomal-recessive nonsyndromic hearing impairment. Am J Hum Genet 2010; 86: 138-147.
4. Shearer AE, Smith RJ: Genetics: advances in genetic testing for deafness. Curr Opin Pediatr 2012; 24: 679-686.
5. Delmaghani S, Aghaie A, Michalski N, Bonnet C, Weil D, Petit C: Defect in the gene encoding the EAR/EPTP domain-containing protein TSPEAR causes DFNB98 profound deafness. Hum Mol Genet 2012; 21: 3835-3844.
6. Sirmaci A, Erbek S, Price J et al: A truncating mutation in SERPINB6 is associated with autosomal-recessive nonsyndromic sensorineural hearing loss. Am J Hum Genet 2010; 86: 797-804.
7. von Ameln S, Wang G, Boulouiz R et al: A mutation in PNPT1, encoding mitochondrial-RNA-import protein PNPase, causes hereditary hearing loss. Am J Hum Genet 2012; 91: 919-927.
8. Friedman LM, Dror AA, Avraham KB: Mouse models to study inner ear development and hereditary hearing loss. Int J Dev Biol 2007; 51: 609-631.
9. Gagnon LH, Longo-Guess CM, Berryman M et al: The chloride intracellular channel protein CLIC5 is expressed at high levels in hair cell stereocilia and is essential for normal inner ear function. J Neurosci 2006; 26: 10188-10198.
10. Theunissen EJ, Huygen PL, Folgering HT: Vestibular hyperreactivity and hyperventilation. Clin Otolaryngol Allied Sci 1986; 11: 161-169.
11. Livak KJ, Schmittgen TD: Analysis of relative gene expression data using real-time quantitative PCR and the 2(-Delta Delta C(T)) Method. Methods 2001; 25: 402-408.
12. Luijendijk MW, van de Pol TJ, van Duijnhoven G et al: Cloning, characterization, and mRNA expression analysis of novel human fetal cochlear cDNAs. Genomics 2003; 82: 480-490.
13. Pfaffl MW: A new mathematical model for relative quantification in real-time RT-PCR. Nucleic Acids Res 2001; 29: e45.
14. Bosman AJ SG: Woordenlijst voor spraakaudiometrie (Compact Disc) Gouda, the Netherlands: Electro Medical Instruments bv & Veenhuis Medical Audio bv, 1992.
15. Prolo LM, Vogel H, Reimer RJ: The lysosomal sialic acid transporter sialin is required for normal CNS myelination. J Neurosci 2009; 29: 15355-15365.

16. Nagy E, Maquat LE: A rule for termination-codon position within intron-containing genes: when nonsense affects RNA abundance. Trends Biochem Sci 1998; 23: 198-199.
17. Pierchala BA, Munoz MR, Tsui CC: Proteomic analysis of the slit diaphragm complex: CLIC5 is a protein critical for podocyte morphology and function. Kidney Int 2010; 78: 868-882.
18. Wegner B, Al-Momany A, Kulak SC et al: CLIC5A, a component of the ezrin-podocalyxin complex in glomeruli, is a determinant of podocyte integrity. Am J Physiol Renal Physiol 2010; 298: F1492-1503.
19. Bradford EM, Miller ML, Prasad V et al: CLIC5 mutant mice are resistant to diet-induced obesity and exhibit gastric hemorrhaging and increased susceptibility to torpor. Am J Physiol Regul Integr Comp Physiol 2010; 298: R1531-1542.
20. Dulhunty A, Gage P, Curtis S, Chelvanayagam G, Board P: The glutathione transferase structural family includes a nuclear chloride channel and a ryanodine receptor calcium release channel modulator. J Biol Chem 2001; 276: 3319-3323.
21. Ashley RH: Challenging accepted ion channel biology: p64 and the CLIC family of putative intracellular anion channel proteins (Review). Mol Membr Biol 2003; 20: 1-11.
22. Berryman M, Bretscher A: Identification of a novel member of the chloride intracellular channel gene family (CLIC5) that associates with the actin cytoskeleton of placental microvilli. Mol Biol Cell 2000; 11: 1509-1521.
23. Jiang L, Phang JM, Yu J et al: CLIC proteins, ezrin, radixin, moesin and the coupling of membranes to the actin cytoskeleton: A smoking gun? Biochim Biophys Acta 2014; 1838: 643-657.
24. Salles FT, Andrade LR, Tanda S et al: CLIC5 stabilizes membrane-actin filament linkages at the base of hair cell stereocilia in a molecular complex with radixin, taperin, and myosin VI. Cytoskeleton (Hoboken) 2013.
25. Sakaguchi H, Tokita J, Naoz M, Bowen-Pope D, Gov NS, Kachar B: Dynamic compartmentalization of protein tyrosine phosphatase receptor Q at the proximal end of stereocilia: implication of myosin VI-based transport. Cell Motil Cytoskeleton 2008; 65: 528-538.
26. Kitajiri S, Fukumoto K, Hata M et al: Radixin deficiency causes deafness associated with progressive degeneration of cochlear stereocilia. J Cell Biol 2004; 166: 559-570.
27. Goodyear RJ, Legan PK, Wright MB et al: A receptor-like inositol lipid phosphatase is required for the maturation of developing cochlear hair bundles. J Neurosci 2003; 23: 9208-9219.
28. Self T, Sobe T, Copeland NG, Jenkins NA, Avraham KB, Steel KP: Role of myosin VI in the differentiation of cochlear hair cells. Dev Biol 1999; 214: 331-341.

SUPPLEMENTAL FIGURES AND TABLES

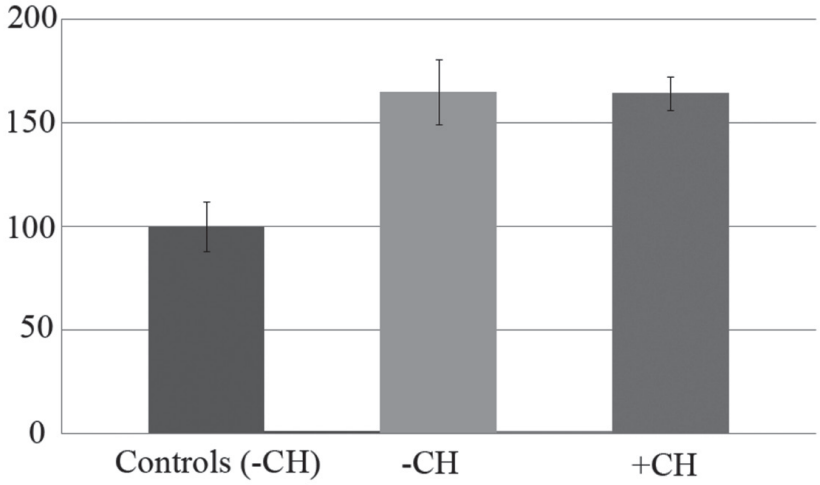

Supplemental Figure 1. The homozygous mutation *CLIC5* c.96T>A (p.(Cys32Ter)) in family W05-009 does not result in nonsense mediated mRNA decay (NMD)

Shown is the mean expression of *CLIC5* in Epstein-Barr-virus (EBV)-transformed lymphoblastoid cells of affected individuals II.2 and II.3 (n=2) and controls (n=10) treated with (+CH) and without (-CH) cycloheximide. Quantifications were normalized against *GUSB* expression. Differences in expression between the affected individuals and 10 controls were calculated by using the delta delta Ct method.[11] The p-value was derived from the standard score (Z-value) calculated for untreated samples (-CH) as compared to the normal distribution of the 10 controls. Since we assume a lower expression level as a result of NMD, a one-sided test was enough to reject the null hypothesis (p=0.376). Also, no difference was seen in *CLIC5* expression between treated and untreated patient samples. In conclusion, occurrence of NMD could not be confirmed.

Supplemental Table S1. Primer sequences and PCR conditions for genomic PCR, sequence analysis and QPCR

Target	Oligonucleotides		Product size (bps)	Annealing Temperature (°C)
Primers for genomic PCR and sequence analysis of *CLIC5, MYO6* and *ESPN*				
CLIC5 Exon 1	Forward primer	CCAGGACCAGCTCTGTCTC	733	56
	Reverse primer	AACCTGCCTTCCTCCATTC		
CLIC5 Exon 2	Forward primer	TTATTGAGCCCTTACATGCTG	484	56
	Reverse primer	ACTTGCCTTTGCAGACTCTC		
CLIC5 Exon 3	Forward primer	ACAGGCATGTTGGATAGCAC	653	56
	Reverse primer	GTCACTGGGTTACCCTTTCC		
CLIC5 Exon 4	Forward primer	GCTGGAAAGGGAAGTATTGC	306	56
	Reverse primer	CTCTGGCCCAAGTATTTGAC		
CLIC5 Exon 5	Forward primer	TCCAGGTATTCTGCAGTGTG	431	56
	Reverse primer	AGGTTCTTGACCAACAGGTG		
CLIC5 Exon 6	Forward primer	AAAGAAGACAGCACTGCCAC	427	56
	Reverse primer	GCCTCAAGGCAGTGATACAG		
CLIC5 Exon 1a*	Forward primer	TCCAATGGACTTGTGGTTTG	885	56
	Reverse primer	TGACTGATTTAGTCCCTCCG		
MYO6 Exon 1	Forward primer	TCCGTAGCCGTGACGTG	532	56
	Reverse primer	TCGGGCAGTGAACAGAAG		
MYO6 Exon 2	Forward primer	TGGGCAGATGTGTTTGTTAG	388	56
	Reverse primer	TGCTTTCCCAAATATCTACCTC		
MYO6 Exon 3	Forward primer	GTATGCAACCAATTAAGCCC	262	56
	Reverse primer	TAGATTGTTTCTGAACCCGC		
MYO6 Exon 4	Forward primer	TAGGGTTTACATCAGCCAGG	337	56
	Reverse primer	TCAAGCATGATTTTCTGTTAGAC		
MYO6 Exon 5	Forward primer	TGGGTCCCTATAAAGATCAGG	471	56
	Reverse primer	CCCTGTGTAAAATACTTGCTCC		
MYO6 Exon 6	Forward primer	TGATTTCTTTAAGAGTAAGTGGTCC	322	58
	Reverse primer	TACAGTGAGCTGTGGTGGTG		
MYO6 Exon 7	Forward primer	TGATGATCTAGGTTTCAGTTTTATATG	238	56
	Reverse primer	TGAGAGAAGAACATTCCAGACC		
MYO6 Exon 8	Forward primer	GCATGAGCCACTGTGTCC	324	56
	Reverse primer	TGCAAATACAGCACCAACTG		
MYO6 Exon 9	Forward primer	AACCTCTTTGATAGACAAATGG	651	58
	Reverse primer	CAGGCTCAAGCAATCCATC		
MYO6 Exon 10	Forward primer	TTCATGGTTGGCACTATTTG	353	56
	Reverse primer	CAACAAGAGGTATAAAGTATTACACTG		
MYO6 Exon 11	Forward primer	AGTGCATTAATTGACCTGGTG	363	58
	Reverse primer	TTTAAGCAAACTGCATATAAAGAGAC		
MYO6 Exon 12	Forward primer	AAAAGTTACAAATAAGCCTTGCC	375	56
	Reverse primer	TTTTGATCTACCAAGCTCAGG		

Supplemental Table S1. Continued

Target	Oligonucleotides		Product size (bps)	Annealing Temperature (°C)
Primers for genomic PCR and sequence analysis of *CLIC5, MYO6* and *ESPN*				
MYO6 Exon 13	Forward primer	GTTTAGGTGCACTCTGTGGC	376	56
	Reverse primer	CATATTATGAAATGTGAGTGTGGAC		
MYO6 Exon 14	Forward primer	TGAGAACATTTGGGAAGTATAGAAC	351	56
	Reverse primer	ATACACCATCCATCCACACC		
MYO6 Exon 15	Forward primer	TTCAGAAACAGTGCAAAATTC	295	56
	Reverse primer	CTTCCAGGCAGTAATACAGAAG		
MYO6 Exon 16	Forward primer	TGTTGTTTCTGATCAGTCCTTG	389	56
	Reverse primer	TCCATCTAAGGAAGATACTGTGC		
MYO6 Exon 17	Forward primer	CTTACACCTATTTTCTTTCCTAAGAG	500	56
	Reverse primer	TCACCACTAGTCAGTGTGGAC		
MYO6 Exon 18	Forward primer	AAGTTCCTTTGGACAGAGCC	390	56
	Reverse primer	CAAATATCAACAATGCAGGG		
MYO6 Exon 19	Forward primer	CCAGGAGGTTGTTAAACTGG	267	56
	Reverse primer	CAGGGTTACTATGCCTACTTGC		
MYO6 Exon 20	Forward primer	CCCAGCCTTGAGTTCTTTAG	361	56
	Reverse primer	AAGATGAAAATTTTATTGCACTG		
MYO6 Exon 21-22	Forward primer	TCTCATAAATTGCCCGTTTC	580	56
	Reverse primer	TGTTGTTAGTGACCATATAATTCAAG		
MYO6 Exon 23	Forward primer	TGCCAAGGCCTATGTAATTG	354	56
	Reverse primer	AGCATCACCTCTGAGACAGC		
MYO6 Exon 24	Forward primer	GGTCGTCAAGATTTCATGTTTC	307	56
	Reverse primer	AAAACCTGAGTATCCAAACTGC		
MYO6 Exon 25	Forward primer	TTGAAAACAGAAGTGAAATACCC	375	56
	Reverse primer	GTCTCAACACATTTTGTAATTTTG		
MYO6 Exon 26	Forward primer	GCTGTATTTGCATATTGGAGTAG	460	56
	Reverse primer	TTGTCATTAACCACTGTCAATACC		
MYO6 Exon 27	Forward primer	TTCCCAATCTGTTACCTTTG	309	56
	Reverse primer	TTGATCTCCTGACCTCGTG		
MYO6 Exon 28	Forward primer	GGGGCAGTTATGCTTTCC	336	56
	Reverse primer	TTCTGCATGGAAATGAGAGG		
MYO6 Exon 29	Forward primer	CACAAATTTGCACAATCCAG	271	56
	Reverse primer	AGCACCATACAAGAGCATTAAAC		
MYO6 Exon 30	Forward primer	TGTGTTACGGCTAGATTTGTTG	309	56
	Reverse primer	TCATGTAACAGGTTCTGGTCC		
MYO6 Exon 31	Forward primer	TCCGGTTTTCAAACTTATGC	367	56
	Reverse primer	GTGCATTCATGGACCAAAAG		
MYO6 Exon 32	Forward primer	GCTTATCCTTATGAATAATTAGCTTAC	431	56
	Reverse primer	GCCATCAAGGCTGTATTAGG		
MYO6 Exon 33	Forward primer	ACTTTTCAGTCACCACCTCG	296	56
	Reverse primer	TCCACTGAAAATTGTAGCAAAAC		
MYO6 Exon 34	Forward primer	GGGGTATATTTTAGGATTAAAGGC	438	58
	Reverse primer	TGGAAATGTGATTTAACCGC		

Supplemental Table S1. Continued

Target	Oligonucleotides		Product size (bps)	Annealing Temperature (°C)
Primers for genomic PCR and sequence analysis of *CLIC5, MYO6* and *ESPN*				
MYO6 Exon 35_1	Forward primer	ATTGAAAGGGTCCTTGATGG	831	56
	Reverse primer	TGCCTTGATCATTTTAAGTGG		
MYO6 Exon 35_2	Forward primer	CCGCTGTAATTCCCAAAAC	614	56
	Reverse primer	TCCAGTTAAGCCACTATGCC		
MYO6 Exon 35_3	Forward primer	GCACAATGTGTGTTGCTGTC	658	56
	Reverse primer	CCTAACTGAGGTAATCTTTCTAGGG		
ESPN Exon 1	Forward primer	ATTCGAACCCAGTTTTGCTG	1010	58
	Reverse primer	CCACCCACTTCCAGGACTAC		
ESPN Exon 2	Forward primer	AGGAAGGGTGGAGAGATC	859	58
	Reverse primer	ATGTTGAGTGGGAGCCATTT		
ESPN Exon 3-5	Forward primer	GAGGTCAGACACAGCAGGTG	1954	58
	Reverse primer	AGCGTGGGTTTCCAGTTATG		
ESPN Exon 3-5S#	Forward primer	AGGTGAGCTGCACCGACGTG	NA	NA
	Reverse primer	TGACCTCTAGCTCCCCGTTC		
ESPN Exon 6	Forward primer	GGAACCTGGGTCCTGCTG	552	58
	Reverse primer	CCTCCCCATGTTTAAGAGCA		
ESPN Exon 7	Forward primer	TGGTCTTCCCCCAGTAAGTG	673	58
	Reverse primer	TACTCTCCTCCCAGTCCAGTG		
ESPN Exon 8	Forward primer	GCTGCCCACTGTGAGAACC	933	58
	Reverse primer	GGGAGGCCCTTTCTAGCTG		
ESPN Exon 9	Forward primer	CCATCCAATCTTGGCTTAGG	377	58
	Reverse primer	ACTGGTGACAGTGCAGGTGA		
ESPN Exon 10	Forward primer	CACAGTGTTCTCAGGCATCG	444	58
	Reverse primer	GATGGGCTGTGCATCCAG		
ESPN Exon 11-12	Forward primer	TCCCAGCTACTTGTTCTCTGC	691	58
	Reverse primer	GTGGGGTTAGGTTAACTGAAGG		
ESPN Exon 13	Forward primer	CTCAGTAACCCACCCCTTG	741	58
	Reverse primer	ATCTGGGTCAGAGAGGAAGG		
Primers for *MYO6* mRNA analysis				
MYO6 mRNA Ex1-9	Forward primer	TTCACCCGTACAGGTAGCC	826	56
	Reverse primer	TTCCTCTTTGCCTTGAACAC		
MYO6 mRNA Ex8-13	Forward primer	CTTTGGAAATGCGAAGACTG	787	56
	Reverse primer	TCCAATAAAATAGGATGATGTTTC		
MYO6 mRNA Ex13-19	Forward primer	GCAAGCAAACAATGCTCG	738	56
	Reverse primer	CTTCGAAGTTTATCCAGAAGC		
MYO6 mRNA Ex18-26	Forward primer	TGAATCCAGAGATAAGTTTATACGG	851	56
	Reverse primer	GTTCCTGCGTCATCATAGTG		
MYO6 mRNA Ex25-31	Forward primer	TGATGGTCTGGTTAAGGTGG	750	56
	Reverse primer	TCACGTAGTTCTGCATATTTCC		
MYO6 mRNA Ex30/31-35	Forward primer	TTTGAGTAGAGGTCCTGCTG	754	56
	Reverse primer	GGGCACACACCCTACCTAAG		

Supplemental Table S1. Continued

Target	Oligonucleotides		Product size (bps)	Annealing Temperature (°C)
Primers for genomic PCR and sequence analysis of *CLIC5, MYO6* and *ESPN*				
Primer for QPCR				
CLIC5 Exon2-3	Forward primer	CGGCAACTGTCCTTTCTCTC	115	60
	Reverse primer	GGCTAGGTTGTGCAGGTCAG		
GUSB Exon2-3	Forward primer	AGAGTGGTGCTGAGGATTGG	80	60
	Reverse primer	CCCTCATGCTCTAGCGTGTC		

The reference sequences for exon numbering *CLIC5, MYO6* and *ESPN* were NM_016929.4, NM_004999.3 and NM_031475.2, respectively. *This is the first exon of an alternative *CLIC5* transcript (NM_001114086.1) #These primers were only used for sequence analysis.

Supplemental Table S2. Overview of homozygous regions shared by the affected individuals of family W05-009

Start SNP		End SNP			Start	End	Size	Known
Name	rsId	Name	rsId	Chr.	position	position	(Mb)	arNSHI gene
SNP_A-4193053	rs2477828	SNP_A-2248124	rs2057276	6	41430495	88865821	47.38	*MYO6*
SNP_A-2227424	rs196004	SNP_A-2061244	rs153219	16	23966086	29215298	5.25	-
SNP_A-1794682	rs10915317	SNP_A-2070006	rs12119878	1	5081066	9218721	4.16	*ESPN*
SNP_A-2090773	rs11152920	SNP_A-2155415	rs783403	7	48809712	50903934	2.09	-
SNP_A-2152234	rs17238567	SNP_A-1980966	rs1366419	5	20964216	22916852	1.95	-
SNP_A-2013197	rs1912515	SNP_A-4224094	rs11018855	11	88287451	89835267	1.55	-
SNP_A-2303650	rs8105809	SNP_A-2059039	rs3745836	19	55123464	56652592	1.53	-
SNP_A-2194601	rs1447595	SNP_A-1974496	rs10513030	3	135476532	136877493	1.40	-
SNP_A-4212479	rs2159579	SNP_A-2215144	rs7800245	7	84845546	86103733	1.26	-
SNP_A-1993002	rs10503951	SNP_A-4216078	rs6996639	8	33665680	34843712	1.18	-
SNP_A-2146287	rs1124531	SNP_A-1860565	rs891974	5	169773687	170902780	1.13	-
SNP_A-2206226	rs9302387	SNP_A-2138415	rs11642765	16	20478724	21582734	1.10	-
SNP_A-4227577	rs308409	SNP_A-2214677	rs3113377	4	123752692	124834671	1.08	-
SNP_A-4195575	rs16840977	SNP_A-4239672	rs277638	3	99034331	100079447	1.05	-
SNP_A-4203661	rs1631550	SNP_A-2048940	rs2979684	8	23786381	24817441	1.03	-
SNP_A-1826210	rs7118543	SNP_A-2013513	rs4483549	11	89949097	90955972	1.01	-

Genomic position were determined using the UCSC Genome Browser website (http://genome-euro.ucsc.edu/index.html, hg19).

[1]Department of Otorhinolaryngology, Hearing and Genes, Radboud university medical center, Nijmegen, the Netherlands, [2]Radboud Institute for Molecular Life Sciences, Radboud university medical center, Nijmegen, the Netherlands, [3]Department of Otorhinolaryngology Head & Neck Surgery, College of Medicine, University of Maryland, Baltimore, MD, USA, [4]COMSATS Institute of Information Technology, Park Road, Islamabad, Pakistan, [5]Department of Physiology, College of Medicine, University of Kentucky, Lexington, KY, USA,[6]Institute of Human Genetics, Helmholtz Zentrum München, German Research Center for Environmental Health, Neuherberg, Germany, [7]Developmental Biology, Cincinnati Children's Hospital Medical Center, Cincinnati, OH, USA, [8]Al-Nafees Medical College & Hospital, Isra University, Islamabad, Pakistan, [9]Department of Human Genetics, Radboud university medical center, Nijmegen, The Netherlands, [10]Department of Otorhinolaryngology/Head and Neck Surgery, University of Groningen, University Medical Center Groningen, Groningen, the Netherlands, [11]Department of Clinical Genetics, University of Groningen, University Medical Center Groningen, Groningen, the Netherlands.

Chapter 4

Novel and recurrent *CIB2* variants, associated with non-syndromic deafness, do not affect calcium buffering and localization in hair cells

Celia Zazo Seco[1,2,*], Arnaud P. Giese[3,*], Sobia Shafique[4,*], Margit Schraders[1,2], Anne M. M. Oonk[1], Mike Grossheim[5], Jaap Oostrik[1,2], Tim Strom[6], Rashmi Hegde[7], Erwin van Wijk[1,2], Gregory I. Frolenkov[5], Maleeha Azam[4], Helger G. Yntema[2,9], Rolien H. Free[10], Saima Riazuddin[3], Joke B.G.M. Verheij[11], Ronald J. Admiraa[11], Raheel Qamar[4,8,#], Zubair M. Ahmed[3,#], Hannie Kremer[1,2,9,#]

*,#Authors contributed equally

European journal of human genetics 2015 Jul 15. doi: 10.1038/ejhg.2015.157

ABSTRACT

Variants in *CIB2* can underlie either Usher syndrome type I (USH1J) or nonsyndromic hearing impairment (DFNB48). Here, a novel homozygous missense variant c.196C>T and compound heterozygous variants, c.[97C>T];[196C>T], were found respectively in two unrelated families of Dutch origin. Besides, the previously reported c.272T>C functional missense variant in *CIB2* was identified in two families of Pakistani origin. The missense variants are demonstrated not to affect subcellular localization of *CIB2* in vestibular hair cells in ex vivo expression experiments. Furthermore, these variants do not affect the ATP-induced calcium responses in COS-7 cells. However, based on the residues affected, the variants are suggested to alter αIIβ integrin binding. Hearing impairment was nonsyndromic in all four families. However, deafness segregating with the c.272T>C variant in one Pakistani family is remarkably less severe than that in all other families with this mutation. Our results contribute to the insight in genotype-phenotype correlations of *CIB2* mutations.

INTRODUCTION

Genetic defects are important in the etiology of sensorineural hearing impairment (HI) especially in the early onset cases.[1] Hereditary sensorineural HI is nonsyndromic (NSHI) in the majority of early onset cases but part of these will be diagnosed with syndromic HI later in life. Usher syndrome is the most common sensorineural HI syndrome with a prevalence of 3-6.[2] per 100,000 and the first symptoms of retinitis pigmentosa most often in the first or second decade of life.[2] Vestibular defects occur in part of the subjects with Usher syndrome and lead to delayed motor development.[2] To date, there are 13 loci and 10 genes known to be involved in the three clinical types of Usher syndrome.[3-6] Mutations in six of these genes, *MYO7A*[7-10], *CDH23*[11,12], *PCDH15*[13,14], *WHRN*[15,16], *SANS*[17] and *CIB2*[4], can lead to either Usher syndrome or autosomal recessive NSHI (arNSHI). Mutations in *USH2A* can lead to either Usher syndrome or nonsyndromic retinitis pigmentosa.[18,19]

CIB2 belongs to a family of calcium and integrin-binding proteins. CIB2 contains three predicted EF hand domains, of which only the two most C-terminal EF hands are able to bind Ca^{2+}.[20,21] Upon Ca^{2+}-binding, conformational changes occur which create a hydrophobic pocket that mediates the interaction with the C-terminal tail of integrin.[22,23] *CIB2* has a broad expression pattern that includes the inner ear where it is immunohistochemically detected in supporting cells and in stereocilia and cuticular plate of hair cells in the cochlea and the vestibular system.[4] Based on the functional impairment of hair cells in *Cib2* zebrafish morphants, it has been suggested that Cib2 is important for Ca^{2+} homeostasis in sensory hair cells, and that loss of Cib2 function might affect processes like mechanotransduction, adaptation, electromotility, and synaptic transmission.[4,24] Similarly, through functional studies in *Drosophila*, CIB2 was found to be essential for adequate phototransduction and maintenance of photoreceptor cells.[4] Furthermore, CIB2 has been demonstrated to be integrated into the Usher interactome via the association with whirlin and myosin VIIa.[4]

In this study, we present molecular identity of functional variants in *CIB2* in NSHI affected families of Dutch and Pakistani origin (Figure 1). One is the recurrent c.272T>C *CIB2* missense variant[4] present homozygously in two Pakistani families with moderate-to-severe and profound prelingual arNSHI, respectively. The second is the novel c.196C>T missense variant found homozygously and in compound heterozygous state with the c.97C>T nonsense variant in two families of Dutch origin with profound arNSHI. We analyzed the effect of these deafness-associated alleles on the expression, subcellular localization and calcium binding abilities of CIB2.

MATERIALS AND METHODS

Patients and their clinical and audiological evaluation

The current study conformed to the tenets of the Helsinki declaration. Informed consent was obtained from all participating subjects of two families from Pakistan W09-1575 and W09-1600 (Figure 1A) and from the Dutch families W06-0987 and 07-1069 (Figure 1B and 1C). This study was approved by the Department of Biosciences Ethics Review Board of the COMSATS Institute of Information Technology, Islamabad, Pakistan and the local ethics committee of the Radboud university medical center, Nijmegen, the Netherlands.

In all four families, other possible causes of HI, previous ear surgery and external ear deformities were excluded by a general ENT examination. Additionally, a computed tomography (CT) scan of the temporal bone was performed for the affected individual of family W06-0987 and one affected member (II.1) of family 07-1069 in order to exclude possible anatomical causes of HI. Pure tone audiometry was performed to determine hearing thresholds at 0.25, 0.5, 1, 2, 4 and 8 kHz. Both air conduction and bone conduction thresholds were obtained to exclude a conductive hearing loss. Brainstem evoked response audiometry (BERA) was performed for the affected individual of family W06-0987 and individual II.1 of family 07-1069 according to current standards. Visual Reinforcement Audiometry (VRA) was performed before the age of three years in the affected individual of family W06-0987.[25] GraphPad Prism 5.00 (GraphPad, San Diego, Ca, USA) was employed for linear regression analysis to evaluate whether or not HI in family W06-0987 was progressive. Classification of the HI is in accordance with the GENDEAF guidelines (Hereditary Hearing Loss Homepage). For families W06-0987 and 07-1069 vestibular function was assessed by electronystagmography, rotatory tests and calorisation as previously described.[26] To evaluate retinal involvement in the disease, fundoscopy was performed. In addition, renal, liver and thyroid functions were assessed in family W06-0987.

Genetic studies and functional evaluation of variants

Genomic DNA was isolated from peripheral-blood lymphocytes by standard procedures. DNA of individual II.3 from family W06-0987 was genotyped with the Affymetrix GeneChip Human Mapping 250K Nsp SNP array according to the manufacturer's protocol. Genotype calling and calculation of the regions of homozygosity was performed with the Genotyping Console software (Affymetrix) and default settings. For families W09-1575 (IV:2, IV:6,

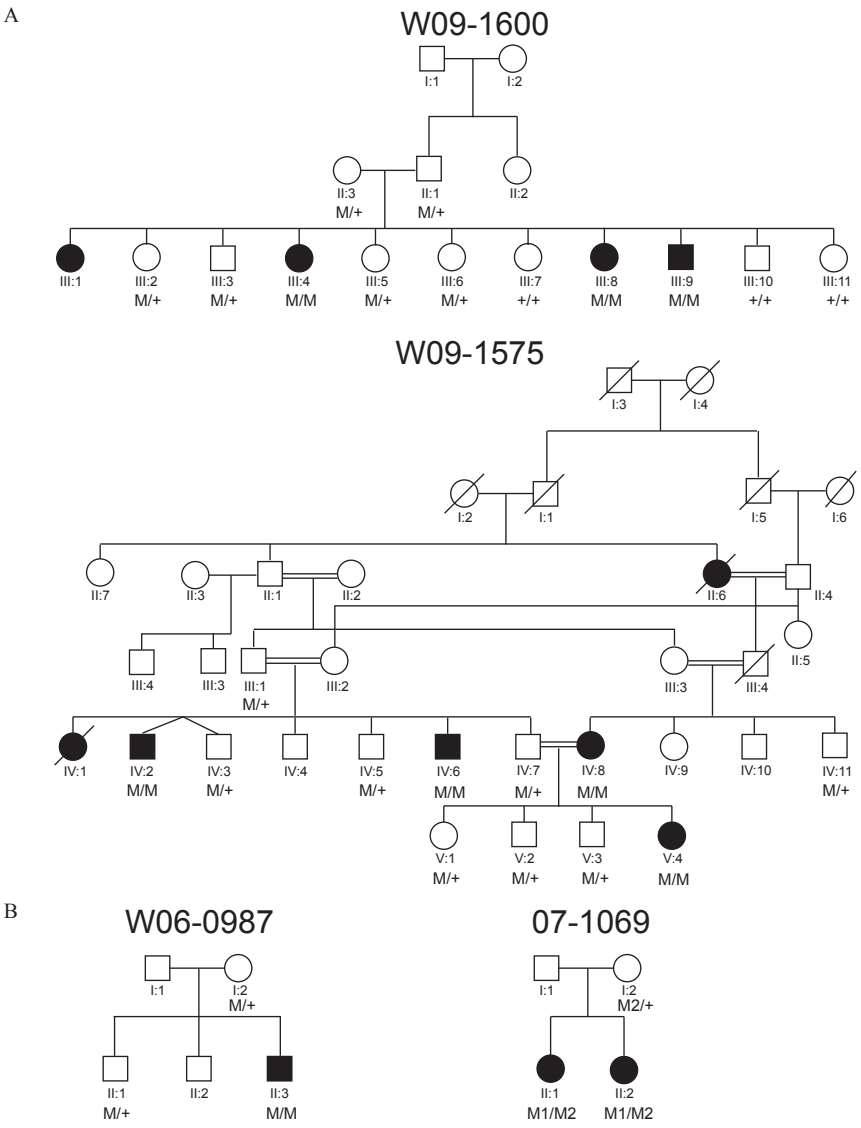

Figure 1. Pedigrees and segregation of *CIB2* variants

A) Pedigrees and segregation of the c.272T>C variant in the consanguineous Pakistani families W09-1575 and W09-1600. "M" represents the mutated allele c.272C and "+" the wild type allele, c.272T.**B)** Pedigree and segregation of c.196C>T variant in family W06-0987 of Dutch origin. "M" represents the mutated allele c.196T and "+" the wild type allele, c.196C. **C)** Pedigree and segregation of c.97C>T, indicated as M1, and c.196C>T, indicated as M2, variants in family 07-1069 of Dutch origin. The "+" represents the wild type allele, c.97C. Individual II.1 underwent WES.

IV:8, V:4) and W09-1600 (III:1, III:4, III:8, III:9), genotyping with Illumina HumanOmniExpress 700K arrays was performed. Homozygous regions were determined using the online tool Homozygosity Mapper with default settings. All exons of *CIB2* including exon-intron boundaries were analysed for the presence of variants as previously described4 employing NM_006383.2 as reference sequence. Mutation analysis of *TRIOBP* was performed by Sanger sequencing.[27] Primer sequences are available upon request. As a reference sequence NM_001039141.2 and NM_138632.2 were employed.

For affected member II.1 of family 07-1069, mutations and the common deletion in the *GJB2* associated with DFNB1 have been excluded by Sanger sequencing and allele-specific PCR. Other known mutations in genes associated with severe congenital hearing loss i.e. *CDH23, MYO7A, PCDH15, USH1C, USH1G, USH2A, GPR98, USH3A, DFNB31*, were excluded by using the Asper biotech array (version 6.0 with 612 variants) for Usher syndrome (Asper biotech, Tartu, Estonia). Subsequently, variants in a set of 104 deafness genes (URL Gene list) were identified by whole exome sequencing (WES) followed by data filtering and interpretation. Library preparation was performed using 3 µg of purified DNA of affected member II.1 of family 07-1069. For enrichment the SOLiD optimized Sure Select All Human Exon Kit (50 Mb; Agilent Technologies, Santa Clara, CA, USA) was employed, followed by sequencing on 5500XL sequencers (Life Technologies, Carlsbad, CA, USA). Sequence reads were aligned to the human genome (hg19) using Lifescope v2.1 (Life Technologies), followed by variant calling on the aligned sequence. Variants were annotated using a custom analysis pipeline.[28] The criteria to filter and interpret variants in the set of 104 genes known to be associated with deafness was as described previously.[28,29] An in-house-developed graphical user interface was used for data visualization and filtering within the respective gene set.

Molecular modeling, expression of *CIB2* in hair cells by Helios gene gun transfection and calcium response assays of DsRed-tagged $CIB2^{Phe91Ser}$, $CIB2^{Arg66Trp}$ and $CIB2^{WT}$ were performed as previously described.[4]

All variants identified in this study were submitted to the Leiden Open Variant Database with the following IDs: c.97C>T, #05182; c.196C>T, #05182; c.272T>C, #05182.

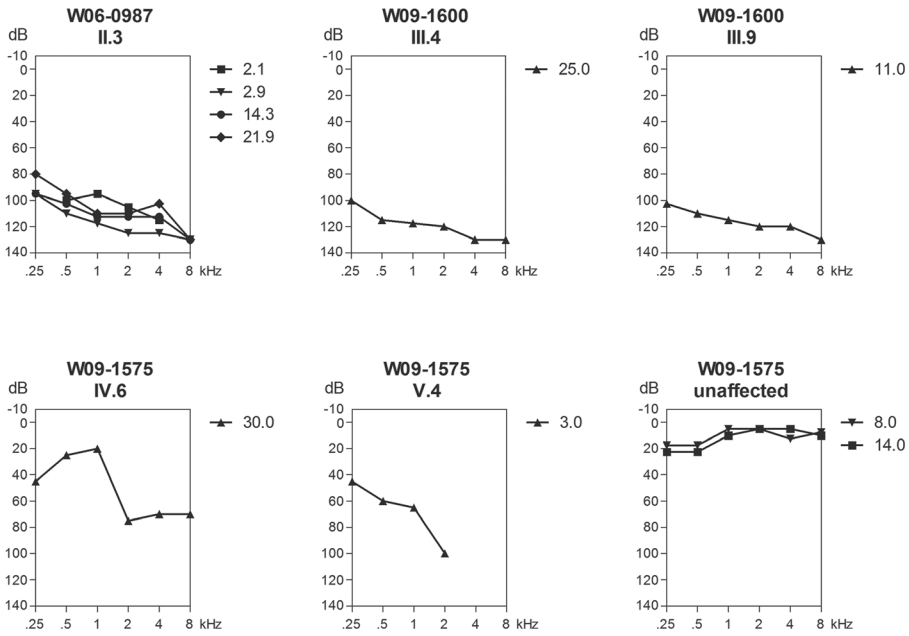

Figure 2. Audiograms of affected individuals of families W06-0987, W09-1575 and W09-1600

Longitudinal binaural mean air-conduction pure tone thresholds are shown of the hearing impaired member of family W06-0987. Binaural mean air-conduction pure tone thresholds are shown of affected members III.4 and III.9 of family W09-1600, individual V.4 and two unaffected members of family W09-1575 (IV:7 at 14 years of age and V:3 at 8 years of age). For individual IV.6 of W09-1575, the air-conduction thresholds of the left ear are depicted. Age (years) at which measurements are performed are indicated with a symbol key.

RESULTS

Patient evaluation

For none of the hearing-impaired individuals additional abnormalities were found during ENT examination. Affected individuals of Pakistani family W09-1575 (Figure 1A) were diagnosed with prelingual, bilateral, moderate-to-severe sensorineural HI (Figure 2). In another Pakistani family W09-1600 the HI was profound, prelingual, bilateral and sensorineural (Figure 2). There were no symptoms of retinal degeneration in the hearing impaired individuals of these two families. The ages of the affected individuals at last visit were 5, 13, 24 and 29 years for family W09-1575 and 11, 15, 25 and 32 years for family W09-1600. However, no ophthalmologic examinations could be performed and therefore

subclinical retinal abnormalities cannot be excluded. Individual II.3 of Dutch family W06-0987 (Figure 1B) presented with prelingual HI, probably congenital but diagnosed by a hearing test at nine months of age. BERA performed before the age of one year demonstrated a response at 80 dB Hl. VRA and pure tone audiometry revealed bilateral, profound sensorineural HI with a stable character and a gently downsloping audiogram configuration (Figure 2). A CT scan did not show any structural abnormalities of the temporal bone. Renal, liver and thyroid function were found to be normal. Vestibular examination showed a slight hyperreflexia. Ophthalmologic examination including fundoscopy at the age of 24 years revealed no abnormalities except for bilateral epicanthic folds. Both individuals of Dutch family 07-1069 (Figure 1C) were diagnosed with congenital, profound sensorineural hearing loss since they both failed the neonatal hearing screening. During BERA no responses were found for both individuals. Vestibular examination in II.1 displayed excitable vestibules with normal responses on the right and an unilateral weakness at the left vestibule. This was examined after cochlear implantation at the left ear. A CT scan in individual II.1 displayed no temporal bone abnormalities. Also, ophthalmologic and renal examination in the same child revealed no abnormalities. Both hearing impaired members of family 07-1069 received a cochlear implant with good results. At their last visit in the clinic at the ages of 7 (II.1) and 4 years (II.2), the affected sibs did not have any signs night blindness as an early symptom of retinitis pigmentosa.

Genetic analyses

As a first step in the genetic analyses of the presented families, functional variants in *GJB2* were excluded through Sanger sequencing and allele specific PCR was employed to exclude the common GJB2/GJB6 deletion. Homozygosity mapping was subsequently performed in families W06-0987, W09-1575 and W09-1600 as part of a larger project directed towards the identification of genetic defects underlying sensorineural HI in consanguineous Pakistani families and non-consanguineous families of the Netherlands.[27,30] In the only affected individual II.3 of family W06-0987, homozygosity mapping revealed nine homozygous regions larger than 1 Mb (Table 1). The second large homozygous region harbored *TRIOBP*, the gene associated with the known arNSHI type DFNB28.[31,32] No variants with a predicted functional effect were identified in *TRIOBP* by Sanger sequencing of the exons and exon-intron boundaries. The largest homozygous region of 16 Mb (SNP_A-1814998 ; SNP_A- A-1821537) contained the *CIB2* gene, associated with DFNB48 and USH1J by allelic functional variants.[4]

Table 1. Homozygosity mapping in families W06-0987, W09-1575 and W09-1600

# Family	Start SNP	End SNP	Chr.	Genome Browser (Feb. 2009)	Size (Mb)	Known arNSHI gene
W06-0987	SNP_A-1814998	SNP_A-1821537	15	chr15:68,705,697-84,705,110	16.00	*CIB2*
	SNP_A-1920225	SNP_A-1945927	22	chr22:36,758,849-40,089,893	3.33	*TRIOBP*
	SNP_A-2032497	SNP_A-2091266	2	chr2:82,534,958-85,096,481	2.56	-
	SNP_A-2033819	SNP_A-2145805	14	chr14:82,354,342-84,798,493	2.44	-
	SNP_A-2210335	SNP_A-1965012	2	chr2:135,471,415-137,880,893	2.41	-
	SNP_A-2277801	SNP_A-1876469	9	chr9:94,682,964-96,757,868	2.07	-
	SNP_A-2029422	SNP_A-4193502	1	chr1:58,894,050-60,899,424	2.01	-
	SNP_A-1856228	SNP_A-2043311	8	chr8:50,258,845-52,029,738	1.77	-
	SNP_A-1934688	SNP_A-4209616	3	chr3:102,434,617-103,440,905	1.01	-
W09-1575	rs4438265	rs12912915	15	chr15:70,826,268-92,013,118	21.19	*CIB2*
W09-1600	rs8036698	rs2732151	15	chr15:68,716,776-84,203,685	15.49	*CIB2*

Homozygous regions larger than 1 Mb in the affected individual of family W06-0987 and homozygous regions larger than 3 Mb shared by affected individuals in the consanguineous families W09-1575 and W09-1600.

Genotyped affected individuals of the consanguineous family W09-1575 shared only one homozygous region larger than 3 Mb which overlapped with the only shared homozygous region larger than 3 Mb in genotyped affected individuals of family W09-1600. *CIB2* is located in the overlapping chromosomal segment (Table 1). In family W09-1575, an additional homozygous region of 4 Mb (rs1516570; rs12186082) was identified on chromosome 3. However, the affected individuals were homozygous for different alleles. Therefore this region was not further analyzed.

Mutation analysis of *CIB2* in the affected individual of family W06-0987 revealed a homozygous variant c.196C>T that is predicted to cause a substitution of a tryptophan for an arginine (p.(Arg66Trp)) (Supplemental figure 1A). The mother and unaffected sibling were carriers of this variant (Figure 1B). *CIB2* c.196C>T affects all known CIB2 protein isoforms except isoform CIB2-006 as indicated in ENSEMBL (GRCh38) and in the Genome Browser (GRCh37) (Supplemental figure 2).[4] The c.196C>T variant is not present in the NCBI dbSNP138 database, the NHLBI Exome Sequencing Project (Exome Variant Server), the 1000 Genomes Project and the Nijmegen exome database (5031 exomes). In addition, c.196C>T is predicted to have a deleterious effect on protein function according to Polymorphism phenotyping version 2 (Polyphen2) with a score of 0.98 (range 0-1, 0 being benign and 1 being probably damaging), mutation taster with a score of 0.99 (range 0-1, 0 being benign and 1 being

probably damaging) and Sorting Intolerant From Tolerant (SIFT) with a score of 0 (≤ 0.05 predicted to be damaging, >0.05 predicted to be tolerated). The c.196C>T missense variant affects the codon for amino acid residue Arg66 that is moderately conserved with a score of 4 (9; conserved, 1; variable) according to the ConSeq online bioinformatic tool. The arginine residue at position 66 is conserved across the CIB2 orthologs and CIB4 paralogs in a wide range of species. In the paralogs CIB1 and CIB3 and several of the CIB2 orthologs, lysine is found at this position that is, like arginine, a positively charged amino acid (Supplemental figure 1B).

Sanger sequencing of *CIB2* in families W09-1575 and W09-1600 revealed a homozygous missense variant c.272T>C (Supplemental figure 1A) which is predicted to substitute a serine for a phenylalanine. This functional variant was previously described to be a founder mutation and a common cause of arNSHI in the Pakistani population.4 However, in contrast to previously reported Pakistani families homozygous for the variant c.272T>C, the affected individuals of family W09-1575 had moderate-to-severe sensorineural HI (Figure 2).

For family 07-1069, DNA diagnostics was requested after the diagnosis of profound sensorineural HI. Known functional variants in genes for Usher syndrome were excluded. Subsequent analysis of 104 deafness genes in individual II.1 of family 07-1069 revealed only two likely functional variants: c.196C>T and c.97C>T in *CIB2*. The latter is a nonsense variant of the codon for Arg33 (p.(Arg33*)) and the former variant was already detected homozygously in family W06-0987). The presence of the variants was confirmed by Sanger sequencing in both II.1 and her affected sister, II.2. They inherited c.97C>T from their unaffected mother (Figure 1C), indicating that the variants in the two affected children are present in the compound heterozygous state (c.[97C>T];[196C>T]). Variant c.97C>T is a rare SNP, rs201845656, found three times in 8586 alleles in the European American population (allele frequency of 0,03%) in EVS and eight times in the Nijmegen exome database (n=5031, allele frequency of 0,08%). The c.97C>T variant affects the CIB2 isoforms B and C but not isoforms A and CIB2-006 (Supplemental figure 2).4 The c.97C>T variant is predicted to result in nonsense-mediated decay, since it introduces a premature termination codon more than 54 bp upstream of the last intron.33

The c.196C>T and c.272T>C variants do not affect targeting of CIB2 to the stereocilia tip of vestibular hair cells

CIB2 is localized along the stereocilia of cochlear and vestibular hair cells as well as at the stereocilia tips.[4] The mechanism that permits the targeting of

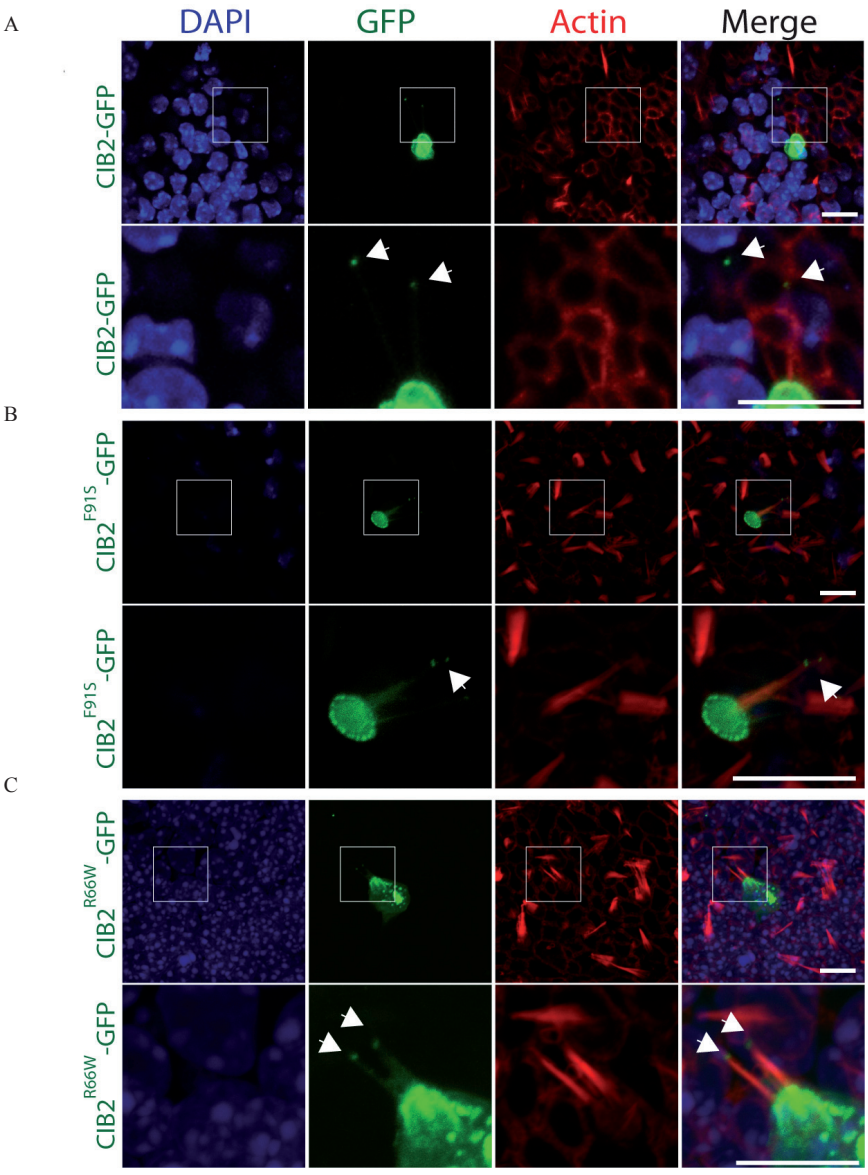

Figure 3. The c.196C>T variant does not affect the localization of CIB2 in hair cells of the vestibular system

(A,B,C) $CIB2^{WT}$-GFP, $CIB2^{Arg66Trp}$-GFP and $CIB2^{Phe91Ser}$-GFP constructs were overexpressed in the P2 vestibular system of mouse using the gene gun technology. The $CIB2^{WT}$-GFP variant is targeted to the tip of the stereocilia (green, arrows) and accumulates in the cuticular plate of sensory hair cells **(A)**. The localization of CIB2 is not disrupted when c.196C>T and c.272T>C variants were introduced **(B, C)**. Phalloidin labeling is in red and DAPI staining in blue. Scale bar: 10µm.

CIB2 to the region of the mechanotransduction machinery is still unclear. We transiently overexpressed a $CIB2^{Arg66Trp\text{-}GFP}$ and $CIB2^{Phe91Ser\text{-}GFP}$ constructs in P2 vestibular system explants in order to investigate their effect on CIB2 targeting. We found that, like wild type control ($CIB2^{WT}$-GFP), $CIB2^{Arg66Trp\text{-}GFP}$, as well as $CIB2^{Phe91Ser\text{-}GFP}$, accumulate in the cuticular plate, along and at the tip of the stereocilia of vestibular hair cells (Figure 3). These results suggest that, at least *ex vivo*, the arNSHI associated variants do not affect CIB2 targeting in vestibular sensory hair cells (Figure 3).

The c.196C>T and c.272T>C variants do not affect the calcium buffering property of CIB2

To test the calcium buffering property of $CIB2^{Arg66Trp}$ variant, we performed a ratiometric Ca^{2+} imaging assay on transiently transfected COS-7 cells and measured ATP-induced inositol triphosphate (IP_3)-dependent calcium responses. Cells overexpressing DsRed-$CIB2^{WT}$ had a significant decrease in ATP-induced Ca^{2+} release as compared to mock-transfected cells (Figure 4C). The calcium responses of cells transfected with DsRed-$CIB2^{Phe91Ser}$ or DsRed-$CIB2^{Arg66Trp}$ constructs were comparable to cells transfected with a DsRed-$CIB2^{WT}$ construct showing that the amino acid substitutions do not affect the calcium-buffering ability of CIB2 (Figure 4C).

Molecular modeling suggests impaired interaction of CIB2 with effector molecules due to the c.196C>T and c.272T>C variants

When modeled using the known crystal structure of CIB1 as backbone[4,21,34] in CIB2 the p.Arg66 maps to the N-terminal domain of CIB2 within a region that has been implicated in the interaction of CIB protein with the carboxy terminal, unstructured, negatively charged tail of αIIβ integrin. CIB1 is involved in the activation of integrin αIIβ3. It is thought that hydrophobic interactions between the αIIβ helix and the C-terminal domain of CIB1 primarily drive the interaction, with the N-domain involved in electrostatic stabilizing interactions with the negatively charged unstructured C-terminal tail of αIIβ (residues P_{998}PLEEDDEEGQ$_{1008}$). Implicated in this interaction are residues p.Arg33 and p.Lys65 of CIB1. By structure-based sequence alignment this corresponds to p.Arg33 and p.Arg66 of CIB2. Therefore, an amino acid change at p.Arg66 would likely destabilize the interaction with integrin and thus attenuate integrin activation (Figure 4 A, B).[22,34] In consistence with our calcium imaging data, Arg66 is located away from the Ca^{2+} binding pockets[20,21], and thus the substitution of tryptophan for arginine at position 66 is predicted not to alter

calcium buffering abilities of CIB2. Similarly, the substitution of serine for phenylalanine at position 91 is also predicted to weaken the interaction of CIB2 with αIIβ integrin.[4]

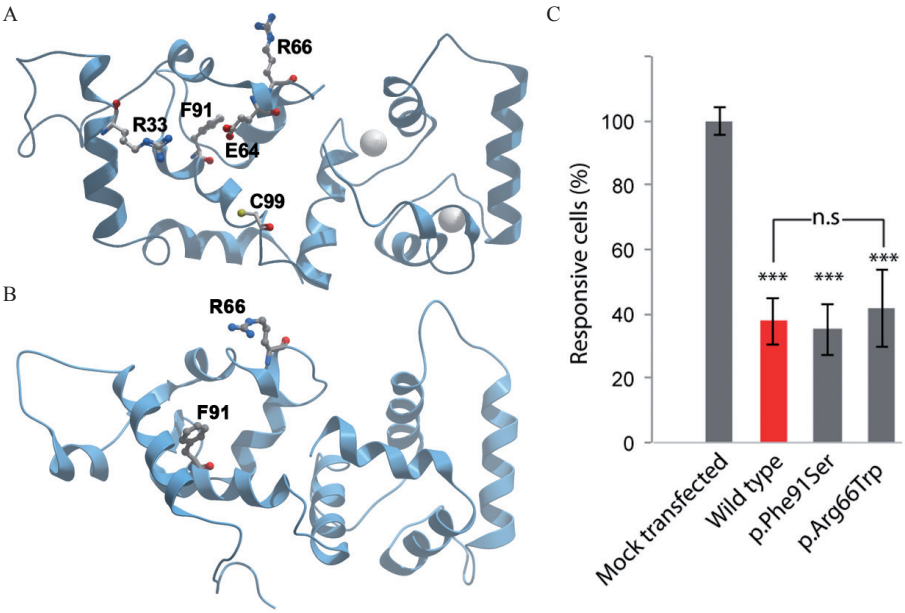

Figure 4. (A, B) Molecular modeling of CIB2

The p.(Arg66Trp) and p.(Phe91Ser) missense mutations in CIB2, associated with arNSHI are predicted to alter the interaction of CIB2 with effector molecules. For molecular modeling, we used **(A)** the NMR structure of CIB1 bound to αIIβ integrin peptide and **(B)** the Protein Data Bank (PDB) 1XO5 crystal structure of Ca^{2+}-CIB1. Two Ca^{2+} ions are represented by grey spheres.

(C) The c.196C>T variant does not affect the calcium buffering ability of CIB2

COS-7 cells were transfected with DsRed-$CIB2^{WT}$, DsRed-$CIB2^{Arg66Trp}$ and DsRed-$CIB2^{Phe91Ser}$ constructs. The increase of cytosolic calcium concentration in response to the application of 1 μM of ATP was measured with ratiometric Fura-2 imaging as previously described.[4] The ATP-evoked calcium responses decreased when DsRed-$CIB2^{WT}$ (Red bar) is overexpressed due to the ability of CIB2 to bind and buffer Calcium. The p.(Phe91Ser) and p.(Arg66Trp) substitutions did not alter calcium buffering ability of CIB2 (grey bars on the right). Data are normalized to the average response of mock-transfected cells and are shown as mean ± s.e.m. ***P < 0.001; **P < 0.01; *P < 0.05.

DISCUSSION

In this study we present a new homozygous functional variant, c.97C>T, and a compound heterozygous variants, c.[97C>T];[196C>T] in *CIB2* underlying DFNB48 arNSHI in an isolated case (W06-0987) and in a family (07-1609), respectively, of Dutch origin. Additionally, we report two consanguineous families of Pakistani origin (W09-1575 and W09-1600) with arNSHI carrying the previously described and recurrent CIB2 variant, c.272T>C. Due to this founder variant, defects in *CIB2* are the major cause of arNSHI in Pakistan.[4]

DFNB48 and USH1J are caused by allelic *CIB2* variants.[4] Patients of the so far only family with USH1J present with prelingual, bilateral profound HI. Retinitis pigmentosa in the USH1J family progressed from mild to complete vision loss and was detected as early as 10 years of age. Besides that, vestibular dysfunction, later confirmed by ENG, was suspected since there was a delayed onset of ambulation.[35] The DFNB48 phenotype found in three of the four families reported in the present study is consistent with the previously described DFNB48 phenotype[4,36], severe to profound, prelingual bilateral HI without signs of retinitis pigmentosa and vestibular dysfunction. However, the HI in family W09-1575 with the recurrent homozygous variant, is less severe. The age at last evaluation of affected individuals in this family, who were diagnosed in early childhood, varies from 5 to 29 years and there are no signs of progression to profound HI. Genetic modifying factors might contribute to the less severe HI as compared to that in the previously descriDFNB48 families.[4] Therefore, it is worthwhile to perform more extensive genotyping in this family in order to identify candidate modifying DNA variants for *CIB2* defects which may provide insight into pathogenic mechanisms.

Interestingly, the c.196C>T variant associated with arNSHI is located very close to the c.192G>C variant associated with the USH1J phenotype.[4] At their most recent evaluation at the ages of 24 years (family W06-0987) and seven and four years (family 07-1069), the hearing impaired individuals with the c.196C>T variant in the homozygous or compound heterozygous state did not have any symptoms of early retinitis pigmentosa. Since electroretinography could not be performed, we cannot exclude an early stage of retinitis pigmentosa in these individuals. However, classical Usher syndrome type I as diagnosed in the USH1J family with the c.192G>C variant in the homozygous state[4,35] is excluded in the present families because of absence of vestibular areflexia and for family W06-0987 in addition because of lack of symptoms of retinal degeneration at 24 years of age.[2] The difference in phenotypic effect of the

c.192G>C (p.(Glu64Asp)) and c.196C>T (p.(Arg66Trp)) variants in *CIB2* might be the result of a larger negative effect of the former mutation because of loss of a salt bridge between residues Arg33 and Glu64 which is formed in the absence of integrin.[4] The associations of CIB2 with the Usher proteins myosin VIIa (USH1B) and whirlin (USH2D)[16] are candidates for being affected differently by the two mutations but so far the region(s) of CIB2 that mediate(s) these direct or indirect interactions is still elusive. The identification of additional USH1J and DFNB48 families can shed light on the underlying reasons for the phenotypic differences, DFNB48 and USH1J, of mutations that affect neighboring amino acid residues. Phenotypes varying from arNSHI, Usher syndrome type I and hearing impairment combined with a variable age of onset of retinitis pigmentosa or asymptomatic retinitis pigmentosa-like findings has previously been described for functional variants in *CDH23*.[37] Screening of *CIB2* in more families in different populations will add more information on the frequency of functional variants of *CIB2* and will contribute to define phenotype-genotype correlations of *CIB2* variants.

Acknowledgements

We are grateful to the families for their participation in this study. We thank Saskia van der Velde-Visser for excellent technical assistance. This work was financially supported by grants from The Oticon Foundation [09-3742, to H.K.], ZonMW [40-00812-98-09047, to H.K; 016.136.088, to M.S.; 016.136.091 to E.v.W. and 40-42900-98-1006 to E.v.W.]. This study was partially sponsored by the National Institute on Deafness and Other Communication Disorders (NIDCD/NIH) research grants [R01 DC012564 to Z.M.A. and R01 DC011803 to S.R.]. Part of this work was supported by a core grant from the COMSATS Institute of Information Technology.

WEB RESOURCES

1000 Genomes Project: http://www.1000genomes.org/
Conseq: http://conseq.tau.ac.il/
ENSEMBL: http://www.ensembl.org/Homo_sapiens/Info/Index
Exome variant server: EVS, http://evs.gs.washington.edu/EVS/
Genome browser: http://genome-euro.ucsc.edu
Gene list: https://www.radboudumc.nl/Informatievoorverwijzers/Genoomdiagnostiek/en/Pages/Hearingimpairment.aspx)
Hereditary Hearing Loss Homepage: http://hereditaryhearingloss.org/
Homozygosity Mapper: www.homozygositymapper.org
Interpro: http://www.ebi.ac.uk/interpro/
LOVD: http://databases.lovd.nl/shared/variants/0000053133#05182; http://databases.lovd.nl/shared/variants/0000053131#05182; http://databases.lovd.nl/shared/variants/0000053132#05182
Mutation Taster: www.mutationtaster.org
Polymorphism phenotyping 2: Polyphen2 , http://genetics.bwh.harvard.edu/pph2/
Sorting Intolerant From Tolerant: SIFT, http://sift.jcvi.org/

REFERENCES

1. Mehl AL, Thomson V: The Colorado newborn hearing screening project, 1992-1999: on the threshold of effective population-based universal newborn hearing screening. Pediatrics 2002; 109: E7.
2. Cohen M, Bitner-Glindzicz M, Luxon L: The changing face of Usher syndrome: clinical implications. Int J Audiol 2007; 46: 82-93.
3. Millan JM, Aller E, Jaijo T, Blanco-Kelly F, Gimenez-Pardo A, Ayuso C: An update on the genetics of usher syndrome. J Ophthalmol 2011; 2011: 417217.
4. Riazuddin S, Belyantseva IA, Giese AP et al: Alterations of the CIB2 calcium- and integrin-binding protein cause Usher syndrome type 1J and nonsyndromic deafness DFNB48. Nat Genet 2012; 44: 1265-1271.
5. Jaworek TJ, Bhatti R, Latief N, Khan SN, Riazuddin S, Ahmed ZM: USH1K, a novel locus for type I Usher syndrome, maps to chromosome 10p11.21-q21.1. J Hum Genet 2012; 57: 633-637.
6. Cosgrove D, Zallocchi M: Usher protein functions in hair cells and photoreceptors. Int J Biochem Cell Biol 2014; 46: 80-89.
7. Weil D, Blanchard S, Kaplan J et al: Defective myosin VIIA gene responsible for Usher syndrome type 1B. Nature 1995; 374: 60-61.
8. Liu XZ, Walsh J, Mburu P et al: Mutations in the myosin VIIA gene cause non-syndromic recessive deafness. Nat Genet 1997; 16: 188-190.
9. Weil D, Kussel P, Blanchard S et al: The autosomal recessive isolated deafness, DFNB2, and the Usher 1B syndrome are allelic defects of the myosin-VIIA gene. Nat Genet 1997; 16: 191-193.
10. Liu XZ, Walsh J, Tamagawa Y et al: Autosomal dominant non-syndromic deafness caused by a mutation in the myosin VIIA gene. Nat Genet 1997; 17: 268-269.
11. Wayne S, Der Kaloustian VM, Schloss M et al: Localization of the Usher syndrome type ID gene (Ush1D) to chromosome 10. Hum Mol Genet 1996; 5: 1689-1692.
12. Bork JM, Peters LM, Riazuddin S et al: Usher syndrome 1D and nonsyndromic autosomal recessive deafness DFNB12 are caused by allelic mutations of the novel cadherin-like gene CDH23. Am J Hum Genet 2001; 68: 26-37.
13. Ahmed ZM, Riazuddin S, Bernstein SL et al: Mutations of the protocadherin gene PCDH15 cause Usher syndrome type 1F. Am J Hum Genet 2001; 69: 25-34.
14. Ahmed ZM, Riazuddin S, Ahmad J et al: PCDH15 is expressed in the neurosensory epithelium of the eye and ear and mutant alleles are responsible for both USH1F and DFNB23. Hum Mol Genet 2003; 12: 3215-3223.
15. Mburu P, Mustapha M, Varela A et al: Defects in whirlin, a PDZ domain molecule involved in stereocilia elongation, cause deafness in the whirler mouse and families with DFNB31. Nat Genet 2003; 34: 421-428.

16. Ebermann I, Scholl HP, Charbel Issa P et al: A novel gene for Usher syndrome type 2: mutations in the long isoform of whirlin are associated with retinitis pigmentosa and sensorineural hearing loss. Hum Genet 2007; 121: 203-211.
17. Oonk AM, van Huet RA, Leijendeckers JM et al: Nonsyndromic Hearing Loss Caused by USH1G Mutations: Widening the USH1G Disease Spectrum. Ear Hear 2014.
18. Eudy JD, Weston MD, Yao S et al: Mutation of a gene encoding a protein with extracellular matrix motifs in Usher syndrome type IIa. Science 1998; 280: 1753-1757.
19. Rivolta C, Sweklo EA, Berson EL, Dryja TP: Missense mutation in the USH2A gene: association with recessive retinitis pigmentosa without hearing loss. Am J Hum Genet 2000; 66: 1975-1978.
20. Blamey CJ, Ceccarelli C, Naik UP, Bahnson BJ: The crystal structure of calcium- and integrin-binding protein 1: insights into redox regulated functions. Protein Sci 2005; 14: 1214-1221.
21. Gentry HR, Singer AU, Betts L et al: Structural and biochemical characterization of CIB1 delineates a new family of EF-hand-containing proteins. J Biol Chem 2005; 280: 8407-8415.
22. Huang H, Vogel HJ: Structural basis for the activation of platelet integrin alphaIIbbeta3 by calcium- and integrin-binding protein 1. J Am Chem Soc 2012; 134: 3864-3872.
23. Blazejczyk M, Sobczak A, Debowska K et al: Biochemical characterization and expression analysis of a novel EF-hand Ca2+ binding protein calmyrin2 (Cib2) in brain indicates its function in NMDA receptor mediated Ca2+ signaling. Arch Biochem Biophys 2009; 487: 66-78.
24. Ahmed ZM, Frolenkov GI, Riazuddin S: Usher proteins in inner ear structure and function. Physiol Genomics 2013; 45: 987-989.
25. Widen JE, Folsom RC, Cone-Wesson B et al: Identification of neonatal hearing impairment: hearing status at 8 to 12 months corrected age using a visual reinforcement audiometry protocol. Ear Hear 2000; 21: 471-487.
26. Theunissen EJ, Huygen PL, Folgering HT: Vestibular hyperreactivity and hyperventilation. Clin Otolaryngol Allied Sci 1986; 11: 161-169.
27. Schraders M, Lee K, Oostrik J et al: Homozygosity mapping reveals mutations of GRXCR1 as a cause of autosomal-recessive nonsyndromic hearing impairment. Am J Hum Genet 2010; 86: 138-147.
28. Neveling K, Feenstra I, Gilissen C et al: A post-hoc comparison of the utility of sanger sequencing and exome sequencing for the diagnosis of heterogeneous diseases. Hum Mutat 2013; 34: 1721-1726.
29. de Ligt J, Willemsen MH, van Bon BW et al: Diagnostic exome sequencing in persons with severe intellectual disability. N Engl J Med 2012; 367: 1921-1929.
30. Shafique S, Siddiqi S, Schraders M et al: Genetic spectrum of autosomal recessive non-syndromic hearing loss in Pakistani families. PLoS One 2014; 9: e100146.

31. Riazuddin S, Khan SN, Ahmed ZM et al: Mutations in TRIOBP, which encodes a putative cytoskeletal-organizing protein, are associated with nonsyndromic recessive deafness. Am J Hum Genet 2006; 78: 137-143.
32. Shahin H, Walsh T, Sobe T et al: Mutations in a novel isoform of TRIOBP that encodes a filamentous-actin binding protein are responsible for DFNB28 recessive nonsyndromic hearing loss. Am J Hum Genet 2006; 78: 144-152.
33. Nagy E, Maquat LE: A rule for termination-codon position within intron-containing genes: when nonsense affects RNA abundance. Trends Biochem Sci 1998; 23: 198-199.
34. Huang H, Ishida H, Yamniuk AP, Vogel HJ: Solution structures of Ca2+-CIB1 and Mg2+-CIB1 and their interactions with the platelet integrin alphaIIb cytoplasmic domain. J Biol Chem 2011; 286: 17181-17192.
35. Ahmed ZM, Riazuddin S, Khan SN, Friedman PL, Riazuddin S, Friedman TB: USH1H, a novel locus for type I Usher syndrome, maps to chromosome 15q22-23. Clin Genet 2009; 75: 86-91.
36. Ahmad J, Khan SN, Khan SY et al: DFNB48, a new nonsyndromic recessive deafness locus, maps to chromosome 15q23-q25.1. Hum Genet 2005; 116: 407-412.
37. Astuto LM, Bork JM, Weston MD et al: CDH23 mutation and phenotype heterogeneity: a profile of 107 diverse families with Usher syndrome and nonsyndromic deafness. Am J Hum Genet 2002; 71: 262-275.

SUPPLEMENTAL FIGURES

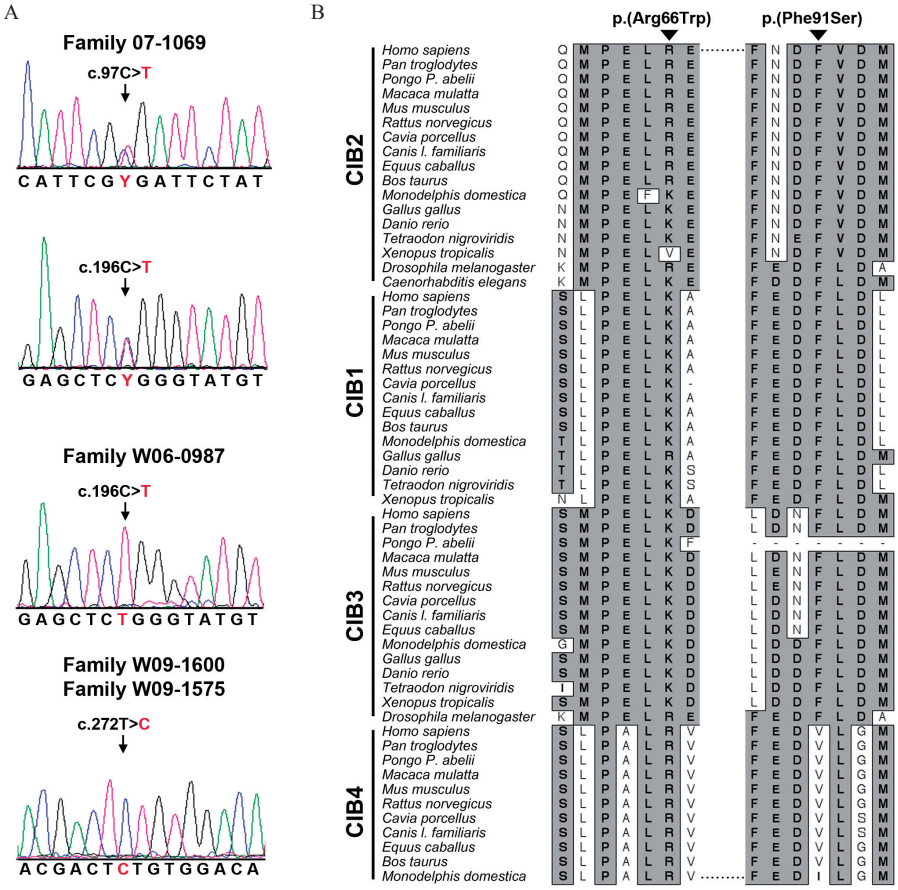

Supplemental figure 1. *CIB2* variants causing arNSHI

A) DNA sequence chromatograms of exon 3 and exon 4 of *CIB2* depicting wild type sequences and the homozygous mutations c.196C>T and c.272T>C, respectively, and chromatograms of exon 3 with the compound heterozygous mutations c.97C>T and c.196C>T and wild type sequences. Nucleotide positions are according to human CIB2 isoform A (accession no. NM_006383.2). **B)** Clustal W alignment of CIB family members revealed that the p.Arg66 residue in human *CIB2* (accession no. EAW99186) is either an arginine or a lysine in orthologs and homologs in a wide variety of species. Furthermore, residue phenylalanine at position 91 is highly conserved across homologs and orthologous as shown previously.[4]

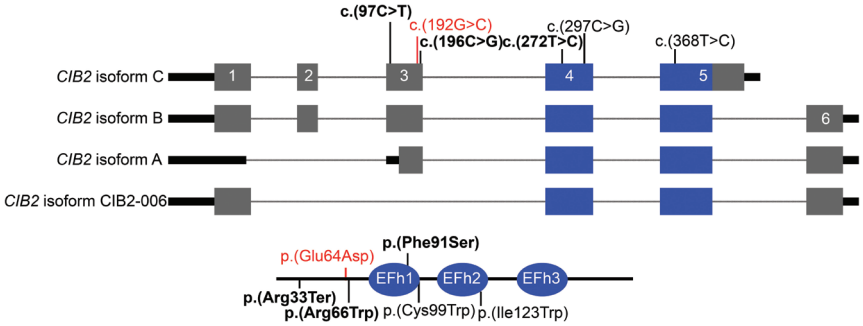

Supplemental figure 2. Schematic representation of the genomic structure of *CIB2* and of the isoforms of the encoded protein

In blue the exonic parts encoding the predicted EF hands, in red the only *CIB2* mutation described causing USH1J [4], in bold black the mutations described here to cause DFNB48 and in regular black the *CIB2* mutations previously described to cause DFNB48.[4] The accession numbers for the cDNA sequences encoding the respective isoforms are uc002bdc.2 for isoform A, uc002bdb.2 for isoform B, uc010ums.2 for isoform C and uc031qta.1 for isoform CIB2-006, according to the UCSC Genome Browser (GRCh37/hg19).

[1] Department of Otorhinolaryngology, Hearing & Genes, Radboud university medical center, Nijmegen, 6525GA, the Netherlands; [2] The Radboud Institute for Molecular Life Sciences, Radboud university medical center, Nijmegen, 6525GA, the Netherlands; [3] Servicio de Genética, Instituto Ramón y Cajal de Investigación Sanitaria (IRYCIS), Madrid, 28034, Spain; [4] Centro de Investigación Biomédica en Red de Enfermedades Raras (CIBERER), Madrid, 28034, Spain; [5] Radboud Institute for Health Sciences, Radboud university medical center, Nijmegen, 6525GA, the Netherlands; [6] Human Genome Sequencing Center, Baylor College of Medicine, Houston, TX 77030 USA; [7] Department of Human Genetics, Radboud university medical center, Nijmegen, 6525GA, the Netherlands; [8] Centre for Molecular and Biomolecular Informatics, Radboud university medical center, Nijmegen, 6525GA, the Netherlands; [9] Department of Endocrinology & Nutrition, Hospital Universitario Ramón y Cajal, Universidad de Alcalá , IRYCIS, Centro de Investigación Biomédica en Red Diabetes y Enfermedades Metabólicas Asociadas (CIBERDEM), Madrid, 28034, Spain; [10] Donders Institute for Brain, Cognition and Behaviour, Radboud University Nijmegen Medical Centre, Nijmegen, 6525GA, The Netherlands [11] Department of Psychiatry (966), Donders Institute for Brain, Cognition and Behavior, Radboud University Nijmegen Medical Center, Nijmegen, 6525GA, The Netherlands; [12] Department of Cognitive Neuroscience, Radboud university medical center, Nijmegen, 6525GA, the Netherlands; [13] Department of Laboratory Medicine, Laboratory of Hematology, Radboud university medical center, Nijmegen, 6525GA, the Netherlands; [14] Department of Hematology, Radboud university medical center, Nijmegen, 6525GA, the Netherlands; [15] Department of Dermatology, Radboud university medical center, Nijmegen, 6525GA, the Netherlands; [16] Department of Molecular and Human Genetics, Baylor College of Medicine, Houston, TX 77030 USA; [17] Department of Pediatrics, Baylor College of Medicine, Houston, TX 77030 USA; [20] Department of Otorhinolaryngology and Head and Neck Surgery, Rudolf Magnus Institute of Neuroscience, University Medical Center Utrecht, Utrecht, 3584CX, the Netherlands; [21] Department of Clinical Genetics, Erasmus MC, University Medical Center Rotterdam, 3000DR Rotterdam, the Netherlands [22] Hubrecht Institute, Royal Netherlands Academy of Arts and Sciences (KNAW) and UMC Utrecht, 3584CT Utrecht, The Netherlands

CHAPTER 5

Allelic mutations of *KITLG*, encoding KIT ligand, cause asymmetric and unilateral hearing loss and Waardenburg syndrome type II

Celia Zazo Seco[1,2,*], Luciana Serrão de Castro[3,4,*], Josephine W. van Nierop[1,5,*], Matías Morín[3,4,*], Shalini Jhangiani[6], Eva J.J. Verver[1,20], Margit Schraders[1,2], Nadine Maiwald[7], Mieke Wesdorp[1,2], Hanka Venselaar[8], Liesbeth Spruijt[7], Jaap Oostrik[1,2], Jeroen Schoots[7], Baylor-Hopkins Center for Mendelian Genomics[6], Jeroen van Reeuwijk[7], Stefan H. Lelieveld[2,7], Patrick L. M. Huygen[1], María Insenser[9], Ronald J.C. Admiraal[1,10], Ronald J.E. Pennings[1,5], Lies H. Hoefsloot[7,21], Alejandro Arias-Vásquez[7,11,12], Joep de Ligt[7,22], Helger G. Yntema[7], Joop H. Jansen[13,14], Donna M. Muzny[6], Gerwin Huls[13,14], Michelle M. van Rossum[15], James R. Lupski[6,16,17], Miguel Angel Moreno-Pelayo[3,4,#], Henricus P. M. Kunst[1,5,#], Hannie Kremer[1,2,7,#].

*,#Authors contributed equally

American journal of human genetics, in press

ABSTRACT

Linkage analysis combined with whole-exome sequencing in a large family with Non-Syndromic, congenital and stable Unilateral and Asymmetric Hearing Loss (NS-UHL/AHL) revealed a heterozygous truncating mutation, c.286_303delinsT (p.Ser96Ter), in *KITLG*. This mutation co-segregated with the NS-UHL/AHL as a dominant trait with reduced penetrance. By screening a panel of probands with NS-UHL/AHL, an additional mutation, c.200_202del (p.His67_Cys68delinsArg), was found. *In vitro* studies revealed that the p.His67_Cys68delinsArg transmembrane isoform of KITLG is not detectable at the cell membrane supporting pathogenicity. *KITLG* encodes a ligand for the KIT receptor. Also, KITLG-KIT signaling and MITF are suggested to mutually interact in melanocyte development. Since mutations in *MITF* are causative of Waardenburg syndrome type II (WS II), we screened *KITLG* in suspected WS II probands. A heterozygous missense mutation, c.310C>G (p.Leu104Val), was identified which segregated with WS II in a small family. *In vitro* studies revealed that the p.Leu104Val transmembrane isoform of KITLG is at the cell membrane as is wild-type KITLG. However, in culture medium of transfected cells, the p.Leu104Val soluble isoform of KITLG was reduced whereas no soluble p.His67_Cys68delinsArg and p.Ser96Ter KITLG could be detected. These data suggest that mutations in *KITLG* associated with NS-UHL/AHL have a loss-of-function effect. The mechanism of the mutation underlying WS II leading to membrane incorporation and reduced secretion of KITLG we speculate occurs via a dominant negative or gain-of-function effect. Our study unveils different phenotypes associated with *KITLG*, previously associated with pigmentation abnormalities and will thereby improve the genetic counseling of individuals with *KITLG* variants.

INTRODUCTION

Familial Non-Syndromic sensorineural Unilateral and Asymmetric Hearing Loss (NS-UHL/AHL) (MIM 125000) is rare with only a few families described in literature and no genes or loci known to date.[1-3] Like symmetric hearing loss (HL), UHL/AHL can negatively affect the life of individuals because of cognitive and social developmental delay. UHL/AHL can also be inherited as part of a syndrome, *e.g.* Waardenburg syndrome (WS) (PS193500) or Pendred syndrome (MIM 274600), or it can be induced by environmental factors such as prematurity, trauma and meningitis.

WS is a dominantly inherited auditory-pigmentary syndrome with an estimated prevalence of 5-10:100,000. To date, four types of WS (I to IV) are distinguished and seven genes are found to be associated with the syndrome. The classification of WS is based on the presence of specific clinical features in addition to pigmentary abnormalities of hair, skin, and eyes and congenital HL as in WS II.[4] These additional clinical features are craniofacial defects in WS I, craniofacial and limb defects in WS III and Hirschsprung disease in WS IV. All WS genes function in the same pathways involved in development of neural crest-derived melanocytes by influencing *Mitf* expression and/or activity.[5-9]

Besides WS, there are other HL syndromes accompanied by hypopigmentation due to melanocyte defects.[10] One of these is the piebald trait (MIM 172800). Piebaldism is characterized by congenital regional absence of melanocytes in the skin and hair caused by heterozygous loss of function mutations in *KIT* (MIM 164920).[10] Very occasionally, piebald trait has been found to be associated with congenital HL indicating that they might be part of the same disorder.[11,12]

By using a combined strategy of linkage analysis and whole-exome sequencing (WES) in a large Dutch family with NS-UHL/AHL, a truncating mutation, c.286_303delinsT (NM_003994.5 and NM_000899.4, p.Ser96Ter), of *KITLG* (MIM 184745) was identified. Targeted gene testing of a panel of NS-UHL/AHL affected individuals identified an in-frame deletion, c.200_202del (NM_003994.5 and NM_000899.4, p.His67_Cys68delinsArg), in a family of Spanish origin. Due to the dual regulation of melanocyte development by KIT-KITLG signaling and MITF,[6,8,13] a cohort of WS II affected individuals was tested for mutations in *KITLG* which revealed a missense mutation, c.310C>G (NM_003994.5 and NM_000899.4, p.Leu104Val), that was segregating with WS II in another family from the Netherlands. We analyzed the effect of these mutations on subcellular localization and secretion of the transmembrane and soluble KITLG isoforms, respectively.

SUBJECTS AND METHODS

Subject evaluation

The current study was approved by the medical ethics committee of the Radboud university medical center, the Hospital Universitario Ramón y Cajal and the Institutional Review Board of Baylor College of Medicine. Written informed consent was obtained from all participating subjects.

The medical history was taken from all participants, paying special attention to hearing impairment, vestibular symptoms and possible causes of acquired deafness. In family W09-1628 (Figure 1A), 26 people participated in the Ear, Nose and Throat (ENT) evaluation (II:4, III:1, III:3, III:4, III:5, III:6, III:7, III:9, IV:1, IV:3, IV:4, IV:5, IV:6, IV:7, IV:8, V:1, V:2, V:3, V:4, V:5, V:6, V:7, V:8, V:9, V:10, V:11). In family S1489, the index case III:1 and his father II:1 took part in an ENT examination (Figure 1B). From family 12-01744, two individuals, the index II:1 and his mother I:2, both affected with WS II, participated in an ENT evaluation (Figure 1C). The affection status of the other family members was based information provided by close relatives.

Individuals were considered to be affected if at least one ear showed three pure tone thresholds below the 95th percentile (P_{95}) at the last evaluation. AHL was indicated when the difference between the hearing thresholds of both ears was more than 10 dB at three or more frequencies or more than 15 dB at two or more frequencies. The HL was indicated as unilateral if three or more frequencies were beyond the P_{95} value in only one ear, with normal hearing in the contralateral ear.

Audiometric examination comprised conventional pure-tone audiometry in a sound-treated room according to the International Organization for Standardization (ISO) standards 389 and 8253-1 (ISO 389. 1985; ISO 8253. 1989). Air conduction thresholds were measured in dB HL at 0.25, 0.5, 1, 2, 4, and 8 kHz. Bone conduction thresholds were measured to exclude conductive or mixed HL. The P95 threshold values in relation to the person's age and sex were derived for each frequency using the ISO 7029 method (ISO 7029. 1984).[14] In family W09-1628, speech-audiometry was performed under the above-mentioned conditions using standard monosyllabic (consonant-vowel-consonant) Dutch word lists. For individual II:1 of family 12-01744 play-audiometry with blocks was performed at the age of three years. Thresholds were measured in dB HL at 0.5, 1, and 4 kHz.

Six affected members of family W09-1628 (III:5, IV:1, V:1, V:5, V:6, V:7) underwent vestibular and ocular motor tests. Ocular motor evaluation comprised

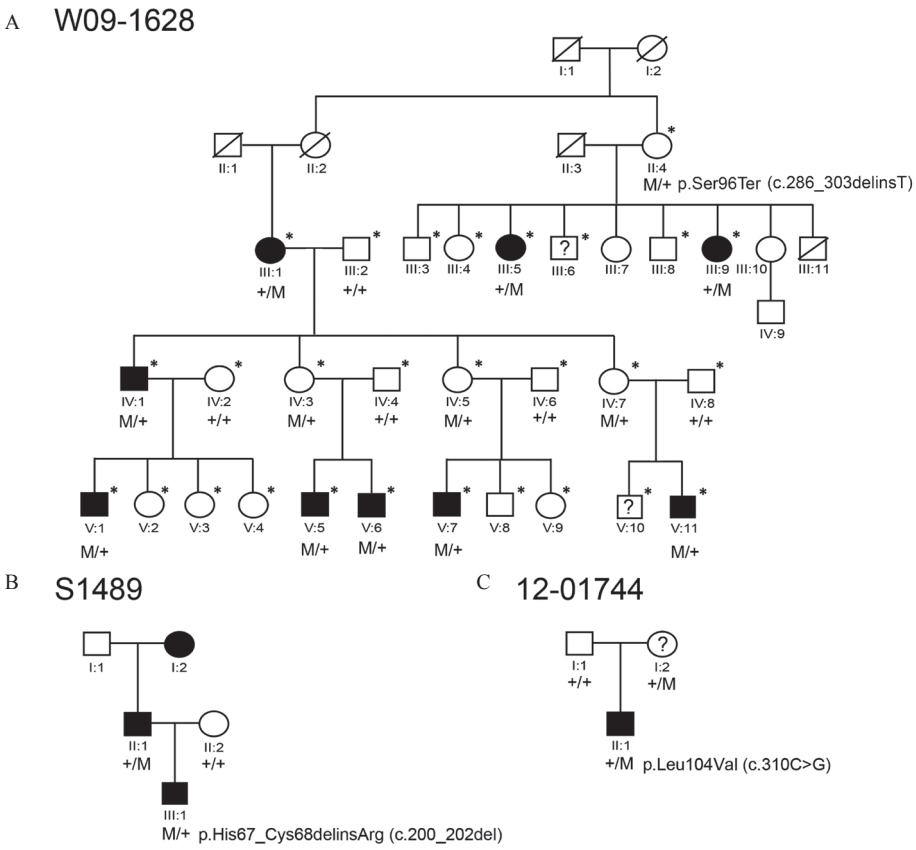

Figure 1. Families affected by *KITLG* mutations. A) Pedigree of family W09-1628 with NS-UHL/AHL. Asterisks mark individuals who were genotyped with HumanOmniExpress BeadChip arrays. 'M' represents the mutant allele c.286_303delinsT and '+' the wild-type allele. For privacy reasons, the genotype for the c.286_303delinsT has not been indicated for unaffected individuals except for those with affected offspring. B) Pedigree of family S1489 with NS-AHL. 'M' represents the c.200_202del variant and '+' the wild-type allele. C) Pedigree of family 12-01744 with WS II. 'M' represents the variant c.310C>G, '+' the wild-type allele and '?' indicates an unclear affection status.

saccades, smooth pursuit, optokinetic nystagmus, as well as gaze evoked and spontaneous nystagmus. Vestibulo-ocular reflexes (VOR) were evaluated using electronystagmography (ENG) with computer analysis. Vestibular stimulation comprised rotary and caloric tests.[15] The diagnosis of hyporeflexia in the rotary test was based on finding parameter values below the 5th percentile of normal. When the response parameters had directional preponderance values of >25%, VOR asymmetry was considered to be significant. The finding of

caloric asymmetry relates to a difference in response levels larger than 20%. Caloric hyporeflexia indicates a response level of < 7º/sec for cold and < 10 º/sec for warm. According to ANSI (1999) procedures, we have established normative laboratory data using the 95% confidence limit for the normal population. To avoid underestimation, we have calculated the lower limit of acceptance by using 2.34 times the standard deviation from the mean to define a hyporeactivity of the caloric responses (*i.e.* 7º/sec and 10 º/sec for cold and warm irrigation, respectively).[16]

High resolution spiral computed tomography (CT) images of the temporal bones of both ears, with 0.6 mm axial sections and coronal reconstructions, were obtained to detect possible inner ear anomalies in one affected individual (V:7) of family W09-1628. The images were analyzed by an experienced head and neck radiologist.

In the index case III:1 of family S1489 magnetic resonance imaging (MRI) was performed to exclude inner ear defects and retrocochlear pathology.

To evaluate the presence of pigmentation abnormalities, history was taken and physical examination was performed in all three families W09-1628, 12-01744 and S1489. Fourteen individuals of family W09-1628 participated in a dermatological evaluation, 10 of whom were heterozygous for the mutation underlying the HL in the family (eight had HL, in one of whom the HL was not associated with the mutation in the family, two did not show HL) and four of whom were controls without the mutation. Dermatological evaluation included determination of skin type (I - VI), eye color, hair color, poliosis of the head, cilia and eyebrows, skin depigmentation, hypopigmentation, hyperpigmentation, number of naevi, allergic reactions, other observed skin abnormalities and treatment of skin abnormalities in the past. The whole body was examined and a Wood's lamp was used to analyze the hypo-, hyper- and depigmentations. If necessary, skin abnormalities were reviewed with a dermatoscope. Examination with a Wood's lamp was also performed for the affected individuals of family 12-01744.

To evaluate the presence of abnormalities in hematopoiesis, blood samples were collected of the 14 individuals that underwent dermatological evaluation. Blood samples were evaluated for haemoglobin concentration, mean corpuscular haemoglobin concentration (MCHC), erythrocyte-counts, mean corpuscular volume (MCV), red blood cell count distribution width (RDW), reticulocyte counts, hematocrit, trombocyte counts, leukocyte counts and differentiated leukocytes (neutrophilic granulocytes, lymphocytes, eosinophilic granulocytes, basophil granulocytes and monocytes) by microscopic analysis and an automated protocol. As a reference the Radboud university medical center standard was used.[17]

Description of subject cohorts

The cohort of 64 probands of Dutch origin, with a clinical suspicion of WS II consisted of three classes of affected individuals: (1) 31 subjects with bilateral symmetric HI and hair, eye and/or skin pigmentation abnormalities, (2) nine subjects with AHI of whom five had additional hair, eye and/or skin pigmentation abnormalities and (3) 24 subjects with UHL of whom 15 had pigmentation abnormalities of hair, eye, and/or skin. Because AHL is described in WS II, *MITF* testing was requested in routine diagnostics and excluded. In the index case of family 12-01744 of this cohort, all genes known to be involved in WS II (*MITF, SOX10, SNAI2*) were analyzed by Sanger sequencing and no potentially pathogenic variants were found. The NS-UHL/AHL cohort consisted of 23 index cases, 10 with NS-UHL and 13 with NS-AHL. In all subjects of this cohort the c.35delG *GJB2* (MIM 121011) mutation (NM_004004.5, p.Gly12Valfs*2) and the m.1555A>G mutation in *MT-RNR1* (MIM 561000, NC_012920.1) were excluded. These subjects were not pretested for *MITF* mutations.

Linkage analysis

Genomic DNA was isolated from peripheral blood lymphocytes by standard procedures. The HumanOmniExpress BeadChip arrays (Illumina) with a total of 733,202 SNPs covering the genome at a median of 2.2 kb intervals were used for genotyping DNA from individuals' blood (Figure 1A). SuperLink online SNP 1.1 software was employed for multipoint LOD score calculations using a window size of ten SNPs.[18] In order to select independent SNPs, pruning (r^2=0.025) was performed by using PLINK.[19] The disease was assumed to be an autosomal dominant disorder with a disease allele frequency of 0.001. The penetrance of the disease allele was set at 70%.

In order to confirm the linkage region defined by Superlink, genotyping of variable number of tandem repeat (VNTR) genetic markers was performed.[20] Touchdown PCR was used to amplify the VNTR markers. Marker heterozygosity, order and genetic location were derived from the Marshfield genetic map. VNTR markers were selected to encompass the linkage interval, on chromosome 12, region q21.32-q23.1. The alleles were assigned using Gene Mapper v.4.0 software (Applied Biosystems).

Whole-exome sequencing

WES was performed at the Human Genome sequencing center (HGSC) at Baylor College of Medicine through the Baylor-Hopkins Center for Mendelian Genomics initiative. Using 0.5 µg of DNA, an Illumina paired-end pre-capture

library was constructed according to the manufacturer's protocol (Illumina Multiplexing_SamplePrep_Guide_1005361_D) with modifications as described in the "BCM-HGSC Illumina Barcoded Paired-End Capture Library Preparation" protocol. Four pre-captured libraries were pooled and then hybridized in solution to the HGSC CORE design (52Mb, NimbleGen) according to the manufacturer's protocol "NimbleGen SeqCap EZ Exome Library SR User's Guide (Version 2.2)" with minor revisions.[21] The sequencing run was performed in paired-end mode using the Illumina HiSeq 2000 platform, with sequencing-by-synthesis reactions extended for 101 cycles from each end and an additional seven cycles for the index read. With a sequencing yield of 10.4 Gb, the samples achieved 91% of the targeted exome bases covered to a depth of 20X or greater. The overall coverage in the linkage interval was optimal with 97.7% and 94.4% of base pairs covered ≥10X for individuals IV:1 and III:9, respectively. Illumina sequence analysis was performed using the HGSC Mercury analysis pipeline,[22,23] which moves data through various analysis tools from the initial sequence generation on the instrument to annotated variant calls (SNPs and intra-read insertions and deletions).

Sanger sequence analysis

Primers for amplification of exons and exon-intron boundaries of *KITLG* (NM_003994.5 and NM_000899.4) and *KITLG* rs642742 and rs12821256 were designed with ExonPrimer (Table S1). Amplification by PCR was performed on 40 ng of genomic DNA with Taq DNA polymerase (Roche or Invitrogen). PCR fragments were purified with NucleoFast 96 PCR plates (Clontech) or ExoI/FastAP (Fermentas) in accordance with manufacturer's protocols. Sequence analysis was performed with the ABI PRISM BigDye Terminator Cycle Sequencing V2.0 Ready Reaction kit and analyzed with the ABI PRISM 3730 DNA analyzer (Applied Biosystems). As reference sequence NM_003994.5 and NM_000899.4 were employed.

The presence of the *KITLG* c.286_303delinsT mutation was determined in 153 ethnicity matched control individuals. To do so, exon 4 of *KITLG* was amplified and fragments were analyzed by agarose gel electrophoresis. The presence of the *KITLG* c.200_202del variant was investigated in 200 controls of Spanish origin by a size-based screening with one primer labeled with a 6-FAM fluorophore. Allele size was determined by capillary electrophoresis in an ABI PRISM 3100 genetic analyzer (Applied Biosystems) and analysis with the GeneScan software (Applied Biosystems). For all three *KITLG* variants absence was verified in the following databases: the Exome Variant Server (>200,000 exomes), the

Nijmegen WES database (5031 exomes), Exome Aggregation Consortium database (ExAC, 65,000 exomes), the "Centro de Investigación Biomédica en Red de Enfermedades Raras" (CIBERER) Exome Sever (403 exomes), and the WES database of the Baylor-Hopkins Center for Mendelian Genomics (~5000 exomes).

A possible effect of the *KITLG* variants was predicted with the following software tools included in Alamut (Interactive Biosoftware): Sorting Intolerant from Tolerant (SIFT), Polymorphism phenotyping version 2 (Polyphen2), Mutation Taster, NetGene, BDGP Splice prediction site and Human Splice Finder. The conservation of the substituted amino acids was scored by using the Conseq online tool.

pCR4-Topo cloning

Exon 4 of *KITLG* from individual IV:1 in family W09-1628, and index case III:1 from family S1489 were amplified (primers as for sequencing) and cloned into a pCR4-Topo vector (Invitrogen) according to the manufacturer's protocol. Plasmid DNA was isolated from transformed *E. coli* DH5α with the NucleoSpin Plasmid (NoLid) kit (Machery Nagel) and analyzed by Sanger sequence analysis as described above.

Expression of KITLG in NIH3T3 cells

Total RNA was extracted from human control peripheral blood using QIAamp® RNA Blood mini Kit (Qiagen) following the manufacturer's instructions. Reverse transcription was carried out using 1µg of RNA and random hexamers with the Transcriptor First Strand cDNA Synthesis Kit (Roche). Full-length transcripts encoding the human *KITLG* transmembrane (NM_003994.5) and soluble (NM_000899.4) isoforms were amplified using modified primers; the forward primer contains a BamHI site and the reverse primers (R2-XhoI or R1-XhoI) contain a XhoI restriction site (Table S1). Amplimers were cloned in the eukaryotic expression vector pIRES-hrGFP-1a (Stratagene) to obtain two different sets of plasmids suitable to generate respectively: 1) the human soluble KITLG protein (with the region encoded by exon 6) and 2) the KITLG protein (without the region encoded by exon 6) fused to three FLAG epitopes at the C-terminal end.

Plasmids encoding the aberrant KITLG, p.His67_Cys68delinsArg, p.Ser96Ter and p.Leu104Val, were generated by direct mutagenesis with the QuickChange Site-Directed Mutagenesis Kit (Stratagene) and verified by Sanger sequencing. Cell culture, transfection and detection of proteins by immunofluorescence were

performed as previously described.[24] Cells were transiently transfected with 500 ng of wild-type or mutated constructs using Lipofectamine 2000 (111668, Invitrogen) according to the manufacturer's protocol. As primary antibodies, the monoclonal anti-FLAG M2 mouse antibody (1:500; SIGMA, F1804) or with anti-KITLG antibody (1:1000; Abcam, ab52603, anti-SCF) were used and as secondary antibodies the Alexa Fluor 488-conjugated goat anti-mouse IgG (1:1000; Molecular Probes, A-11017; Invitrogen) or Alexa Fluor 594-conjugated goat anti-rabbit (1:500. Molecular Probes, A11037; Invitrogen) were employed. Slides were mounted using Fluorsave™ Reagent (Calbiochem). Images were acquired and analyzed by confocal microscopy (Nikkon C1 plus ECLIPSE Ti-e microscope and an 60X Plan Apo VC OIL objective with NA 1.4).

Enzyme-linked immunosorbent assay (ELISA)

In order to assess the levels of the soluble KITLG isoform, a commercial ELISA kit (ab100636 SCF Human ELISA kit) was employed according to manufacturer's instructions (Abcam). NIH3T3 cells were independently transfected with plasmids encoding soluble wild- type KITLG or soluble KITLG containing the mutations identified in this study (p.Ser96Ter, p.Leu104Val, and p.His67_Cys68delinsArg). After cells were cultured for 24 hrs, cell-free supernatants were collected by centrifuging at 15000 rpm for 10 min at 4 ºC. Samples were stored at -70ºC until the ELISAs were performed. Samples were diluted with one volume of 1X assay diluent B. The detection limit was 2 pg/ml and the mean intra- and inter-assay coefficients of variability were < 10% and < 12%, respectively. Samples were assayed in quadruplicate and at least four independent transfections were performed. Transfection levels of cells with the wild-type and mutant constructs were determined by detection of GFP and KITLG by (immuno)fluorescence of permeabilized cells. For detection of the latter, the anti-KITLG antibody (Abcam, ab52603, anti-SCF. Figure S1) was employed. The dosage of the soluble form detected by ELISA in the medium was normalized to the quantity of transfected cells per well in each case. Cells were examined with a fluorescence inverted microscope (Olympus IX81) equipped with a UPLFLN40X, PLAPON60XO and UPLSAPO100XO objectives. Images were recorded with a cooled CCD-F View II (Soft Imaging System) camera and processed using Cell R software (Olympus). We verified that the ELISA kit allowed the identification of the aberrant KITLG proteins, including the truncated form (p.Ser96Ter), by using cellular extracts of permeabilized cells transfected with constructs encoding FLAG-tagged transmembrane KITLG aberrant isoforms (Figure S2).

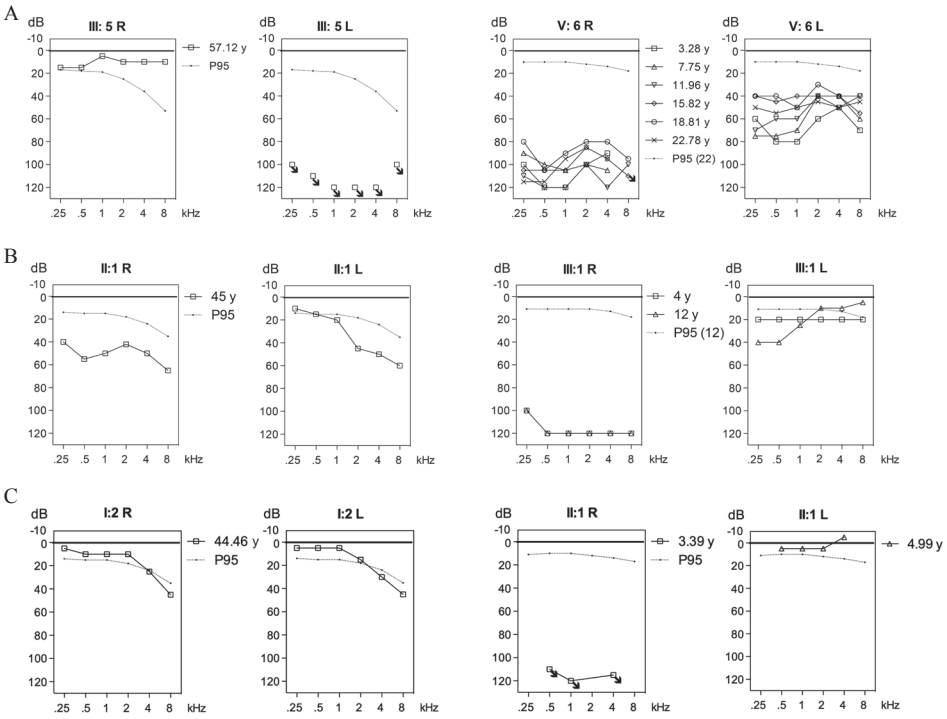

Figure 2. Pure tone audiometry in families affected by *KITLG* mutations. A) Pure tone audiograms for individuals of family W09-1628 with UHL (III:5) and AHL (V:6). B) Pure tone audiograms for family S1489 with AHL. C) Pure tone audiograms for family 12-01744 with WS II. R, right ear; L, left ear, P_{95} represents thresholds according to the P_{95} of presbyacusis (ISO 7029. 1984).[14]

RESULTS

Clinical characterization of families with NS-UHL/AHL and WS II

Family W09-1628 A large Dutch family, W09-1628 (Figure 1A), with autosomal dominant, congenital, non-syndromic sensorineural HL and a large inter- and intra-individual variation of severity and audiogram configuration was ascertained. Otoscopy was normal for all but two individuals, V:7 and V:8 (for details see the Supplemental Note).

In cases with UHL, either the left or the right ear was affected and severity of the HL varied from mild to profound (Figure 2A and Figure S3). Overall, five individuals presented with NS-AHL (III:9, V:1, V:5, V:6, V:11) and four individuals with NS-UHL (III:1, III:5, IV:1, V:7) (Figure S3). HL was only affecting or more pronounced in the lower frequencies (< 2 kHz) in four

ears. Interaural differences in audiogram configuration were observed in one individual (III:9, Figure S3). Additional information on individual cases is provided in the Supplemental Note.

Analysis of longitudinal data revealed that HL was stable in all individuals. Only minor "negative progression" was seen in individual longitudinal data which is likely to be explained by the young age at which first thresholds were determined. The genetic defect underlying the NS-UHL/AHL in this family has a reduced penetrance since four individuals transmitting the disease to their offspring were unaffected (II:4, IV:3, IV:5 and IV:7) (Figure 1A).

Vestibular function was evaluated in six of the hearing impaired family members (Table S2). Three individuals displayed asymmetry on calorisation, corresponding with the side of the worst ear (V:1, IV:1, III:5). One person (V:7) displayed a marginal hyporeflexia on both sides while he had UHL; the other ear had a dip at 4 kHz only although no history of excessive noise exposure was reported. In the remaining two individuals (V:5 and V:6), vestibular function was found to be normal (Table S2). Except for individual II:4, none of the individuals who carried the mutation reported vestibular symptoms. During history taking, individual II:4 indicated a possible Meniére disease.

Since KITLG functions in the proliferation, migration and survival of hematopoietic stem cells and melanoblasts,[25-28] blood cell counts as well as skin, hair, and eye color were evaluated in members of family W09-1628 with and without the *KITLG* mutation. All determined hematological parameters were within the normal range although individuals IV:1, IV:3 and V:4 were treated in the past with ferrofumarate for anemia (Table S3). These findings suggest that the *KITLG* mutation in the present family, in the heterozygous state does not affect steady state hematopoiesis.

All evaluated individuals had skin type I or II, blond hair and blue eyes (Table S4). Heterochromia iridis and dystopia canthorum were not observed. Hypo- and depigmentations of the skin were not found in the younger generation (V). In the older generations, hypo- and depigmentations were present in individuals with and without *KITLG* mutation (Table S4). These pigmentation characteristics are age-related and a common feature in the population.[29] Our findings suggest that the heterozygous *KITLG* mutation in this family does not lead to pigmentation abnormalities of skin, eyes or hair.

Family S1489 The index case of family S1489 (Figure 1B) and his father presented with AHL and variability in severity and audiogram configuration (Figure 2B) as was observed in family W09-1628. The AHL in the propositus (III:1) was reported to be of prelingual onset without progression. The earliest

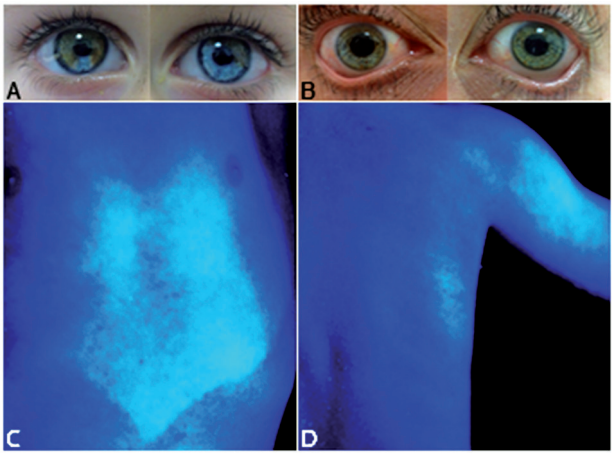

Figure 3. Eye and skin hypopigmentation phenotypes in family 12-01744 with WS II. A) Heterochromia iridis in the index case (II:1). B) Signs of heterochromia iridis in his mother (I:2). C) A hypopigmented sharply demarcated macule on the thorax of case II:1 and D) on the upper arm and a nummular sharply demarcated hyperpigmented macula at the back, detected by a Wood's lamp.

clinical evidence of HL was obtained at the age of four years. HL was profound at all frequencies in the right ear and mild in the left ear, affecting the low frequencies. The father of the propositus (II:1) presented with moderate bilateral AHL. Audiogram configuration was downsloping for the left ear and flat for the right ear. No vestibular symptoms were reported by the affected father and son. Examination of the skin revealed no hypo- or hyperpigmentation features. Additional information is provided in the Supplemental Note.

Family 12-01744 In family (Figure 1C), otoscopy demonstrated otitis media with effusion for the right ear of the index case (II:1) at the age of almost 5 years. Therefore, reliable thresholds could only be measured for the left ear which were normal. At the age of three years, play audiometry had been performed elsewhere which revealed profound HL for the right ear (Figure 2C). The mother of the index case (I:2) did not present any abnormalities in otoscopy and her hearing was normal with only two frequencies, 4 kHz and 8 kHz, below the P_{95} values (Figure 2C). The index case had heterochromia iridis that is suggested to be present in his mother as well by small blue spots in the iris (Figure 3A, B). Both individuals had skin type III. The index case had brown/blond hair. On the thorax and upper arms, he had a hypopigmented partially sharply demarcated macule which was already present at birth. Furthermore, a nummular sharply demarcated hyperpigmented macule at the back was seen (Figure 3C, D).

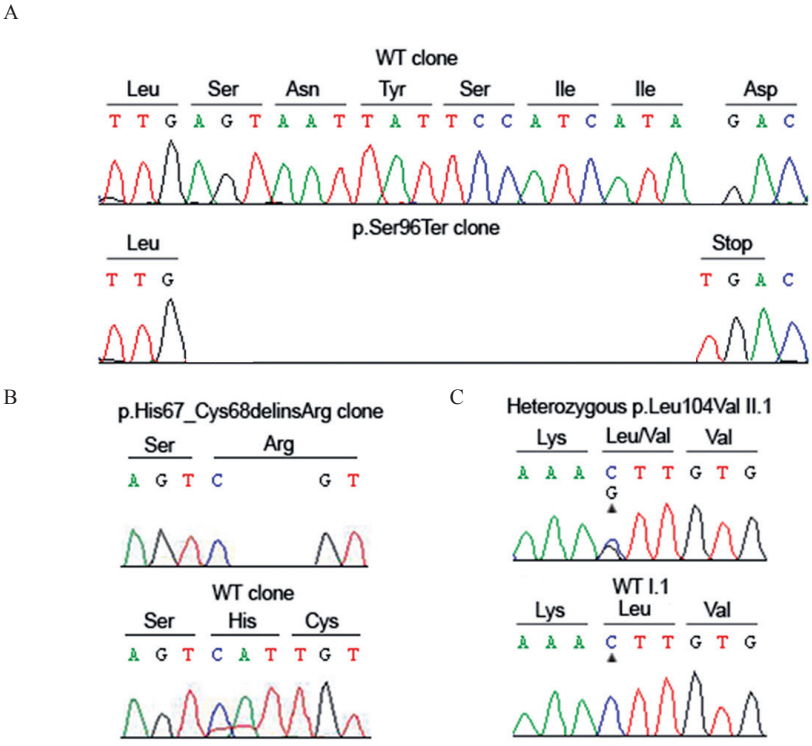

Figure 4. Genetic defects underlying UHL and AHL and schematic representation of the genomic structure of *KITLG* and of the encoded KITLG isoforms. A) Electropherograms of pCR4-topo clones representing the wild-type and c.286_303delinsT alleles of *KITLG* exon 4 of individual IV:1 (family W09-1628). B) Electropherograms of pCR4-topo clones representing the wild-type and c.200_202del alleles of *KITLG* exon 4 of individual III:1 (family S1489). C) Partial nucleotide sequences of *KITLG* exon 4 of case II:1 of family 12-01744. The mutated nucleotide is marked by an arrowhead. As reference sequences NM_003994.5 and NM_000899.4 were used. D) Exon 6 is alternatively spliced. The yellow dots represent the gain of function mutations c.98C>T, c.100A>C and c.107A>G, causative of familial hyper- and hypopigmentation syndromes. The green and red dots represent the mutations identified in the present study to be causative of NS-UHL/AHL. The white dot represents the mutation identified in a family with WS II. All depicted variants affect the KIT ligand domain of both the soluble and transmembrane isoforms of KITLG. "WT" means wild-type.

D

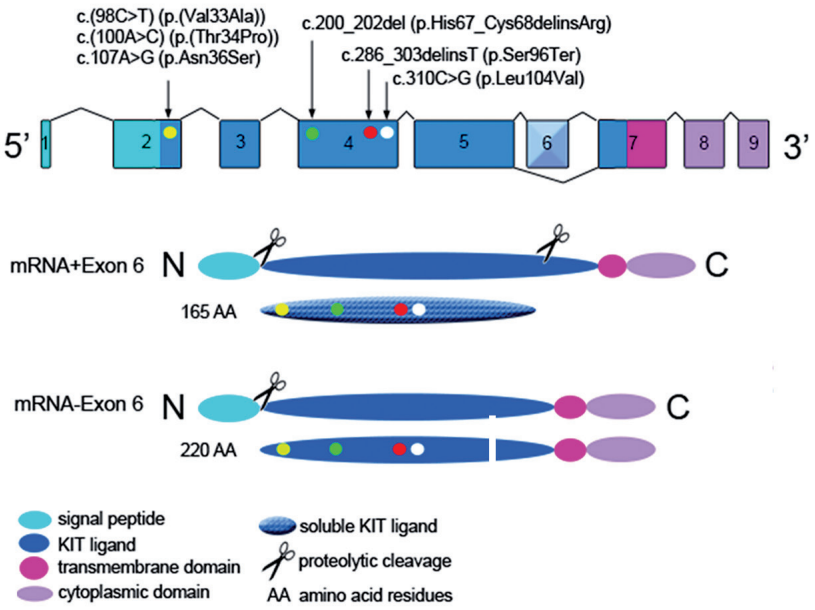
c.(98C>T) (p.(Val33Ala))
c.(100A>C) (p.(Thr34Pro))
c.107A>G (p.Asn36Ser)
c.200_202del (p.His67_Cys68delinsArg)
c.286_303delinsT (p.Ser96Ter)
c.310C>G (p.Leu104Val)
5'
1
2
3
4
5
6
7
8
9
3'
mRNA+Exon 6
N
C
165 AA
mRNA-Exon 6
N
C
220 AA
signal peptide
KIT ligand
transmembrane domain
cytoplasmic domain
soluble KIT ligand
proteolytic cleavage
AA amino acid residues

A locus for NS-UHL/AHL on chromosome 12q21.32-q23.1

In family W09-1628 genotyping was performed with high density SNP arrays (Figure 1A). Genome-wide multipoint LOD scores were calculated using 14,488 independent SNPs which revealed a single linkage interval of 13.15 Mb on chromosome 12q21.32-q23.1, delimited by rs10459171 and rs35723 (chr12:87,808,426-100,960,087; GRCh37/hg19). A maximum LOD score of 4.27 was calculated for rs7132875 and rs7309222 (Figure S4). There were no other regions with a LOD score suggestive of linkage (≥ 2.0) (Figure S4).

As a next step, linkage of the disease to the 12q21.32-q23.1 region was confirmed by genotyping of VNTR genetic markers and recombination events delimited the linkage interval to a region flanked by markers D12S88 and D12S346 (12q21.31-q23.1; chr12:86,371,384-99,528,530 GRCh37/hg19) (Figure S5). According to the UCSC Genome Browser (GRCh37/hg19), 82 RefSeq genes were present in the critical region but none was reported to be related to deafness in humans before and in mouse, only the ortholog of *KITLG* (*Kitl*) was associated with sensorineural HI (Mouse Genome Informatics database).

WES discovers a truncating mutation in *KITLG*

Because of the size of the critical region, WES was performed for the affected individuals III:9 and IV:1 to identify the genetic defect underlying the NS-UHL/AHL in family W09-1628. Multiple filter steps of the initial 87,751 variants that were shared by individuals III:9 and IV:1 (Table 1) revealed two heterozygous candidate variants in exon 4 of *KITLG*, c.286_303del and c.303insT. Sanger sequencing after cloning of *KITLG* exon 4 amplimers demonstrated that both variants are present *in cis* and thus are likely to represent one mutational event (c.286_303delinsT) (Figure 4A). The predicted effect of the c.286_303delinsT variant is a shift of the reading frame and a premature termination of protein synthesis, p.Ser96Ter. The variant was detected heterozygously in all affected individuals of the family, in all unaffected individuals who transmit the mutation to their offspring, in one individual with an unknown affection status, and in an additional unaffected individual (Figure 1A). The *KITLG* variant c.286_303delinsT was neither present in 153 ethnicity-matched control individuals nor in exome databases (see 'Subjects and Methods'). CNV analysis of WES data did not reveal any CNV in the linkage interval and no CNVs that were shared by the two individuals (Table S5).

Based on the segregation pattern of the c.286_303delinsT variant in *KITLG*, we calculated a penetrance of 60-67%. The SNPs rs642742 and rs12821256

Table 1. Filter steps applied on sequence variants identified in WES of individuals III:9 and IV:1 of family W09-1628.

Filter steps	# Variants
Shared exome	87,751
In linkage region 12q21.31-q23.1	241
≤ 0.5 % dbSNP132-Nijmegen in-house frequency	50
Exonic missense, nonsense, indels, non- and canonical splice sites	9
Confirmed by Sanger sequecing	2 in *KITLG*

Indicated are the number of variants as compared to reference genome GRCh37 (hg19) after each filter step.

are located in *KITLG* enhancers ~326 kb and ~350 kb upstream of the *KITLG* transcription start site, respectively, and are described to alter enhancer activity.[30,31] To evaluate a possible contribution of these SNPs to the penetrance of HL in the family, they were genotyped in all with the mutation (Figure S5). No correlation was observed between the SNP genotypes and the penetrance of the mutation in this family.

KITLG variants in NS-UHL/AHL and WS II

We further addressed involvement of *KITLG* mutations in both NS-UHL/AHL and in WS II. HL in individuals with WS II is variable, being asymmetric and/or unilateral in some of the cases.[32,33] Furthermore, function of *MITF* (MIM 156845) that is associated with WS II, is influenced by KITLG-KIT signaling.[8] We selected two panels of affected individuals. The first panel consisted of 64 probands with a clinical suspicion of WS II. The second panel consisted of 23 unrelated probands with autosomal dominant NS-UHL/AHL, mainly of Spanish origin. Further details on the panels are provided in 'Subjects and Methods'. Two additional heterozygous *KITLG* variants were identified, an in-frame deletion, c.200_202del (p.His67_Cys68delinsArg) (Figure 4B), in an index case of Spanish origin with NS-AHL and a missense variant, c.310C>G (p. Leu104Val; Figure 4C) in a WS II case of Dutch origin with UHL.

The *KITLG* variant c.200_202del was heterozygously present in the father of the proband who also presented with NS-AHL (Figure 1B, Figure 2B). The c.200_202del variant was neither detected in 200 ethnicity-matched control alleles nor in exome databases (see 'Subjects and Methods'). The predicted effect of the deletion of three nucleotides on the encoded protein is an amino

A

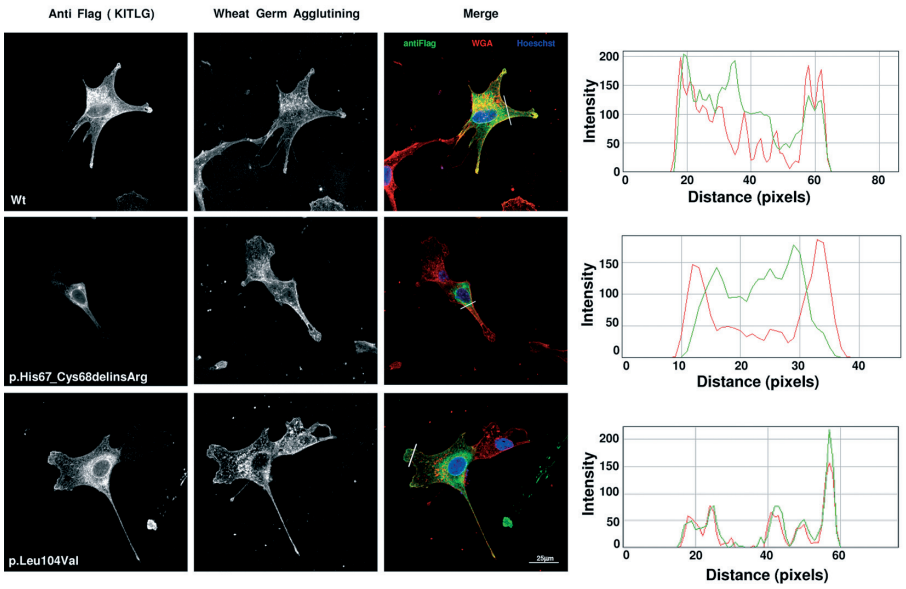

Figure 5. Effect of *KITLG* mutations on subcellular localization and excretion of the transmembrane and soluble KITLG isoforms, respectively. A) WGA staining of NIH3T3 cells transfected with constructs encoding the FLAG-tagged wild-type, p.His67_Cys68delinsArg and p.Leu104Val transmembrane isoform of KITLG. Cells were incubated with anti-FLAG antibodies and Alexa 488-conjugated goat anti mouse (left column), WGA Texas Red-X is visualized in the middle column. In the right column, the signals of the left and middle columns are merged. Co-localization of WGA with wild-type and p.Leu104Val KITLG was observed at the cell membrane but not with p.His67_Cys68delinsArg KITLG. WGA (red) and KITLG (green) fluorescence intensities profiles were plotted as a function of distance using ImageJ software. Scale bar = 25 µm. B) The amount of soluble p.Leu104Val KITLG is significantly reduced ($p < 10^{-3}$, Student's t-test) in the medium of transfected NIH3T3 cells as measured by ELISA. No soluble KITLG was detected for the p.His67_CysdelinsArg and p.Ser96Ter mutations. Data are means ±SD of four independent experiments. "WT" means wild-type.

B

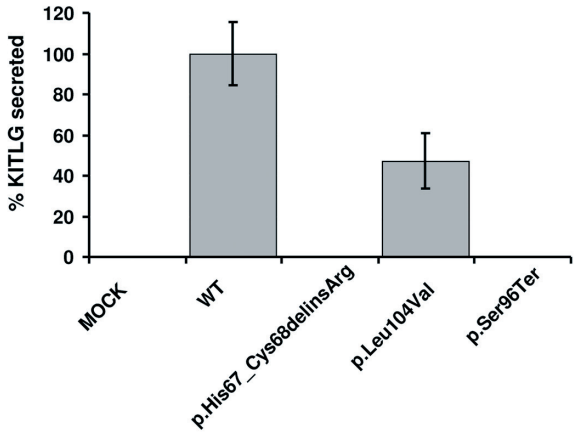

acid deletion and a substitution (p.His67_Cys68delinsArg). Cys68 is highly conserved with a score of 9 in the ConSeq online bioinformatic tool (9; conserved, 1; variable). The Cys68 residue forms an intramolecular Cys-Cys bond with Cys163 which is essential for the full biological activity of KITLG.[25,34-36] The loop in which Cys68 is located connects a β-sheet to an α-helix. Homology modeling of *KITLG* p.His67_Cys68delinsArg predicts that when residue Cys68 is not present and the Cys68-Cys163 bond thus cannot be formed, the local structure of KITLG around the loop is affected. Also, a reactive Cys (Cys163) is left without a binding partner which could lead to even larger structural changes than predicted (Figure S6A, B). The interaction with the KIT receptor is predicted to be preserved (Figure S6B). In aggregate, these data suggest that the cysteine at position 68 has a critical role in maintaining the structural and functional integrity of the protein.

In family 12-01744, *KITLG* c.310C>G was inherited from the mother (Figure 1C). The variant is predicted to substitute valine for leucine at position 104 (p.Leu104Val) and is not present in any of the exome databases (see 'Subjects and Methods) which include at least 4000 exomes of individuals of Dutch origin. The amino acid substitution is predicted to be deleterious for protein function according to Polyphen2 with a score of 0.998 (range 0-1; 0, benign; 1, probably damaging), mutation taster with a score of 1 (range 0-1; 0, benign; 1, probably

damaging), and SIFT with a score of 0.04 (≤ 0.05, probably damaging; >0.05 predicted tolerated). Leu104 is highly conserved with a score of 9 in ConSeq. Leu104 is buried inside an α-helix and therefore not interacting with the KIT receptor. The substitution Leu104Val is predicted to have a small, local effect on the structure since valine is predicted not to be exactly at the same position as leucine (Figure S6C, D). Although Leu104 is buried in the protein, neighboring residues can contact the KIT receptor. Therefore, a small effect on the position of these contacting residues is expected, but since the contact surfaces of KITLG and KIT receptor are much larger, the interaction is not predicted to be severely impaired by the Leu104Val substitution (Figure S6C, D).

KITLG encodes two KITLG isoforms through alternative splicing and proteolytic processing, a transmembrane isoform and a soluble isoform (Figure 4D). In mouse, it appears that soluble KITLG plays a role in melanocyte migration and/or early survival and transmembrane KITLG in melanocyte survival at or close to the destination.[26,37] All three KITLG mutations identified in this study affect both KITLG isoforms (Figure 4D).

KITLG variants affect protein localization and/or secretion

We studied the effect of the p.His67_Cys68delinsArg and p.Leu104Val variants on subcellular localization of transmembrane KITLG. NIH3T3 cells were transiently transfected with a set of plasmids to express the FLAG-tagged wild-type or variant human transmembrane KITLG (Figure 5A). The expression of wild-type and aberrant variants of KITLG was verified by Western blot analysis (Figure S7). Localization of KITLG at the cell membrane was addressed by labelling of the membrane with wheat germ agglutinin (WGA), a member of the lectin family, which binds to N-acetyl-D-glucosamine and sialic acid residues on the surface of cells. Both FLAG-tagged wild-type and p.Leu104Val KITLG were detected in the cytoplasm and at the cell membrane, also in lamellipodia and filipodia (Figure 5A). In contrast, p.His67_Cys68delinsArg KITLG staining did not overlap with the WGA-labeling (Figure 5A). This indicates that the transmembrane p.His67_Cys68delinsArg KITLG fails to reach the cell membrane and therefore will not or only to a very limited extent in comparison to controls, be integrated in the cell membrane which supports functional consequences of the mutation and the pathogenic effect of this variant.

As a next step, we investigated whether the p.His67_Cys68delinsArg, p.Leu104Val, and p.Ser96Ter variants affect proteolytic processing and subsequent secretion of soluble KITLG. After expression of wild-type and variant soluble KITLG in NIH3T3 cells, secreted KITLG was measured by

ELISA of the growth medium. The amount of soluble p.Leu104Val KITLG was significantly reduced as compared to wild-type soluble KITLG whereas no p.His67_Cys68delinsArg and p.Ser96Ter soluble KITLG could be detected (Figure 5B). These findings support a pathogenic effect of all three KITLG variants.

Since KITLG can be detected in human blood,[34] we assessed by Western blot analysis whether the levels of KITLG were significantly reduced in peripheral blood samples of affected individuals with the c.286_303delinsT, c.200_202del and c.310C>G mutations as compared to levels in control individuals. No clear differences were observed (Figure S8). Moreover, the truncated protein encoded by the c.286_303delinsT *KITLG* allele was not detected. This suggests that either the truncated protein is not stable and/or that the transcript is degraded by nonsense-mediated decay (NMD). Since the truncating variant is in exon 4, not in the last or penultimate exon, the transcript is predicted to be subject to NMD.[38]

Kitl expression in the mouse cochlea

Since expression of *KITLG/Kitl* in cochlear tissue was not demonstrated previously, we assessed transcription of *Kitl* in mouse cochlea by RT-PCR employing as templates cDNA derived from RNA of P2 and P28 mice. Two amplification products were obtained that corresponded to *Kitl* transcripts with and without exon 6. Moreover, q-PCR demonstrated that the relative levels of both *Kitl* alternative transcripts were increased at P28 as compared with those at P2 (Figure S9). Although blood in cochlear vessels might have contributed to the detected *Kitl* transcripts, our data suggest that *Kitl* functions postnatally in mouse inner ear.

DISCUSSION

Here, we present variant alleles of *KITLG*, alternatively called *SCF* (Stem Cell Factor) or *MGF* (Mast Cell Growth Factor), and provide evidence that these disease associated alleles underlie dominantly inherited NS-UHL/AHL and WS II. A combined strategy of linkage analysis and WES, revealed a heterozygous truncating mutation, c.286_303delinsT, in *KITLG* in a large Dutch pedigree (W09-1628) with NS-UHL/AHL. The HL is inherited as a dominant trait with incomplete penetrance. By further testing of *KITLG*, two additional mutations were identified in a small family with NS-UHL/AHL and in a family with WS

II. The HL in all three families with mutations in *KITLG* was congenital, stable and variable with regard to the affected ear as well as audiogram configuration and severity. Based on the variable expression of *KITLG* mutations, bilateral symmetric HI might be seen as a phenotypic outcome. However, no potentially pathogenic variants were identified in WES data of 231 cases with bilateral and symmetric HI (87 adNSHI and 144 isolated cases). This indicates that KITLG mutations are not a frequent cause of bilateral symmetric sensorineural HI.

KITLG-KIT signaling plays a role in proliferation, migration from the neural crest, and survival and differentiation of hematopoietic precursor cells, primordial germ cells and melanoblasts.[25-28,39] In mouse, severe mutations in *Kitl* (*Sl* locus) and *Kit* (*W* locus) are embryonic lethal in the homozygous state but viable when compound heterozygous with less severe defects as are semi-dominant mutations.[40-42] Mice homozygous for the semi-dominant alleles W^v of *kit* and Sl^d of *kitl* are viable and display similar phenotypes i.e. macrocytic anemia, sterility, absence of coat pigmentation and abnormal pigmentation of the iris and of the stria vascularis in the inner ear.[28,31,43-47] Absence or reduction of highly specialized melanocytes, the intermediate cells, in the stria vascularis leads to no or a reduced endocochlear potential (EP) and consequently to HL. This EP is the driving force for the transduction of sound via influx of K^+ and other cations into hair cells.[48,49] Steel *et al.* (1992)[47] demonstrated that in Sl^d/Sl^d mice, both the survival and targeting of melanoblasts to the developing inner ear is affected but not early melanoblast differentiation and migration. At 11 days of gestation, lower numbers of melanoblasts could be detected near the otic vesicle in mutants than in control animals and these numbers further decreased during development.[26,47]

In most of the studied inner ears of six days old W^v/W^v mice, no melanocytes could be detected in the stria vascularis which explains that no EP was measured. However, the penetrance of this phenotype was incomplete since in some ears, the EP was nearly normal and intermediate cells were present as in control mice.[28] This variability in severity of the hearing impairment and affected ear is reminiscent of the phenotype in the presented families with *KITLG* mutations. In W^v/W^v mice, this variability in inner ear phenotype was found to reflect the number of melanocytes present and how far they migrated along each cochlea.[28] Also, a stria vascularis with structural anomalies was found to be capable of maintaining a normal EP[50] which can contribute to the variable expressivity of the *KITLG* mutations in the presented families W09-1628 and 12-01744. Findings on secondary hair cell degeneration have been reported in *Kit* and *Kitl* mutant mice compound heterozygous for a null allele and an allele with the less severe mutations, W^v and Sl^d respectively.[27, 51] We have no indications for secondary hair

cell loss in the presented families since the HL was found or reported to be stable. However, we cannot exclude progressive degeneration of hair cells in the prenatal stage, especially in those cases with severe to profound HL in one ear.

In family W09-1628 vestibular testing in six individuals with the mutation and with HL revealed abnormal, vestibular responses in four of the subjects. However, these subjects did not report vestibular symptoms during history taking. The only individual that complained about balance problems was not tested on vestibular function because of her high age. In conclusion, it seems that vestibular dysfunction could be part of the inner ear phenotype associated with *KITLG* mutations. However, this seems to lead to subclinical abnormal function, since the majority of individuals with the mutation did not report vestibular symptoms which suggests sufficient compensatory mechanisms.

In families W09-1628 and S1489, there are no indications for phenotypes of the tissues that are affected in the *Kit* and *Kitl* mutant mice, other than the inner ear *i.e.* hematopoietic tissues, gonads, eye, hair and skin. This suggests dominance of the wild-type *KITLG* allele over the mutant allele in those tissues. For the KITLG mutation in family 12-01744 this does not hold true for the iris and skin.

Interestingly, activating *KITLG* mutations and variants in regulatory sequences of *KITLG* affect pigmentation of skin and hair. Firstly, missense mutations in *KITLG* are causative for familial progressive 2 hyperpigmentation and/or hypopigmentation syndromes (Figure 4D) (MIM 145250). Mutations underlying these syndromes are demonstrated (c.107A>G, p.Asn36Ser (NM_003994.5 and NM_000899.4)) or predicted (c.107A>G, p.(Val33Ala) and c.100A>C, p.(Thr34Pro)) to have an activating effect since all three are in the conserved VTNN motif.[52,53] Protein modeling suggests that mutations in this domain may affect the affinity of KITLG for KIT.[52] Secondly, SNPs in *KITLG* regulatory regions are associated with skin and hair pigmentation (rs642742 and rs12821256, MIM 611664).[31] These data, together with the facts that KIT signaling regulates MITF function[13,54,55] and that genes associated with hypopigmentation-deafness disorders function in the KIT-MITF pathway,[8,56] pinpointed *KITLG* as a candidate gene for WS II. Indeed, we have identified a missense mutation in *KITLG* to be associated with WS II in family 12-01744. The HL phenotype in this family is similar to that in families W09-1628 and S1489. The pigmentation abnormalities of skin and iris in this WSII family suggest a more severe effect of the p.Leu104Val substitution in these tissues, as compared to the p.Ser96Ter and the p.His67_Cys68delinsArg mutations which might be through a gain of function or dominant negative effect for either of

the transmembrane isoform of p.Leu104Val KITLG or the soluble isoform or both. To activate KIT, dimerization occurs for both isoforms.[57,58] The p.Ser96Ter and the p.His67_Cys68delinsArg defects are likely to have a loss of function effect since the transmembrane isoform of p.His67_Cys68delinsArg KITLG is not detectably integrated into the membrane which will also be the case for the p.Ser96Ter KITLG since it lacks the transmembrane domain. Also, for both defects, the soluble isoform could not be detected in ELISA of the medium of cultured cells.

Our findings add *KITLG* to the family of genes associated with pigmentation-deafness disorders *i.e. KIT, PAX3* (MIM 606597), *SOX10* (MIM 602229), *EDN3* (MIM 131242), *EDNRB* (MIM 131244), and *MITF*. As presented here for *KITLG*, the phenotypic variability of mutations in several of these hypopigmentation-deafness genes depends on whether the effect of the mutation is loss of function (dosage), (presumably) dominant negative or activating. Loss of function mutations in *MITF* for example are dominant and cause WS II. Mutations in *MITF* that underlie Tietz syndrome are assumed to have a dominant negative effect. Tietz syndrome (MIM 103500) is more severe than WS II and characterized by fully penetrant bilateral, congenital and profound HL with fair and blond skin, so called "born as snow white".[59]

In conclusion, we demonstrate that allelic mutations in *KITLG* can underlie different clinical conditions and these findings extend the set of genes known to be associated with hypopigmentation-deafness disorders as KITLG is now shown to be associated with WS II and with NS-UHL/AHL. Analogous to mouse, the severity of the human phenotype is likely to reflect the number of melanocytes that have reached the inner ear and skin and/or survived in these tissues.

Acknowledgements

The authors thank Mrs. Saskia van der Velde-Visser for technical assistance and Dr. Christian Gilissen for assistance in bioinformatics. We are grateful to Rafael Gonzalo-Gobernado (Microscopy Unit, IRYCIS) for the technical assistance and to Prof. Guy Richardson for kindly providing mRNA of mouse cochlea for RT-PCR experiments. We would like to thank Dr. Andy Beynon for the fruitful discussions about audiometric phenotypes. This work was supported by the Oticon Foundation (09-3742, to HK), by ZonMW (40-00812-98-09047, to HK and 90700388, to RJEP), by the Heinsius Houbolt Foundation (to HK and HPK), by ISCIII (PI11/1215, PI14/0948, to MAMP) and Fundación Ramón Areces (to MAMP), and by US NHGRI/NHBLI Baylor Hopkins Center for

Mendelian Genomics (HG006542). LSdC was supported by a post-doctoral training grant from Programa Ciência sem Fronteiras/CNPq (Conselho Nacional de Desenvolvimento Científico e Tecnológico, Brazil) - 201399/2012-1.

WEB RESOURCES

Alamut Visual: http://www.interactive-biosoftware.com/alamut-visual/
CIBERER Exome Server: http://bioinfo.cipf.es/apps-beta/exome-server/beta/
Exome Aggregation Consortium: http://exac.broadinstitute.org/
Exome variant server: http://evs.gs.washington.edu/EVS/
ExonPrimer: http://ihg.gsf.de/ihg/ExonPrimer.html
Genome browser: http://genome.ucsc.edu/
Mammalian genotyping service (Marshfield map): http://research.marshfieldclinic.org/
Mouse Genome Informatics: https://www.jax.org/research-and-faculty/tools/hereditary-hearing-impairment/hearing-mice-table-two
Mutation Taster: www.mutationtaster.org
Online Mendelian Inheritance in Man (OMIM) phenotypic series: http://omim.org/phenotypicSeries/
OMIM: http://www.omim.org/
Plink: http://pngu.mgh.harvard.edu/~purcell/plink/
Polyphen2: http://genetics.bwh.harvard.edu/pph2/
SIFT: http://sift.jcvi.org/
SuperLink online SNP 1.1 software: http://cbl-hap.cs.technion.ac.il/superlink-snp/
The Conseq server: http://conseq.tau.ac.il/
WHAT IF Twinset: http://swift.cmbi.ru.nl/whatif/
HGSC Mercury analysis pipeline: https://www.hgsc.bcm.edu/software/mercury
Yasara: http://www.yasara.org/

Accession numbers

Variants were submitted to LOVD (ID#: 0000065309, 0000065310 and 0000065311).

REFERENCES

1. Everberg, G. (1957). Hereditary unilateral deafness. Acta Otolaryngol. 47, 303-311.
2. Everberg, G. (1960). Further studies on hereditary unilateral deafness. Acta Otolaryngol. 51, 615-635.
3. Dikkers, F.G., Verheij, J.B., and van Mechelen, M. (2005). Hereditary congenital unilateral deafness: a new disorder? Ann. Otol. Rhinol. Laryngol. 114, 332-337.
4. Pingault, V., Ente, D., Dastot-Le Moal, F., Goossens, M., Marlin, S., and Bondurand, N. (2010). Review and update of mutations causing Waardenburg syndrome. Hum. Mutat. 31, 391-406.
5. Perez-Losada, J., Sanchez-Martin, M., Rodriguez-Garcia, A., Sanchez, M.L., Orfao, A., Flores, T., and Sanchez-Garcia, I. (2002). Zinc-finger transcription factor Slug contributes to the function of the stem cell factor c-kit signaling pathway. Blood 100, 1274-1286.
6. Sato-Jin, K., Nishimura, E.K., Akasaka, E., Huber, W., Nakano, H., Miller, A., Du, J., Wu, M., Hanada, K., Sawamura, D., et al. (2008). Epistatic connections between microphthalmia-associated transcription factor and endothelin signaling in Waardenburg syndrome and other pigmentary disorders. FASEB J. 22, 1155-1168.
7. Read, A.P., and Newton, V.E. (1997). Waardenburg syndrome. J. Med. Genet. 34, 656-665.
8. Hou, L., and Pavan, W.J. (2008). Transcriptional and signaling regulation in neural crest stem cell-derived melanocyte development: do all roads lead to Mitf? Cell Res. 18, 1163-1176.
9. Lang, D., Lu, M.M., Huang, L., Engleka, K.A., Zhang, M., Chu, E.Y., Lipner, S., Skoultchi, A., Millar, S.E., and Epstein, J.A. (2005). Pax3 functions at a nodal point in melanocyte stem cell differentiation. Nature 433, 884-887.
10. Fleischman, R.A., Saltman, D.L., Stastny, V., and Zneimer, S. (1991). Deletion of the c-kit protooncogene in the human developmental defect piebald trait. Proc. Natl. Acad. Sci. USA 88, 10885-10889.
11. Comings, D.E., and Odland, G.F. (1966). Partial albinism. JAMA 195, 519-523.
12. Spritz, R.A., and Beighton, P. (1998). Piebaldism with deafness: molecular evidence for an expanded syndrome. Am. J. Med. Genet. 75, 101-103.
13. Hemesath, T.J., Price, E.R., Takemoto, C., Badalian, T., and Fisher, D.E. (1998). MAP kinase links the transcription factor Microphthalmia to c-Kit signalling in melanocytes. Nature 391, 298-301.
14. De Leenheer, E.M., Huygen, P.L., Coucke, P.J., Admiraal, R.J., van Camp, G., and Cremers, C.W. (2002). Longitudinal and cross-sectional phenotype analysis in a new, large Dutch DFNA2/KCNQ4 family. Ann. Otol. Rhinol. Laryngol. 111, 267-274.
15. Theunissen, E.J., Huygen, P.L., and Folgering, H.T. (1986). Vestibular hyperreactivity and hyperventilation. Clin. Otolaryngol. Allied Sci. 11, 161-169.
16. Wuyts, F.L., Furman, J., Vanspauwen, R., and Van de Heyning, P. (2007). Vestibular function testing. Curr. Opin. Neurol. 20, 19-24.

17. Pekelharing JM, H.O., de Jonge R, Lokhoff J, Sodikromo J, Spaans M, Brouwer R, de Lathouder S, Hinzmann R. (2010). Haematology reference intervals for established and novel parameters in healthy adults. Diagnostic Perspectives, 1-11.
18. Silberstein, M., Weissbrod, O., Otten, L., Tzemach, A., Anisenia, A., Shtark, O., Tuberg, D., Galfrin, E., Gannon, I., Shalata, A., et al. (2013). A system for exact and approximate genetic linkage analysis of SNP data in large pedigrees. Bioinformatics 29, 197-205.
19. Purcell, S., Neale, B., Todd-Brown, K., Thomas, L., Ferreira, M.A., Bender, D., Maller, J., Sklar, P., de Bakker, P.I., Daly, M.J., et al. (2007). PLINK: a tool set for whole-genome association and population-based linkage analyses. Am. J. Hum. Genet. 81, 559-575.
20. Schraders, M., Haas, S.A., Weegerink, N.J., Oostrik, J., Hu, H., Hoefsloot, L.H., Kannan, S., Huygen, P.L., Pennings, R.J., Admiraal, R.J., et al. (2011). Next-generation sequencing identifies mutations of SMPX, which encodes the small muscle protein, X-linked, as a cause of progressive hearing impairment. Am. J. Hum. Genet. 88, 628-634.
21. Bainbridge, M.N., Wang, M., Wu, Y., Newsham, I., Muzny, D.M., Jefferies, J.L., Albert, T.J., Burgess, D.L., and Gibbs, R.A. (2011). Targeted enrichment beyond the consensus coding DNA sequence exome reveals exons with higher variant densities. Genome Biol. 12, R68.
22. Reid, J.G., Carroll, A., Veeraraghavan, N., Dahdouli, M., Sundquist, A., English, A., Bainbridge, M., White, S., Salerno, W., Buhay, C., et al. (2014). Launching genomics into the cloud: deployment of Mercury, a next generation sequence analysis pipeline. BMC Bioinformatics 15, 30.
23. Challis, D., Yu, J., Evani, U.S., Jackson, A.R., Paithankar, S., Coarfa, C., Milosavljevic, A., Gibbs, R.A., and Yu, F. (2012). An integrative variant analysis suite for whole exome next-generation sequencing data. BMC Bioinformatics 13, 8.
24. Morin, M., Bryan, K.E., Mayo-Merino, F., Goodyear, R., Mencia, A., Modamio-Hoybjor, S., del Castillo, I., Cabalka, J.M., Richardson, G., Moreno, F., et al. (2009). In vivo and in vitro effects of two novel gamma-actin (ACTG1) mutations that cause DFNA20/26 hearing impairment. Hum. Mol. Genet. 18, 3075-3089.
25. Broudy, V.C. (1997). Stem cell factor and hematopoiesis. Blood 90, 1345-1364.
26. Wehrle-Haller, B., and Weston, J.A. (1995). Soluble and cell-bound forms of steel factor activity play distinct roles in melanocyte precursor dispersal and survival on the lateral neural crest migration pathway. Development 121, 731-742.
27. Schrott, A., Melichar, I., Popelar, J., and Syka, J. (1990). Deterioration of hearing function in mice with neural crest defect. Hear. Res. 46, 1-7.
28. Cable, J., Barkway, C., and Steel, K.P. (1992). Characteristics of stria vascularis melanocytes of viable dominant spotting (Wv/Wv) mouse mutants. Hear. Res. 64, 6-20.
29. Rerknimitr, P., Disphanurat, W., and Achariyakul, M. (2013). Topical tacrolimus significantly promotes repigmentation in idiopathic guttate hypomelanosis: a double-blind, randomized, placebo-controlled study. J. Eur. Acad. Dermatol. Venereol. 27, 460-464.

30. Miller, C.T., Beleza, S., Pollen, A.A., Schluter, D., Kittles, R.A., Shriver, M.D., and Kingsley, D.M. (2007). cis-Regulatory changes in Kit ligand expression and parallel evolution of pigmentation in sticklebacks and humans. Cell 131, 1179-1189.
31. Guenther, C.A., Tasic, B., Luo, L., Bedell, M.A., and Kingsley, D.M. (2014). A molecular basis for classic blond hair color in Europeans. Nat. Genet. 46, 748-752.
32. Pandya, A., Xia, X.J., Landa, B.L., Arnos, K.S., Israel, J., Lloyd, J., James, A.L., Diehl, S.R., Blanton, S.H., and Nance, W.E. (1996). Phenotypic variation in Waardenburg syndrome: mutational heterogeneity, modifier genes or polygenic background? Hum. Mol. Genet. 5, 497-502.
33. Reynolds, J.E., Meyer, J.M., Landa, B., Stevens, C.A., Arnos, K.S., Israel, J., Marazita, M.L., Bodurtha, J., Nance, W.E., and Diehl, S.R. (1995). Analysis of variability of clinical manifestations in Waardenburg syndrome. Am. J. Med. Genet. 57, 540-547.
34. Langley, K.E., Wypych, J., Mendiaz, E.A., Clogston, C.L., Parker, V.P., Farrar, D.H., Brothers, M.O., Satygal, V.N., Leslie, I., Birkett, N.C., et al. (1992). Purification and characterization of soluble forms of human and rat stem cell factor recombinantly expressed by Escherichia coli and by Chinese hamster ovary cells. Arch. Biochem. Biophys. 295, 21-28.
35. Jones, M.D., Narhi, L.O., Chang, W.C., and Lu, H.S. (1996). Refolding and oxidation of recombinant human stem cell factor produced in Escherichia coli. J. Biol. Chem. 271, 11301-11308.
36. Nishikawa, M., Tojo, A., Ikebuchi, K., Katayama, K., Fujii, N., Ozawa, K., and Asano, S. (1992). Deletion mutagenesis of stem cell factor defines the C-terminal sequences essential for its biological activity. Biochem. Biophys. Res. Commun. 188, 292-297.
37. Tabone-Eglinger, S., Calderin-Sollet, Z., Pinon, P., Aebischer, N., Wehrle-Haller, M., Jacquier, M.C., Boettiger, D., and Wehrle-Haller, B. (2014). Niche anchorage and signaling through membrane-bound Kit-ligand/c-kit receptor are kinase independent and imatinib insensitive. FASEB J. 28, 4441-4456.
38. Nagy, E., and Maquat, L.E. (1998). A rule for termination-codon position within intron-containing genes: when nonsense affects RNA abundance. Trends Biochem. Sci. 23, 198-199.
39. Hoyer, P.E., Byskov, A.G., and Mollgard, K. (2005). Stem cell factor and c-Kit in human primordial germ cells and fetal ovaries. Mol. Cell. Endocrinol. 234, 1-10.
40. Huang, E., Nocka, K., Beier, D.R., Chu, T.Y., Buck, J., Lahm, H.W., Wellner, D., Leder, P., and Besmer, P. (1990). The hematopoietic growth factor KL is encoded by the Sl locus and is the ligand of the c-kit receptor, the gene product of the W locus. Cell 63, 225-233.
41. Copeland, N.G., Gilbert, D.J., Cho, B.C., Donovan, P.J., Jenkins, N.A., Cosman, D., Anderson, D., Lyman, S.D., and Williams, D.E. (1990). Mast cell growth factor maps near the steel locus on mouse chromosome 10 and is deleted in a number of steel alleles. Cell 63, 175-183.

42. Rajaraman, S., Davis, W.S., Mahakali-Zama, A., Evans, H.K., Russell, L.B., and Bedell, M.A. (2002). An allelic series of mutations in the Kit ligand gene of mice. II. Effects of ethylnitrosourea-induced Kitl point mutations on survival and peripheral blood cells of Kitl(Steel) mice. Genetics 162, 341-353.
43. Zsebo, K.M., Williams, D.A., Geissler, E.N., Broudy, V.C., Martin, F.H., Atkins, H.L., Hsu, R.Y., Birkett, N.C., Okino, K.H., Murdock, D.C., et al. (1990). Stem cell factor is encoded at the Sl locus of the mouse and is the ligand for the c-kit tyrosine kinase receptor. Cell 63, 213-224.
44. Geissler, E.N., Cheng, S.V., Gusella, J.F., and Housman, D.E. (1988). Genetic analysis of the dominant white-spotting (W) region on mouse chromosome 5: identification of cloned DNA markers near W. Proc. Natl. Acad. Sci. USA 85, 9635-9639.
45. Geissler, E.N., Ryan, M.A., and Housman, D.E. (1988). The dominant-white spotting (W) locus of the mouse encodes the c-kit proto-oncogene. Cell 55, 185-192.
46. Chabot, B., Stephenson, D.A., Chapman, V.M., Besmer, P., and Bernstein, A. (1988). The proto-oncogene c-kit encoding a transmembrane tyrosine kinase receptor maps to the mouse W locus. Nature 335, 88-89.
47. Steel, K.P., Davidson, D.R., and Jackson, I.J. (1992). TRP-2/DT, a new early melanoblast marker, shows that steel growth factor (c-kit ligand) is a survival factor. Development 115, 1111-1119.
48. Takeuchi, S., Ando, M., and Kakigi, A. (2000). Mechanism generating endocochlear potential: role played by intermediate cells in stria vascularis. Biophys. J. 79, 2572-2582.
49. Hudspeth, A.J. (2014). Integrating the active process of hair cells with cochlear function. Nat. Rev. Neurosci. 15, 600-614.
50. Brown, P.G., and Ruben, R.J. (1969). The endocochlear potential in the Shaker-1 (sh-1-sh-1) mouse. Acta Otolaryngol. 68, 14-20.
51. Deol, M.S. (1970). The relationship between abnormalities of pigmentation and of the inner ear. Proc R Soc Lond B Biol Sci. 175, 201-217.
52. Amyere, M., Vogt, T., Hoo, J., Brandrup, F., Bygum, A., Boon, L., and Vikkula, M. (2011). KITLG mutations cause familial progressive hyper- and hypopigmentation. J. Invest. Dermatol. 131, 1234-1239.
53. Wang, Z.Q., Si, L., Tang, Q., Lin, D., Fu, Z., Zhang, J., Cui, B., Zhu, Y., Kong, X., Deng, M., et al. (2009). Gain-of-function mutation of KIT ligand on melanin synthesis causes familial progressive hyperpigmentation. Am. J. Hum. Genet. 84, 672-677.
54. Opdecamp, K., Nakayama, A., Nguyen, M.T., Hodgkinson, C.A., Pavan, W.J., and Arnheiter, H. (1997). Melanocyte development in vivo and in neural crest cell cultures: crucial dependence on the Mitf basic-helix-loop-helix-zipper transcription factor. Development 124, 2377-2386.

55. Wu, M., Hemesath, T.J., Takemoto, C.M., Horstmann, M.A., Wells, A.G., Price, E.R., Fisher, D.Z., and Fisher, D.E. (2000). c-Kit triggers dual phosphorylations, which couple activation and degradation of the essential melanocyte factor Mi. Genes Dev. 14, 301-312.
56. Sommer, L. (2011). Generation of melanocytes from neural crest cells. Pigment. Cell Melanoma Res. 24, 411-421.
57. Paulhe, F., Wehrle-Haller, M., Jacquier, M.C., Imhof, B.A., Tabone-Eglinger, S., and Wehrle-Haller, B. (2009). Dimerization of Kit-ligand and efficient cell-surface presentation requires a conserved Ser-Gly-Gly-Tyr motif in its transmembrane domain. FASEB J. 23, 3037-3048.
58. Zhang, Z., Zhang, R., Joachimiak, A., Schlessinger, J., and Kong, X.P. (2000). Crystal structure of human stem cell factor: implication for stem cell factor receptor dimerization and activation. Proc. Natl. Acad. Sci. USA 97, 7732-7737.
59. Smith, S.D., Kelley, P.M., Kenyon, J.B., and Hoover, D. (2000). Tietz syndrome (hypopigmentation/deafness) caused by mutation of MITF. J. Med. Genet. 37, 446-448.

SUPPLEMENTAL CLINICAL INFORMATION, FIGURES, TABLES AND LEGENDS

Supplemental Note

Family W09-1628

Individual V:7. Otoscopy revealed a fragile appearance of the malleus and an underdeveloped superior part of the auricle. These abnormalities were also seen in his brother (V:8) with normal hearing. CT imaging revealed no inner ear anomalies.

A dip at 4 kHz in the right ear was observed in pure tone audiometry. Such a dip is specifically associated with noise exposure although no excessive noise exposure was reported by the affected individual.

Individual III:6. The affection status of III:6 is indicated with a question mark in the pedigree (Figure 1) because his hearing loss (HL) might well be caused by other factors than the segregating genetic defect (Figure 1 and Figure S5). The HL in the left ear of individual III:6 had an onset between 45.56 and 46.46 years of age. Before the age of 45 years hearing was normal, as shown in Figure S3.

Individual V:10. This individual has a symmetric, mild mixed HL which can be explained by his recurrent otitis media.

Individual III:2. This individual, indicated to have balance problems while walking on uneven ground and when walking on a straight line. He is a spouse and does not carry the genetic defect segregating in the family.

Individual III:5. With regard to hair and eye color, individual III:5 was lighter than all other family members. She heterozygously carries the rs12821256 G allele that is associated with blond hair (Figure S5).[1]

Family S1489

Otoscopy did not reveal any abnormalities for the affected father and son (II:1 and III:1, respectively) and there was no evidence of non-genetic causes of the HL. MRI did neither demonstrate inner ear abnormalities nor cerebellopontine angle pathology. Propositus III:1 indicated to have suffered from atopic dermatitis in the past.

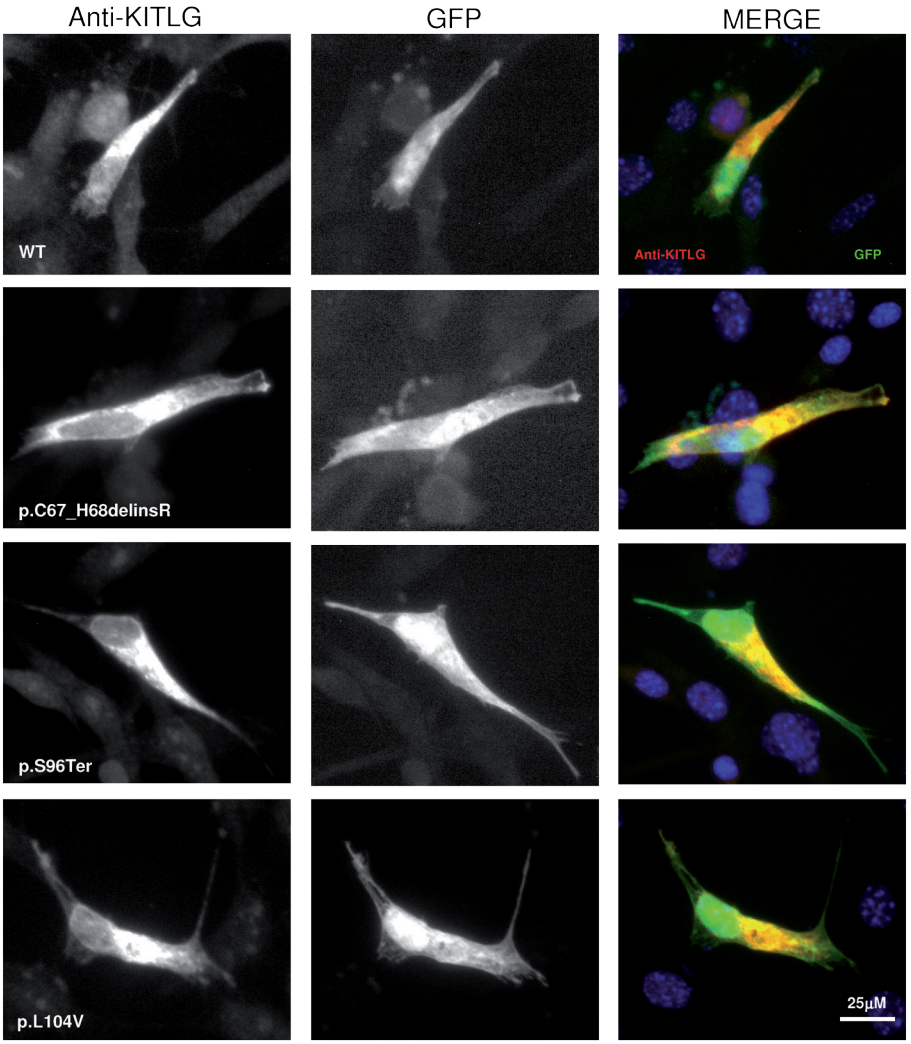

Figure S1. Expression of wild-type and aberrant soluble KITLG as detected by inmunofluorescence in transfected NIH3T3 cells used in the ELISA assays.

Cells were permeablized and incubated with anti-KITLG and Alexa488 goat anti mouse (left column), GFP signal (middle column) and merged (right column). Nuclei were stained with Hoechst (in blue). "WT" means wild-type.

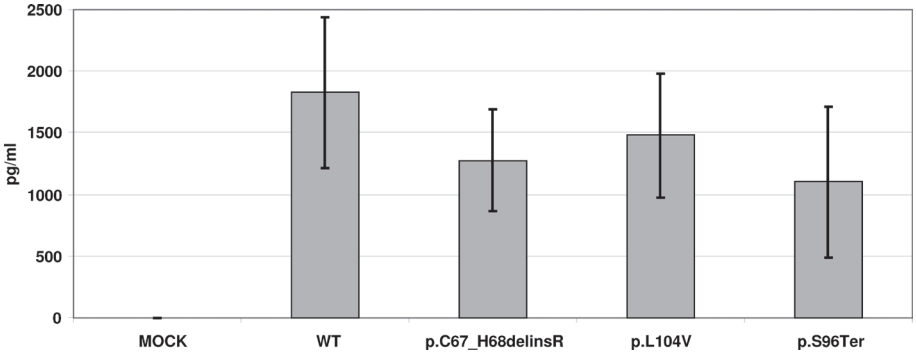

Figure S2. KITLG concentrations determined by ELISA. NIH3T3 cells transfected with a set of plasmids encoding FLAG-tagged wild-type and aberrant transmembrane KITLG were lysed and 10 µl of cell extracts were analysed by ELISA. Expression of wild-type and aberrant KITLG was readily detected. Data are means ±SD. "WT" means wild-type.

A

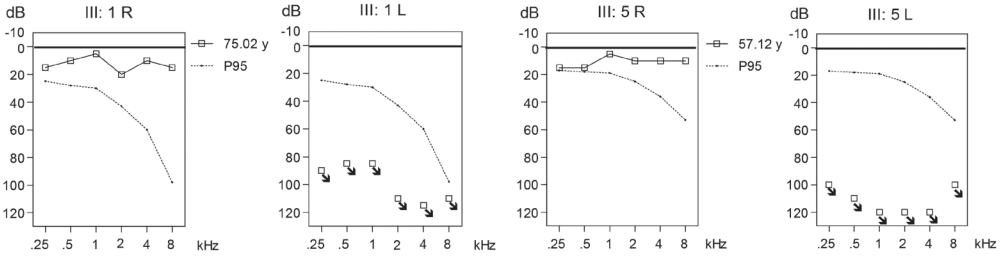
dB
III: 1 R
75.02 y
P95
III: 1 L
III: 5 R
57.12 y
III: 5 L
IV: 1 R
51.63 y
IV: 1 L
V: 7 R
3.82 y
5.08 y
7.71 y
10.44 y
14.10 y
22.56 y
P95 (22)
V: 7 L
-10
0
20
40
60
80
100
120
.25 .5 1 2 4 8
kHz

B

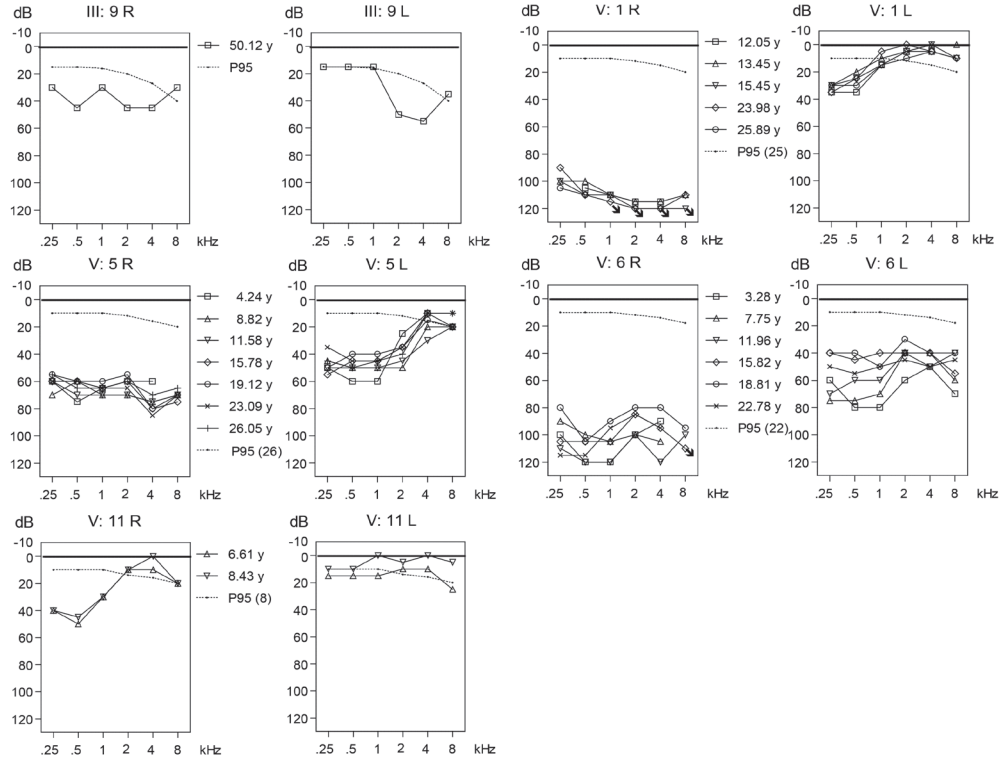
dB
III: 9 R
50.12 y
P95
III: 9 L
V: 1 R
12.05 y
13.45 y
15.45 y
23.98 y
25.89 y
P95 (25)
V: 1 L
V: 5 R
4.24 y
8.82 y
11.58 y
15.78 y
19.12 y
23.09 y
26.05 y
P95 (26)
V: 5 L
V: 6 R
3.28 y
7.75 y
11.96 y
15.82 y
18.81 y
22.78 y
P95 (22)
V: 6 L
V: 11 R
6.61 y
8.43 y
P95 (8)
V: 11 L
-10
0
20
40
60
80
100
120
.25 .5 1 2 4 8
kHz

C

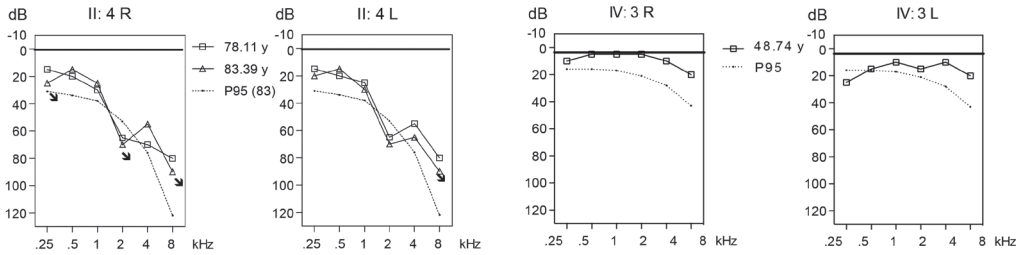

D

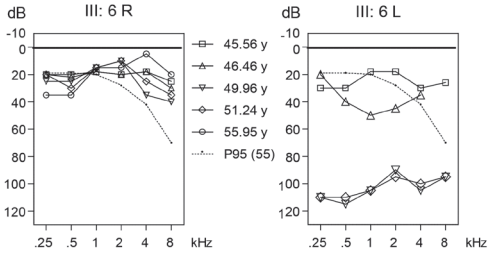

Figure S3. Pure tone air-conduction audiograms of individuals of family W09-1628 who have the *KITLG* c.286_303delinsT variant. Thresholds of the right (R) and left (L) ears are shown separately. Age is indicated in years between the audiograms of R and L ears. When available, longitudinal data are shown. The dashed lines in the audiograms represent the P95 thresholds related to the person's sex and age at the last measurement. Audiograms of individuals with UHL (A), AHL (B), normal hearing (C) and questionable affection status (D) are indicated.

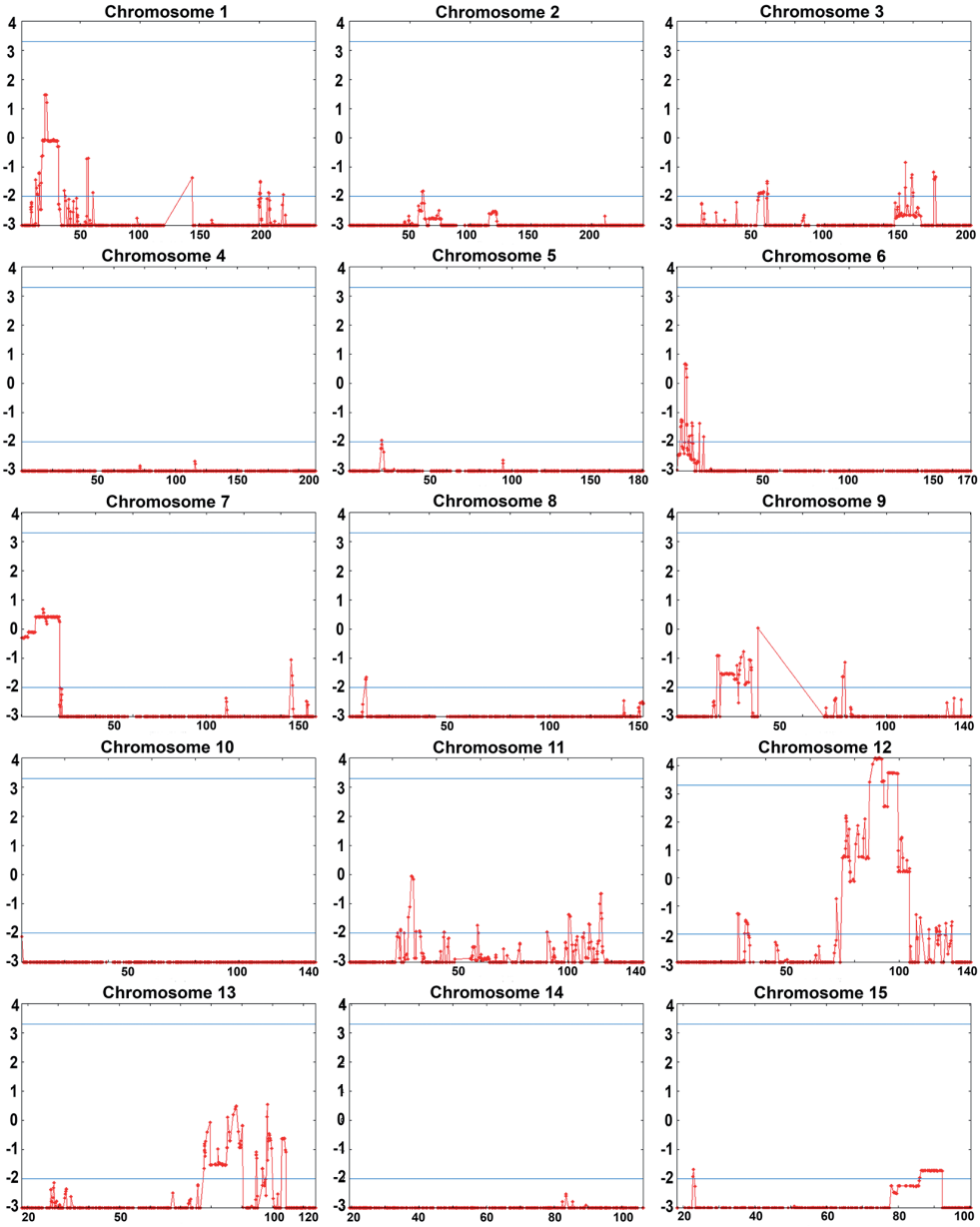
Chromosome 1
Chromosome 2
Chromosome 3
Chromosome 4
Chromosome 5
Chromosome 6
Chromosome 7
Chromosome 8
Chromosome 9
Chromosome 10
Chromosome 11
Chromosome 12
Chromosome 13
Chromosome 14
Chromosome 15

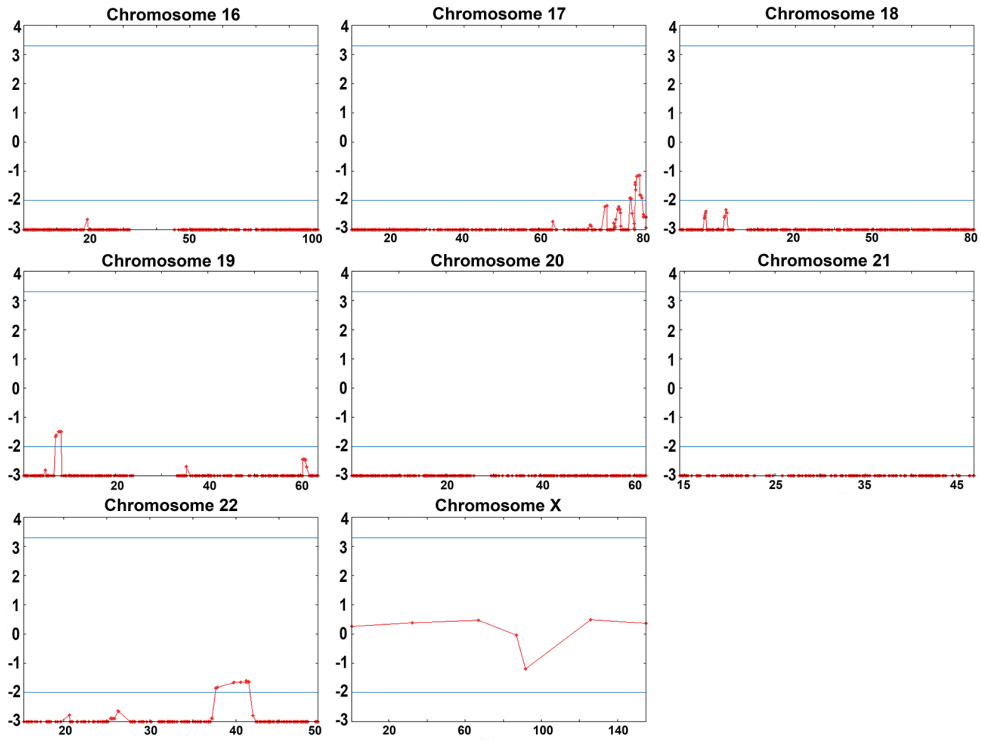

Figure S4. Genome wide LOD scores as calculated using SuperLink online SNP 1.1 software. The Y axis represents LOD scores and the X axis genetic distance in centimorgans (cM), per chromosome. The blue lines mark a LOD score of 3.3 indicating genome wide significance and a LOD score of -2.0 indicating exclusion of linkage. In the calculations, windows of 10 SNPs were used; penetrance was set at 70% and the disease allele frequency at 0.001. There is only one region in chromosome 12q21.32-q23.1, delimited by rs10459171 and rs35723, (chr12:87,808,426-100,960,087; GRCh37, hg19) with a significant maximum LOD score of 4.27 for rs7132875 and rs7309222.

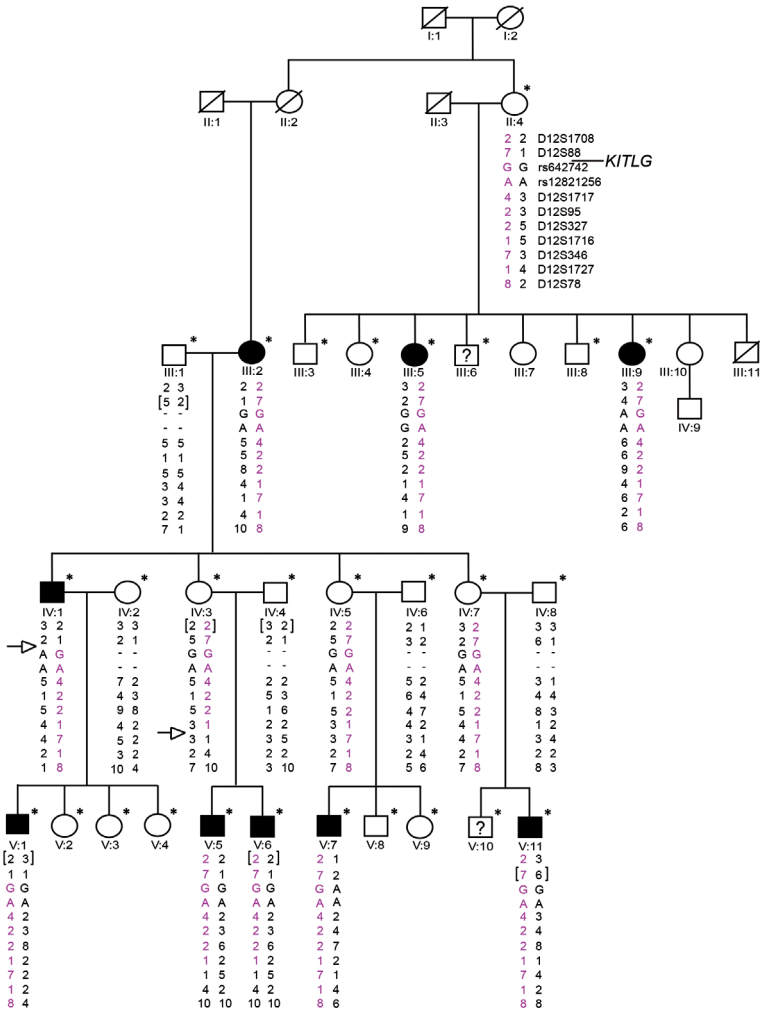

Figure S5. Genotypes of VNTR markers and SNPs in regulatory sequences of *KITLG*. VNTR marker order is according to the Marshfield map. In brackets, the genotypes are indicated which were inferred from the pedigree information. For privacy reasons, the genotypes for the disease allele have not been indicated for unaffected individuals with the c.286_303delinsT mutation except for those with affected offspring. Recombination events in individuals IV:1 and IV:3 define the disease allele (in pink) flanked by D12S88 to D12S346. Only one individual of unclear affection status (III:6) and three symptomatic individuals with the mutation (III:9, IV:1, V:7) were heterozygous for the A allele of SNP rs6427402 (allele frequency 92% in West Africans[2]). The G allele of rs12821256, which is associated with blond hair, is most prevalent in northern Europe.1 Only individual III:5 has a G allele for rs12821256. Her hair and eye color are lighter blond and blue, respectively, when compared to the other family members (Table S4).

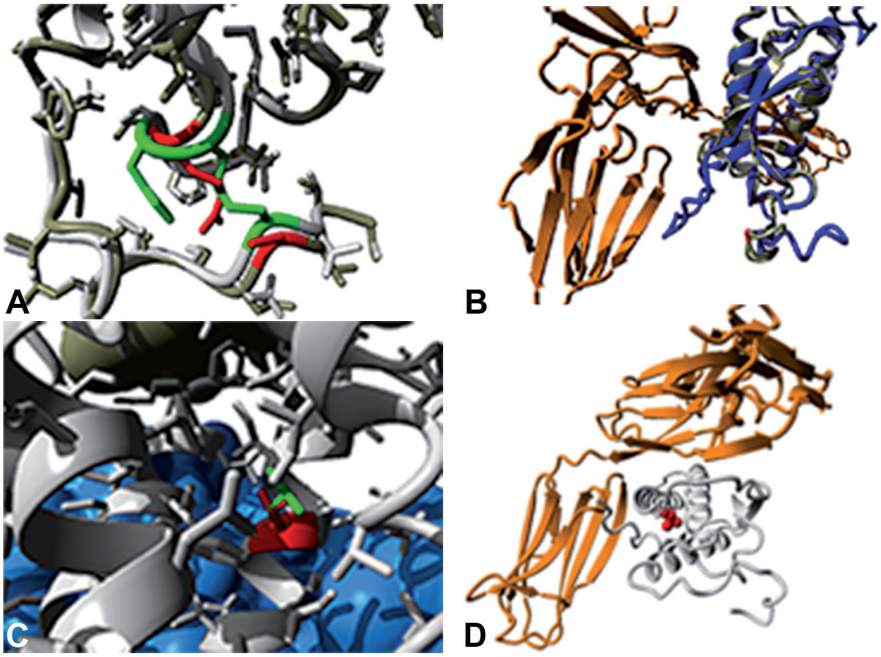

Figure S6. A molecular modeling of the KITLG variants p.His67_Cys68delinsArg and p.Leu104Val using PDB files 1cfs and 2o26. The model for KITLG and KIT was constructed using the PDB files 1scf and 2o26 as templates.[3] The 1scf file contains the structure of human KITLG. In order to study the interaction of KITLG with the KIT receptor we constructed the Kit-Kitl complex using PDB-file 2o26. The 2o26 file contains the structures for KITLG and KIT from mouse, which are 77% and 67% identical to respectively KITLG and KIT in humans. The generated human KIT model was superposed on the mouse KIT-KITLG complex. The YASARA[4] and WHAT IF Twinset[5] were employed (with default parameters) for model building and subsequent analyses.[6] A) A close-up of the loop affected by the p.His67_Cys68delinsArg variant. In green, the intramolecular disulfide bond formed by Cys68 and Cys163 is presented. The inserted Arg and Cys163 that is left without a binding partner are presented in red. Loss of the Cys68-Cys163 intramolecular bond is predicted to affect the local structure of the loop and the overall active KITLG conformation. The wild- type protein is in grey, the substituted in moss-green. B) Overview of the KIT receptor in orange, the wild-type KITLG in blue, and the KITLG with p.His67_Cys68delinsArg in grey. The amino acid residue affected by the substitution is in red. C) A close-up of the α-helix affected by the p.Leu104Val variant. In green, the wild-type Leu104 is shown and in red the variant Val104. Valine is smaller than leucine and it prefers β-sheets rather than α-helices. Therefore, p.Leu104Val might have a disruptive effect on the secondary structure of KITLG. D) Overview of the KIT receptor (orange) and the KITLG (grey) with the substituted Leu104, the side chain of this residue is shown as red balls.

Figure S7

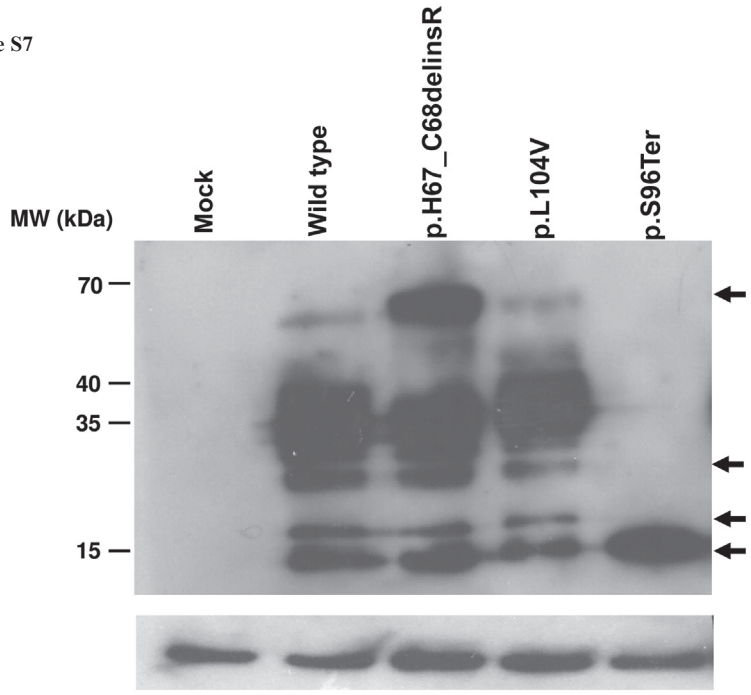

Figure S8

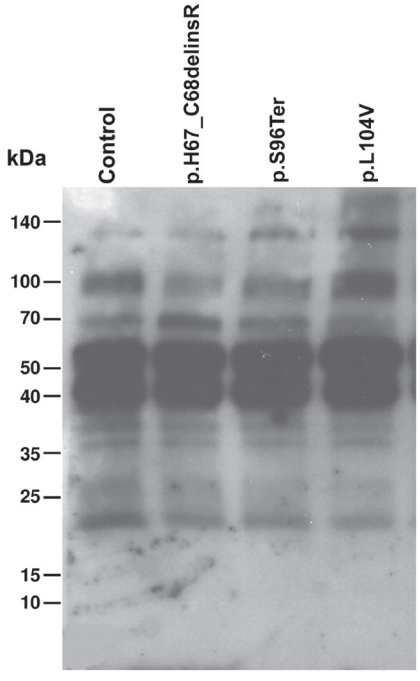

Figure S7. KITLG detection on Western blot of NIH3T3 cells transfected with constructs encoding transmembrane wild-type, p.His67_Cys68delinsArg, p.Leu104Val and p.Ser96Ter KITLG. Transfected NIH3T3 cells were homogenized in lysis buffer (150 mM NaCl, 50 mM Tris HCl, pH 7.4, 5 mM EGTA, 5 mM EDTA, 1% Triton X-100, 25 lg/ml leupeptin, and 1 mM phenylmethylsulphonylfluoride) and kept on ice for 30 min. After centrifugation at 10,000g (4ºC) for 5 min, 50 µg of protein were mixed 1:1 with SDS-PAGE sample buffer (50 mM Tris–Cl, pH 6.8, 50 mM DTT, 2% SDS, 10% glycerol, 5% βME). Proteins were separated in a SDS-PAGE gel and transferred electrophoretically to nitrocellulose membranes. After blocking with 5% skimmed dry milk in 1% TBS (pH 7.6), 0.1% Tween 20 for 1 hr at RT, blots were incubated with the mouse anti-FLAG antibody (1:1000) (SIGMA, F1804)) overnight at 4ºC. After washing, membranes were incubated with sheep anti-mouse IgG (1:10000) conjugated with HRP (Amersham Biosciences) for 1 hr at RT. Bands were visualized by enhanced chemiluminiscence (Clarity Western ECL substrate; Biorad) and exposed to X-ray film at different time points. Beta-actin was used as loading control. Arrows indicate bands of ~15, ~16, ~28 and ~68 kDa, respectively. Shown data is a representative of three independent experiments. Besides the ~28 kDa band corresponding to the expected size of FLAG-tagged KITLG, several other bands spanning a molecular weight range of about 28-35 kDa were detected, indicating extensive and heterogeneous glycosylation.[7,8] An additional band of 15 kDa was readily detected for the truncated p.Ser96Ter KITLG and was also present in the other samples, but with less intensity. This protein might represent the usage of an alternative ATG codon, downstream of the codon of Serine 96, and in frame with the three FLAG tags. A lighter second band of around 16 kDa was also detected in all samples which might be the result of proteolytic processing of the protein. Although the transmembrane isoform, expressed in this experiment, lacks the proteolytic cleavage site (encoded by exon 6), alternative proteolytic might have occurred as has been proposed for the murine Kitl.[9] Finally, a band of ~68 kDa was detected which is more intense for the p.His67_Cys68delinsArg mutation than for the other mutations and control suggesting an increased tendency to aggregate. The bands of about 16 and 15 kDa were not detected when we used the anti-KITLG antibody that is directed against the N-terminal region of the human KITLG (data not shown).

Figure S8. p.His67_Cys68delinsArg, p.Ser96Ter and p.Leu104Val aberrations do not lead to clear alterations of KITLG levels in blood. To analyze KITLG expression in human blood, 1 ml of blood was collected from individuals II:1 of family 12-01744, V:1 of family W09-1628 and II:1 of family S1489. Blood samples were centrifuged for 15 min at 15000 rpm at 4 ºC. One µl of supernatant was used for Western blot analysis with the anti-KITLG antibody (abcam, ab52603, anti-SCF) as primary antibody (1:1000) and the sheep anti-rabbit IgG (1:10000) conjugated with HRP (Amersham Biosciences) as secondary antibody. Western blot analysis was performed as described in the legend of Figure S7. Samples were analyzed on 12% SDS-PAGE followed by Western blotting with polyclonal anti-KITLG. No differences were observed between samples of control individuals and those of individuals with a KITLG mutation. There was no band visible that could expectedly represent the truncated p.Ser96Ter KITLG.

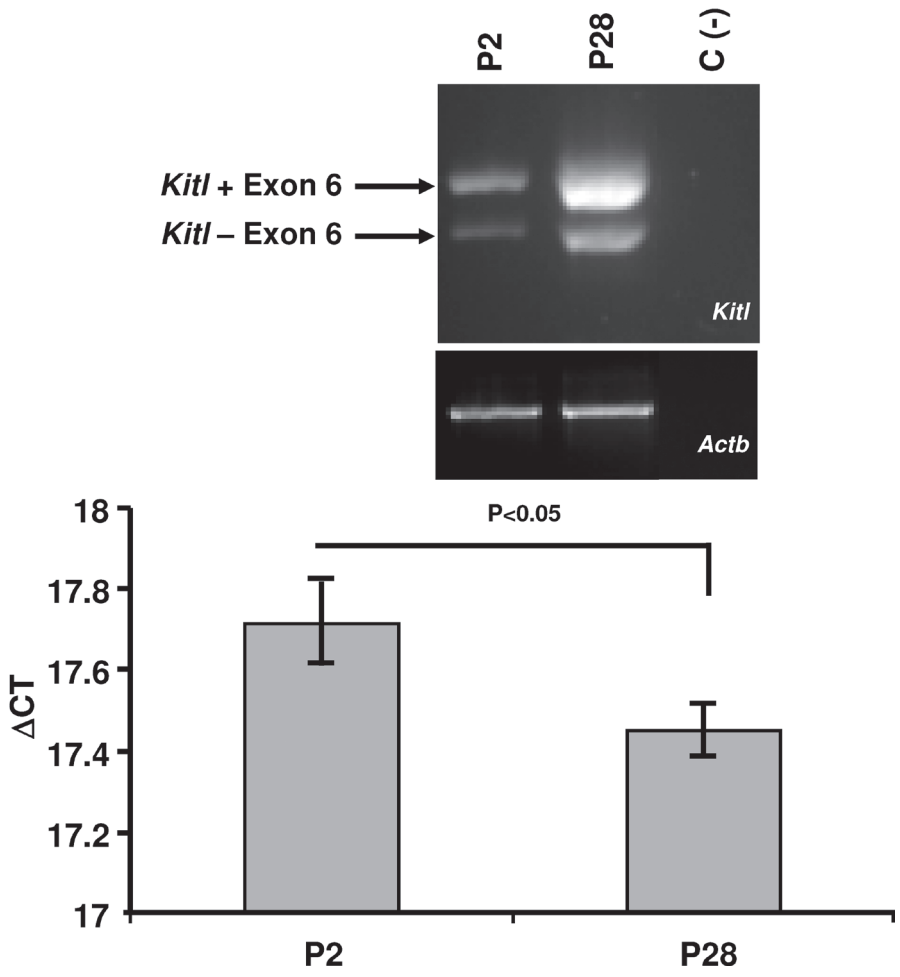

Figure S9. *Kitl* expression in mouse cochlea. Cochlea cDNA derived from cochlea RNA of postnatal (P) days P2 and P18 129sv wild-type mice was kindly provided by Prof. Guy Richardson (Sussex University, UK). PCR was performed with this cDNA as template and primers for *Actb* and *Kitl* and subsequently size-separated on 1% agarose gel according to standard protocols. To quantify *Kitl* expression, one µl of cDNA was used as template for quantitative PCR with SYBR Green (11066420, SYBR Green I Master, Roche Diagnostics). The gene for ribosomal 18S rRNA was employed as housekeeping gene for data normalization. The differences in expression were calculated by subtracting the obtained CT values of *Kitlg* and 18S rRNA, respectively, according to the following equation: ΔCT = CT (*Kitlg*) – CT (18S rRNA). A) Transcripts of *Kitl* in P2 and P28 mouse cochlea. *Actb* was employed as control. B) Quantitative PCR revealed changes of relative *KITLG* transcript levels during functional maturation of the mouse cochlea. For statistical evaluation the Student's t-test was performed. Bars represent standard error of means.

Table S1. Primer sequences.

Target	Primer	Oligonucleotides
rs642742	Forward	TGGGGTTTAAAGCATAGACTG
	Reverse	TGTGGTAATGGGTGAGTCTG
rs12821256	Forward	AAGTATGCCCAAAGGATAAGG
	Reverse	GAGTGCTTTGTTCCAACTTAGTC
*KITLG*_mRNA_ NM_003994.5_BamHI_F	Forward	CGCTGCGGATCCTTATGAAGAAGACA
*KITLG*_mRNA_ NM_003994.5_XhoI_R1	Reverse	CGAAAGTAACAGTGTTGACTCGAGCCACAA
*KITLG*_mRNA_ NM_003994.5_XhoI_R2	Reverse	ACAAGCCACTCGAGCACTTCTTGAAACTCTC
*KITLG*_intron ex3-4_ gateway_F	Forward	GGGGACAAGTTTGTACAAAAAAGCAGGCTTCGGAAGTTTGAGACAGCCTGG
*KITLG*_intron ex4-5_ gateway_R	Reverse	GGGGACCACTTTGTACAAGAAAGCTGGGTCGCAGGACTGATTTTGCATTG
pCI-Neo-Rho-Insert Fw	Forward	CGGAGGTCAACAACGAGTCT
pCI-Neo-Rho-Insert Rev	Reverse	AGGTGTAGGGGATGGGAGAC
*KITLG*_Exon1	Forward	GCTCCAGAACAGCTAAACGG
	Reverse	CAGCTGCAAGTCCCAGG
*KITLG*_Exon2	Forward	GGTGAGCATAGCTTGAATGC
	Reverse	GCAGTGGTGTGCAACTAGC
*KITLG*_Exon3	Forward	TGCTTTTCTCCAAAGCACTAC
	Reverse	CAATAAGCAAGCTCCTAAATAGC
*KITLG*_Exon4	Forward	TGGCAGGCACTTGTAATCTG
	Reverse	CTTGTTTTCTTTGCTCATCTG
*KITLG*_Exon5	Forward	CATACGTTAAAACAGCCATCTAAAAG
	Reverse	TCTTGCTACAGCTTAACACAGAGG
*KITLG*_Exon6	Forward	AGACCTGGCAAGTAATCTGG
	Reverse	AGAAGACCATAAAAGGAATAACAG
*KITLG*_Exon7	Forward	CTTGCAAAAGCAATATTCAGC
	Reverse	TCAGCTAGAGGGATTGTCTCC
*KITLG*_Exon8	Forward	CAGCTTCTTTATTACTCTTTAGCCC
	Reverse	ATGGAGATGCAGCACTGAAG
*KITLG*_Exon9	Forward	AGAAGGTAGGCTCCCCATTC
	Reverse	ACAATGGAGCCTGTCATGG
*KITLG*_control testing_p. His67_Cys68delinsArg	Forward	6FAM CTCCGAGTTTTATGGCACTTAC
	Reverse	CTTGTTTTCTTTGCTCATCTG
*KITLG*_control testing_p. Ser96Ter	Forward	GACAGCTTGACTGATCTTCTGG
	Reverse	GAGTTTTCTTTCACGCACTCC
*Kitl*_qPCR_cochlea	Forward	TATGATAACCCTCAACTATGTCGC
	Reverse	TTGTCCAGAAGAGTAGTCAAGC
18S rRNA	Forward	CGGCTACCACATCCAAGGA
	Reverse	AATTACCGCGGCTGCTG
Actb	Forward	GATGGTGGGCATGGGTCAGA
	Reverse	GGATGTCCACGTCACACTTCATGA
Kitl	Forward	CGGGAATCCTGTGACTGATAA
	Reverse	CCACTGTGCGAAGGTAACAA

For the primer design to amplify *KITLG*, NM_003994.5 and NM_000899.4 were used. For *Actb*, uc009ajk.1 was employed and for *Kitl*, uc007gxp.1.

Table S2. Overview of the results of audiometry, otoscopic examination, and vestibular function tests in family W09-1628.

Subject	Age at evaluation	Type of hearing	PTA (1,2,4 kHz)		Speech discrimination		Otoscopic examination	Vestibular function test	
			R	L	R	L		Rotary chair	Caloric test
II:4a	83	Normal	50	55	40% at 100 dB	30% at 100 dB	Normal	NT	NT
III:1	75	UHL	12	≥108	100% at 60 dB	0% at 80 dB	Normal	NT	NT
III:5	57	UHL	8	>120	100% at 60 dB	0% at 120 dB	Normal	Asymmetry Hyporeflexia	Asymmetry to the detriment of L
III:6b	55	AHL	18	116	0% at 120 dB	100% at 60 dB	Normal	NT	NT
III:9	50	AHL	40	40	90% at 100 dB	88% at 80 dB	Normal	NT	NT
IV:1	51	UHL	13	3	100% at 80 dB	NT	Normal	Hyporeflexia	Asymmetry to the detriment of R and hyporeflexia R
IV:3a	48	Normal	8	12	NT	NT	Normal	NT	NT
IV:5a	47	Normal	5	5	NT	NT	Normal	NT	NT
IV:7a	37	Normal	8	8	NT	NT	Normal	NT	NT
V:1	25	AHL	>120	8	0% at 120 dB	100% at 60 dB	Normal	Normal	Asymmetry to the detriment of R and hyporeflexia R
V:5	26	AHL	65	32	80% at 110 dB	100% at 80 dB	Normal	Normal	Normal
V:6	22	AHL	92	48	0% at 120 dB	100% at 90 dB	Normal	Normal	Normal
V:7	22	UHL	20	108	95% at 60 dB	0% at 120 dB	R+L: fragile malleus	Hyporeflexia	Bilateral marginal caloric hyporeflexia
V:11	8	AHL	17	12	97% at 80 dB	97% at 50 dB	Normal	NT	NT

Listed individuals are heterozygous for the *KITLG* c.286_303delinsT mutation. Data for unaffected individuals with the mutation but without affected offspring are not indicated. [a] normal hearing; [b] other causes of HL cannot be excluded; NT, not tested. PTA of 1,2,4 kHz of the last audiogram is presented.

Table S3. Overview of the results of the hematological evaluations in family W09-1628.

Subject	Age at evaluation	Gender	p.Ser96Ter	HL	Anemia by history	Haemoglobin Mmol/L	Hematocrit	Erythrocytes 10^{12}/L	MCHC mmol/L	MCV fL	MCH fmol	RDW %	Trombocytes 109/L
III: 1	63	F	Yes	Yes	No	8.20	0.39	4.27	20.90	92.00	1.92	12.80	216.00
III.5	62	F	Yes	Yes	No	8.60	0.40	4.31	21.30	94.00	2.00	13.40	286.00
III:6	63	M	Yes	Yes	No	9.90	0.44	4.93	22.30	90.00	2.01	13.00	206.00
III:10	53	F	No	No	Yes	9.40	0.44	5.11	21.30	86.00	1.84	12.80	296.00
IV: 1	56	M	Yes	Yes	Yes	8.80	0.40	4.43	21.80	91.00	1.99	12.70	204.00
IV: 3	53	F	Yes	No	Yes	7.50	0.36	3.88	20.60	94.00	1.93	12.80	190.00
IV: 7	42	F	Yes	No	No	8.40	0.38	4.15	22.40	90.00	2.02	13.20	289.00
IV:9	25	F	No	No	Yes	9.10	0.41	4.55	22.00	91.00	2.00	12.80	309.00
V: 1	31	M	Yes	Yes	No	9.00	0.41	4.49	21.90	92.00	2.00	12.50	246.00
V: 2	29	F	No	No	No	8.30	0.41	4.52	20.40	90.00	1.84	13.10	252.00
V: 3	26	F	No	No	No	8.00	0.38	4.11	20.80	94.00	1.95	12.70	245.00
V: 5	31	M	Yes	Yes	No	8.70	0.41	4.32	21.30	95.00	2.01	12.30	250.00
V: 6	28	M	Yes	Yes	No	9.10	0.43	4.45	21.40	96.00	2.04	12.40	169.00
V: 11	13	M	Yes	Yes	No	8.50	0.37	4.41	22.70	85.00	1.93	12.50	314.00

Table S3. Continued.

Subject	Age at evaluation	Gender	p.Ser96Ter	HL	Leukocytes 10^9/L	Reticulocytes permille	Reticulocytes absolute 10^9/L	Reticulocyte haemoglobin equivalent fmol	Auto diff. neutrophils 10^9/L	Auto diff. lymphocytes 10^9/L	Auto diff. monocytes 10^9/L	Auto diff. eosinophilic granulocytes 10^9/L	Auto diff. granulocytes 10^9/L
III: 1	63	F	Yes	Yes	7.30	10.00	41.00	2.12	3.15	2.92	0.54	0.60	0.09
III.5	62	F	Yes	Yes	7.20	10.00	41.80	2.31	4.02	2.45	0.62	0.12	0.03
III:6	63	M	Yes	Yes	5.00	8.00	40.40	2.29	2.28	2.06	0.48	0.13	0.02
III:10	53	F	No	No	7.20	8.00	41.40	2.10	3.43	2.90	0.72	0.15	0.04
IV: 1	56	M	Yes	Yes	7.40	7.00	30.10	2.27	5.42	1.38	0.40	0.13	0.03
IV: 3	53	F	Yes	No	5.60	10.00	37.20	2.26	3.09	1.93	0.42	0.13	0.02
IV: 7	42	F	Yes	No	6.40	10.00	39.40	2.27	3.74	2.20	0.30	0.12	0.03
IV:9	25	F	No	No	6.20	11.00	50.10	2.21	2.91	2.57	0.60	0.10	0.02
V: 1	31	M	Yes	Yes	4.20	6.00	28.70	2.14	2.14	1.64	0.32	0.04	0.02
V: 2	29	F	No	No	7.10	12.00	52.40	2.16	4.30	1.99	0.62	0.14	0.04
V: 3	26	F	No	No	6.60	10.00	39.00	2.10	3.78	2.13	0.41	0.25	0.02
V: 5	31	M	Yes	Yes	8.10	12.00	51.00	2.45	4.95	2.40	0.62	0.13	0.01
V: 6	28	M	Yes	Yes	4.50	13.00	58.70	2.42	2.10	1.72	0.45	0.24	0.01
V: 11	13	M	Yes	Yes	6.00	19.00	82.50	2.17	2.76	2.36	0.58	0.30	0.03

The normal values are 1) for males: haemoglobin 8.4-10.8 mmol/L; hematocrit 0.41-0.53; erythrocytes 4.5-5.9 x 10^{12}/L; MCV 80-100 fL; trombocytes: 150-400 x10^9/L; leucocytes 4-11 x 10^9/L; 2) for females: haemoglobin 7.4-9.9 mml/L; hematocrit 0.36-0.46; erythrocytes 4-5.2 x 10^{12}/L; MCV 80-100 fL; trombocytes: 150-400 x10^9/L; leucocytes 4-11 x 10^9/L.

MCHC, Mean corpuscular haemoglobin concentration; MCV, mean corpuscular volume; RDW, red blood cell distribution width.

Table S4. Overview of the results of the dermatological evaluations in family W09-1628.

Pedigree	Age at evaluation	Gender	p.Ser96Ter	HL	Skin type	Eye colour	Dystopia canthorum	Hair colour	Age at greying	Skin depigmentation patches	Skin hypo-pigmentation patches	Skin hyper-pigmentation patches	Poliosis	Naevi
III: 1	63	F	Yes	Yes	x	blue	No	dark blond	60	No	x	x	x	x
III:5	62	F	Yes	Yes	I	light blue	No	white blond	50	Yes	Yes	No	Yes	<50
III:6	63	M	Yes	Yes	I	blue	No	blond	40	No	Yes	No	No	<50
III:10	53	F	No	No	II	blue	No	dark blond	no greying	Yes	Yes	No	No	50-100
IV: 1	56	M	Yes	Yes	I	blue	No	blond	50	No	Yes	No	No	<50
IV: 3	53	F	Yes	No	II	blue	No	blond	no greying	Yes	Yes	No	No	<50
IV: 7	42	F	Yes	No	II	blue	No	blond	no greying	Yes	Yes	No	No	50-100
IV:9	25	F	No	No	I	blue	No	dark blond	no greying	No	No	No	No	<50
V: 1	31	M	Yes	Yes	II	blue	No	light blond	no greying	No	No	No	No	<50
V: 2	29	F	No	No	II	blue	No	dark blond	no greying	No	No	No	No	<50
V: 3	26	F	No	No	I	blue	No	blond	no greying	No	Yes	No	Yes	<50
V: 5	31	M	Yes	Yes	II	blue	No	dark blond	no greying	No	Yes	No	No	<50
V: 6	28	M	Yes	Yes	II	blue	No	dark blond	no greying	Yes	No	No	No	<50

x; examinations could not be performed.

Table S5. Filter steps applied on total CNV data from WES of individuals III:9 and IV:1 of family W09-1628.

Filter steps	# Variants
Total CNVs	26
CNVs ≥ 5Kb	24
Exonic CNV	22
< 70% overlapping with control population	4
Linkage region 12q21.31-q23.1	0

Indicated is the number of CNVs, compared to reference genome GRCh37 (hg19), after every filter step. Total CNVs indicates the number of CNVs called in individuals III:9 and IV:1. The control dataset consisted of 721 genotypes of control individuals with Cytoscan HD arrays (Affymetrix) and 1251 genotypes of control individuals with Affymetrix 6.0 arrays (Affymetrix).

REFERENCES

1. Guenther, C.A., Tasic, B., Luo, L., Bedell, M.A., and Kingsley, D.M. (2014). A molecular basis for classic blond hair color in Europeans. Nat. Genet. 46, 748-752.
2. Miller, C.T., Beleza, S., Pollen, A.A., Schluter, D., Kittles, R.A., Shriver, M.D., and Kingsley, D.M. (2007). cis-Regulatory changes in Kit ligand expression and parallel evolution of pigmentation in sticklebacks and humans. Cell 131, 1179-1189.
3. Yuzawa, S., Opatowsky, Y., Zhang, Z., Mandiyan, V., Lax, I., and Schlessinger, J. (2007). Structural basis for activation of the receptor tyrosine kinase KIT by stem cell factor. Cell 130, 323-334.
4. Krieger, E., Koraimann, G., and Vriend, G. (2002). Increasing the precision of comparative models with YASARA NOVA--a self-parameterizing force field. Proteins 47, 393-402.
5. Vriend, G. (1990). WHAT IF: a molecular modeling and drug design program. J. Mol. Graph. 8, 52-56, 29.
6. Krieger, E., Joo, K., Lee, J., Lee, J., Raman, S., Thompson, J., Tyka, M., Baker, D., and Karplus, K. (2009). Improving physical realism, stereochemistry, and side-chain accuracy in homology modeling: Four approaches that performed well in CASP8. Proteins 77 Suppl 9, 114-122.
7. Jiang, X., Gurel, O., Mendiaz, E.A., Stearns, G.W., Clogston, C.L., Lu, H.S., Osslund, T.D., Syed, R.S., Langley, K.E., and Hendrickson, W.A. (2000). Structure of the active core of human stem cell factor and analysis of binding to its receptor kit. EMBO J. 19, 3192-3203.
8. Arakawa, T., Yphantis, D.A., Lary, J.W., Narhi, L.O., Lu, H.S., Prestrelski, S.J., Clogston, C.L., Zsebo, K.M., Mendiaz, E.A., Wypych, J., et al. (1991). Glycosylated and unglycosylated recombinant-derived human stem cell factors are dimeric and have extensive regular secondary structure. J. Biol. Chem. 266, 18942-18948.
9. Majumdar, M.K., Feng, L., Medlock, E., Toksoz, D., and Williams, D.A. (1994). Identification and mutation of primary and secondary proteolytic cleavage sites in murine stem cell factor cDNA yields biologically active, cell-associated protein. J. Biol. Chem. 269, 1237-1242.

[1]Department of Otorhinolaryngology, Hearing & Genes, Radboud university medical center, Nijmegen, 6525GA, the Netherlands;

[2]The Radboud Institute for Molecular Life Sciences, Radboud university medical center, Nijmegen, 6525GA, the Netherlands;

[3]Department of Human Genetics, Radboud University Medical Center, Nijmegen, 6525GA, The Netherlands;

[4]Donders Institute for Brain, Cognition and Behaviour, Radboud University Medical Center, Nijmegen, 6525GA, The Netherlands;

[5]Department of Cellular Neurobiology, University of Göttingen, Julia-Lermontowa-Weg 3, Göttingen, 37077, Germany;

[6]Human Genetics, Genome Institute of Singapore, Agency for Science, Technology and Research, Singapore, 138672, Singapore;

[7]Laboratory of Molecular Imaging, Singapore Bioimaging Consortium, A*STAR, Singapore; Singapore Institute for Clinical Sciences, A*STAR, Singapore; Clinical Imaging Research Centre, NUS-A*STAR, Singapore, 138667, Singapore;

[8]Singapore Institute for Clinical Sciences, A*STAR, 117609, Singapore.

[9]Institute of Biomedical and Genetic Engineering (IBGE), Islamabad, Pakistan;

[10]Center for Molecular and Biomolecular Informatics, Radboud university medical center, Nijmegen, 6525GA, the Netherlands;

[11]Department of Molecular Developmental Biology, Faculty of Science, Radboud Institute for Molecular Life Sciences Radboud University, Nijmegen, 6525GA, The Netherlands;

[12]Wilhelm Johannsen Centre for Functional Genome Research, Department of Cellular and Molecular Medicine (ICMM), The Panum Institute, University of Copenhagen, Copenhagen, 2200, Denmark;

[13]Department of Otorhinolaryngology, Head & Neck Surgery and Audiology, Bispebjerg Hospital/Rigshospitalet, 2400, Copenhagen, Denmark;

[14]Clinical Genetic Clinic, Kennedy Center, Copenhagen University Hospital, Rigshospitalet, Glostrup, 2600, Denmark;

[15]National Institute of Rehabilitation Medicine (NIRM), Islamabad, Pakistan;

[16]Neurogenetics Group, VIB-Department of Molecular Genetics, University of Antwerp, Campus Drie Eiken, Universiteitsplein 1, 2610, Antwerp, Belgium;

[17]Department of Neurology, Antwerp University Hospital, Antwerp, 2000, Belgium.

[18]Laboratories of Neurogenetics and Neuropathology, Institute Born-Bunge, University of Antwerp, Antwerp, 2000, Belgium;

[19]Department of Neurology, Donders Institute for Brain, Cognition, and Behaviour, Nijmegen, Radboud University Medical Center, 6525GA, the Netherlands;

[20]Genome Institute of Singapore, 60 Biopolis Street, #02-01 Genome, 138672 Singapore;

[21]COMSATS Institute of Information Technology, Islamabad, Pakistan;

[22]Al-Nafees Medical College & Hospital, Isra University, Islamabad, Pakistan;

CHAPTER 6

A homozygous nonsense mutation in *FITM2* causes Siddiqi syndrome, a deafness-dystonia syndrome with ichthyosis-like features and signs of sensory neuropathy

Celia Zazo Seco[1,2,*], Anna Castells-Nobau[3,4,*], Seol-hee Joo[5], Margit Schraders[1,2], Jian Nee Foo[6], Sambasivam Sendhil Velan[7], Jaap Oostrik[1,2], Erik de Vrieze[1,3], Atika Mansoor[8], Martijn Huijnen[9], Radek Szklarczyk[9], Martin Oti[9,10], Lisbeth Tranebjærg[11,12,13], Erwin van Wijk[1], Saadat Siddique[14], Jonathan Baets[15,16,17], Peter de Jonghe[18,19,20], Syed Ali Raza Kazmi[8], Jolanda M. Scheffer-de Gooyert[3,4], Suresh Anand Sadananthan[7,21], Bonnie Nijhof[3,4], Bart van de Warrenburg[22], Khor Chiea Chuen[23], Monique van der Voet[3,4], Martin C. Göpfert[5], Raheel Qamar[24,25,#], Annette Schenck[3,4,#], Hannie Kremer[1,2,3,#], Saima Siddiqi[8,#]

*,#Authors contributed equally

Manuscript in preparation

ABSTRACT

A combined strategy of linkage analysis and whole exome sequencing in a consanguineous family of Pakistani origin with a novel syndrome of progressive sensorineural hearing impairment, dystonia, regression of motor skills, signs of sensory neuropathy and ichthyosis-like features revealed a homozygous nonsense mutation, c.4G>T (p.Glu2*), in *FITM2*. FITM2 and its paralog FITM1 constitute an evolutionary conserved protein family involved in partitioning of triglycerides into cellular lipid droplets. Despite the role of FITM2 in neutral lipid storage and metabolism, no indications for lipodystrophy were observed in the affected individuals. In order to obtain independent support of the involvement of *FITM2* in the human pathology, downregulation of the single *Fitm* ortholog, CG10671, in *Drosophila melanogaster* was pursued by using RNA inter ference. Phenotypic characteristics of the syndrome were recapitulated in *Drosophila* by progressive locomotor impairment, hearing loss and morphological abnormalities of type IV sensory neurons as well as neuromuscular junctions. This confirms that the *FITM2* mutation is indeed causative of the syndrome. The phenotypic characteristics of the affected individuals indicate that FITM2 function in humans goes beyond neutral lipid storage and metabolism.

INTRODUCTION

Hearing is a complex process involving the inner ear for transformation of sound into an electrical signal that is further processed in the central nervous auditory pathway and cortex. Therefore it comes as no surprise that mutations in more than a hundred genes are causative of malfunction of the auditory system resulting in hearing impairment (See URL, Hereditary hearing loss homepage). Expression of these genes and the function of the encoded proteins are not private to the auditory system in most of the cases.[1, 2] Defects in the proteins involved in hearing can give rise to hearing impairment only (non-syndromic hearing impairment) or can result in a multisystem disorder (syndromic hearing impairment) as it is described for more than 400 syndromes with hearing impairment in literature and Online Mendelian Inheritance in Man (See URL, OMIM).[3]

Cells have the ability to store neutral lipids in specialized organelles, the lipid droplets (LDs) which thereby are important for energy storage and lipid metabolism.[4] However, the role of LDs goes beyond this since functions in modulation of cellular signaling, transcription regulation and autophagy are emerging as well as functions in immunity.[5] Defects in genes that have a role in LD formation and/or function can lead to hereditary lipodystrophies but also to motor neuropathies without obvious effects on lipid storage and metabolism.[6] For example, Seipin, which is encoded by *BSCL2* (MIM# 606158), is an endoplasmic reticulum (ER) resident protein involved in LD formation and maintenance as well as in adipocyte differentiation.[7,8] Loss-of-function mutations in *BSCL2* result in Berardinelli-Seip congenital lipodystrophy (MIM# 269700) whereas gain-of-toxic-function mutations in *BSCL2* cause a motor neuron disease (MIM# 600794) due to neuronal ER stress without metabolic implications.[9-11] Spartin, encoded by SPG20 (MIM# 607111), is associated with LDs[12] and functions in lipid droplet turnover. Loss of function mutations in SPG20 are causative of Troyer syndrome (MIM# 275900), a hereditary spastic paraplegia, which is not associated with defects in lipid metabolism.[13]

The Fat storage-Inducing TransMembrane (FITM) protein family is a novel two-member family of highly conserved proteins, FITM1 and FITM2, involved in LD partitioning and energy metabolism.[14-17] FITM1 (MIM# 612028) is primarily expressed in skeletal muscle and, at lower levels, in heart. Expression of mouse Fit2 (MIM# 612029) is highest in brown and white adipose tissue and further ubiquitous at a low level in both humans and mouse.[15] Expression in human adipose tissue has not been described yet. Deficiency of FIT2 in mouse

adipose tissue results in progressive lipodystrophy and postnatal whole body *Fit2* knock-out in mouse is lethal.[18, 19] So far, no phenotype in humans has been linked to mutations in either of the two *FITM* genes. However, *FITM2* is part of the *FITM2-R3HDML-HNF4A* locus that is associated with type 2 diabetes.

In this study, we identified a homozygous truncating mutation in *FITM2* in a consanguineous family of Pakistani origin with a characteristic constellation of clinical features of sensorineural hearing impairment, dystonia, regression of motor skills, signs of sensory neuropathy and an ichthyosis-like appearance of the skin. No indications for a lipodystrophy were present in the affected subjects. RNAi-induced gene ablations in *Drosophila melanogaster* recapitulated the human phenotype which supports the involvement of *FITM2* in the presented novel human phenotype.

MATERIALS AND METHODS

Patient evaluation

Written informed consent was obtained from individuals I-1 and I-2. The human subjects review boards of Biomedical and genetic Engineering, Islamabad, Pakistan, the medial ethics committee of the Radboud university medical center, Nijmegen, the Netherlands, and the Domain Specific Review Board for ethics of the National Healthcare Group Singapore approved the study protocol.

Patients of the presented family (W09-1008; Figure 1A) were evaluated by medical specialists in Pediatrics, Otorhinolaryngology, and Neurology.

Tmpanometry, pure-tone audiometry, Brainstem Evoked Response Audiometry (BERA), Magenetic Resonance Imaging (MRI) of the brain, measurements of fasting levels of glucose and triglycerides in serum and neurophysiological evaluations were performed according to standard protocols. Muscle tissue derived from a musculus vastus lateralis biopsy was embedded in paraffin and stained with hematoxilin-eosin according to standard protocols.

MRI of abdomen

The abdominal MR images were acquired from a 3T MR scanner (Tim Trio Siemens) using two-point Dixon sequence (TR = 5.28 *ms*, TE1 = 2.45 *ms*, TE2 = 3.68 *ms*, FA = 9 *deg*, bandwidth1 = 500 *Hz/Px*, bandwidth2 = 780 *Hz/Px*) after anatomical localization. For the parent (I-1), 80 axial slices with 3 *mm* thickness, 0.6 *mm* interslice gap and in-plane resolution of 1.25 × 1.25 *mm* were acquired and 52 slices with in-plane resolution of 1.02 × 1.02 *mm* were acquired for two

affected children (II-5 and II-6). A fully automated segmentation technique was employed to segment and quantify the abdominal fat volumes between the first (L1) and fifth (L5) lumbar vertebrae.[43] First, the fat tissues were separated from non-fat tissues by intensity thresholding. The extracted fat tissues were then classified into subcutaneous (SAT) and visceral (VAT) adipose tissues using graph theoretic segmentation.

MR spectroscopy of the liver

Fat content in the liver was determined using ^{1}H magnetic resonance spectroscopy (MRS). The liver spectra were obtained from a 2 × 2 × 2 cm^3 voxel from two locations (right and left lobes) using a point-resolved spectroscopy sequence (echo time (TE) = 30 ms, repetition time (TR) = 2000 ms) and a Siemens body matrix coil. The acquired spectra were fitted using the linear combination of model spectra (LCModel).[43] The liver fat was determined from the concentration of methyl and methylene groups of lipids and the unsuppressed water signal and corrected for T2 losses.[44]

Genetic analyses

SNP Genotyping

Genomic DNA was isolated from peripheral-blood lymphocytes by standard procedures. All family members were genotyped employing the HumanOmniExpress BeadChip v1.1 (Illumina, Inc., San Diego, CA) arrays with 719,659 SNPs. Homozygosity mapping using 696,513 autosomal SNPs with genotype calls in all samples (364,151 polymorphic) using PLINK v1.07 was performed.(45) Overlapping homozygous regions >5 Mb in size present in all affected and absent in the unaffected individuals were selected. Family relationships among genotyped individuals using identity-by-descent checks were performed. We further conducted a genome-wide linkage scan using MERLIN 1.1.2 on a subset of 53,028 independent SNPs, based on inheritance of the same ancestral mutant allele (0.001) from both parents (coded as first cousins) under a recessive model.[46]

Sequence analysis; Whole exome sequencing (WES) and Sanger sequencing

In family W09-1008, WES was performed in the non-affected parents, I-1 and I-2, and in two affected siblings, II-5 and II-6 using the Nimblegen SeqCap EZ exome v3 kit and protocol (Roche). The captured libraries were barcoded, pooled and sequenced on a single lane in a multiplexed 2x101 base pair Illumina HiSeq 2000 sequencing run. Reads were mapped against the UCSC Genome

Browser Hg19 assembly (build 37) using BWA v1.7 and variants were called using the Genome Analysis Toolkit (GATK) v2 following the recommended guidelines. All four samples were sequenced to a mean depth of 79.5x with >96% of the exome covered by ≥10 reads. Identified variants were evaluated with the SIFT tool and checked against public databases of exomic or genomic variants (1000 genomes, HapMap and NHLBI exome variant server).

Primers for amplification of exons and exon-intron boundaries of *FITM2* (uc002xlr.1) were designed with ExonPrimer. Amplification by PCR was performed on 40 ng of genomic DNA with Taq DNA polymerase (Roche) or Amplitaq (Life Technologies). Primer sequences are provided in Table S1. PCR fragments were purified with NucleoFast 96 PCR plates (Clontech) in accordance with the manufacturer's protocol. Sequence analysis was performed with the ABI PRISM BigDye Terminator Cycle Sequencing V2.0 Ready Reaction kit and analyzed with the ABI PRISM 3730 DNA analyzer (Applied Biosystems). Presence of the *FITM2* c.4G>T transversion was determined in 137 ethnically matched healthy controls by restriction analysis of amplicons encompassing *FITM2* exon 1 (primers as indicated in Table S1)which were purified as described above and digested with *NspI* (New England Biolabs) in accordance with the manufacturer's protocol. Restriction fragments were analyzed on 2% agarose gels. The mutation removes a restriction site. The absence of the *FITM2* c.4G>T variant was also verified in the Nijmegen WES database (5031 exomes) and Exome Aggregation Consortium database (ExAC, 65,000 exomes).

Expression analysis of *FITM2* in HEK293T cells

Wild-type and c.4G>T *FITM2* cDNA were cloned in an expression vector containing a C-terminal Streptavidin-FLAG-tag (SF-TAP)[47] using gateway technology (Life Technologies) according to the manufacturer's instructions. HEK293T cells were cultured in high glucose DMEM AQmedia (Sigma Aldrich), supplemented with 10% FCS, 1% penicillin/streptomycin and 1 mM sodium pyruvate. For DNA transfections, HEK293T cells were seeded in 6-well plates, grown overnight, and transfected with 2 µg of plasmid using PEI transfection reagent (Merck Millipore). Twenty-four hours after transfection cells were washed with PBS and lysed on ice in lysis buffer (50 mM Tris-HCl pH 7.5, 150 mM NaCl, 0.5% Triton-X-100 supplemented with complete protease inhibitor cocktail (Roche). Affinity purification of SF-TAP-tagged proteins was performed on cleared lysates using anti-FLAG M2 affinity gel (Sigma Aldrich). Lysates were incubated for four hours at 4°C and subsequently precipitated by centrifugation and washed three times in lysis buffer. Protein lysates and

affinity purified samples were analyzed on Western blots of NuPAGE® Novex® 12% Bis-Tris Protein Gels (Life technologies) and imaged by using the Odyssey Infrared Imaging System (LI-COR, USA). Tagged molecules were detected by anti-FLAG polyclonal antibodies (Sigma Aldrich) and IRDye800 goat-anti-rabbit IgG (Licor) as described.[48]

RNAi and phenotypic analyses in *Drosophila melanogaster*

Drosophila melanogaster stocks and maintenance

Conditional RNA-mediated interference (RNAi) knockdown of *Fitm* (CG10671) was achieved with the *UAS*-GAL4 system.[49] *UAS*-RNAi stocks against CG10671 and their genetic background controls were obtained from the Vienna *Drosophila* RNAi Centre (VDRC).[50] Experiments were replicated in multiple stocks, two from the GD RNAi library (v44433 and v44435; referred to as *Fitm* RNAi-1A and *Fitm* RNAi-1B, respectively) with the corresponding genetic background control (Control-1; v60000) and one from the KK RNAi library (v109895; *Fitm* RNAi-2) with the corresponding genetic background control (v60100; Control-2). The stocks are based on two independent RNAi constructs: GD3580 (v44433 and v44435) and KK107999 (v109895).

RNAi expression was induced by a variety of GAL4 driver lines, which carry a tissue-specific promoter driving the expression of GAL4. The *w; C7*-GAL4; *UAS*-Dcr-2 (fat body expression) was kindly provided by Marek Jindra.[51] The GAL4 promoter driver lines, *w;; αTub84B-GAL4/ TM6C, Sb1 Tb1* (5138) (ubiquitous expression) and *w, UAS*-Dcr-2; *Mef2*-GAL4 (25756) (skeletal muscle expression) were obtained from the *Drosophila* Bloomington Stock Center (BDSC). The *w;; elav*-GAL4 (8760) was obtained from the BDSC and combined with *w; UAS*-Dcr-2 (60009) from VDRC to create *w; UAS*-Dcr-2; *elav*-GAL4 (pan-neuronal expression). A copy of *UAS*-Dcr-2 was included to improve the efficiency of knockdown.[50] The *w; 477*-GAL4, *UAS*-mCD8::GFP; +/ *ppk*-GAL4 driver (expression in class IV dendritic arborization (da) neurons) was assembled from *yw*, *477*-GAL4, *UAS*-mCD8::GFP (8768) and *w;; ppk*-GAL4 (32079), both from BDSC. Crosses were maintained according to standard procedures at 28°C.

Confirmation of *Fitm* knockdown by qRT-PCR

In order to evaluate the efficiency of RNAi-induced knockdown, *Fitm* RNAi-1A, *Fitm* RNAi-1B and *Fitm* RNAi-2 lines were crossed to the *αTub84B*-GAL4 driver (ubiquitious). One day old males of the appropriate genotype were selected for qRT-PCR. The extraction of mRNA, cDNA synthesis and qPCR were

performed as previously described.[52] RNA polymerase II (*RpII215*) was used as a reference gene. Primer pairs for amplification of *Fitm* and *RpII215* transcripts were designed using ExonPrimer software (http://ihg.gsf.de/ihg/ExonPrimer.html). For each genotype, three biological and two technical replicates were performed. Differential gene expression was calculated using the $2^{\Delta\Delta Ct}$ method.[53] For statistical analysis of the qRT-PCR data, *p* values were calculated with the two sided T-test in Excel 2007 (Microsoft).

Island assay

Fitm RNAi lines and the corresponding genetic background control lines were crossed to the *αTub84B*-GAL4 (ubiquitous), the *Mef2*-GAL4 (skeletal muscle) and the *C7*-GAL4 (fat body) driver lines, respectively. Progeny of the appropriate genotypes and age were subjected to the island assay.[22] In brief, flies were thrown to a platform in the middle of a soap bath and their escape response was videotaped. Flies remaining on the platform after 10 seconds were manually counted. Flight ability, wing and leg movements were visually evaluated.[21] If an abnormal locomotion behavior was found, at least one additional experiment was performed to confirm the observed behavioral defects. The SPSS statistics 20 package (IBM) was used for the ANOVA statistical comparisons.

All behavioral experiments were performed at room temperature under standard light conditions. Aged flies were transferred to fresh food vials every three to four days.

***Drosophila* neuromuscular junction (NMJ) morphology**

The *Fitm* RNAi-1A and *Fitm* RNAi-2 lines and the corresponding control lines were crossed to the *Mef2*-GAL4 (skeletal muscle) driver line. Wandering L3 male larvae were dissected and fixed in 3.7% paraformaldehyde in PBS for 30 min. Type 1b NMJs of muscle 4 were co-labeled for bruchpilot (brp) and discs large 1 protein (dlg1). Brp was revealed using the primary antibody nc82 (1:125) (Developmental Studies Hybridoma Bank, University of Iowa) applied overnight at 4°C, and a secondary Alexa 488-labelled goat anti-mouse antibody (1:250; Invitrogen) for 2h. Discs large 1 was visualized using the primary antibody anti-dlg1 (1:25; Developmental Studies Hybridoma Bank) in combination with the Zenon Alexa Fluor 568 Mouse IgG1 labeling kit (Invitrogen) assembled according to the manufacturer's protocol. Incubation times for antibodies was of 1.5hrs. Antibodies were diluted in PBS-Triton and each incubation period was followed by 5x 10min washing on PBS-T. NMJ images were obtained using an automated high-content Leica microscope (DMI6000B). Individual synapses

were imaged and the NMJ area, length, longest branching length, amount of active zones, branches and branching points were quantitatively assessed using an in-house developed macro for the Fiji image processing software. Data was collected from larvae selected from two independent experiments.

Dendritic morphology of class IV dendritic arborization neurons

Male L3-stage larvae were dissected following a ventral midline incision for imaging of the dorsal class IV dendritic arborization C (ddaC) neurons. The *Fitm* RNAi-1A and *Fitm* RNAi-2 lines and the corresponding controls were crossed to *w; 477*-GAL4, *UAS*-mCD8::GFP; +/*ppk*-GAL4 driver line. Dendritic neurons were stained with rat anti-mouse CD8a (1:100; Thermo Fisher Scientific MCD0800) and goat-anti-rat Alexa Fluor 488 (1:200; Thermo Fisher Scientific A-11006). Z-stack images were taken at a Zeiss LSM 510 confocal microscope with a 20x objective. Z-stacks were imported into NeuronStudio (version 0.9.92) for generation of neuronal reconstructions and Sholl analysis (10 µm interval).(54) Tracing files were analyzed with L-Measure (version v5.2 (55)) and statistical significance was analyzed using the One-Sample T-Test in GraphPad Prism (version 5.00 for Windows, GraphPad Software). Data was collected from larvae selected from two independent experiments.

Hearing test

To assess sound responses of the *Drosophila* Johnston's organ (JO), antennal vibrations and ensuing antennal nerve potentials were measured in adult flies three days after eclosion as previously described.[27] The *Fitm* RNAi-1A, *Fitm* RNAi-1B and *Fitm* RNAi-2 lines and the corresponding controls were crossed to the *elav*-GAL4 and *αTub84B*-GAL4 drivers. In brief, antennal vibrations were monitored at the tip of the antennal arista using a PSV-400 scanning laser Doppler vibrometer (LDV) with an OFV-500 close up unit (Polytec GmbH). Pure tones adjusted to the mechanical best frequency of the antenna were used as sound stimuli. The resulting sound particle velocity was measured with an Emkay NR3158 pressure gradient microphone (distributed by Knowles Electronics Inc.) at the position of the fly. In line with previous reports,[27] the individual best frequency of each antenna was determined from the power spectrum of its mechanical free fluctuations in the absence of sound stimulation, and tone evoked antennal vibration amplitudes were measured as Fourier amplitudes at the frequency of sound stimulation. Ensuing nerve potentials were measured in the form of compound action potentials (CAPs) from the axonal projections of JO neurons in the antennal nerve via an electrolytically tapered

tungsten electrode inserted between the antenna and the head.[28] A tungsten wire inserted into the thorax served as indifferent electrode. CAP amplitudes were plotted against the corresponding sound particle velocities. Hill fits were used to determine the sound particle velocity threshold of the CAPs, whereby the particle velocity corresponding to 10% of the maximum amplitude approached by the fit was used as the threshold criterion.[10] To quantify the amplification gain exerted by motile responses of JO neurons, the antenna's mechanical sensitivity, measured as antennal displacement amplitudes normalized to the corresponding sound particle velocities, was plotted against the particle velocity of the stimulus tones. The amplification gain was then measured as the ratio between the antenna's mechanical sensitivity in the low and high intensity regimes.[27, 28] Data analysis was performed using Polytec-VIB (Polytec GmbH), Spike 2 (Cambridge Electronic Design), Excel 2007 (Microsoft), SigmaPlot 10 (Systat Software) and Prism (GraphPad Software) software.

Fat body analysis

Fitm RNAi lines and the corresponding controls were crossed to the *C7*-GAL4 driver line (fat body). Progeny was transferred to vials with fresh food every two days. Fat bodies of female flies were dissected at the indicated adult age, fixed in PBS with 3.7% paraformaldehyde for 20 min, rinsed with PBS, stained with Bodipy (1:2000; C3922, Life technologies) for 20 min at room temperature, and mounted in Vectashield with DAPI (Vector Laboratories). Pictures were obtained using a Zeiss Axio Imager ZI fluorescence microscope (Zeiss). Data was collected from flies selected from two independent experiments.

RESULTS

Clinical and paraclinical evaluation of the family

Clinical observations of affected individuals

A consanguineous family (Figure 1A) was ascertained from the Punjab region in Pakistan with five sibs affected by syndromic hearing impairment and three healthy sibs and parents. All affected individuals had global developmental delay and subsequent neuro-regression. Sensorineural hearing impairment was the first symptom of the disease at the age of about six months which progressed until profound in about ten years (Figure 1B). Speech was limited to single words. No intervention was undertaken for the hearing impairment of the subjects. Delayed motor development was evident in all five affected subjects. Four of them only

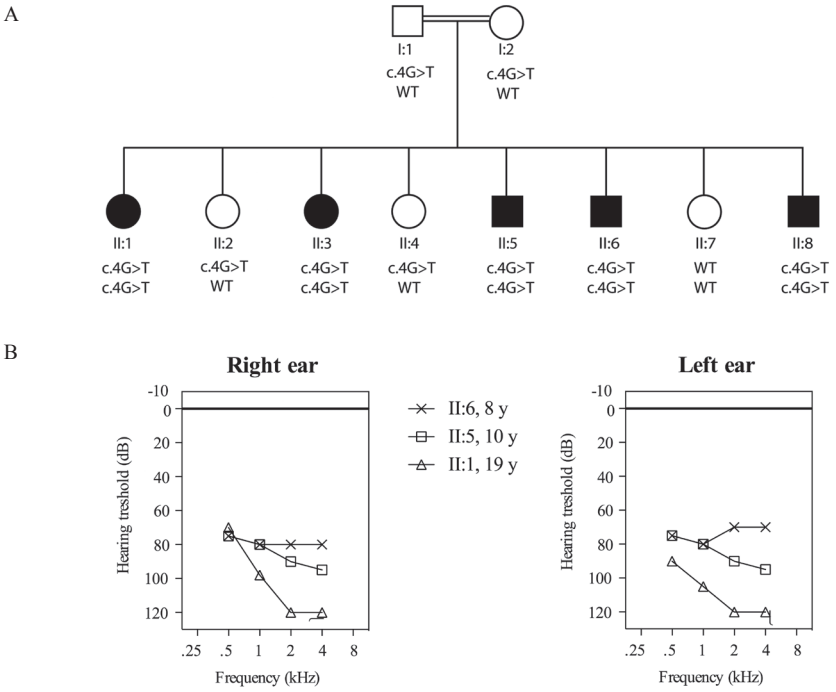

Figure 1. (A) Pedigree of family W09-1008 and segregation of the c.4G>T (p.Glu2*) mutation in *FITM2* and (B) pure tone audiometry of individuals II:1, II:5 and II:6.

walked independently at the age of three years and subject II-6 never walked independently. The three oldest subjects displayed regression in their motor skills from six years of age, with gradual loss of head control, ability to sit and walk by ten years. Fine motor skills were poor due to dystonic hand movements and finger deformities. Subjects were only able to feed themselves but needed assistance in other daily tasks such as dressing and toileting. Significant dystonic limb movements affected three subjects and truncal dystonia was observed in subjects II-5 and II-8. Contractures, including *pes cavus* deformities, were seen in all three dystonic individuals due to long-standing immobility and dystonia. There were no signs of spasticity. Muscle wasting of the lower limbs was observed, found to be more likely due to immobility and poor nutritional status rather than to myopathy or motor neuropathy. All affected subjects had sensory disturbances with two complaining of non-specific pain in their joints and the remaining three experiencing paraesthesia or 'burning sensation' in their limb peripheries, joints and trunk. Pain sensation was tested in subjects II-5 and II-6 and found to be absent in the upper limbs and face but preserved in the trunk and lower limbs.

Table 1. Clinical features of affected subjects with the homozygous c.4G>T (p.Glu2*) mutation in *FITM2*

Characteristics	II.1	II.3	II.5	II.6	II.8
Age (years)	26	22	13	9	6
Gender	Female	Female	Male	Male	Male
Onset of HI (months)	6				
Current speech	Single words				
Sensory disturbances	Frequent pain in joints		Daily burning sensation in peripheries		
Autonomic features	Urinary incontinence from 12 years; daily diarrhea from 16 years	Normal			
Motor function	Delayed walking at 3 years; bedridden by 10 years	Delayed walking at 3 years; loss of ambulation by 10 years		Crawled at 2 years; never walked independently	Delayed walking at 3.5 years; unable to run
Dystonic movements	Dystonic limb movements from 2 years	None	Dystonic limb movements from 2 years		None
Seizures	Daily seizures from 15 years	None			
Skin features	Ichthyosis-like features, most prominent at the shin				
Height (m)/ weight (kg)/ BMI/age at measurement (yrs)	1.36/32.0/17.2/23	1.38/31.0/16.1/19	1.21/22.0/14.8/12	1.06/17.0/15.2/8	0.91/15.0/18.1/5

For comparison, the BMI of two healthy sibs (II.2 and II.7) was 23.5 and 21.0 at the ages of 22 years and 12 years, respectively.

All five affected individuals displayed ichthyosis-like whitish scaling of the skin with more prominent abnormalities on the shin and also scarring alopecia. Furthermore, they were poorly thrived and had low weights. Affected subjects did not display dysmorphic features and their daily life behaviour did not suggest severe cognitive dysfunction or visual abnormalities. The salient clinical features of the affected individuals are summarised in Table 1.

Clinical examinations of affected individuals

Otological examination, tympanometry and pure-tone audiometry were performed in subjects II-1, II-5 and II-6 at the ages of 19, 10, and 8 years, respectively. No external or middle ear abnormalities were noticed and tympanograms were

Table 2. Biochemical evaluation of serum and liver fat content of affected subjects.

Measurements	II.1	II.5	II.6	Control values
Fasting glucose (mg/dl)	101	110	94	60-110
SGOT (AST) (U/L)	27 (32)	25 (38)	ND	In brackets per indvidual
CPK (U/L)	136 (26-140)	150 (38-174)	ND	In brackets per individual
LDH (U/L)	263	397	ND	240-480
Aldolase (U/L)	4.5 (0.1-7.6)	3.0 (0.2-15.2)	ND	In brackets per indvidual
Urea (mg/dL)	30	45	ND	10-50
Creatinine (mg/dL)	0.8	0.7	ND	0.7-1.19
Triglycerides (mmol/L)	ND	1.31	1.21	<1.7
Liver fat (%)	ND	3.63	ND	<10%

SGOT, serum levels of glutamic oxaloacetic transaminase; CPK, creatine phosphokinase; LDH, lactate dehydrogenase; ND, not determined.

normal for both ears. Pure-tone audiograms display bilateral, symmetric, severe or profound hearing impairment which is sensorineural since bone conduction thresholds were in accordance with air conduction thresholds (Figure 1B). BERA was performed for II-1 and II-5 and did not reveal any waveforms up to 90 dB, for both ears. There are no signs of muscle damage or liver or kidney dysfunction since serum levels of glutamic oxaloacetic transaminase (SGOT), creatine phosphokinase (CPK), lactate dehydrogenase (LDH) and aldolase were found to be within the normal range for both subjects II-1 and II-5 (Table 2). Fasting glucose levels were determined to be normal for all three, II-1, II-5 and II-6. Also, fasting serum levels of triglycerides were normal (II-5 and II-6) (Table 2).

Nerve conduction studies were performed for individual II-1 at the age of 14 years. For the left tibial nerve, small Compound Muscle Action Potentials (CMAP) were measured with normal motor conduction velocity. Normal CMAP and motor conduction velocity were observed in the left Median and Ulnar nerves. Also, action potentials and conduction velocities in the left sensory Median and Ulnar nerves were found to be normal. Needle EMG was normal in

deltoid, anterior tibial and gastrocnemius muscles. Findings were interpreted as resulting from decreased muscle bulk.

MRI of the abdomen of individuals II-5 and II-6, and of II-1 as a control did not demonstrate any signs of lipodystrophy. Values of liver fat content and subcutaneous adipose tissue (SAT) and visceral adipose tissue (VAT) volumes were in the normal range. MRI of the brain was performed for individuals II-1 and II-5 and showed no abnormalities, particularly not in the basal ganglia.

A skeletal muscle biopsy of individual II-1 did not display myopathic or neurogenic changes.

In summary, the syndrome in the family is characterized by progressive hearing impairment and delayed motor development followed by regression of motor function which can be accompanied by dystonia and signs of sensory neuropathy. The described evaluations did not provide insight in the primary defect or the pathogenic mechanisms underlying the syndrome.

Whole exome sequencing (WES) identified a nonsense mutation in *FITM2*

Homozygosity mapping and linkage analysis of all family members revealed a single homozygous region of 8.4 Mb on chromosome 20q12-q13.2 (rs2903624-rs6096425). LOD score calculations using 58,023 SNPs in linkage disequilibrium revealed a maximum LOD score of 4.00 (Figure S1). The only linkage region contained 125 genes (USCS, Ref Seq, hg19). WES was performed in the non-affected parents, I.1 and I.2, and in two affected siblings, II.5 and II.6. The single homozygous region on chromosome 20q12-q13.2 was fully covered by Nimblegen SeqCap EZ exome v3. In the linkage region, only nonsynonymous exonic and canonical splice-site variants were selected, occurring with a frequency of less than 5% in the 1000 genomes and HapMap populations, and that were shared by both affected siblings homozygously and were heterozygously in the parents. This revealed a single homozygous nonsense mutation in the second codon, c.4G>T (p.Glu2*, NM_001080472.1; Figure S2A), of *FITM2* that cosegregated with the disease in the family (Figure 1A). This *FITM2* c.4G>T variant was neither present in 274 Pakistani control alleles nor in whole genome or exome databases (see 'Subjects and Methods'). The variant was submitted to Leiden open variation database (LOVD, see URL) (variant ID #0000079006).

Since postnatal whole-body *Fit2* knock-out in mouse is lethal (19), we hypothesized that the present mutation might not lead to complete loss of *FITM2* function due to usage of downstream alternative translation initiation sites. We expressed FLAG-tagged wild-type and p.Glu2* FITM2 in HEK293T

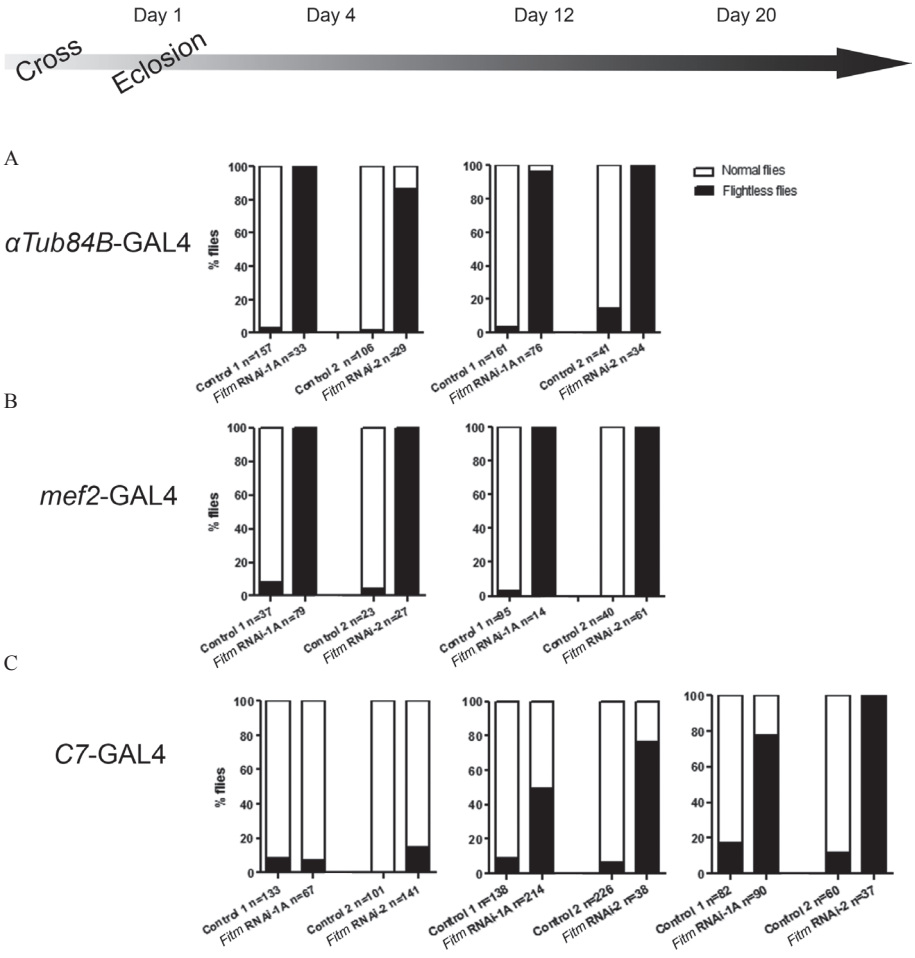

Figure 2. Downregulation of *Fitm* impairs the locomotor abilities in *Drosophila*

The upper horizontal arrow represents the time points in days and developmental stage at which the flies were evaluated. Stacked bar graphs show the percentage of flightless flies (black bars) and flies that were able to clear the platform during the first 10 seconds (white bars). *Fitm* RNAi-1A and *Fitm* RNAi-2 flies with *Fitm* downregulated ubiquitously and in skeletal muscle with the *αTub84B*-GAL4 (A) and *Mef2*-GAL4 (B) promoters, respectively, showed a severe locomotor impairment at 4 days after eclosion and thereafter. (C) *Fitm* knockdown in the fat body (*C7*-GAL4 driver) using the *Fitm* RNAi-1A and *Fitm* RNAi-2 lines revealed a progressive locomotor impairment starting at 12 days after eclosion as compared to corresponding age-matched control flies. Statistical significance was reached between knockdown flies and corresponding controls in all tests depicted (p=0.000).

cells to identify potential shorter FITM2 peptides. Even after FLAG-affinity purification, no indication for significant amounts of alternative FITM2 peptides were obtained (Figure S2B). Therefore, we conclude that the *FITM2* mutation results in loss of FITM2 function.

To further address the involvement of *FITM2* mutations in hearing impairment syndromes with characteristics overlapping those in the present family, *FITM2* was analyzed for the presence of mutations in six index patients with deafness and a sensory polyneuropathy. Also, four index cases were tested who were suspected of Mohr-Tranebjaerg syndrome, a dystonia-deafness syndrome, or with several characteristics of the syndrome and who did not carry *TIMM8A* mutations. This did not reveal any potentially pathogenic *FITM2* variants.

Drosophila models of *FITM2*

To gain independent support for the role of *FITM2* in the phenotype of the presented family and to dissect the underlying tissue-specific pathologies and mechanisms, we turned to an efficient genetic model organism, the fruit fly *Drosophila melanogaster*, that has already been successfully employed to study specific aspects of the observed human pathology.[8, 20-23] The *Drosophila* genome harbors a single, so far uncharacterized gene representing the human FITM protein family (FITM1 and FITM2), CG10671. According to ModEncode and FlyAtlas systematic expression databases,[24, 25] *Fitm* is widely expressed throughout developmental stages and tissues, with highest expression found in adult fat body, heart and carcass. From here on we will refer to CG10671 as *Fitm*.

We modeled loss of human *FITM2* expression by conditional knockdown in *Drosophila*, employing two independent, inducible RNAi constructs (ID #3580 and ID #107999) and the *UAS*-GAL4 system. The efficacy of downregulation of *Fitm* was determined by qRT-PCR after ubiquitous knockdown using the *αTub84B*-GAL4 driver. The relative mRNA expression upon *Fitm* knockdown was 14.67% (p=0.03) for *Fitm* RNAi-1A and 7.04% for *Fitm* RNAi-2 (p=3x10-4) as compared to the respective control lines.

Knockdown of *Drosophila Fitm* causes locomotor impairment

To evaluate locomotor function, impaired in the presented Pakistani family, we first subjected *Fitm* knockdown models to the island assay. This revealed that ubiquitous *Fitm* knockdown leads to severe locomotor impairment, resulting in more than 86% of flightless flies at four and at 12 days after eclosion (Figure 2A). Upon downregulation of *Fitm* in skeletal muscle more than 98% of the

flies displayed the flightless phenotype at 4 and at 12 days after eclosion (Figure 2B). The effect of fat body-specific *Fitm* knockdown on locomotion was evaluated, because of the evolutionary conserved role of *FITM2* in lipid droplet formation in adipose tissue[15, 18] and high *Fitm* expression in *Drosophila* fat body. A progressive locomotor impairment was observed from 49% at 12 days after eclosion to more than 78% of flightless flies at 20 days after eclosion (Figure 2C).

In addition to quantification of the flightless phenotype, we visually evaluated body and wing movements of the flightless flies, since sensory motor coordination is essential for flight initiation and a sensory neuropathy is part of the phenotype in the Pakistani family. At the initiation of flight, flies first raise their wings to a stable position that will be held for a few seconds before takeoff for flight.[26] A

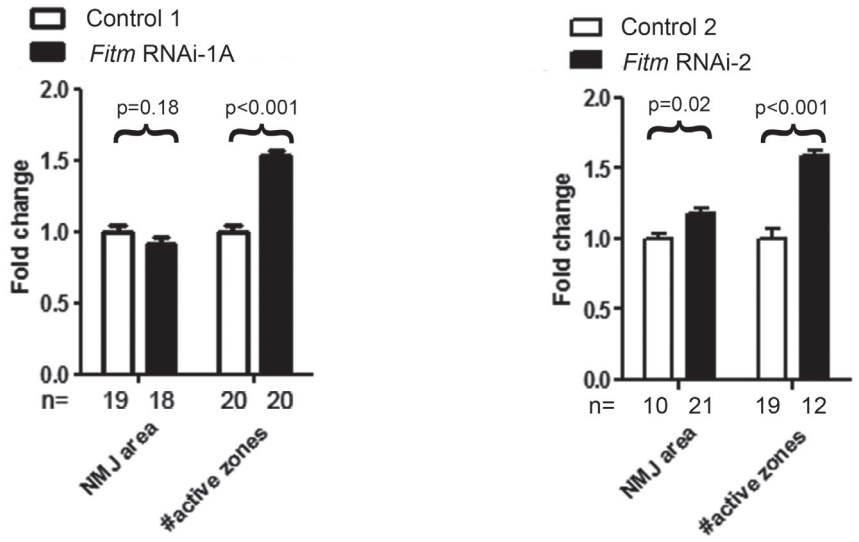

Figure 3. Muscle-specific downregulation of *Fitm* leads to an increased number of active zones in NMJs

Synapse morphology was determined in muscle 4 of L3 larvae with *Fitm* downregulated in the skeletal muscle (*Mef2*-GAL4 driver) using the RNAi lines *Fitm* RNAi-1A and *Fitm* RNAi-2 and compared to the corresponding controls. *Fitm* RNAi flies demonstrated a significant increase in active zones without a significant change in NMJ area. Values for all parameters were normalized against values of the corresponding controls. Bar graphs represent the fold change of the knockdown condition compared to its corresponding control; error bars represent normalized standard error of the mean (SEM). *P*-values were determined using two-sided T-tests and are indicated in the graphs. The number of NMJ images is indicated with "n".

subset of *Fitm* knockdown flies displayed uncontrolled movements as compared to controls. The knockdown flies failed to upstroke their wings for take-off and instead displayed fast wing movements, and uncontrolled jumping and shaking of their corpus. This locomotion phenotype was highly consistent in both RNAi lines tested with all three ubiquitous, skeletal muscle and fat body promoters. In conclusion, loss of *Fitm* expression in *Drosophila* causes locomotor phenotypes and *Fitm* knockdown in either skeletal muscle or fat body suffices to induce these phenotypes.

Fitm is required in muscle for normal development of NMJ synaptic terminals

Since locomotor function and motor coordination require proper signal transduction in neuromuscular synapses, we investigated NMJ architecture in *Drosophila* L3 larvae upon muscle and pan-neuronal knockdown of *Fitm* by assessing various morphological parameters (Figure 3, Figure S3, Figure S4). While gross morphology and organization of NMJs were unaffected by muscle-specific knockdown of *Fitm* (Figure S3), we observed a significant increase in the number of the so-called active zones, the microdomains of synaptic vesicle release within the presynaptic terminal (Figure 3). No consistent differences in other NMJ parameters were found upon pan-neuronal *Fitm* knockdown (Figure S4). Therefore, we conclude that reduced expression of *Fitm* in skeletal muscle of *Drosophila* L3 larvae positively affects active zone development in NMJs independent of NJM area.

Downregulation of _Fitm_ causes abnormal dendrite branching and field coverage of _Drosophila_ multi-dendritic sensory neurons

Since a sensory neuropathy is part of the syndrome caused by a nonsensense mutation in *FITM2*, we evaluated the role for *Fitm* in sensory neuron development by imaging the ddaC class IV dendritic arborization neurons in *Drosophila* L3 larvae. These nociceptive ddaC neurons have a complex, but rather stereotypic dendritic branching pattern with a large field of coverage (Figure 4A, C) that, together with other class IV dendritic arborization neurons, tile the larval body wall. We expressed RNAi transgenes in class IV dendritic arborization neurons using the *477*-GAL4 and *ppk*-GAL4 drivers, simultaneously inducing expression of the fluorescent marker *UAS*-mCD8::GFP. Knockdown of *Fitm* in the independent RNAi lines *Fitm* RNAi-1A and *Fitm* RNAi-2, resulted in a strong dendrite field coverage defect in a subset of larvae, which was not observed in their respective controls (Figure 4A–D). The abnormal tiling phenotype was strongest in *Fitm*

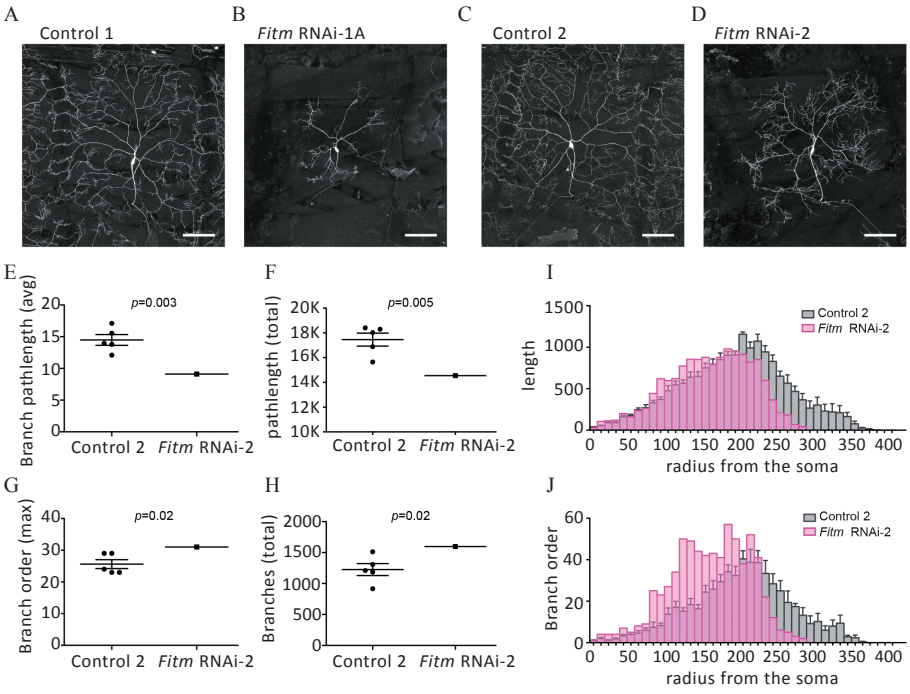

Figure 4. *Fitm* knockdown in *Drosophila* interferes with nociceptive multi-dendritic sensory neuron morphology

(A)–(D) Confocal projections of class IV da neurons within segment A3 of L3 larvae, visualized with the class IV da-specific drivers *477*-GAL4 and *ppk*-GAL4 and *UAS*-mCD8::GFP. The ddaC neurons show abnormal dendritic morphology in a subset of *Fitm* RNAi larvae. (A) Control-1 shows contact to neighboring neurons. (B) Knockdown of *Fitm* RNAi-1A results in a severe outgrowth defect, observed in 5/18 larvae. (C) Representative Control-2, (D) Knockdown of *Fitm* RNAi-2 results in an abnormal phenotype in 1/11 larvae. As for *Fitm* RNAi-1A all contact to the neighboring sensory neurons is lost, but the outgrowth phenotype is less severe. With manual tracing and quantitative analysis the extent of the *Fitm* RNAi-2 phenotype was further analyzed (E–J). (E)–(H) Quantitative analysis of dendritic trees reveals that the affected *Fitm* RNAi-2 neuron has E) a reduced average branch path length (p=0.003), (F) a reduced accumulative branch path length (p=0.005), (G) an increased maximal branch order (p=0.02), and H) increased number of branches (p=0.02). (I)–(J) Sholl analysis reveals defects as a measure of the soma distance, to reveal spatial defects. (I) The dendritic length is increased between 80–150 µm, but drops 200 µm from the soma. The field coverage is reduced by 100 µm. (J) The branch order is increased sharply from 80 µm and drops prematurely due to reduced field coverage. Dorsal is up in (A)–(D), scale bar is 100 µm, error bars in (E)–(J) indicate the SEM.

A

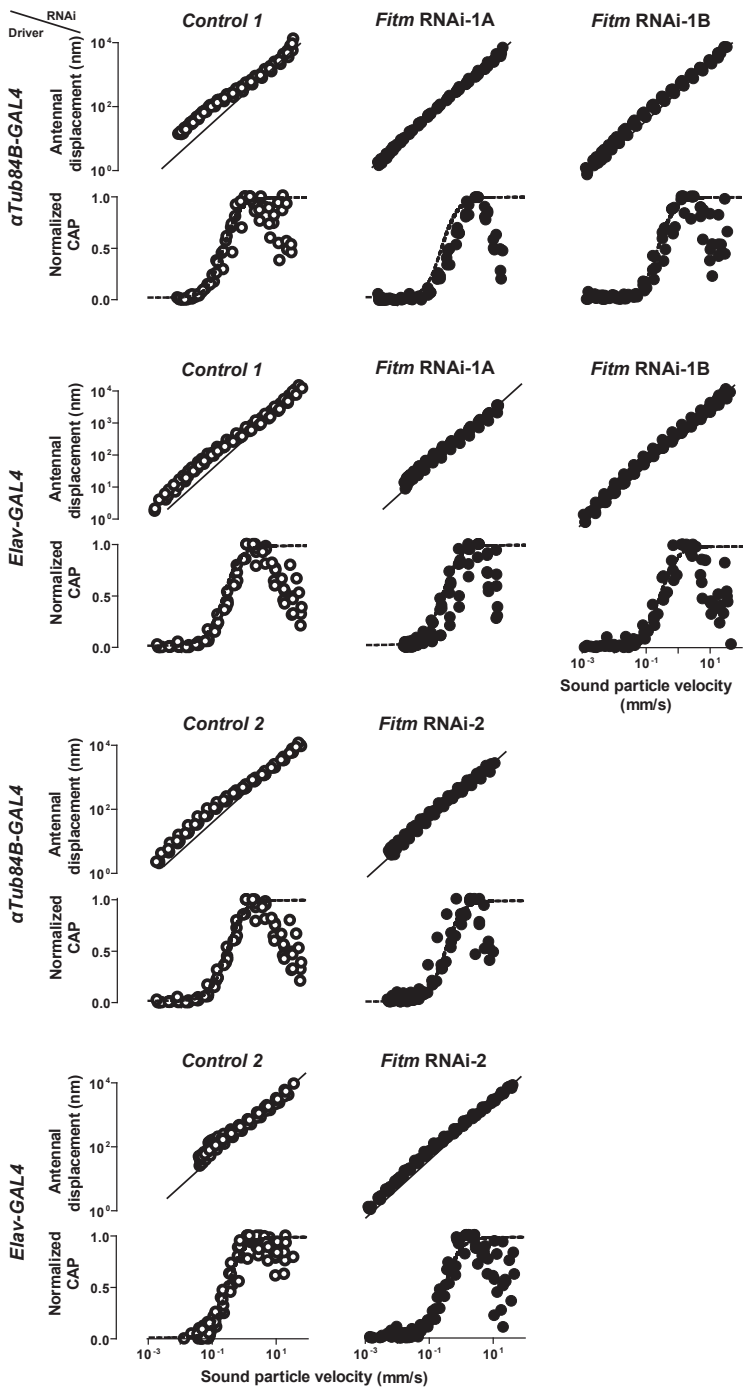
RNAi
Driver
Control 1
Fitm RNAi-1A
Fitm RNAi-1B
αTub84B-GAL4
Elav-GAL4
Antennal displacement (nm)
Normalized CAP
Control 2
Fitm RNAi-2
Sound particle velocity (mm/s)

B

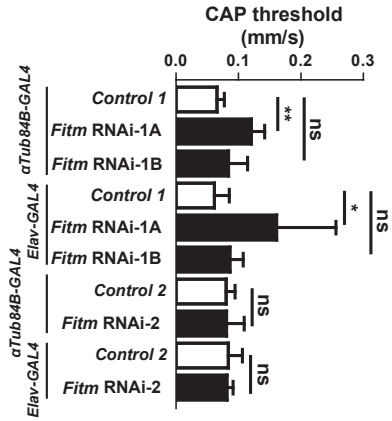

C

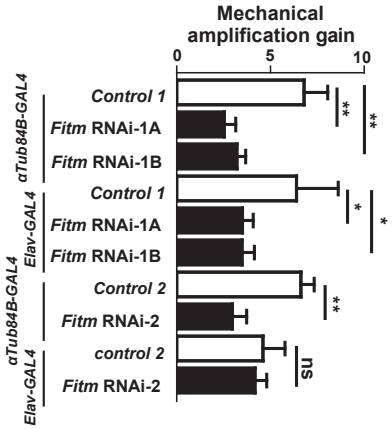

Figure 5. Knockdown of *Fitm* impairs *Drosophila* hearing

Antennal vibrations and ensuing antennal nerve potentials were measured in the *Fitm* RNAi-1A, *Fitm* RNAi-1B and *Fitm* RNAi-2 lines and the corresponding controls (Control-1 and Control-2, respectively) crossed to the pan-neuronal *elav*-GAL4 and ubiquitous *αTub84B*-GAL4 drivers[27] three days after eclosion. (A) Sound-evoked antennal displacement amplitudes (upper panels, log scale) and normalized compound action potential (CAP) amplitudes as functions of the sound particle velocity. Each circle indicates a single data point. Solid (upper panels) and dashed (lower panels) lines indicate linear auditory mechanics, as observed upon the loss of auditory sensory neuron motility and active mechanical amplification,[28] and Hill fits to the pooled CAP responses of each strain, respectively. N = 5 flies per strain. (B) Respective CAP thresholds, deduced from Hill fits to the CAP amplitudes of each individual. (C) Respective mechanical amplification gains provided by auditory sensory neuron motility. Significances: **: $p<0.01$, *: $p<0.05$, and ns: not significant (Mann-Whitney U-tests).

RNAi-1A (Figure 4B), but *Fitm* RNAi-2 also shows this same defect, were contact to the neighboring sensory neurons is completely absent (Figure 4D).
To gain more insight in the underlying defects of the abnormal field coverage, we performed manual tracing and quantitative analysis on the *Fitm* RNAi-2 neuron (Figure S5). Analysis of the mutant and control dendritic trees revealed a reduced average branch path length (p=0.003, Figure 4E) and a reduced accumulative branch path length (p=0.005, Figure 4F), both in concordance with the reduced field of coverage. The maximal branch order and number of branches was not decreased, but displayed a slight increase with respect to the control panel (both p=0.02, Figure 4G, H). To test for space-constrained effects that would explain this result we performed Sholl analyses, where the length or branch order are plotted as a function of the distance from the soma. The analysis revealed that dendritic length was increased slightly between 80–150 µm from the soma, but then decreased prematurely (Figure 4I). The branch order was strongly increased between 80–210 µm (Figure 4J), but prematurely dropped after 210 µm. The final field coverage of the neuron was reduced by 100 µm. Taken together, our results demonstrate that *Fitm* is required for normal branching and dendritic field coverage of *Drosophila* ddaC nociceptive sensory neurons.

Fitm is required for normal hearing in *Drosophila*

Affected members of the presented family displayed postnatal sensorineural hearing impairment that progressed to profound. Therefore, we aimed at testing whether *Fitm* is implicated in *Drosophila* hearing. To do so, we analyzed sound-evoked mechanical and electrical responses of the antennal hearing organ (Figure 5). Three RNAi lines, *Fitm* RNAi-1A, *Fitm* RNAi-1B and *Fitm* RNAi-2 were tested, whereby *Fitm* expression was knocked down ubiquitously or pan-neuronally. A third *Fitm* RNAi line was included, *Fitm* RNAi-1B, which harbors the same RNAi construct (ID #3580) as *Fitm* RNAi-1A but inserted in a different genomic position. This line was included to strengthen the phenotypic effect of *Fitm* knockdown on hearing, which was relatively mild in the RNAi-2 line. The relative mRNA expression upon *Fitm* RNAi-1B knockdown by using *αTub84B*-GAL4 was of 17.64% (p=0.02). To evoke sound-responses, we exposed the flies to pure tones of different intensities at the individual mechanical best frequency of their antennal sound receiver[27] and measured the resulting vibrations of this receiver as well as the ensuing compound action potentials (CAPs) propagated by the axonal projections of the fly's auditory sensory neurons in the antennal nerve (Figure 5A). In genetic background controls, sound particle velocities

exceeded ca. 0.05 mm/s evoked CAP responses (Figure 5B), consistent with published data on wild-type flies.[28] As in wild-type flies, the sound-induced displacement of the antenna also scaled nonlinearly with the intensity of sound stimulation (Figure 5A), displaying a compressive nonlinearity that, arising from motile responses of auditory sensory neurons,[28] actively amplifies the antennal displacement response to faint sounds with an amplification gain of approximately seven (Figure 5C). Both ubiquitous and pan-neuronal knockdown of *Fitm* using *Fitm* RNAi-1A significantly increased the threshold of the sound-evoked CAP responses (Figure 5B), documenting a reduced auditory sensitivity. The same trend, although not significant, was seen in flies expressing *Fitm* RNAi-1B, whereas auditory sensitivity seemed uncompromised in flies expressing *Fitm* RNAi-2 (Figure 5B). Significant hearing impairment was also detected in the latter flies when we examined the nonlinear scaling of their antennal vibrations, which provides a more sensitive measure of auditory sensory neuron integrity.[28] Consistently, all three RNAi constructs significantly

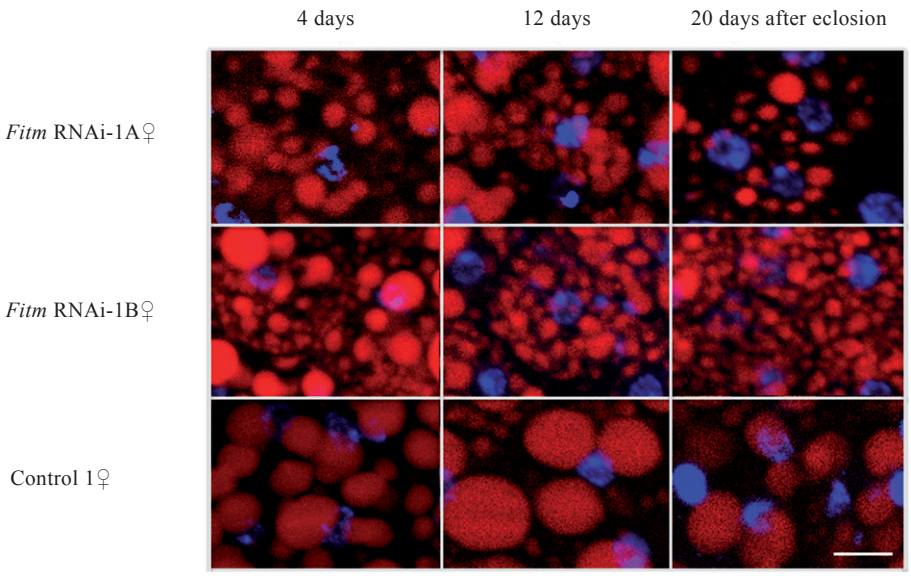

Figure 6. Lipid droplet size is altered by downregulation of *Fitm*

Lipid droplets labeled with Bodipy (red) in fat bodies of females of the *Fitm* RNAi-1A and *Fitm* RNAi-1B lines upon RNAi expression induced by the fat body (*C7*-GAL4) driver as compared to the corresponding female control flies. Nuclei were stained with DAPI (blue). RNAi expression leads progressive decrease of lipid droplet size as compared to that in controls evaluated at 4, 12 and 20 days after eclosion. The scale bar is 10 µm.

reduced this nonlinear scaling, as witnessed by significantly lowered mechanical amplification gains (Figure 5C). Only in flies with pan-neural *Fitm* RNAi-2 expression, amplification gains resembled those of control flies, which already displayed severely reduced amplification gains. Together, these results document that *Drosophila* auditory sensory neurons require *Fitm* for normal mechanical amplification in hearing, which is linked to auditory stimulus transduction and auditory neuron integrity.[28]

Fitm* is important for lipid droplet size in the fat body of adult *Drosophila

Having shown striking parallels between human and *Drosophila* phenotypes, we finally sought to evaluate whether *Drosophila Fitm* functions in lipid droplet formation, as previously reported in other organisms.[15, 17, 18] For this, we knocked down *Fitm* expression in the fat body and evaluated lipid droplet size in female flies. *Fitm* RNAi-1A knockdown flies demonstrated a diminished lipid droplet size as compared to flies of the Control-1 background line at 2, 7 and 12 days after eclosion (Figure 6). The *Fitm* RNAi-2 line exhibited a strong variation in lipid droplet size and therefore was not suitable for the experiment (Figure S6). The lipid droplet phenotype as seen in fat bodies of *Fitm* RNAi-1A knockdown flies was reproduced in the *Fitm* RNAi-1B line (Figure 6). Therefore, we can conclude that *Fitm* function in lipid droplet formation is conserved in *Drosophila*.

DISCUSSION

We have described a unique family with a novel homozygous truncating mutation, c.4G>T (p.Glu2*), in *FITM2*. Affected subjects display a syndrome characterized by progressive sensorineural hearing impairment, delayed motor development, dystonia and signs of sensory neuropathy and ichthyosis. The syndrome is further associated with reduced BMI. The chronic diarrhea of the oldest affected sib might also be associated with the symdrome as postnatal *Fit2* deletion in mouse results in a malabsorptive enteropathy.[19] The combination of the disease characteristics is novel although observed phenotypic characteristics in the family are overlapping with several known monogenic neurological conditions such as, obviously, other dystonia-deafness syndromes including Mohr-Tranebjaerg syndrome (MIM #304700), and Megdel syndrome (MIM #614739, and also Troyer syndrome (MIM #275900). We propose to call the syndrome in the presented family “Siddiqi syndrome” after Dr. Saima Siddiqi, who initiated the research in this family. The causative association of the

syndrome with a loss-of-function mutation in *FITM2* is supported by modeling of the disease in *Drosophila melanogaster* which has been proven to be a suitable model for studying conserved aspects of lipid metabolism and LD biology.[8, 29] RNAi knockdown of the single *Drosohila FITM* ortholog recapitulated hearing impairment , impaired locomotion, and abnormalities of the sensory system.

Affected subjects do not have signs of a lipodystrophy which is in contrast to the findings in mouse in which post-differentiation adipose-specific knockout of *Fit2* results in progressive reduction of white adipose tissue.[18] Functional redundancy in human adipose tissue might exist for FITM2 through FITM1 which is apparently not the case in mouse. In the latter, FIT2 is prominently expressed in adipose tissue in which FIT1 was not detected.[15] The relative expression of *FITM1* and *FITM2* in human adipose tissue is still elusive.

Sensorineural hearing impairment is the first symptom of Siddiqi syndrome. The audiometric evaluations did not allow to discriminate whether the hearing impairment has a cochlear or retrocochlear neuronal origin. The hearing phenotype resulting from *Fitm* knockdown in *Drosophila* was reflecting impaired auditory stimulus transduction and auditory neuron function which might support a neuronal component in the human phenotype *e.g.* progressive loss of spiral ganglion cells as has been demonstrated in a patient with Mohr-Tranebjaerg syndrome.[30] A cochlear component, however, might well contribute to progressive dysfunction of the auditory system in the patients. Interestingly, LDs are prominent constituents of Hensen cells which are highly specialized cells in the organ of Corti. Hensen cell LDs have been suggested to function in an anti-inflammatory response to prevent cochlear damage.[31-34] Additionally, a mechanical function in modulating sound detection has been proposed for LDs in Hensen cells.[31] Whether vestibular dysfunction is part of the inner ear phenotype could not be evaluated. Therefore, it remains undetermined whether impaired balance contributed to the delayed motor developments of the subjects.

Deafness-dystonia is clinically and etiologically heterogeneous and in many of the investigated cases the underlying cause remained elusive.[35, 36] For part of the genetically solved cases, involvement of mitochondrial dysfunction is emerging as a common theme. This is obvious for Mohr-Tranebjaerg (MIM# 304700) syndrome with mutations in *TIMM8A*[37] (MIM# 300356), for a number of rare mitochondrial disorders with mutations in mitochondrial genes as well as for *SUCLA2*-associated disease (MIM #612073), an atypical type of methylmalonic aciduria, as *SUCLA2* encodes the ATP-forming β subunit of mitochondrial succinyl-CoA ligase.[38] However, also for *SERAC1* (MIM #614725) defects in patients with MEGDEL syndrome (MIM# 614739) impaired mitochondrial energy metabolism is part of the

pathogenic mechanisms. SERAC1 is associated with the endoplasmatic reticulum (ER) and suggested to localize at the ER-mitochondrial interface. It functions in remodeling of phosphatidylglycerol and cholesterol trafficking.[39] TIMM8A is located in the mitochondrial intermembrane space and is important for maintenance of mitochondrial morphology.[40] Interestingly, there is increasing data that suggest a functional connection between LDs, and thus FITM2, and other organelles including mitochondria.[41] Based on these findings, it is tempting to speculate that impaired mitochondrial function or otherwise impaired energy supply in the affected tissues might be part of the disease mechanism in the present family with a defect in *FITM2*. In this light, it is interesting that overexpression of *Fit2* in mouse skeletal muscle led to increased energy expenditure which indicated an unexpected function of FIT2 and thereby LDs in regulation of energy metabolism.[14] The underlying mechanism of the latter is still elusive but might well be related to the expanding functions of LDs.[5]

Alternative and/or additional pathogenic mechanisms for the presented syndrome might be related to ER-stress analogous to the disease mechanism of specific gain of function mutations in *BSCL2* that underlie motor neuropathies.[9] Also impairment of other recently proposed roles of LDs *e.g.* in immunity, modulation of nuclear functions, protein degradation, autophagy, and lipid signaling should be considered to contribute to the phenotypic characteristics of the presented family.[5, 42] Further studies are needed to elucidate the molecular mechanisms underlying the syndrome for which *Drosophila melanogaster* would be an excellent model as well as patient cells.

In conclusion, we have elucidated the genetic defect in *FITM2* to underlie a novel dystonia-deafness syndrome which was modeled in *Drosophila*. The phenotype of the affected individuals suggests human FITM2 to be essential for biological processes other than neutral lipid storage and metabolism.

Acknowledgements

We are grateful to the family for participation in this study. We thank the Bloomington *Drosophila* Stock Center (NIH P40OD018537) at Indiana University, and Vienna *Drosophila* RNAi center for providing transgenic RNAi fly stocks used in this study. This research was supported in part by the Netherlands Organization for Scientific Research (NWO) VENI grant 91.614.084 to MV, ZonMW TOP subsidy 40-00812-98-09047 to HK, a post-doc scholarship of the Higher Education Commission, Pakistan to SS and a Higher Education Commission (HEC) grant 2155 to RQ under the National Research Program for Universities. We acknowledge Prof. dr. R.A. Wevers, A. Beynon, E.-J. Kamsteeg and Mieke Wesdorp for discussions.

WEB RESOURCES

1000 genomes: http://www.1000genomes.org/
Drosophila Bloomington Stock Center: http://flystocks.bio.indiana.edu/
Exome Aggregation Consortium: http://exac.broadinstitute.org/
ExonPrimer: http://ihg.gsf.de/ihg/ExonPrimer.html
Hereditary hearing loss homepage: http://hereditaryhearingloss.org/
HapMap: hapmap.ncbi.nlm.nih.gov
Leiden open variation database (LOVD): http://databases.lovd.nl/
NeuronStudio: http://research.mssm.edu/cnic/tools-ns.html
NHLBI exome variant server: http://evs.gs.washington.edu/EVS/
OMIM: http://www.ncbi.nlm.nih.gov/omim
SIFT: http://sift.jcvi.org/
USCS: https://genome.ucsc.edu/
Vienna *Drosophila* RNAi Centre: http://stockcenter.vdrc.at/control/main

REFERENCES

1 Seco, C.Z., Oonk, A.M., Dominguez-Ruiz, M., Draaisma, J.M., Gandia, M., Oostrik, J., Neveling, K., Kunst, H.P., Hoefsloot, L.H., del Castillo, I. et al. (2015) Progressive hearing loss and vestibular dysfunction caused by a homozygous nonsense mutation in CLIC5. Eur. J. Hum. Genet., 23, 189-194.

2 Yariz, K.O., Duman, D., Seco, C.Z., Dallman, J., Huang, M., Peters, T.A., Sirmaci, A., Lu, N., Schraders, M., Skromne, I. et al. (2012) Mutations in OTOGL, encoding the inner ear protein otogelin-like, cause moderate sensorineural hearing loss. Am. J. Hum. Genet., 91, 872-882.

3 Toriello, H.V., Reardon, W., Gorlin, R.J. and Gorlin, R.J. (2004) Hereditary hearing loss and its syndromes. Oxford University Press, Oxford ; New York.

4 Walther, T.C. and Farese, R.V., Jr. (2012) Lipid droplets and cellular lipid metabolism. Annu. Rev. Biochem., 81, 687-714.

5 Welte, M.A. (2015) Expanding Roles for Lipid Droplets. Curr. Biol., 25, R470-R481.

6 Fujimoto, T. and Parton, R.G. (2011) Not just fat: the structure and function of the lipid droplet. Cold Spring Harb. Perspect. Biol., 3.

7 Cui, X., Wang, Y., Tang, Y., Liu, Y., Zhao, L., Deng, J., Xu, G., Peng, X., Ju, S., Liu, G. et al. (2011) Seipin ablation in mice results in severe generalized lipodystrophy. Hum. Mol. Genet., 20, 3022-3030.

8 Tian, Y., Bi, J., Shui, G., Liu, Z., Xiang, Y., Liu, Y., Wenk, M.R., Yang, H. and Huang, X. (2011) Tissue-autonomous function of Drosophila seipin in preventing ectopic lipid droplet formation. PLoS Genet., 7, e1001364.

9 Ito, D. and Suzuki, N. (2009) Seipinopathy: a novel endoplasmic reticulum stress-associated disease. Brain, 132, 8-15.

10 Magre, J., Delepine, M., Khallouf, E., Gedde-Dahl, T., Jr., Van Maldergem, L., Sobel, E., Papp, J., Meier, M., Megarbane, A., Bachy, A. et al. (2001) Identification of the gene altered in Berardinelli-Seip congenital lipodystrophy on chromosome 11q13. Nat. Genet., 28, 365-370.

11 Yagi, T., Ito, D., Nihei, Y., Ishihara, T. and Suzuki, N. (2011) N88S seipin mutant transgenic mice develop features of seipinopathy/BSCL2-related motor neuron disease via endoplasmic reticulum stress. Hum. Mol. Genet., 20, 3831-3840.

12 Eastman, S.W., Yassaee, M. and Bieniasz, P.D. (2009) A role for ubiquitin ligases and Spartin/SPG20 in lipid droplet turnover. J. Cell Biol., 184, 881-894.

13 Patel, H., Cross, H., Proukakis, C., Hershberger, R., Bork, P., Ciccarelli, F.D., Patton, M.A., McKusick, V.A. and Crosby, A.H. (2002) SPG20 is mutated in Troyer syndrome, an hereditary spastic paraplegia. Nat. Genet., 31, 347-348.

14 Miranda, D.A., Koves, T.R., Gross, D.A., Chadt, A., Al-Hasani, H., Cline, G.W., Schwartz, G.J., Muoio, D.M. and Silver, D.L. (2011) Re-patterning of skeletal muscle energy metabolism by fat storage-inducing transmembrane protein 2. J. Biol. Chem., 286, 42188-42199.

15 Kadereit, B., Kumar, P., Wang, W.J., Miranda, D., Snapp, E.L., Severina, N., Torregroza, I., Evans, T. and Silver, D.L. (2008) Evolutionarily conserved gene family important for fat storage. Proc. Natl. Acad. Sci. USA, 105, 94-99.

16 Gross, D.A., Snapp, E.L. and Silver, D.L. (2010) Structural insights into triglyceride storage mediated by fat storage-inducing transmembrane (FIT) protein 2. PLoS One, 5, e10796.

17 Gross, D.A., Zhan, C. and Silver, D.L. (2011) Direct binding of triglyceride to fat storage-inducing transmembrane proteins 1 and 2 is important for lipid droplet formation. Proc. Natl. Acad. Sci. USA, 108, 19581-19586.

18 Miranda, D.A., Kim, J.H., Nguyen, L.N., Cheng, W., Tan, B.C., Goh, V.J., Tan, J.S., Yaligar, J., Kn, B.P., Velan, S.S. et al. (2014) Fat storage-inducing transmembrane protein 2 is required for normal fat storage in adipose tissue. J. Biol. Chem., 289, 9560-9572.

19 Goh, V.J., Tan, J.S., Tan, B.C., Seow, C., Ong, W.Y., Lim, Y.C., Sun, L., Ghosh, S. and Silver, D.L. (2015) Postnatal deletion of Fat storage-inducing Transmembrane Protein 2 (FIT2/FITM2) causes lethal enteropathy. J. Biol. Chem., in press.

20 Storkebaum, E., Leitao-Goncalves, R., Godenschwege, T., Nangle, L., Mejia, M., Bosmans, I., Ooms, T., Jacobs, A., Van Dijck, P., Yang, X.L. et al. (2009) Dominant mutations in the tyrosyl-tRNA synthetase gene recapitulate in Drosophila features of human Charcot-Marie-Tooth neuropathy. Proc. Natl. Acad. Sci. USA, 106, 11782-11787.

21 Lee, D.W., Seo, J.B., Ganetzky, B. and Koh, Y.H. (2009) DeltaFY mutation in human torsin A [corrected] induces locomotor disability and abberant synaptic structures in Drosophila. Mol. Cells, 27, 89-97.

22 Schmidt, I., Thomas, S., Kain, P., Risse, B., Naffin, E. and Klambt, C. (2012) Kinesin heavy chain function in Drosophila glial cells controls neuronal activity. J. Neurosci., 32, 7466-7476.

23 Niehues, S., Bussmann, J., Steffes, G., Erdmann, I., Kohrer, C., Sun, L., Wagner, M., Schafer, K., Wang, G., Koerdt, S.N. et al. (2015) Impaired protein translation in Drosophila models for Charcot-Marie-Tooth neuropathy caused by mutant tRNA synthetases. Nat. Commun., 6, 7520.

24 Chintapalli, V.R., Wang, J. and Dow, J.A. (2007) Using FlyAtlas to identify better Drosophila melanogaster models of human disease. Nat. Genet., 39, 715-720.

25 Graveley, B.R., Brooks, A.N., Carlson, J.W., Duff, M.O., Landolin, J.M., Yang, L., Artieri, C.G., van Baren, M.J., Boley, N., Booth, B.W. et al. (2011) The developmental transcriptome of Drosophila melanogaster. Nature, 471, 473-479.

26 Card, G. and Dickinson, M. (2008) Performance trade-offs in the flight initiation of Drosophila. J. Exp. Biol., 211, 341-353.

27 Gopfert, M.C., Albert, J.T., Nadrowski, B. and Kamikouchi, A. (2006) Specification of auditory sensitivity by Drosophila TRP channels. Nat. Neurosci., 9, 999-1000.

28 Senthilan, P.R., Piepenbrock, D., Ovezmyradov, G., Nadrowski, B., Bechstedt, S., Pauls, S., Winkler, M., Mobius, W., Howard, J. and Gopfert, M.C. (2012) Drosophila auditory organ genes and genetic hearing defects. Cell, 150, 1042-1054.

29 Baker, K.D. and Thummel, C.S. (2007) Diabetic larvae and obese flies-emerging studies of metabolism in Drosophila. Cell Metab., 6, 257-266.

30 Merchant, S.N., McKenna, M.J., Nadol, J.B., Jr., Kristiansen, A.G., Tropitzsch, A., Lindal, S. and Tranebjaeizrg, L. (2001) Temporal bone histopathologic and genetic studies in Mohr-Tranebjaerg syndrome (DFN-1). Otol. Neurotol., 22, 506-511.

31 Merchan, M.A., Merchan, J.A. and Ludena, M.D. (1980) Morphology of Hensen's cells. J. Anat., 131, 519-523.

32 Bell, A. and Fletcher, N.H. (2004) The cochlear amplifier as a standing wave: "squirting" waves between rows of outer hair cells? J. Acoust. Soc. Am., 116, 1016-1024.

33 Kalinec, F., Webster, P., Maricle, A., Guerrero, D., Chakravarti, D.N., Chakravarti, B., Gellibolian, R. and Kalinec, G. (2009) Glucocorticoid-stimulated, transcription-independent release of annexin A1 by cochlear Hensen cells. Br. J. Pharmacol., 158, 1820-1834.

34 Urrutia, R.A. and Kalinec, F. (2015) Biology and pathobiology of lipid droplets and their potential role in the protection of the organ of Corti. Hear. Res., in press.

35 Kojovic, M., Parees, I., Kassavetis, P., Palomar, F.J., Mir, P., Teo, J.T., Cordivari, C., Rothwell, J.C., Bhatia, K.P. and Edwards, M.J. (2013) Secondary and primary dystonia: pathophysiological differences. Brain, 136, 2038-2049.

36 Kojovic, M., Parees, I., Lampreia, T., Pienczk-Reclawowicz, K., Xiromerisiou, G., Rubio-Agusti, I., Kramberger, M., Carecchio, M., Alazami, A.M., Brancati, F. et al. (2013) The syndrome of deafness-dystonia: clinical and genetic heterogeneity. Mov. Disord., 28, 795-803.

37 Jin, H., May, M., Tranebjaerg, L., Kendall, E., Fontan, G., Jackson, J., Subramony, S.H., Arena, F., Lubs, H., Smith, S. et al. (1996) A novel X-linked gene, DDP, shows mutations in families with deafness (DFN-1), dystonia, mental deficiency and blindness. Nat. Genet., 14, 177-180.

38 Elpeleg, O., Miller, C., Hershkovitz, E., Bitner-Glindzicz, M., Bondi-Rubinstein, G., Rahman, S., Pagnamenta, A., Eshhar, S. and Saada, A. (2005) Deficiency of the ADP-forming succinyl-CoA synthase activity is associated with encephalomyopathy and mitochondrial DNA depletion. Am. J. Hum. Genet., 76, 1081-1086.

39 Wortmann, S.B., Vaz, F.M., Gardeitchik, T., Vissers, L.E., Renkema, G.H., Schuurs-Hoeijmakers, J.H., Kulik, W., Lammens, M., Christin, C., Kluijtmans, L.A. et al. (2012) Mutations in the phospholipid remodeling gene SERAC1 impair mitochondrial function and intracellular cholesterol trafficking and cause dystonia and deafness. Nat. Genet., 44, 797-802.

40 Engl, G., Florian, S., Tranebjaerg, L. and Rapaport, D. (2012) Alterations in expression levels of deafness dystonia protein 1 affect mitochondrial morphology. Hum. Mol. Genet., 21, 287-299.

41 Barbosa, A.D., Savage, D.B. and Siniossoglou, S. (2015) Lipid droplet-organelle interactions: emerging roles in lipid metabolism. Curr Opin Cell Biol, 35, 91-97.

42 Pol, A., Gross, S.P. and Parton, R.G. (2014) Review: biogenesis of the multifunctional lipid droplet: lipids, proteins, and sites. J. Cell Biol., 204, 635-646.

43 Sadananthan, S.A., Prakash, B., Leow, M.K., Khoo, C.M., Chou, H., Venkataraman, K., Khoo, E.Y., Lee, Y.S., Gluckman, P.D., Tai, E.S. et al. (2015) Automated segmentation of visceral and subcutaneous (deep and superficial) adipose tissues in normal and overweight men. J. Magn. Reson. Imaging, 41, 924-934.

44 Cowin, G.J., Jonsson, J.R., Bauer, J.D., Ash, S., Ali, A., Osland, E.J., Purdie, D.M., Clouston, A.D., Powell, E.E. and Galloway, G.J. (2008) Magnetic resonance imaging and spectroscopy for monitoring liver steatosis. J. Magn. Reson. Imaging, 28, 937-945.

45 Purcell, S., Neale, B., Todd-Brown, K., Thomas, L., Ferreira, M.A., Bender, D., Maller, J., Sklar, P., de Bakker, P.I., Daly, M.J. et al. (2007) PLINK: a tool set for whole-genome association and population-based linkage analyses. Am. J. Hum. Genet., 81, 559-575.

46 Abecasis, G.R., Cherny, S.S., Cookson, W.O. and Cardon, L.R. (2002) Merlin--rapid analysis of dense genetic maps using sparse gene flow trees. Nat. Genet., 30, 97-101.

47 Gloeckner, C.J., Boldt, K., Schumacher, A., Roepman, R. and Ueffing, M. (2007) A novel tandem affinity purification strategy for the efficient isolation and characterisation of native protein complexes. Proteomics, 7, 4228-4234.

48 Roosing, S., Lamers, I.J., de Vrieze, E., van den Born, L.I., Lambertus, S., Arts, H.H., Group, P.B.S., Peters, T.A., Hoyng, C.B., Kremer, H. et al. (2014) Disruption of the basal body protein POC1B results in autosomal-recessive cone-rod dystrophy. Am. J. Hum. Genet., 95, 131-142.

49 Brand, A.H. and Perrimon, N. (1993) Targeted gene expression as a means of altering cell fates and generating dominant phenotypes. Development, 118, 401-415.

50 Dietzl, G., Chen, D., Schnorrer, F., Su, K.C., Barinova, Y., Fellner, M., Gasser, B., Kinsey, K., Oppel, S., Scheiblauer, S. et al. (2007) A genome-wide transgenic RNAi library for conditional gene inactivation in Drosophila. Nature, 448, 151-156.

51 Rynes, J., Donohoe, C.D., Frommolt, P., Brodesser, S., Jindra, M. and Uhlirova, M. (2012) Activating transcription factor 3 regulates immune and metabolic homeostasis. Mol. Cell Biol., 32, 3949-3962.

52 Mukhopadhyay, A., Kramer, J.M., Merkx, G., Lugtenberg, D., Smeets, D.F., Oortveld, M.A., Blokland, E.A., Agrawal, J., Schenck, A., van Bokhoven, H. et al. (2010) CDK19 is disrupted in a female patient with bilateral congenital retinal folds, microcephaly and mild mental retardation. Hum. Genet., 128, 281-291.

53 Livak, K.J. and Schmittgen, T.D. (2001) Analysis of relative gene expression data using real-time quantitative PCR and the 2(-Delta Delta C(T)) Method. Methods, 25, 402-408.

54 Wearne, S.L., Rodriguez, A., Ehlenberger, D.B., Rocher, A.B., Henderson, S.C. and Hof, P.R. (2005) New techniques for imaging, digitization and analysis of three-dimensional neural morphology on multiple scales. Neuroscience, 136, 661-680.

55 Scorcioni, R., Polavaram, S. and Ascoli, G.A. (2008) L-Measure: a web-accessible tool for the analysis, comparison and search of digital reconstructions of neuronal morphologies. Nat. Protoc., 3, 866-876.

SUPPLEMENTAL FIGURES, TABLES AND LEGENDS

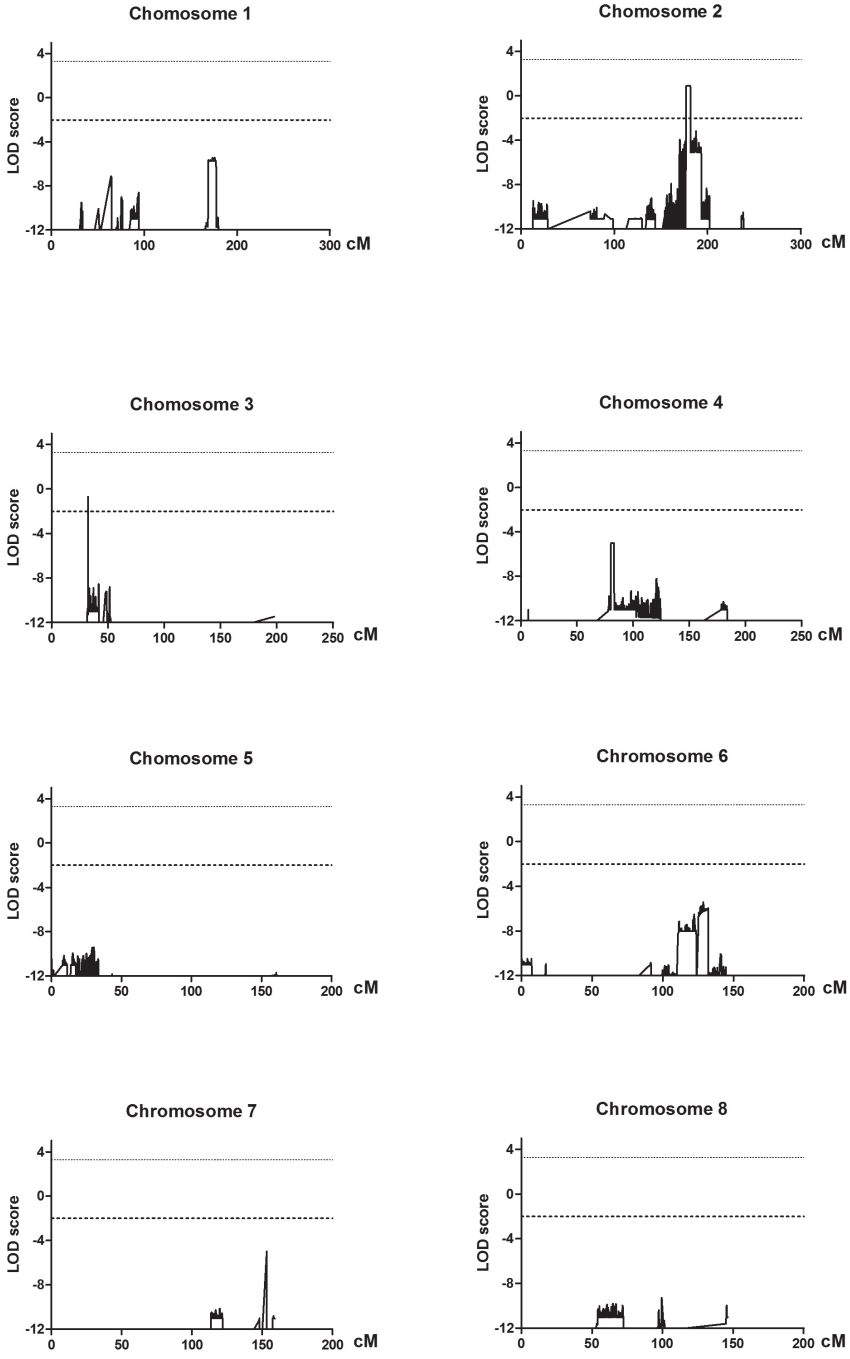

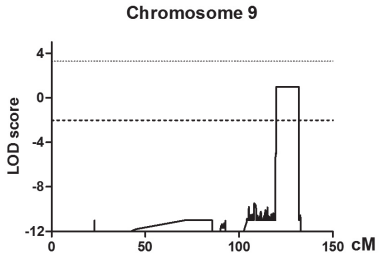
Chromosome 9
LOD score
4
0
-4
-8
-12
0
50
100
150
cM

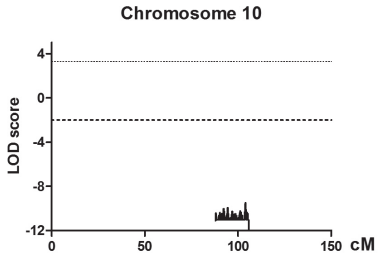
Chromosome 10
LOD score
4
0
-4
-8
-12
0
50
100
150
cM

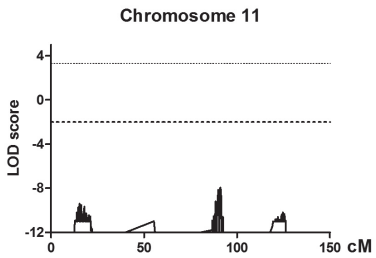
Chromosome 11
LOD score
4
0
-4
-8
-12
0
50
100
150
cM

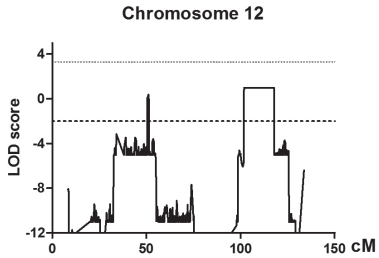
Chromosome 12
LOD score
4
0
-4
-8
-12
0
50
100
150
cM

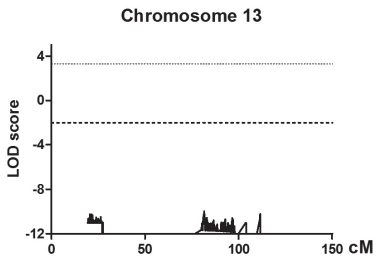
Chromosome 13
LOD score
4
0
-4
-8
-12
0
50
100
150
cM

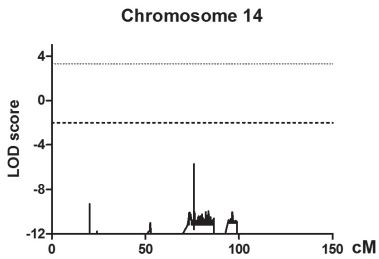
Chromosome 14
LOD score
4
0
-4
-8
-12
0
50
100
150
cM

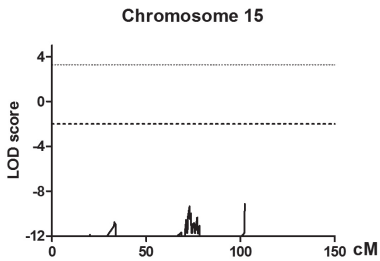
Chromosome 15
LOD score
4
0
-4
-8
-12
0
50
100
150
cM

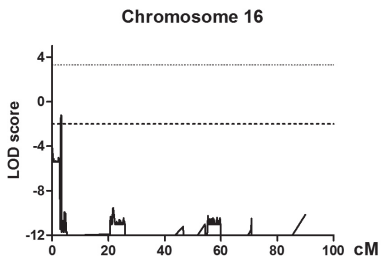
Chromosome 16
LOD score
4
0
-4
-8
-12
0
20
40
60
80
100
cM

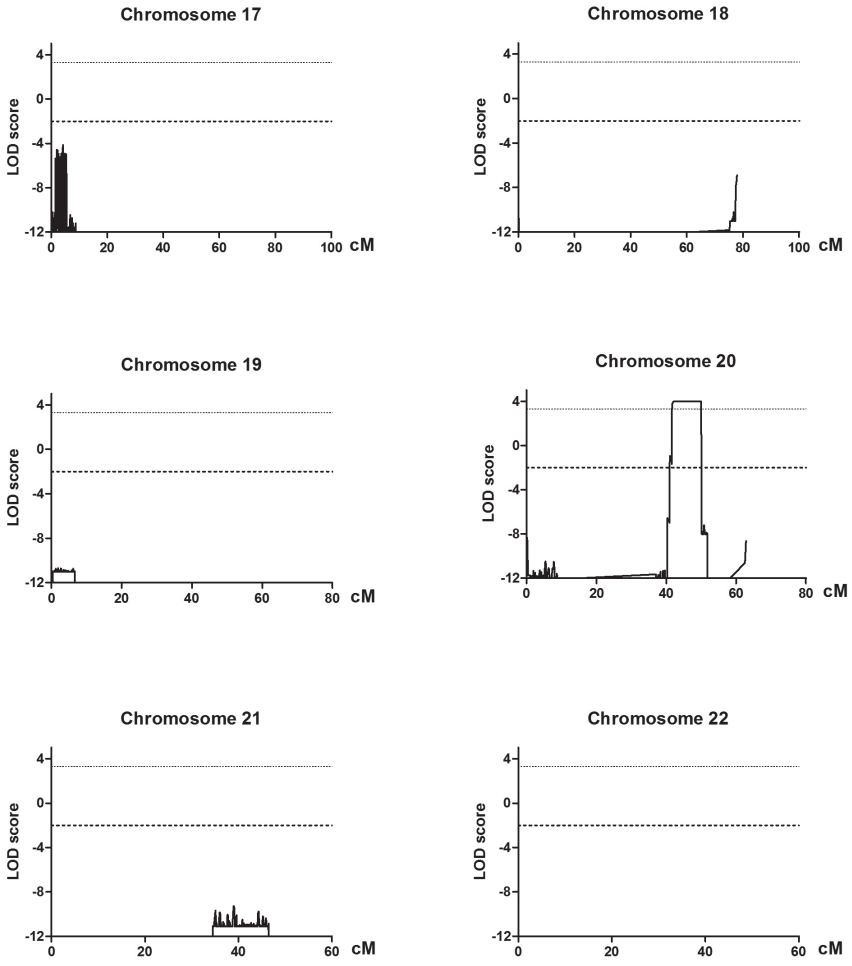

Figure S1. Genome wide LOD scores as calculated using MERLIN 1.1.2

The Y axis represents LOD scores and the X axis genetic distance in centimorgans (cM), per chromosome. The dotted line mark a LOD score of 3.3 indicating genome wide significance and the dashed line mark a LOD score of -2.0 indicating exclusion of linkage. In the calculations, the disease allele frequency at 0.001. There is only one region in chromosome 20q12-q13.2, delimited by rs2903624 and rs6096425 (chr20:41,616,510-50,037,207; GRCh37, hg19) with a significant maximum LOD score of 4.

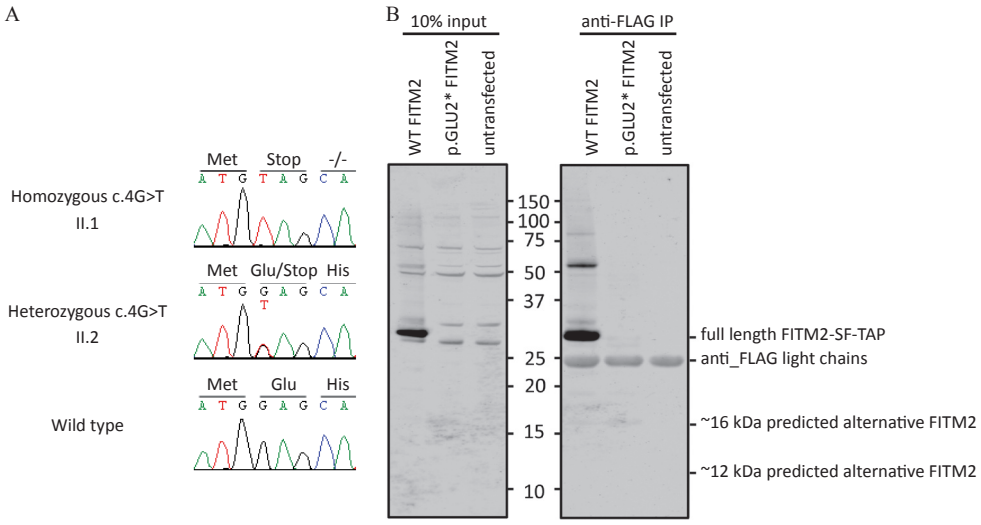

Figure S2. identification of genetic defects underlying Siddiqi syndrome in family W09-1008 and expression analysis of wild-type and p.Glu2* FITM2 fused to a flag TAG in HEK293T cells

(A) Partial sequences of *FITM2* exon 1 are shown from an affected member, an unaffected heterozygous sib and an unaffected wild-type sib of family W09-1008. The predicted amino acid changes and the surrounding amino acids are indicated above the sequence. As reference sequence NM_001080472.1 was employed. (B)The left panel shows a Western blot of a gel on which 10 % of the cell lysate was loaded (before affinity purification). The right panel shows a Western blot of a gel on which 10 µl of the lysate after affinity purification (anti-FLAG) was loaded. Wildtype (WT) FITM2 migrates around 29kDa and it is absent upon transfection of the p.Glu2* FITM2 construct expressed. After affinity purification, a very weak band is observed at ~16kDa. However, the intensity of the 16 kDa band is about 2700 fold lower than the wild-type FITM2 band and therefore it is likely to have little or none biological impact. The gel was immunostained with an anti FLAG polyclonal antibody. Of four ATG-triplets in the original reading-frame, three (codon positions 94, 493 and 508) are predicted to be potential translation initiation sites by the Netstart 1.0 algorithm.[1] Accordingly, alternative proteins would consist of 285 amino acids (aa) (26.2 kDa), 152 aa (11.2 kDa), and 147 aa (10.6 kDa), respectively. Expression constructs encode FITM2 fused to a C-terminal Strep-FLAG-tag (SF-TAP),[2] adding approximately 6 kDa to the proteins. Wild-type FITM2 was found to migrate according to molecular weight of ~29 kDa, which is lower as compared to the predicted mass of the complete protein (Figure S2). However, fragments of similar length are observed with anti-FITM2 staining in the work of Duckert *et al.* and pro-peptide cleavage is predicted by the ProP algorithm.[3] Marker size is indicated between the panels and given in kDa.

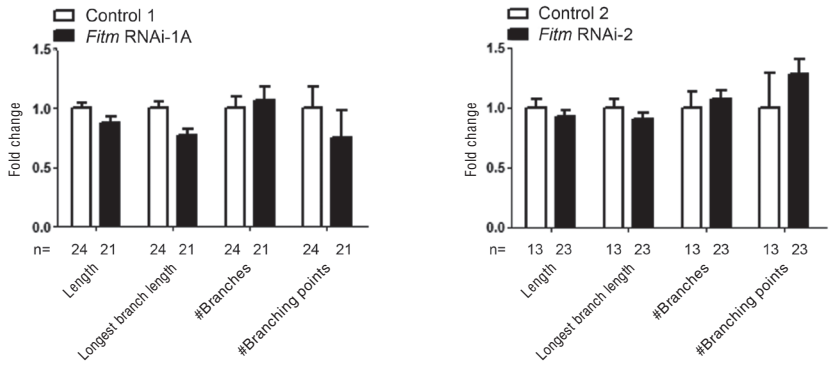

Figure S3. Downregulation of *Fitm* in the skeletal muscle has no effect on NMJ length, longest branch length, number of branches and number of branching points

Synapse morphology was determined in muscle 4 of L3 larvae with *Fitm* downregulated in the skeletal muscle by the *Mef2*-GAL4 driver in the RNAi lines *Fitm* RNAi-1A, and *Fitm* RNAi-2 and compared to the corresponding controls with no consistent differences in the presented parameters. All the parameter values were normalized with the respective control values. Bar graphs represent the fold change of the knockdown condition compared to its corresponding control, error bars represent normalized SEM. P-values were determined using two-sided T-tests. The number of NMJ images is indicated with "n".

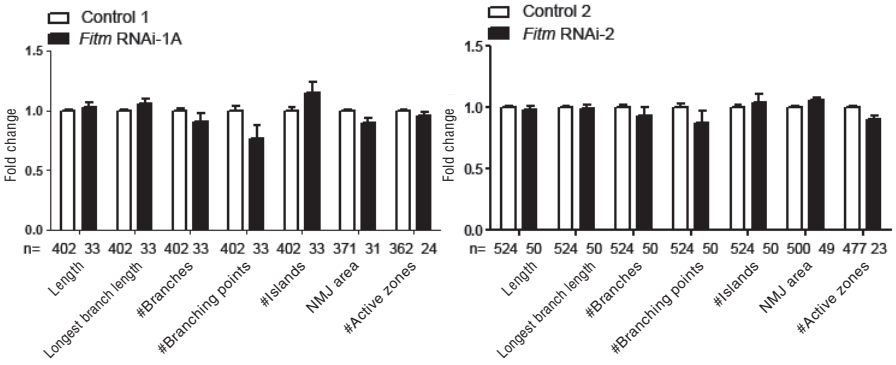

Figure S4. No consistent differences in NMJ parameters were found upon pan-neuronal *Fitm* knockdown

Synapse morphology was determined in muscle 4 of L3 larvae with *Fitm* downregulated pan-neurally using the *elav*-GAL4 driver in the RNAi lines *Fitm* RNAi-1A, and *Fitm* RNAi-2 and compared to the corresponding controls, no significant differences were found in any of the quantified NMJ parameters. All the parameter values were normalized with the respective control values. Bar graphs represent averages and error bars represent SEM. Significance was determined using two-sided T-test. The number of NMJ images is indicated with "n".

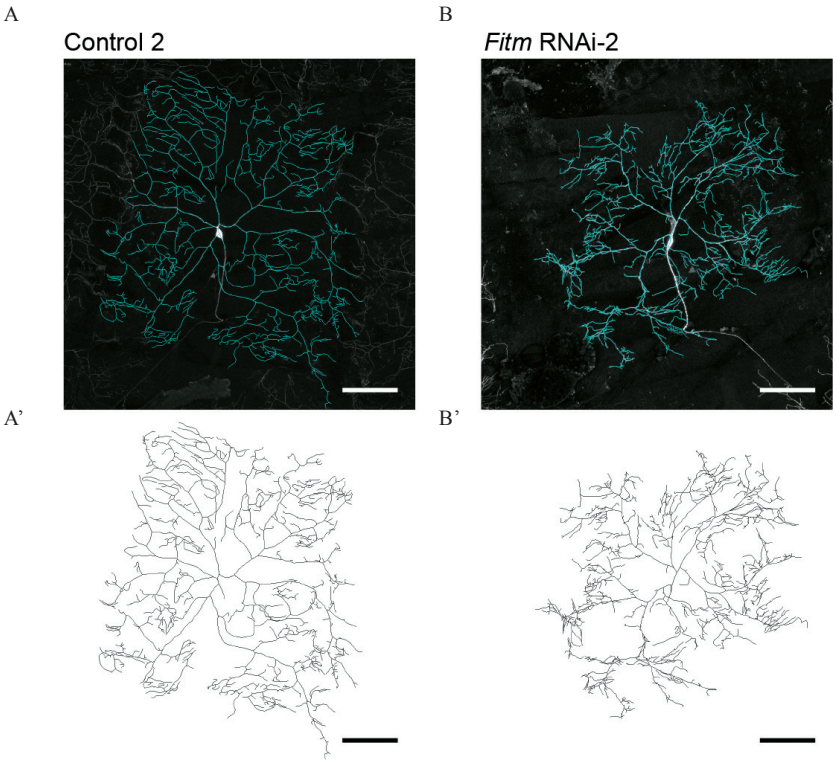

Figure S5. Manual tracing representation of the type IV neurons of *Drosophila*

(A), (B) Control and *Fitm* RNAi-2 neuron with the manual tracing overlaid in cyan. (A'), (B') Isolated manual tracing reconstruction. Scale bar 100 μm.

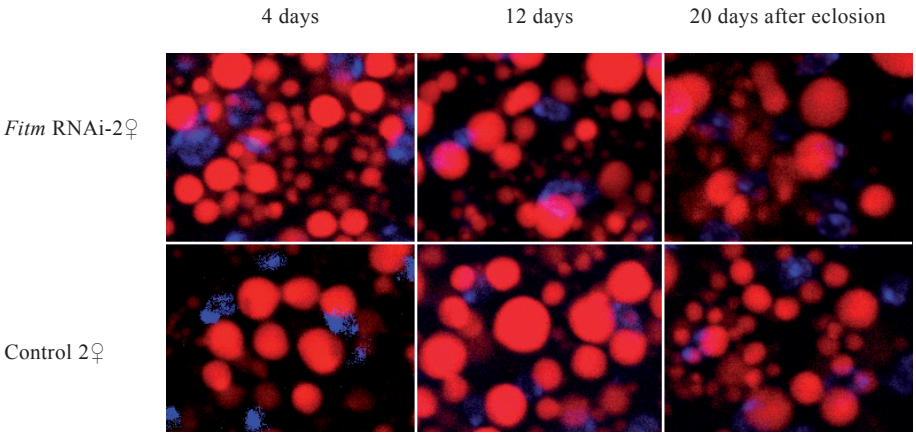

Figure S6. Lipid droplet size in *Drosophila* after dowregulation of *Fitm*

Lipid droplets labeled with Bodipy (red) in fat bodies of females of the *Fitm* RNAi-2 upon RNAi expression induced by the *C7*-GAL4 driver as compared to Control-2 flies. Nuclei were stained with DAPI (blue). Differences in lipid droplet size between *Fitm* RNAi-2 females and controls at 4, 12 and 20 days after eclosion were not detected because the size of lipid droplets of Control-2 was not uniform. The scale bar is 10 μm.

Table S1. Primer sequences and PCR conditions for genomic PCR and Sanger sequence analysis of *FITM2* (uc002xlr.1)

PCR amplicon	Oligonucleotides (5` to 3`)
*FITM2*_Exon 1_forward	agaggagacgagcgagttc
*FITM2*_Exon 1_reverse	ctccaatgactcgtccacc
*FITM2*_Exon 2_forward	cccctgacagtgtagagacc
*FITM2*_Exon 2_reverse	aagtgcctaactgggaatgg
*FITM2*_Exon 1 _Digestion_forward	ggcacggagaggaggac
*FITM2*_Exon 1_Digestion_reverse	cactcacacgttgaggacg
*Fitm*_Exon1_forward	cgtcatagccaccttcttctg
*Fitm*_Exon1-2_reverse	gtcgcataaccctttgtgg
*RpII215*_Exon 3_forward	ccgcgatacttctctccac
*RpII215*_Exon 4_reverse	gaccagctaggcgacattc

REFERENCES

1. Pedersen, A.G., and Nielsen, H. (1997). Neural network prediction of translation initiation sites in eukaryotes: perspectives for EST and genome analysis. Proc. Int. Conf. Intell. Syst. Mol. Biol. 5, 226-233.
2. Gloeckner, C.J., Boldt, K., and Ueffing, M. (2009). Strep/FLAG tandem affinity purification (SF-TAP) to study protein interactions. Curr Protoc Protein Sci Chapter 19, Unit19 20.
3. Duckert, P., Brunak, S., and Blom, N. (2004). Prediction of proprotein convertase cleavage sites. Protein Eng. Des. Sel. 17, 107-112.

[1]Department of Otorhinolaryngology, Hearing & Genes, Radboud university medical center, Nijmegen, the Netherlands; [2]The Radboud Institute for Molecular Life Sciences, Radboud university medical center, Nijmegen, the Netherlands; [3]Department of Human Genetics, Radboud university medical center, Nijmegen, the Netherlands; [4]Radboud Institute for Health Sciences, Nijmegen, the Netherlands; [5]Department of Clinical Genetics, VU University Medical Center, Amsterdam, the Netherlands; [6]Department of Clinical Genetics, Academic Medical Center, University of Amsterdam, Amsterdam, the Netherlands; [7]Department of Pediatrics, Academic Medical Center, University of Amsterdam, Amsterdam, Netherlands [8]Department of Clinical Genetics, Leiden University Medical Center, Leiden, the Netherlands; [9]University Medical Centre Groningen, Department of Genetics, Groningen, the Netherlands; [10]Department of Clinical Genetics, Maastricht University Medical Centre, Maastricht, the Netherlands; [11]Department of Clinical Genetics, Erasmus Medical Centre, Rotterdam, the Netherlands; [12]Department of Clinical Genetics, Utrecht Medical Center/Wilhelmina Children's Hospital, Utrecht, the Netherlands

CHAPTER 7

The diagnostic yield of whole exome sequencing targeting a gene panel for hearing impairment in the Netherlands

Celia Zazo Seco[1,2,*], Ilse Feenstra[3,*], Rolph Pfundt[2,3], Mieke Wesdorp[1,2], Jayne Y. Hehir Kwa[2,3], Jaap Oostrik[1,2], Steven Castelein[3], Christian Gilissen[3], Ilse J. de Wijs[3], Ronald J.C. Admiraal[1,2], Ronald J.E. Pennings[1,2,4], Henricus P. M. Kunst[1,4], Jiddeke M. van de Kamp[5], S. Tamminga[5], Arjan C. Houweling[5], Astrid S. Plomp[6], Saskia M. Maas[6,7], Pia A.M. de Koning Gans[8], Sarina G. Kant[8], Christa M. de Geus[8], Suzanna G.M. Frints[10], Els K. Vanhoutte[10], Marieke F. van Dooren[11], Marie-José H. van den Boogaard[12], Hans Scheffer[2,3], Marcel Nelen[3], Hannie Kremer[1,2,3], Lies Hoefsloot[3,10], Margit Schraders[1,2,#], Helger G. Yntema[2,3,#]

*,#Authors contributed equally

Manuscript in preparation

ABSTRACT

Purpose: Hearing impairment (HI) is genetically very heterogeneous, which hampers genetic counseling and molecular diagnosis. Testing of several known genes selected based on the type of HI, is laborious and expensive. In this study, we evaluate the diagnostic utility of whole exome sequencing (WES) targeting a panel of HI-related genes.

Methods: Two hundred index patients, mostly of Dutch origin, with presumed hereditary HI underwent WES targeting a HI gene panel.

Results: We found causative variants underlying the HI in 58 of 200 patients (29%). Ten of these patients have a large homozygous deletion, which could only be identified by copy number variation detection in the WES data. Variants of uncertain significance were found in 26 patients (13%). In the remaining 116 cases no potentially causative variants have been detected (58%).

Conclusion: The diagnostic yield for HI using WES targeting a HI gene panel is higher than targeted sequencing of single genes. In our patient cohort, causative variants in *GJB2, STRC, MYO15A*, and *USH2A*, and in *MYO6* were the leading causes for autosomal recessive and dominant HI, respectively. Segregation analysis of variants of uncertain significance in affected or unaffected relatives of index patients will further increase the diagnostic yield of WES.

INTRODUCTION

DNA diagnostics of any genetically heterogeneous disease based on predictive gene testing is highly inefficient, laborious and expensive. High throughput sequencing technologies such as whole exome sequencing (WES) have coped with these disadvantages allowing the analysis of all protein-coding exons in a single cost-effective attempt.[1]

Hearing impairment (HI) is the most common sensory disorder with an incidence of one in 750 newborns (> 40 dB) in developed countries.[2] About half of the cases are attributed to genetic factors with more than a hundred genes known to date (http://hereditaryhearingloss.org/). HI is most frequently manifested as non-syndromic (NSHI) accounting for about 70% of the hereditary cases. About 77% of NSHI cases exhibit autosomal recessive inheritance (arNSHI) with 61 genes and 97 loci known to date, whereas it is dominant (adNSHI) in about 22% of the cases with 33 genes and 67 loci known. The remaining 1% shows an X-linked, a Y-linked or a mitochondrial type of inheritance pattern with six loci and six genes known to date (http://hereditaryhearingloss.org/). NSHI is thus genetically very heterogeneous. Many genes have been described to be involved in only one or a few families with HI.[3-5] Some exceptions are known, *e.g.* mutations in *GJB2* followed by mutations in *STRC* and *MYO15A* are the most common causes for arNSHI worldwide.[6-9]

Since many genes contribute to hereditary HI, targeting all or a selection of protein-coding exons in a single experiment, like in WES, seems ideal and might ultimately be the only choice for a comprehensive genetic analysis of HI individuals. The implementation of WES in a diagnostic setting has been much slower than in scientific research due to the relatively low sensitivity of this method in detection of genetic variation in some exonic regions, *e.g.* extremely GC-rich regions, as compared to Sanger sequencing.[10] Despite this fact, the diagnostic yield in hereditary HI obtained by WES is expected to be higher compared to the approach of phenotype-based pre-testing of one or two genes by Sanger sequencing.[11] Therefore, the aim of this study is to evaluate the diagnostic utility of WES targeting a panel of HI-related genes in a group of 200 Dutch index patients with presumed hereditary HI.

PATIENTS AND METHODS

Patients

WES was performed in 200 patients with HI, mainly of Dutch origin. Non-genetic causes of the HI were excluded by anamnesis. Thirty-seven patients have been previously reported.[11,12] For 142 patients mutations in one or more genes involved in HI have been excluded before WES was performed. For all patients, written informed consent for WES was obtained after counseling by a clinical geneticist.

WES and bioinformatics

Prior to sequencing, genomic DNA fragments of all patients were enriched for exome sequences using the Agilent SureSelectXT Human All Exon 50Mb kit. For 45 patients, WES was performed with a 5500xl machine (Life TechnologiesTM) at the department of Human Genetics, Radboudumc Nijmegen, and data were analyzed using LifeScopeTM software as previously reported.[11] For the remaining patients (N=155) WES was performed at BGI-Europe (Copenhagen, Denmark), employing an Illumina HiSeq2000TM machine. For these samples, "read alignment" using BWA and "variant calling" with GATK were performed at BGI.[13]

For all patients, variants were annotated with an in-house developed annotation and prioritization pipeline.[11] Variants in genes associated with HI were selected and analyzed. In the first 45 patients, a panel of 104 HI genes was analyzed.[10] The remaining 155 patients were analyzed with an updated list of 130 HI genes. Detailed information on both gene lists (DGD_181213 and DGD_200614) can be found at http://genomediagnosticsnijmegen.nl/services/exome-sequencing-diagnostics. All reported variants have been verified by Sanger sequencing.

For all patients 'copy number variant calling' was carried out using CoNIFER 0.2.0,[14] and variant annotation was performed using an in-house developed strategy.[15]

Interpretation and classification of variants

To systematically predict their pathogenicity, variants were sorted based on existing guidelines for classification of variants (http://www.acgs.uk.com/media/774853/evaluation_and_reporting_of_sequence_variants_bpgs_june_2013_-_finalpdf.pdf). Patients were grouped based on the combination of (likely) pathogenic variants and associated phenotype known from literature. Three groups were distinguished: 1) patients with causative variants, 2) patients with variants of uncertain significance, and 3) patients without detected causative variants.

Validation of selected variants

All reported sequence variants have been validated by Sanger sequencing (primer sequences and PCR conditions are available upon request). Copy number variants were validated by MLPA (*STRC*, homemade MLPA kit s139; *USH2A*, MRC-Holland kits P361A1 and P362A2) or deletion-specific PCR (OTOA, kindly provided by Guney Bademci, MD).

MYO15A gene analysis

SNP genotyping was performed on genomic DNA samples isolated from peripheral blood of affected individuals using different single-nucleotide polymorphism (SNP) arrays (Affymetrix mapping 250K NspI, Affymetrix Genechip Genome-Wide Human Arrays 5.0 or Affymetrix Genechip Genome-Wide Human Arrays 6.0) as described previously.[16-18]

To determine the presence of the c.6787G>A transition in a panel of 102 index patients with presumed arNSHI, exon 32 of *MYO15A* (NM_016239.3) was amplified and digestion of PCR products with *PvuII* (New England Biolabs) was performed according to the manufacturer's protocol. Restriction fragments were analyzed on 2% agarose gels; the variant introduces a restriction site. To determine the presence of the c.1137delC variant in the same patient panel, exon 2 was amplified using specific primers with an M13 tail. A second round of amplification was performed using an M13 forward and a fluophore-labeled M13 reverse primer. PCR products were subsequently separated on an ABI Prism 3730 Genetic Analyzer, and analyzed with the GeneMapper software according to the manufacturer's protocol (Life Sciences).

For sequence analysis of *MYO15A* (NM_016239.3), all exons and exon-intron boundaries were amplified and Sanger sequence analysis was performed as described previously.[16] Primer sequences for amplification of exons and exon-intron boundaries of *MYO15A* are available upon request.

RESULTS

The exomes of 200 individuals with presumed hereditary HI, mostly of Dutch origin, were sequenced in this study. The inheritance pattern was suspected to be autosomal dominant in 65 cases, autosomal recessive in 33 cases, X-linked in one case and the remaining 101 cases were isolated. Subsequently, targeted analysis of WES data was performed for a panel of 104 (DGD181213, 45 cases) or 130 (DGD200614, 155 cases) genes associated with HI. The average coverage

per gene is available on our website (http://www.genomediagnosticsnijmegen.nl/services/exome-sequencing-diagnostics).

Diagnostic yield with WES in HI patients

We detected variants predicted to be pathogenic in 29% (58 cases) of the 200 cases with presumed hereditary HI (Table 1, Supplementary Table S1, Supplementary Table S2). In 41 of these patients homozygous or compound heterozygous mutations in genes associated with autosomal recessive HI were detected, being large homozygous deletions of several exons or complete genes in 10 of these cases. *GJB2* was found to be the most frequently mutated gene, followed by *USH2A, MYO15A* and *STRC*, together accounting for 41.4% of the positive cases (Figure 1a).

In the remaining 17 cases heterozygous mutations in ten different genes associated with autosomal dominant were found (Supplementary Table S1, Figure 1b). In three cases, the heterozygous mutations were *de novo*. Mutations in *MYO6* were the leading cause in this cohort of presumed adHI cases (Figure 1b).

The diagnostic yield was related to the type of inheritance of the HI in the patients. For patients with suspected autosomal recessive HI, the diagnostic yield was 54.5% (Table 1, Supplementary Table S2). In 27.7% of the cases without a (known) family history (isolated cases), the molecular etiology could be identified, the majority harboring causative variants in genes associated with arHI (Table 1, Supplementary Table S2). For adHI, presumed causative mutations were found in only 18.5% of the cases (Table 1, Supplementary Table S2).

We identified variants of uncertain significance in 26 cases (13%) (Supplementary Table S2, Supplementary Table S3). In 16 of these, co-segregation of the variant(s) with the disease in the family needs to be performed in order to classify these variants as the putative cause of the HI. In the remaining ten cases segregation analysis was performed. However, the variants could neither yet be classified as the cause of the HI, nor could they be discarded as not pathogenic. In two of these cases a variant has been identified which was previously described as causative for HI, but which does not segregate with the disease in the family (AD21 and ISO34). In one case (ISO31) compound heterozygous variants segregating with the HI were identified in two genes (*SLC26A4* and *USH1G*). In two other cases the reported HI phenotype is different from the phenotype known to be associated with the mutation and/or gene (AD17 and AD23). In three cases, a combination of a missense and a nonsense variant

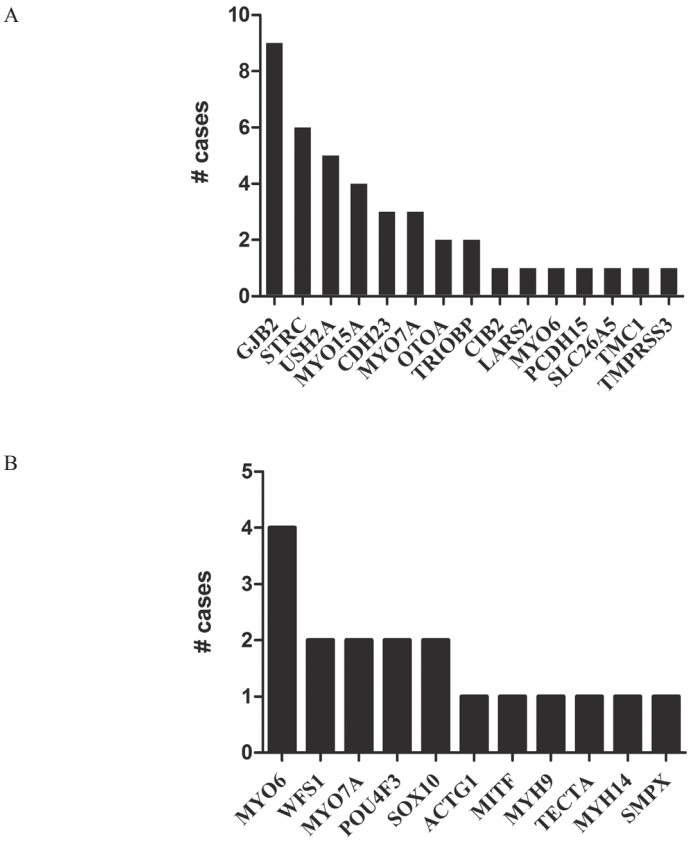

Figure 1. Overview of HI genes and number of cases in which causative variants were identified in these genes. A. cases with arHI. B. cases with adHI.

was found in *LOXHD1* (AR19, ISO29 and ISO35). To date, mostly truncating mutations have been reported for this gene and only a single patient who carries a combination of a missense and a nonsense mutation.[19-23] Finally, in two patients compound heterozygous variants were found in *USH2A* (AR20 and AR21). The significance of the (previously unreported) *USH2A* missense variants in these patients is unclear and they cannot be definitely classified as causative for the HI in these patients, although they are located in trans.

In our study, 58% of the 200 exomes (116 cases) did not reveal causative variants. In the majority of them (92 cases) no putative causative variants were remaining after the data filtering procedure. In 19 cases, the variants were not segregating with the HI in the family. In four cases only a single variant was identified in a gene known to underlie autosomal recessive HI. In two of the

Table 1. List of patients with presumed causal variants.

Patient	Gene	Variant 1	Variant 2	Segregating with HL
AD1[#]	*MYO6* NM_004999.3	c.1546+1G>T (p.?)	-	Yes
AD2	*WFS1* NM_006005.3	c.2051C>T (p.(Ala684Val))[#]	-	ND
AD3	*TECTA* ENST00000392793.1	c.6002G>T (p.(Cys2001Phe))	-	Yes
AD4	*MYO7A* NM_000260.3	c.1373A>T(p.(Asn458Ile))[#]	-	Yes
AD5[#]	*MYO6* NM_004999.3	c.1211del (p.(Gly404Glufs*4))	-	Yes
AD6[#]	*MYH9* NM_002473.4	c.2507C>T (p.(Pro836Leu))	-	Yes
AD7	*POU4F3* NM_002700.2	c.828_829insT (p.(Lys277*))	-	ND
AD8	*MYO7A* NM_000260.3	c.652G>A (p.(Asp218Asn))	-	Yes
AD9	*POU4F3* NM_002700.2	c.668T>C (p.(Leu223Pro))[#]	-	ND
AD10	*MYO6* NM_004999.3	c.3395del (p.(Lys1132Serfs*12))	-	Yes
AD11	*SOX10* NM_006941.3	c.1195C>T (p.(Gln399*))	-	ND
AD12	*MYH14* NM_001145809.1	c.394G>A (p.(Gly32Ser))	-	Yes
AR1[#]	*USH2A* NM_206933.2	c.9372-?_9570+? (p.?)	c.9372-?_9570+? (p.?)	ND
AR2	*OTOA* ENST00000388958	chr16(GRCh37):g.21581229-21771715del[#]	chr16(GRCh37):g.21581229-21771715del#	ND
AR3[#]	*CIB2* NM_006383.2	c.97C>T (p.(Arg33*))	c.196C>T (p.(Arg66Trp))	Yes
AR4	*STRC* NM_153700.2	c.-78-?_5327+?del(p.0?)[#]	c.-78-?_5327+?del(p.0?)[#]	Yes
AR5	*USH2A* NM_206933.2	c.8846-?_9371+?del(p.?)	c.8846-?_9371+?del(p.?)	ND
AR6	*TMC1* NM_138691.2	c.646del (p.(Leu216Serfs*54))	c.790C>T (p.(Arg264*))	ND
AR7	*CDH23* NM_022124.5	c.6442G>A (p.(Asp2148Asn))[#]	c.1545_1547del (p.(Ile515del))[#]	Yes
AR8	*USH2A* NM_206933.2	c.1606T>C (p.(Cys536Arg))[#]	c.9815C>T (p.(Pro3272Leu))[#]	Yes
AR9	*GJB2* NM_004004.5	c.35del (p.(Gly12Valfs*2))[#]	c.71G>A (p.Trp24*))[#]	ND
AR10	*GJB2* NM_004004.5	c.35del (p.(Gly12Valfs*2))[#]	c.35del (p.(Gly12Valfs*2))[#]	Yes
AR11	*CDH23* NM_022124.5	c.2096A>G (p.(Asp699Gly))	c.4564A>G (p.(Asn1521Ser))	Yes
AR12	*GJB2* NM_004004.5	c.-23+1G>A (p.?)[#]	c.35del (p.(Gly12Valfs*2))[#]	Yes
AR13	*MYO7A* NM_000260.3	c.3289C>T(p.(Gln1097*))	c.3862G>C(p.(Ala1288Pro))[#] c.5227C>T(p.(Arg1743Trp))[#]	ND
AR14	*STRC* NM_153700.2	c.-78-?_5327+?del(p.0?)	c.-78-?_5327+?del(p.0?)	ND
AR15	*MITF* NM_000248.3	c.649del (p.(Arg217Aspfs*4))[#]	-	ND
AR16	*PCDH15* NM_033056.3	c.3374-2A>G (r.?)	c.4127C>A (p.(Ala1376Asp))	Yes
AR17	*STRC* NM_153700.2	c.-78-?_5327+?del(p.0?)[#]	c.-78-?_5327+?del(p.0?)[#]	ND
AR18	*STRC* NM_153700.2	c.-78-?_5327+?del(p.0?)[#]	c.-78-?_5327+?del(p.0?)[#]	ND
ISO1[#11]	*MYO15A* NM_016239.3	c.625G>T (p.(Glu209*))	c.1137del (p.(Tyr380Metfs*64))[#]	ND
ISO2[#]	*USH2A* NM_206933.2	c.5385T>A (p.(Tyr1795*))	c.6850_6851insAATC (p.(His2284Glnfs*48))	ND
ISO3	*CDH23* NM_022124.5	c.8480_8481del (p.(Leu2827Hisfs*23))	c.8480_8481del (p.(Leu2827Hisfs*23))	ND
ISO4[#]	*MYO15A* NM_016239.3	c.6764+2T>A (p.?)	c.3844C>T (p.(Arg1282Trp); c.5287C>T (p.(Arg1763Trp))	Yes
ISO5	*GJB2* NM_004004.5	c.101T>C (p.(Met34Thr))[#]	c.109G>A (p.(Val37Ile))[#]	Yes
ISO6	*WFS1* NM_006005.3	c.2051C>T (p.(Ala684Val))[#]	-	ND

Table 1. Continued.

Patient	Gene	Variant 1	Variant 2	Segregating with HL
ISO7	*MYO15A* NM_016239.3	c.6787G>A (p.(Gly2263Ser))	c.7893+1G>A (p.?)	Yes
ISO8	*TRIOBP* NM_001039141.2	c.2653del (p.(Arg885Alafs*120))	c.5014G>T (p.(Gly1672*))	Yes
ISO9	*USH2A* NM_206933.2	c.2299del (p.(Glu767Serfs*21))	c.920_923dup (p.(His308Glnfs*16))	Yes
ISO10	*MYO7A* NM_000260.3	c.3476G>T (p.(Gly1159Val))#	c.5560G>A (p.Val1854Met))#	Yes
ISO11	*GJB2* NM_004004.5	c.250G>C (p.(Val84Leu))	c.269T>C (p.(Leu90Pro))#	Yes
ISO12	*GJB2* NM_004004.5	c.109G>A (p.(Val37Ile))#	c.109G>A (p.(Val37Ile))#	ND
ISO13	*TMPRSS3* NM_024022.2	c.916G>A (p.(Ala306Thr))#	c.1276G>A (p.(Ala426Thr))#	ND
ISO14	*STRC* NM_153700.2	c.-78-?_5327+?del(p.0?)#	c.-78-?_5327+?del(p.0?)#	ND
ISO15	*GJB2* NM_004004.5	c.35del (p.(Gly12Valfs*2))#	c.101T>C (p.(Met34Thr))#	Yes
ISO16	*ACTG1* NM_00199954.1	c.773C>T (p.(Pro258Leu))	-	ND
ISO17	*GJB2* NM_004004.5	c.35del (p.(Gly12Valfs*2))#	c.508_511dup (p.(Ala171Glufs*40))#	ND
ISO18	*MYO15A* NM_016239.3	c.3311dup (p.(Glu1105*))	c.3311dup (p.(Glu1105*))	ND
ISO19	*TRIOBP* NM_001039141.2	c.3460_3461del (p.(Leu1154Alafs*29))	c.3232dup (p.(Arg1078Profs*6))#	ND
ISO20	*MYO7A* NM_000260.3	c.5618G>A (p.(Arg1873Gln))#	c.6028G>A (p.(Asp2010Asn))#	Yes
ISO21	*MYO6* NM_004999.3	c.3610C>T (p.(Arg1204Trp))#	-	ND
ISO22	*SLC26A5* NM_198999.2	c.355C>T (p.(Pro119Ser))	c.355C>T (p.(Pro119Ser))	ND
ISO23	*GJB2* NM_004004.5	c.101T>C (p.(Met34Thr))#	c.109G>A (p.(Val37Ile))#	ND
ISO24	*SOX10* NM_006941.3	c.482G>A (p.(Arg161His))#	-	ND
ISO25	*STRC* NM_153700.2	c.-78-?_5327+?del(p.0?)#	c.-78-?_5327+?del(p.0?)##	ND
ISO26	*MYO6* NM_004999.3	c.3335A>G (p.(Tyr1112Cys))	c.1897del(p.(Gln633Lysfs*19))	Yes
ISO27	*LARS2* NM_015340.3	c.683G>A (p.(Arg228His))	c.880G>A (p.(Glu294Lys))	Yes
ISO28	*OTOA* ENST00000388958	chr16:21581229-21771715#	chr16:21581229-21771715#	ND

AR, autosomal recessive; AD, autosomal dominant; ISO, isolated; Y, yes; ND, not done; # mutations that have been described in literature before, the corresponding references are provided in Supplementary Table S1.

patients the phenotype associated with the gene did not match the phenotype seen in the patient and the gene was not further analyzed. In the other patients the genes were analyzed with Sanger sequencing and/or MLPA which did not reveal a second variant. Finally, in one case a putatively pathogenic variant was identified in *NLRP3*, a gene known to underlie Muckle-Wells syndrome.[24] However, further clinical evaluation in the patient revealed no evidence for this syndrome and the variant was therefore considered not to be the cause of the HI.

Diagnostic yield with targeted sequencing of single genes

To make a proper comparison of the diagnostic yield between single gene testing in DNA diagnostics and WES, an overview was made of all (in-house) gene analysis requests for HI in 2013-2014 and the diagnostic yield (Table 2). In total 436 gene analyses were requested in 206 unique patients for 39 different genes; in 33 (7.6%) of the gene analyses pathogenic variants underlying the HI were identified in 16 different genes. The three genes with the highest diagnostic yield were *GJB2, COCH* and *KCNQ4*. For these three genes, founder or hotspot mutations occur in the Dutch population explaining the high incidence of mutations found in DNA diagnostics.[25-27]

MYO15A mutations in the Dutch HI population

Recently, it has been reported that *MYO15A* mutations are a common cause of arNSHI.[6] Analysis of this gene was not frequently requested for DNA diagnostics; only three times in two years (Table 2) and no causative variants were identified in these cases. However, in the current WES cohort *MYO15A* mutations were identified to underlie the HI in four cases. Therefore, involvement of *MYO15A* mutations in the Dutch arNSHI population was further determined in a panel of patients with arNSHI. First, we analyzed SNP genotyping data of 28 families with at least two individuals with presumed arNSHI. In eight families, affected siblings showed a shared genotype for *MYO15A*. All exons and exon-intron boundaries of *MYO15A* were subsequently screened in the index patient of these eight families. In five of these families causative variants segregating with the HI were identified (Supplementary Table S4). In a second approach, the presence of two mutations (c.1137delC and c.6787G>A) was investigated in a panel of 102 additional index patients with presumed arNSHI. These mutations were selected since these were both identified in our arNSHI panel as well as in the WES cases (ISO1 and ISO7) at that time and we suspected that these might be founder mutations in the Dutch population. The c.1137delC mutation was present in five cases and the c.6787G>A mutation in two patients (homozygously in one).

Table 2. Diagnostic yield for single gene testing in DNA diagnostics

Gene symbol	# of requests	# of positive* requests	% of positive* request per gene
ACTG1	17	0	0
BSND	1	0	0
CLRN1	1	0	0
COCH	19	7	36.8
COL11A1	1	1	100
COL11A2	35	0	0
COL2A1	1	0	0
DFNA5	5	1	20
DFNB59	2	0	0
DIAPH1	8	0	0
EYA1	9	1	11.1
EYA4	22	0	0
GJB2	69	5	7.2
GRXCR1	1	0	0
HOXA2	1	0	0
KCNQ4	26	4	15.4
MITF	18	1	5.6
MYO15A	3	0	0
MYO6	16	0	0
MYO7A	3	1	33.3
NDP	1	1	100
OTOF	4	2	50
OTOG	3	0	0
OTOGL	3	0	0
PAX3	14	1	7.1
POU3F4	1	0	0
POU4F3	11	0	0
PTPRQ	1	0	0
SIX1	5	0	0
SIX5	5	0	0
SLC26A4	8	2	25
SNAI2	10	0	0
SOX10	2	0	0
TECTA	47	2	4.3
TMC1	2	0	0
TMPRSS3	36	2	5.6
TSHZ1	3	0	0
USH2A	5	1	20
WFS1	17	1	5.9

*positive indicates that causative variants were identified.

All exons and exon-intron boundaries of *MYO15A* were subsequently screened in all patients carrying the c.1137delC or the c.6787G>A mutation. In two of these patients the gene could not be completely screened since the DNA was depleted. In total, sequence analysis of the *MYO15A* gene was performed in 13 index patients. In eight of these homozygous or compound heterozygous putatively pathogenic variants were identified that segregated with the HI in the corresponding families (Supplementary Table S4).

To summarize, our targeted analysis of *MYO15A* revealed mutations in eight of 131 families (6.1%). This number might well be higher since we did not screen the complete gene in 97 of the cases. All individuals with causative variants in *MYO15A* presented with congenital severe-to-profound HI (Supplementary Table S4).

DISCUSSION

In this study, we aimed to evaluate the diagnostic yield of WES-based targeted analysis of genes involved in HI. WES technology allowed the efficient identification of single nucleotide variants, indels and large deletions that affect the protein coding regions of HI genes in a single experiment.[11] Our study underlines the great genetic heterogeneity for HI since causative variants were found in 25 different genes (Table 1). Our study also illustrates that there are still many genes to be discovered for HI since in 58% of the cases no putative causative variants were identified in the genes currently known to underlie HI. Part of these cases is likely to be explained by variants in known HI genes that cannot be identified by WES (*e.g.* deep intronic variants affecting splicing, variants in non-coding exons, repeat regions and regulatory regions). For the isolated cases, comprising about half of the subjects in this study, involvement of non-genetic causes cannot be fully excluded. Since *de novo* variants in known adNSHI genes were identified in three of the cases in our study, we hypothesize that novel genes for adNSHI can be identified by a *de novo* strategy (*i.e.* sequencing affected individuals and their unaffected parents). Variants of uncertain significance were mainly reported for patients with presumed autosomal dominant HI (Supplementary Table S2, Supplementary Table S3). Since no family members were available for segregation analysis, the pathogenicity of these variants remained unclear. This highlights the importance of sampling additional family members, and taking an accurate family history.

A subset of the patients (36) in the present study was previously reported in the study by Neveling *et al.* In 16 out of these 36 cases they identified likely pathogenic variants which revealed a diagnostic yield of 44.4% for WES in HI.[11] Segregation analysis was still needed, however, in nine of the families to confirm the genetic diagnosis. This analysis was performed in the current study and in seven families the variants did not segregate with the HI. This lowers the diagnostic yield of the cases included in the study by Neveling *et al.* to 22%, which is comparable to the yield in our study and again underlines the importance of segregation analysis.

The wide use of WES in routine diagnostics and research is producing large amounts of data on sequence variants in HI. Variants that have initially been reported as causative, based on the knowledge at that time, might be reclassified as benign due to increasing availability of allele frequency data.[28] This highlights the importance of population-based allele frequency data to evaluate the causality of variants. However, rare variants can be still difficult to classify since we found that in two cases of our cohort (AD21 and ISO34) previously reported variants did not fully segregate with the HI in the corresponding families (Supplementary Table S3). This makes the causality of these rare variants questionable. Further examples are the novel missense variants that we identified in *USH2A*. We classified these as variants of uncertain significance, despite the facts that 1) they were predicted to be damaging 2) they were not reported in any public database so far, and 3) they segregated with the hearing loss in the corresponding families. However, without support from functional studies, the pathogenicity of these missense variants will remain uncertain since Petrovski *et al.* (2013) calculated a residual variation score of 4.18 for *USH2A* (75th percentile of scored genes, frequency data based on NHLBI Exome Sequencing Project) suggestive of a great tolerance of this gene to genetic variation.[29] This is casting some doubt on the extensive variation in *USH2A* reported as likely pathogenic in public databases such as the Leiden Open Variant Database (LOVD). Importantly, these uncertainties are extremely difficult for genetic counseling, since parents have to be informed about the possible development of Usher syndrome in their children.

CNV detection in our cohort could identify large deletions in 5% of the cases, which is higher than the 2.6% presented in the literature.[30,31] The most likely explanation for this difference is the relatively high frequency of *STRC* deletions in our population (3%). As has also been reported in other populations,[8] deletions of *STRC* seem to be the second most frequent cause of arNSHI in the Netherlands.

We did not find causative variants in genes that are associated with identifiable phenotypes segregating with a recessive inheritance pattern, such as progressive HI with a downsloping audiogram caused by *TMPRSS3* mutations,[7,32] the stable HI with a cookie-bite audiogram configuration caused by mutations in *TECTA*[7] and *SLC26A4*[33] mutations associated with enlarged vestibular aqueducts and/or fluctuating HI. This is most likely due to the fact that these genes are generally tested for mutations in all patients with these identifiable phenotypes.

The most important conclusion from our study is that the diagnostic yield of WES is much higher than that of single gene testing, 29% versus 7.6% (Table 2), respectively. In our cohort we found that mutations in *GJB2, STRC, USH2A, MYO15A* and *MYO6* underlie HI in ~14% of the cases. This is in agreement with previously published studies on the involvement of HI genes in other populations.[6-9,32,34] Moreover, additional targeted testing of *MYO15A* indicated that this gene is relatively frequently involved in prelingual congenital HI in the Dutch population. The main reason for the higher diagnostic yield in WES compared to that of single gene testing in our laboratory is the fact that either no genes have been pretested or the phenotypic variability does not allow successful pretesting by Sanger sequencing. Predictive gene testing is thus highly inefficient. We therefore suggest that for nonsyndromic childhood onset HI it would only be cost-effective to prescreen *GJB2, STRC, USH2A* and *MYO15A*. For recognizable phenotypes (such as Pendred syndrome, Waardenburg syndrome and Usher syndrome) prescreening of specific genes might still be useful. Novel cost-effective technologies, such as molecular inversion probes, will replace Sanger sequencing and allow testing of a panel of genes, such as the genes associated with Usher syndrome, in a single test.[35,36]

Acknowledgements

We are grateful to all participating patients and their families. We also thank Kim van der Donk for expert technical assistance and Rick de Reuver and Nienke Wieskamp for their bioinformatical support. We are thankful to C.C. de Kruiff collecting and referring patients. This work was financially supported by grants from Netherlands Organization for Scientific Research [016.136.088, to M.S], the NUTS-OHRA foundation [1204-076, to H.K.], the Heinsius Houbolt foundation [to H.K.].

REFERENCES

1. Shearer AE, DeLuca AP, Hildebrand MS, et al. Comprehensive genetic testing for hereditary hearing loss using massively parallel sequencing. Proceedings of the National Academy of Sciences of the United States of America. Dec 7 2010;107(49):21104-21109.
2. Morton CC, Nance WE. Newborn hearing screening--a silent revolution. The New England journal of medicine. May 18 2006;354(20):2151-2164.
3. Seco CZ, Oonk AM, Dominguez-Ruiz M, et al. Progressive hearing loss and vestibular dysfunction caused by a homozygous nonsense mutation in CLIC5. European journal of human genetics : EJHG. Feb 2015;23(2):189-194.
4. Schraders M, Ruiz-Palmero L, Kalay E, et al. Mutations of the gene encoding otogelin are a cause of autosomal-recessive nonsyndromic moderate hearing impairment. American journal of human genetics. Nov 2 2012;91(5):883-889.
5. Yariz KO, Duman D, Seco CZ, et al. Mutations in OTOGL, encoding the inner ear protein otogelin-like, cause moderate sensorineural hearing loss. American journal of human genetics. Nov 2 2012;91(5):872-882.
6. Miyagawa M, Nishio SY, Hattori M, et al. Mutations in the MYO15A Gene Are a Significant Cause of Nonsyndromic Hearing Loss: Massively Parallel DNA Sequencing-Based Analysis. The Annals of otology, rhinology, and laryngology. Mar 19 2015.
7. Hoefsloot LH, Feenstra I, Kunst HP, Kremer H. Genotype phenotype correlations for hearing impairment: approaches to management. Clinical genetics. Jun 2014;85(6):514-523.
8. Francey LJ, Conlin LK, Kadesch HE, et al. Genome-wide SNP genotyping identifies the Stereocilin (STRC) gene as a major contributor to pediatric bilateral sensorineural hearing impairment. American journal of medical genetics. Part A. Feb 2012;158A(2):298-308.
9. Vona B, Hofrichter MA, Neuner C, et al. DFNB16 is a frequent cause of congenital hearing impairment: implementation of STRC mutation analysis in routine diagnostics. Clinical genetics. Jan 2015;87(1):49-55.
10. Strom SP, Lee H, Das K, et al. Assessing the necessity of confirmatory testing for exome-sequencing results in a clinical molecular diagnostic laboratory. Genetics in medicine : official journal of the American College of Medical Genetics. Jul 2014;16(7):510-515.
11. Neveling K, Feenstra I, Gilissen C, et al. A post-hoc comparison of the utility of sanger sequencing and exome sequencing for the diagnosis of heterogeneous diseases. Human mutation. Dec 2013;34(12):1721-1726.
12. Seco CZ, Giese AP, Shafique S, et al. Novel and recurrent CIB2 variants, associated with nonsyndromic deafness, do not affect calcium buffering and localization in hair cells. European journal of human genetics : EJHG. Jul 15 2015.

13. Van der Auwera GA, Carneiro MO, Hartl C, et al. From FastQ data to high confidence variant calls: the Genome Analysis Toolkit best practices pipeline. Current protocols in bioinformatics / editoral board, Andreas D. Baxevanis ... [et al.]. Oct 15 2013;11(1110):11 10 11-11 10 33.
14. Krumm N, Sudmant PH, Ko A, et al. Copy number variation detection and genotyping from exome sequence data. Genome research. Aug 2012;22(8):1525-1532.
15. de Ligt J, Boone PM, Pfundt R, et al. Detection of clinically relevant copy number variants with whole-exome sequencing. Human mutation. Oct 2013;34(10):1439-1448.
16. Schraders M, Lee K, Oostrik J, et al. Homozygosity mapping reveals mutations of GRXCR1 as a cause of autosomal-recessive nonsyndromic hearing impairment. American journal of human genetics. Feb 12 2010;86(2):138-147.
17. Maria Oonk AM, van Huet RA, Leijendeckers JM, et al. Nonsyndromic hearing loss caused by USH1G mutations: widening the USH1G disease spectrum. Ear and hearing. Mar-Apr 2015;36(2):205-211.
18. Schraders M, Oostrik J, Huygen PL, et al. Mutations in PTPRQ are a cause of autosomal-recessive nonsyndromic hearing impairment DFNB84 and associated with vestibular dysfunction. American journal of human genetics. Apr 9 2010;86(4):604-610.
19. Edvardson S, Jalas C, Shaag A, et al. A deleterious mutation in the LOXHD1 gene causes autosomal recessive hearing loss in Ashkenazi Jews. American journal of medical genetics. Part A. May 2011;155A(5):1170-1172.
20. Mori K, Moteki H, Kobayashi Y, et al. Mutations in LOXHD1 Gene Cause Various Types and Severities of Hearing Loss. The Annals of otology, rhinology, and laryngology. May 2015;124 Suppl 1:135S-141S.
21. Vozzi D, Morgan A, Vuckovic D, et al. Hereditary hearing loss: a 96 gene targeted sequencing protocol reveals novel alleles in a series of Italian and Qatari patients. Gene. Jun 1 2014;542(2):209-216.
22. Diaz-Horta O, Duman D, Foster J, 2nd, et al. Whole-exome sequencing efficiently detects rare mutations in autosomal recessive nonsyndromic hearing loss. PloS one. 2012;7(11):e50628.
23. Grillet N, Schwander M, Hildebrand MS, et al. Mutations in LOXHD1, an evolutionarily conserved stereociliary protein, disrupt hair cell function in mice and cause progressive hearing loss in humans. American journal of human genetics. Sep 2009;85(3):328-337.
24. Hoffman HM, Mueller JL, Broide DH, Wanderer AA, Kolodner RD. Mutation of a new gene encoding a putative pyrin-like protein causes familial cold autoinflammatory syndrome and Muckle-Wells syndrome. Nature genetics. Nov 2001;29(3):301-305.
25. Fransen E, Verstreken M, Bom SJ, et al. A common ancestor for COCH related cochleovestibular (DFNA9) patients in Belgium and The Netherlands bearing the P51S mutation. Journal of medical genetics. Jan 2001;38(1):61-65.

26. Gasparini P, Rabionet R, Barbujani G, et al. High carrier frequency of the 35delG deafness mutation in European populations. Genetic Analysis Consortium of GJB2 35delG. European journal of human genetics : EJHG. Jan 2000;8(1):19-23.
27. Topsakal V, Pennings RJ, te Brinke H, et al. Phenotype determination guides swift genotyping of a DFNA2/KCNQ4 family with a hot spot mutation (W276S). Otology & neurotology : official publication of the American Otological Society, American Neurotology Society [and] European Academy of Otology and Neurotology. Jan 2005;26(1):52-58.
28. Shearer AE, Eppsteiner RW, Booth KT, et al. Utilizing ethnic-specific differences in minor allele frequency to recategorize reported pathogenic deafness variants. American journal of human genetics. Oct 2 2014;95(4):445-453.
29. Petrovski S, Wang Q, Heinzen EL, Allen AS, Goldstein DB. Genic intolerance to functional variation and the interpretation of personal genomes. PLoS genetics. 2013;9(8):e1003709.
30. Tsai EA, Berman MA, Conlin LK, et al. PECONPI: a novel software for uncovering pathogenic copy number variations in non-syndromic sensorineural hearing loss and other genetically heterogeneous disorders. American journal of medical genetics. Part A. Sep 2013;161A(9):2134-2147.
31. Bademci G, Diaz-Horta O, Guo S, et al. Identification of copy number variants through whole-exome sequencing in autosomal recessive nonsyndromic hearing loss. Genetic testing and molecular biomarkers. Sep 2014;18(9):658-661.
32. Bademci G, Foster J, 2nd, Mahdieh N, et al. Comprehensive analysis via exome sequencing uncovers genetic etiology in autosomal recessive nonsyndromic deafness in a large multiethnic cohort. Genetics in medicine : official journal of the American College of Medical Genetics. Jul 30 2015.
33. Suzuki H, Oshima A, Tsukamoto K, et al. Clinical characteristics and genotype-phenotype correlation of hearing loss patients with SLC26A4 mutations. Acta oto-laryngologica. Dec 2007;127(12):1292-1297.
34. Shearer AE, Black-Ziegelbein EA, Hildebrand MS, et al. Advancing genetic testing for deafness with genomic technology. Journal of medical genetics. Sep 2013;50(9):627-634.
35. Absalan F, Ronaghi M. Molecular inversion probe assay. Methods in molecular biology. 2007;396:315-330.
36. de Vree PJ, de Wit E, Yilmaz M, et al. Targeted sequencing by proximity ligation for comprehensive variant detection and local haplotyping. Nature biotechnology. Oct 2014;32(10):1019-1025.

SUPPLEMENTAL TABLES

Table S1. Additional phenotype and single gene test information regarding patients with causative variants indicated in Table 1.

Patient	Phenotype	Previous single gene tests	Gene	Variant 1	Variant 2	Segregating with HL
AD1[1]	MF/prog.	*TECTA, COL11A2, POU4F3*	*MYO6* NM_004999.3	c.1546+1G>T (p.?)	-	Yes
AD2	HI and optical atrophy	*WFS1, OPA1*	*WFS1* NM_006005.3	c.2051C>T (p.(Ala684Val))[2]	-	ND
AD3	NS	-	*TECTA* ENST00000392793.1	c.6002G>T (p.(Cys2001Phe))	-	Yes
AD4	cong./HF/ profound	*GJB2/GJB6*	*MYO7A* NM_000260.3	c.1373A>T(p.(Asn458Ile))[3]	-	Yes
AD5[1]	HF with a dip at 4kHz/mixed HI	*KCNQ4, WFS1, COL11A2, ACTG1, DFNA5*	*MYO6* NM_004999.3	c.1211del (p.(Gly404Glufs*4))	-	Yes
AD6[1]	HF/prog.	*KCNQ4*	*MYH9* NM_002473.4	c.2507C>T (p.(Pro836Leu))	-	Yes
AD7	young age/ MF with dip at 4kHz	*TECTA, COL11A2*	*POU4F3* NM_002700.2	c.828_829insT (p.(Lys277*))	-	ND
AD8	LF+MF/severe/ prog.	*COCH, MYO6*	*MYO7A* NM_000260.3	c.652G>A (p.(Asp218Asn))	-	Yes
AD9	HF/prog.	*DFNA5, KCNQ4, ACTG1*	*POU4F3* NM_002700.2	c.668T>C (p.(Leu223Pro))[4]	-	ND
AD10	preling./MF	*TECTA, COL11A2*	*MYO6* NM_004999.3	c.3395del (p.(Lys1132Serfs*12))	-	Yes
AD11	cong./flat	-	*SOX10* NM_006941.3	c.1195C>T (p.(Gln399*))	-	ND
AD12	moderate/LF/ bowlshaped	*COL11A2, WFS1, TECTA*	*MYH14* NM_001145809.1	c.394G>A (p.(Gly32Ser))	-	Yes
AR1[1]	Usher type 2	*USH2A, RP-R*	*USH2A* NM_206933.2	c.9372-?_9570+? (p.?)	c.9372-?_9570+? (p.?)	ND
AR2	Cong./ moderate/ flat	*GJB2/GJB6, SLC26A*	*OTOA* ENST00000388958	chr16:21581229-21771715[5]	chr16:21581229-21771715[5]	
AR3[6]	cong./profound	*GJB2/GJB6, Asper array*	*CIB2* NM_006383.2	c.97C>T (p.(Arg33*))	c.196C>T (p.(Arg66Trp))	Yes
AR4	HF/prog.	*COCH, KCNQ4, WFS1, GJB2/ GJB6*	*STRC* NM_153700.2	c.-78-?_5327+?del(p.0?)[7]	c.-78-?_5327+?del(p.0?)[7]	Yes
AR5	cong./HF/ severe/asym. mixed	*GJB2/GJB6, SLC26A4, OTOF*	*USH2A* NM_206933.2	c.8846-?_9371+?del(p.?)	c.8846-?_9371+?del(p.?)	ND
AR6	cong./severe	*GJB2/GJB6, TMPRSS3*	*TMC1* NM_138691.2	c.646del (p.(Leu216Serfs*54))	c.790C>T (p.(Arg264*))	ND
AR7	cong./severe	*GJB2/GJB6*	*CDH23* NM_022124.5	c.6442G>A (p.(Asp2148Asn))[8]	c.1545_1547del (p.(Ile515del))[8]	Yes
AR8	11y.o./HF/RP	-	*USH2A* NM_206933.2	c.1606T>C (p.(Cys536Arg))[9]	c.9815C>T (p.(Pro3272Leu))[9]	Yes
AR9	HF/moderate	-	*GJB2* NM_004004.5	c.35del (p.(Gly12Valfs*2))[10]	c.71G>A (p.Trp24*))[11]	ND
AR10	NS	-	*GJB2* NM_004004.5	c.35del (p.(Gly12Valfs*2))[10]	c.35del (p.(Gly12Valfs*2))[10]	Yes
AR11	profound	*GJB2/GJB6*	*CDH23* NM_022124.5	c.2096A>G (p.(Asp699Gly))	c.4564A>G (p.(Asn1521Ser))	Yes

AR12	cong.	-	*GJB2* NM_004004.5	c.-23+1G>A (p.?)[12]	c.35del (p.(Gly12Valfs*2))[10]	Yes
AR13	cong./HF	-	*MYO7A* NM_000260.3	c.3289C>T(p.(Gln1097*))	c.3862G>C(p.(Ala1288Pro))[13] c.5227C>T(p.(Arg1743Trp))[14]	ND
AR14	4 y.o/ HF/ moderate	*GJB2/GJB6*	*STRC* NM_153700.2	c.-78-?_5327+?del(p.0?)	c.-78-?_5327+?del(p.0?)	ND
AR15	cong.	*GJB2/GJB6*	*MITF* NM_000248.3	c.649del (p.(Arg217Aspfs*4))[15]	-	ND
AR16	cong.	*GJB2/GJB6*	*PCDH15* NM_033056.3	c.3374-2A>G (r.?)	c.4127C>A (p.(Ala1376Asp))	Yes
AR17	HF	-	*STRC* NM_153700.2	c.-78-?_5327+?del(p.0?) [7]	c.-78-?_5327+?del(p.0?) [7]	ND
AR18	cong./ MF/ moderate	*GJB2/GJB6, SLC26A4*	*STRC* NM_153700.2	c.-78-?_5327+?del(p.0?) [7]	c.-78-?_5327+?del(p.0?) [7]	ND
ISO1[1]	HF/prog. with RP	*GJB2/GJB6, TMPRSS3*	*MYO15A* NM_016239.3	c.625G>T (p.(Glu209*))	c.1137del (p.(Tyr380Metfs*64))[16]	ND
ISO2[1]	cong./ HF/ severe/discant	*GJB2/GJB6, TMPRSS3*	*USH2A* NM_206933.2	c.5385T>A (p.(Tyr1795*))	c.6850_6851insAATC (p.(His2284Glnfs*48))	ND
ISO3	Usher syndrome	*GJB2/GJB6, CDH23, MYO7A, USH1C, SANS, UH2A, VLGR1, USH3A*	*CDH23* NM_022124.5	c.8480_8481del (p.(Leu2827Hisfs*23))	c.8480_8481del (p.(Leu2827Hisfs*23))	ND
ISO4[1]	cong./severe/ prog.	*GJB2/GJB6*	*MYO15A* NM_016239.3	c.6764+2T>A (p.?)	c.3844C>T (p.(Arg1282Trp); c.5287C>T (p.(Arg1763Trp))	Yes
ISO5	HF/bowlshaped	-	*GJB2* NM_004004.5	c.101T>C (p.(Met34Thr))[17]	c.109G>A (p.(Val37Ile)) [17]	Yes
ISO6	cong./profound/ prog./optical atrophy	*GJB2/GJB6, MITF*	*WFS1* NM_006005.3	c.2051C>T (p.(Ala684Val))2	-	ND
ISO7	cong./severe	*GJB2/GJB6, MYO7A,KCNE1, KCNQ1, PTPRQ*	*MYO15A* NM_016239.3	c.6787G>A (p.(Gly2263Ser))	c.7893+1G>A (p.?)	Yes
ISO8	HF/prog.	*COL11A2, EYA, TECTA*	*TRIOBP* NM_001039141.2	c.2653del (p.(Arg885Alafs*120))	c.5014G>T (p.(Gly1672*))	Yes
ISO9	cong./flat	*GJB2/GJB6*	*USH2A* NM_206933.2	c.2299del (p.(Glu767Serfs*21))	c.920_923dup (p.(His308Glnfs*16))	Yes
ISO10	HF/mild/prog./ night blindness	*GJB2/GJB6, TMPRSS3, TMC1*	*MYO7A* NM_000260.3	c.3476G>T (p.(Gly1159Val))[18]	c.5560G>A (p.Val1854Met))[19]	Yes
ISO11	cong.	-	*GJB2* NM_004004.5	c.250G>C (p.(Val84Leu))	c.269T>C (p.(Leu90Pro))[20]	Yes
ISO12	LF/prog.	-	*GJB2* NM_004004.5	c.109G>A (p.(Val37Ile))[17]	c.109G>A (p.(Val37Ile)) [17]	ND
ISO13	second decade/ HF/prog.	-	*TMPRSS3* NM_024022.2	c.916G>A (p.(Ala306Thr))[21]	c.1276G>A (p.(Ala426Thr))[22]	ND
ISO14	cong./ MF/ moderate	*GJB2/GJB6*	*STRC* NM_153700.2	c.-78-?_5327+?del(p.0?)[7]	c.-78-?_5327+?del(p.0?)[7]	ND
ISO15	MF	-	*GJB2* NM_004004.5	c.35del (p.(Gly12Valfs*2))[10]	c.101T>C (p.(Met34Thr))[17]	Yes
ISO16	cong./HF/ profound/ID	-	*ACTG1* NM_00199954.1	c.773C>T (p.(Pro258Leu))	-	ND
ISO17	cong./profound	-	*GJB2* NM_004004.5	c.35del (p.(Gly12Valfs*2))[10]	c.508_511dup (p.Ala171Glufs*40))[23]	ND

ISO18	cong./MF+HF/ severe/prog.	*GJB2/GJB6*	*MYO15A* NM_016239.3	c.3311dup (p.(Glu1105*))	c.3311dup (p.(Glu1105*))	ND
ISO19	cong./severe	-	*TRIOBP* NM_001039141.2	c.3460_3461del (p.(Leu1154Alafs*29))	c.3232dup (p.(Arg1078Profs*6))[24]	ND
ISO20	HF/moderate/ prog./asym./ heterochromia iridis	*GJB2/GJB6, TMPRSS3, MITF, PAX3*	*MYO7A* NM_000260.3	c.5618G>A (p.(Arg1873Gln))[25]	c.6028G>A (p.(Asp2010Asn))[26]	Yes
ISO21	5 y.o./ moderate/prog.	*GJB2/GJB6, TECTA, OTOF, MYO15A, TMC1*	*MYO6* NM_004999.3	c.3610C>T (p.(Arg1204Trp))[27]	-	ND
ISO22	cong./ HF/ moderate	*GJB2/GJB6, SLC26A4*	*SLC26A5* NM_198999.2	c.355C>T (p.(Pro119Ser))	c.355C>T (p.(Pro119Ser))	ND
ISO23	6 y.o./HF/prog.	-	*GJB2* NM_004004.5	c.101T>C (p.(Met34Thr))[17]	c.109G>A (p.(Val37Ile))[17]	ND
ISO24	cong./severe/ flat	-	*SOX10* NM_006941.3	c.482G>A (p.(Arg161His))[28]	-	ND
ISO25	39 y.o./ MF+HF/ moderate/ prog.	-	*STRC* NM_153700.2	c.-78-?_5327+?del(p.0?)[7]	c.-78-?_5327+?del(p.0?)[7]	ND
ISO26	HF/ moderate-severe	*GJB2/GJB6, SLC26A, Asper array*	*MYO6* NM_004999.3	c.3335A>G (p.(Tyr1112Cys))	c.1897del(p.(Gln633Lysfs*19))	Yes
ISO27	cong./severe/ vestibular areflexia	*GJB2/GJB6, USH2A, MYO7A, PTPRQ*	*LARS2* NM_015340.3	c.683G>A (p.(Arg228His))	c.880G>A (p.(Glu294Lys))	Yes
ISO28	HF/severe	-	*OTOA* ENST00000388958	chr16:21581229-21771715[5]	chr16:21581229-21771715[5]	

AR, autosomal recessive; AD, autosomal dominant; ISO, isolated; Cong., congenital; LF, low frequencies; MF, mid frequencies; HF, high frequencies; prog., progressive; preling., prelingual; asym., asymmetric;y.o., years old; UHI, unilateral hearing impairment;ID, intellectual disability; ND, not done; NS, not specified.

Table S2. Diagnostics rates of WES based on the type of inheritance of the HI.

		Causative variant(s)		'Uncertain' variant		No variant	
Categories	**# total**	**# cases**	**%**	**# cases**	**%**	**# cases**	**%**
arHI	33	18.0	54.5	3.0	9.1	12.0	36.4
adHI	65	12.0	18.5	11.0	16.9	42.0	64.6
Isolated HI	101	28.0	27.7	11.0	10.9	62.0	61.4
Xlinked-HI	1	0.0	0.0	1.0	100.0	0.0	0.0
Total	200	58.0	29.0	26.0	13.0	116.0	58.0

Table S3. Information on inheritance pattern, phenotype pretested genes and of HI patients with variants of unknown significance identified by WES.

Patient	Phenotype	Previous single gene tests	Gene	Variant 1	Variant 2	Segregating with HL
AD13	HF/prog.	*POU4F3, MYO6*	*MYO7A* NM_000260.4	c.6122T>A (p.(Ile2041Asn))	-	ND
AD14	12y.o./ moderate/prog./ vest.	*COCH*	*SIX1* NM_005982.3	c.58G>C (p.(Val20Leu))	-	ND
AD15	UHI	*PAX3, MITF*	*MYO6* NM_004999.3	c.271G>A (p.(Ala91Thr))	-	ND
AD16	HF/prog.	*MYO6*	*MYO7A* NM_000260.3	c.2617C>T (p.(Arg873Trp))[25]		
-	No					
AD17	cong./ HF/ moderate	*GJB2, GJB6, KCNQ4*	*TECTA* ENST00000392793.1	c.5794A>C (p.(Thr1932Pro))	-	ND
AD18	cong./mild/flat	-	*MYH14* NM_001145809.1	c.5176C>T (p.(Arg1726Trp))	-	ND
AD19	35 y.o./prog./ flat	*EYA4, COL11A2, TECTA*	*COL11A1* NM_001854.3 TECTA ENST00000392793.1	COL11A1:c.2799del (p.(Gly934Alafs*48))	TECTA: c.2128G>A(p.(Glu710Lys))	ND
AD20	MF+flat/prog.	*EYA4, TECTA, COLL11A2*	WFS1 NM_006005.3	c.941G>T (p.(Trp314Leu))	-	ND
AD21[1]	mid-life/ prog./Stickler syndrome	*TECTA, ACTG1, POU4F3, COL11A2*	*COL11A1* NM_001854.3	c.1630-2del (p.?)	-	Yes
AD22	LF/Turner syndrome	*WFS1, DIAPH1*	*ESPN* NM_031475.2	c.2239G>A (p.(Gly747Ser))	-	ND
AD23	childhood/MF/ prog.	-	*WFS1* NM_006005.3	c.2032T>C (p.(Trp678Arg))	-	Yes
AR19	cong./severe	*GJB2/GJB6, USH2A*	*LOXHD1* NM_144612.6	c.1618dup (p.(Thr540Asnfs*24))	c.1730T>G (p.(Leu577Arg))	Yes
AR20	severe/flat	*GJB2/GJB6, SLC26A4*	*USH2A* NM_206933.2	c.1772A>G (p.(Asp591Gly))	c.5018T>C (p.(Leu1673Pro))	Yes
AR21	moderate	-	*USH2A* NM_206933.2	c.5018T>C (p.(Leu1673Pro)) c.7871C>T (p.(Pro2624Leu))	c.2299del (p.(Glu767Serfs*21))	Yes
ISO29	cong./ moderate/flat	-	*LOXHD1* NM_144612.6	c.3061+1G>A (p.?)	c.6353G>A (p.(Gly2118Glu))	ND
ISO30	5y.o./ MF/ moderate/ asym.	-	*MYO6* NM_004999.3	c.584C>A (p.(Ala195Glu))	-	ND
ISO31	cong./profound	-	*SLC26A4* NM_000441.1 USH1G NM_173477.4	SLC26A4:c.505del (p.(Thr169Leufs*3)) ; USH1G: c.83C>T (p.(Pro28Leu))	SLC26A4:c.1334T>G (p.(Leu445Trp))[29];USH1G: c.1258C>G (p.(Leu420Val))	Yes
ISO32	MF/moderate	-	*TECTA* ENST00000392793.1	c.5818G>A (p.(Ala1940Thr))	-	ND
ISO33	MF+HF/prog.	*GJB2/GJB6, TECTA*	*MYO7A* NM_000260.3	c.1846C>T (p.(Arg616Trp))	-	ND

ISO34	cong./ HF/ moderate	-	*TECTA* ENST00000392793.1	c.5597C>T(p.(Thr1866Met))[30]	-	ND
ISO35	preling./prog.	*GJB2/GJB6, TMPRSS3*	*LOXHD1* NM_144612.6	c.3061C>T (p.(Arg1021*))	c.5885C>T (p.(Thr1962Met))	Yes
ISO36	asym.	*GJB2/GJB6*	*OTOGL* NM_173591.3	c.2533T>C (p.(Phe845Leu))	c.4833G>A (p.?)	ND
ISO37	Asperger syndrome	-	*TECTA* ENST00000392793.1	c.2780A>G (p.(His927Arg))	-	ND
ISO38	moderate/prog.	*GJB2/GJB6, MYO6*	*CEACAM16* NM_001039213.3	c.859del (p.(Gln287Argfs*34))	-	ND
ISO39	cong./ asym.	*GJB2/GJB6, TECTA, OTOF, MYO15A, TMC1*	*SLC26A4* NM_000441.1	c.1246A>C(p.(Thr416Pro))	-	ND
XL1[1]	Prog./flat	*GJB2/GJB6, KCNQ4, TMPRSS3*	*SMPX* NM_014332.2	c.132G>A (p.?)	-	ND

AR, autosomal recessive; AD, autosomal dominant; ISO, isolated; Cong., congenital; LF, low frequencies; MF, mid frequencies; HF, high frequencies; prog., progressive; preling., prelingual; asym., asymmetric;y.o., years old; UHI, unilateral hearing impairment; ID, intellectual disability; ND, not done; vest. , vestibular complains.

Table S4. Overview of the *MYO15A* mutations identified in Dutch HI patients in the present study.

Family	Analysis*	Allele 1 (cDNA)*	Allele 1 (Protein)	Allele 2 (cDNA)#	Allele 2 (Protein)
1	A	c.1137delC	p.Thr380MetfsX64	c.6787G>A	p.Gly2263Ser
2	A	c.1137delC	p.Thr380MetfsX64	c.4519C>T	p.Arg1570X
3	A	c.3963A>C	p.Lys1321Asn	c.6764+2T>A	p.?
4	A	c.4497G>T	p.Glu1499Asp	c.5506delC	p.Leu1836CysfsX13
5	A	c.6205C>T	p.Pro2069Ser	c.6764+2T>A	p.?
6	B	c.1137delC	p.Thr380MetfsX64	c.10216+1G>A	p.?
7	B	c.1137delC	p.Thr380MetfsX64	c.6764+2T>A	p.?
8	B	c.6787G>A	p.Gly2263Ser	c.6787G>A	p.Gly2263Ser

* A) shared genotype B) DFNB panel# As a reference sequence NM_016239.3 was used.

REFERENCES

1. Neveling K, Feenstra I, Gilissen C, et al. A post-hoc comparison of the utility of sanger sequencing and exome sequencing for the diagnosis of heterogeneous diseases. Human mutation. Dec 2013;34(12):1721-1726.
2. Rendtorff ND, Lodahl M, Boulahbel H, et al. Identification of p.A684V missense mutation in the WFS1 gene as a frequent cause of autosomal dominant optic atrophy and hearing impairment. American journal of medical genetics. Part A. Jun 2011;155A(6):1298-1313.
3. Luijendijk MW, Van Wijk E, Bischoff AM, et al. Identification and molecular modelling of a mutation in the motor head domain of myosin VIIA in a family with autosomal dominant hearing impairment (DFNA11). Human genetics. Jul 2004;115(2):149-156.
4. Collin RW, Chellappa R, Pauw RJ, et al. Missense mutations in POU4F3 cause autosomal dominant hearing impairment DFNA15 and affect subcellular localization and DNA binding. Human mutation. Apr 2008;29(4):545-554.
5. Bademci G, Diaz-Horta O, Guo S, et al. Identification of copy number variants through whole-exome sequencing in autosomal recessive nonsyndromic hearing loss. Genetic testing and molecular biomarkers. Sep 2014;18(9):658-661.
6. Seco CZ, Giese AP, Shafique S, et al. Novel and recurrent CIB2 variants, associated with nonsyndromic deafness, do not affect calcium buffering and localization in hair cells. European journal of human genetics : EJHG. Jul 15 2015.
7. Verpy E, Masmoudi S, Zwaenepoel I, et al. Mutations in a new gene encoding a protein of the hair bundle cause non-syndromic deafness at the DFNB16 locus. Nature genetics. Nov 2001;29(3):345-349.
8. Astuto LM, Bork JM, Weston MD, et al. CDH23 mutation and phenotype heterogeneity: a profile of 107 diverse families with Usher syndrome and nonsyndromic deafness. American journal of human genetics. Aug 2002;71(2):262-275.
9. Dreyer B, Tranebjaerg L, Rosenberg T, Weston MD, Kimberling WJ, Nilssen O. Identification of novel USH2A mutations: implications for the structure of USH2A protein. European journal of human genetics : EJHG. Jul 2000;8(7):500-506.
10. Zelante L, Gasparini P, Estivill X, et al. Connexin26 mutations associated with the most common form of non-syndromic neurosensory autosomal recessive deafness (DFNB1) in Mediterraneans. Human molecular genetics. Sep 1997;6(9):1605-1609.
11. Rehman AU, Santos-Cortez RL, Drummond MC, et al. Challenges and solutions for gene identification in the presence of familial locus heterogeneity. European journal of human genetics : EJHG. Dec 10 2014.
12. Denoyelle F, Marlin S, Weil D, et al. Clinical features of the prevalent form of childhood deafness, DFNB1, due to a connexin-26 gene defect: implications for genetic counselling. Lancet. Apr 17 1999;353(9161):1298-1303.

13. Bharadwaj AK, Kasztejna JP, Huq S, Berson EL, Dryja TP. Evaluation of the myosin VIIA gene and visual function in patients with Usher syndrome type I. Experimental eye research. Aug 2000;71(2):173-181.
14. Pennings RJ, Huygen PL, Orten DJ, et al. Evaluation of visual impairment in Usher syndrome 1b and Usher syndrome 2a. Acta ophthalmologica Scandinavica. Apr 2004;82(2):131-139.
15. Tassabehji M, Newton VE, Liu XZ, et al. The mutational spectrum in Waardenburg syndrome. Human molecular genetics. Nov 1995;4(11):2131-2137.
16. Vona B, Muller T, Nanda I, et al. Targeted next-generation sequencing of deafness genes in hearing-impaired individuals uncovers informative mutations. Genetics in medicine : official journal of the American College of Medical Genetics. Dec 2014;16(12):945-953.
17. Hoefsloot LH, Feenstra I, Kunst HP, Kremer H. Genotype phenotype correlations for hearing impairment: approaches to management. Clinical genetics. Jun 2014;85(6):514-523.
18. Roux AF, Faugere V, Vache C, et al. Four-year follow-up of diagnostic service in USH1 patients. Investigative ophthalmology & visual science. Jun 2011;52(7):4063-4071.
19. Neveling K, Collin RW, Gilissen C, et al. Next-generation genetic testing for retinitis pigmentosa. Human mutation. Jun 2012;33(6):963-972.
20. Batissoco AC, Abreu-Silva RS, Braga MC, et al. Prevalence of GJB2 (connexin-26) and GJB6 (connexin-30) mutations in a cohort of 300 Brazilian hearing-impaired individuals: implications for diagnosis and genetic counseling. Ear and hearing. Feb 2009;30(1):1-7.
21. Elbracht M, Senderek J, Eggermann T, et al. Autosomal recessive postlingual hearing loss (DFNB8): compound heterozygosity for two novel TMPRSS3 mutations in German siblings. Journal of medical genetics. Jun 2007;44(6):e81.
22. Weegerink NJ, Schraders M, Oostrik J, et al. Genotype-phenotype correlation in DFNB8/10 families with TMPRSS3 mutations. Journal of the Association for Research in Otolaryngology : JARO. Dec 2011;12(6):753-766.
23. Wu BL, Lindeman N, Lip V, et al. Effectiveness of sequencing connexin 26 (GJB2) in cases of familial or sporadic childhood deafness referred for molecular diagnostic testing. Genetics in medicine : official journal of the American College of Medical Genetics. Jul-Aug 2002;4(4):279-288.
24. Riazuddin S, Khan SN, Ahmed ZM, et al. Mutations in TRIOBP, which encodes a putative cytoskeletal-organizing protein, are associated with nonsyndromic recessive deafness. American journal of human genetics. Jan 2006;78(1):137-143.
25. Roux AF, Faugere V, Le Guedard S, et al. Survey of the frequency of USH1 gene mutations in a cohort of Usher patients shows the importance of cadherin 23 and protocadherin 15 genes and establishes a detection rate of above 90%. Journal of medical genetics. Sep 2006;43(9):763-768.

26. Jacobson SG, Aleman TS, Sumaroka A, et al. Disease boundaries in the retina of patients with Usher syndrome caused by MYO7A gene mutations. Investigative ophthalmology & visual science. Apr 2009;50(4):1886-1894.
27. Oonk AM, Leijendeckers JM, Lammers EM, et al. Progressive hereditary hearing impairment caused by a MYO6 mutation resembles presbyacusis. Hearing research. May 2013;299:88-98.
28. Chaoui A, Watanabe Y, Touraine R, et al. Identification and functional analysis of SOX10 missense mutations in different subtypes of Waardenburg syndrome. Human mutation. Dec 2011;32(12):1436-1449.
29. Van Hauwe P, Everett LA, Coucke P, et al. Two frequent missense mutations in Pendred syndrome. Human molecular genetics. Jul 1998;7(7):1099-1104.
30. Brownstein Z, Friedman LM, Shahin H, et al. Targeted genomic capture and massively parallel sequencing to identify genes for hereditary hearing loss in Middle Eastern families. Genome biology. 2011;12(9):R89.

Chapter 8

General discussion

FUNCTIONS OF PROTEINS ENCODED BY NOVEL DEAFNESS GENES

The research described in this thesis has led to the discovery of novel deafness genes that, when mutated, cause hearing impairment (HI) which is the most common sensory disorder worldwide.[47]

In chapters 2 and 3, two novel genes involved in autosomal recessive non-syndromic HI (arNSHI) are reported. *OTOGL* encodes a member of the group of non-collageneous glycoproteins which, together with collagens, form the three acellular membranes of the inner ear: the tectorial membrane, the otoconial membrane and the cupula.[2] These acellular membranes are inertial masses against which the stereocilia of the sensory epithelia in the organ of Corti and in the vestibular system can deflect.[48] As a consequence, mechanotransduction occurs resulting in depolarization of hair cells. To date, the precise functions of the otoconial membrane and the cupula are still under investigation. However, the function of the tectorial membrane has been well studied in mice with mutations in tectorial membrane proteins.[49] These studies revealed that the tectorial membrane has an important role in the tuning properties and sensitivity of the cochlea due to the tectorial membrane longitudinal stiffness gradients.[49] These gradients are determined by the density of collagens and non-collageneous glycoproteins. Among the latter, we find α-tectorin (TECTA), β-tectorin (TECTB), otogelin (OTOG), CEACAM16 and, as previously indicated, otogelin-like (OTOGL).[2,50-53] Recessively inherited mutations in *TECTA* (DFNB21), *OTOG* (DFNB84B) and *OTOGL* (DFNB18B) (Chapter 2) result in a recognizable phenotype of non-progressive mid-frequency HI.[2,51,54] TECTA, OTOG and OTOGL share a similar protein structure with a stretch of von Willebrand (VW) factor and cysteine rich domains (C8) as seen in Figure 1. OTOG and OTOGL lack the zona pellucida (ZP) domain present in TECTB and TECTA (Figure 1). It has been proposed that the ZP domain is a protein polymerization module that may enable TECTA and TECTB to form homo and heteropolymers.[49,55] Therefore, *TECTB* could be considered as a candidate gene for mid-frequency HI as well, even though *Tectb*$^{-/-}$ mice display low-frequency HI.[56]

CEACAM16 is a cell-adhesion protein that is predicted to contain four immunoglobulin domains (Figure 1).[57] CEACAM16 interacts with TECTA at the tectorial membrane-attached crown which connects stereocilia of outer hair cells with the tectorial membrane.[57] Mutations in *CEACAM16*, as specific mutations in *TECTA* (DFNA8/12), cause postlingual adNSHI.[52,54]

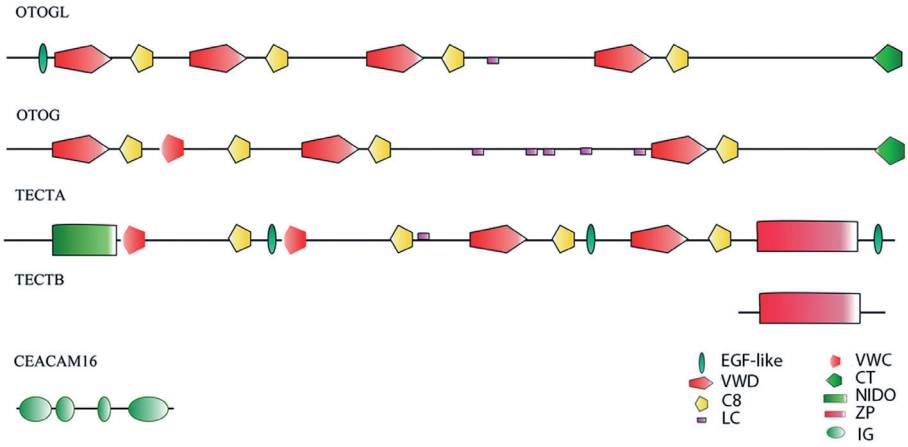

Figure 1. Structural comparison between OTOGL, OTOG, TECTA, TECTB and CEACAM16, the non-collageneous proteins present in the tectorial membrane. The architecture of these proteins was modeled using SMART (http://smart.embl-heidelberg.de/). VWD, von Willebrand factor type D; VWC, von Willebrand factor type C; C8, cysteine rich domain; NIDO, extracelullar domain of unknown function in nidogen; EGF-like, epidermal growth factor like; LC, low complexity; IG, immunoglobulin; CT: C terminal; ZP, zona pellucida.

As presented in chapter 3, a homozygous nonsense mutation in *CLIC5* is the underlying cause of the progressive HI accompanied by vestibular areflexia in two siblings of Turkish origin. The oldest sibling also presented an elevated albumin/creatinine ratio in urine and pre-hypertension which could be the first signs of a nephropathy. The proteinuria, progressive HI and vestibular areflexia phenotypes are all recapitulated in the *Clic5* mutant mouse (*jitterbug*).[58,59] *CLIC5* encodes the chloride intracellular channel 5 protein. However, as discussed in chapter 3, there are many lines of evidence supporting that CLIC5 could have a critical role in stereocilia integrity due to its role in the stabilization of actin filaments rather than in chloride homeostasis.[1,58-60] Therefore, we categorized CLIC5 as a cytoskeleton-associated protein involved in stereocilia morphogenesis.

In chapter 4 mutations in *CIB2*, a gene known to be involved in Usher syndrome 1J and DFNB48[61] were functionally studied. CIB2 belongs to the family of calcium- and integrin- binding proteins. CIB2 contains three predicted EF hand domains of which the two N-terminal ones are predicted to bind calcium. All CIB2 mutations described to date, except for p.Ile123Thr that is located in EF hand 2, are hypothesized to affect the interaction with αIIβ integrin (Table 1).[61]

It was previously suggested that destabilization of the interaction with αIIβ integrin possibly disturbs the capacity of CIB2 to sequestrate calcium, as a result of changes in subcelullar localization.[61] However, we demonstrated that neither the capacity of CIB2 to release calcium nor the subcellular localization of CIB2 were affected by these mutations (Table 1). As previously reported, p.Glu64Asp is causative for Usher syndrome 1J.[61] In the absence of αIIβ integrin, p.Glu64 and p.Arg33 form a salt bridge. Nonetheless, p.Arg33Ter and p.Glu64Asp cause different phenotypes, arNSHI and Usher syndrome 1J, respectively.[61] Therefore, we suggested in chapter 4 that p.Glu64Asp gained a different function in the retina that eventually led to the development of retinitis pigmentosa. Another possibility that cannot be completely ruled out is that p.Gly64Asp is not underlying the retinal phenotype in the presented Usher syndrome 1J family, whose ID is PKDF117.[61] Ahmed *et al.* (2009) reported linkage to a region harboring *CIB2* in family PKDF117.[62] However, the VNTR markers flanking *CIB2*, D15S973 and D15S1027, were not fully informative and an unaffected individual carried the affected haplotype (V:13). Later, Riazuddin *et al.* (2012) reported the *CIB2* p.Glu64Asp mutation underlying Usher syndrome 1J in the PKDF117 family. In this study, segregation analysis of the *CIB2* p.Glu64Asp variant and whole exome sequencing (WES) in order to exclude other possible genetic causes within the linkage region, which for instance also harbours the *NR2E2* gene that is known to be associated with both dominantly and recessively inherited retinitis pigmentosa,[63] were not performed. These facts cast some doubt on the involvement of *CIB2* in the retinal phenotype of the presented Usher syndrome 1J family.

In chapter 5 we demonstrated that loss of function mutations in *KITLG* are the cause of familial non-syndromic unilateral and asymmetric HI (NS-UHI/AHI). Moreover, we identified a missense mutation in *KITLG*, with a possibly dominant negative or gain of function effect, underlying Waardenburg syndrome type II (WS II). The KITLG-KIT pathway functions in the proliferation, migration and survival of melanoblasts. Therefore mice that are homozygous for the semi-dominant alleles W^v of *Kit* and Sl^d of *Kitl* are important models to study the role of melanocytes in the hearing process.[64,65] Both mouse models displayed HI due to a dysfunctional stria vascularis as a consequence of a lack of melanocytes. It has been postulated that melanocytes are important in the formation/function of the stria vascularis during development and/or that they play a role in the maintenance of the endocochlear potential.[64,65] The localization of the K^+ transporter, NKCC, and the K^+ channel, Kir4.1, located at the apical membrane of intermediate cells (melanocytes) in the stria vascularis[66] supports

Table 1. Known mutations in *CIB2* with their effect on calcium release, subcellular localization and predicted effect on integrin binding. In grey the variants that are part of the work performed in chapter 4 are indicated. "USH1J" superscript indicates that this mutation is described to be causative for Usher syndrome type 1J.[61] The ↑ means up-regulated and the ↓ means down-regulated.

Variants in CIB2	Calcium release	Subcellular localization	Integrin binding
p.Arg66Trp	Not affected	Not affected	Impaired
p.Arg33Ter	Nonsense mediated decay predicted		
p.Phe91Ser	Not affected	Not affected	Impaired
p.Glu64Asp^{Ush1J}	Not affected	Not affected	Impaired
p.Cys99Trp	↑	Not affected	Impaired
p.Ile123Trp	↓	Not affected	Not affected

this assumption. We demonstrated that *KITLG* is a novel gene associated with hypopigmentary and HI disorders due to a deficiency in neural crest cell-derived melanocyte development.[67]

In chapter 6, a nonsense mutation in *FITM2* is reported to be causative of a novel syndromic form of HI which is characterized by sensorineural HI, dystonia and sensory neuropathy. The FITM protein family is conserved throughout the evolutionary lineage down to *Saccharomyces cerevisiae*.[13] FITM2 resides in the endoplasmic reticulum and participates in the partitioning of triacylglycerides into lipid droplets. Despite that FITM2 has a role in lipid droplet formation, lipodystrophy or disturbances of lipid storage and/or metabolism were not found to be part of the phenotype in this Pakistani family. This adds *FITM2* to the group of genes that encode proteins involved in lipid metabolism and neurological function and remarkably FITM2 is the first protein involved in lipid droplet formation whose dysfunction results in HI.[68]

WHOLE EXOME SEQUENCING IN INDIVIDUALS WITH HEARING IMPAIRMENT

Although WES has proven to be successful in the identification of the genetic defects in genetically heterogeneous disorders,[69] the lack of coverage of certain exons/genes and the interpretation of the numerous candidate variants obtained are still a challenge.

Challenges

Challenge 1: prediction of the functional effect of variants

Incorrect classification of genetic variants as being pathogenic or non-pathogenic is a systematic issue in HI as it is in human genetics in general. Due to a shared concern in the exponential increase of rare variants and their interpretation, guidelines for their classification have been formulated.[69,70] In order to categorize a variant as clearly pathogenic, the gold standard is to perform a functional assay that supports its effect. However, this cannot be performed routinely due to the large amount of candidate variants that are identified by WES or whole genome sequencing (WGS) studies. Therefore, different computational tools have been developed to predict the effect of any type of mutation on protein structure or function and/or on transcript processing.

Evaluation of missense variants is especially challenging because most of the currently available prediction tools only model loss of function scenarios. However, missense variants can have dominant negative or gain of function effects. The most popular tools are SIFT,[71] that is exclusively based on sequence conservation, and Polyphen 2,[72] that is built upon sequence conservation but also considers the structural properties of the mutated amino acids. To obtain more accurate evaluations, on-line tools that combine the scores obtained by SIFT and Polyphen 2 and other prediction tools, are available. Some examples are Condel, that also includes Mutation Assessor,[73] and combined annotation-dependent depletion (CADD), that uses an algorithm to assess the pathogenicity of any kind of variation.[74] Additionally, when the crystal structure of a protein or a protein domain has been generated and analysed by nuclear magnetic resonance, modelling the effect of missense variants on protein level can be performed by using on-line tools such as project HOPE (http://www.cmbi.ru.nl/hope), YASARA[75] and WHAT IF Twinset.[76] With these tools, you can assess not only the effect of the variant on protein structure but also its impact on protein function in a certain context, *e.g.* effect on protein-protein interactions, as we showed for the mutations found in *KITLG* (chapter 5).

Effects on splicing, especially when they do not alter the canonical splice site sequences, are also difficult to predict because the mechanisms underlying the regulation of alternative splicing are only partially understood.[77,78] Xiong *et al.* (2015) developed a tool that scores the impact of any kind of variation on splicing.[79] Interestingly many of these variants predicted to alter splicing were located more than 30 nucleotides away from a splice site. Xiong *et al.* (2015) also reported that exonic variation (nonsense, synonymous and missense variants) are able to have an impact on splicing.[79] These observations are very important

because the splicing effect of variants outside the canonical splice site regions is not addressed in guidelines that are routinely used in DNA diagnostics.[69,70]

Truncating mutations do not always result in the production of a truncated protein. As indicated above, nonsense variations can result in effects on splicing, especially when located in in-frame exons, by a process named nonsense-associated altered splicing.[80] Alternatively this type of variants can alter splicing of the mutated exon or splicing of surrounding exons, *e.g.* the c.2299delG in *USH2A* exon 13, which is in-frame, results in a frameshift due to the mutation-induced skipping of exons 12 and 13.[81] When a nonsense mutation is located within the first exon an alternative in-frame start codon can be used, which might give rise to a (partially or fully) functional protein.[82] Methods have been developed to predict whether this could occur.[83] Finally, when a premature stop codon is created in the last 54 bp of the 3'-most intron or in the last exon, nonsense mediated decay might not occur, giving rise to a protein that is partially functional or it might gain other functions that are toxic to cell homeostasis (50-bp rule).[84] Rivas *et al.* (2015), who systematically characterized the effect of truncating variants in the transcriptome of a wide range of tissues, reported that the 50-bp rule has a high predictive value.[85]

An important aspect in the evaluation of variants is their frequency in the general and hearing impaired populations. For HI, Shearer A.E. *et al.* (2014) reported that 4.2% of variants described as being pathogenic turned out to be benign due to a relatively high allele frequency in an extensive control data set from different populations.[86] Besides, finding the same or other mutations in a candidate gene in multiple families with a similar phenotype supports the involvement of a candidate gene in a phenotype, but not unequivocally. This assumption was made in many different studies.[87] However, this association by itself is not decisive in assigning or excluding a candidate gene as a disease-associated gene.[88,89] Evidence from other resources like functional evaluation of the variants by analysing the impact of the variants on protein structure and function or animal models that recapitulate the human phenotype, should be taken into account. To date, over a hundred of genes have been associated with NSHI in humans. For about 10% of these genes, only a variant in a single family is reported to date. For most of these genes, supportive evidence for the pathogenicity of the genetic variant is obtained by *in vitro* cell studies or animal models, as we show in chapter 2 and chapter 6, which are indeed decisive to suggest the involvement of a particular gene in a phenotype when a second family with the same or other mutations in the gene of study is lacking.

In conclusion, evaluation of the large numbers of genetic variants identified by WES and WGS is a challenge. The gold standard would be the functional evaluation of every variant, however this is not feasible. Therefore prediction of the effect of variants on the protein level, their frequencies in disease and control populations and all available information on protein structure and animal models are of critical importance.

Challenge 2: coverage

High quality coverage in WES studies is the most important requirement to reliably identify variants and it is also the main challenge behind the implementation of WES in a diagnostics setting which requires high sensitivity and specificity. Due to these requirements, other approaches that allow full coverage of a subset of genes, like molecular inversion probes (MIPs),[90,91] and targeted locus amplification (TLA),[92] have been developed. In chapter 7, we find that mutations in four genes, *GJB2, STRC, USH2A* and *MYO15A* can explain 30.3% of arHI and 13.9% of sporadic cases with HI; and mutations in *MYO6* explain 7.7% of adHI cases. Therefore, a pre-screening of a subset of genes using a targeted approach in large series of probands with arHL should be considered as a more cost- and time-effective approach than WES and WGS.[91]

FUTURE PERSPECTIVES: WHOLE GENOME SEQUENCING AND TRANSCRIPTOMICS

Over a hundred proteins are known to play an essential role in the process of hearing since mutations in the corresponding genes are associated with HI in humans (http://hereditaryhearingloss.org/). In chapter 7, we report that 58% of patients, in whom all known genes involved in HI were evaluated by WES, and in 40% of known DFN loci, a genetic causative variant has not yet been identified. This suggests that, despite the already known large genetic heterogeneity for HI, mutations in additional genes and/or mutations in non-coding regions are likely to underlie HI. Therefore, a step towards WGS and transcriptomics (RNA sequencing) of lymphoblasts or patient-derived pluripotent stem cells (iPSc) can uncover the hidden spectrum of mutations in HI. In Figure 2, I present a diagram of the steps that could be taken to find the genetic cause of HI in suspected hereditary cases. As it is shown, collection of extensive and accurate clinical data and family history is the first step. Excluding environmental factors is essential since their contribution in congenital HI in developed countries is

estimated to be about 50% (chapter 1). Thus, the unknown environmental factors might be partially the reason behind the 61.4% of sporadic cases who remain unsolved in chapter 7. WES of sporadic cases with HI is extremely challenging due to different reasons: 1) the mode of inheritance is unknown, it could be recessive but also dominant with reduced penetrance or there could be a de novo dominant mutation. This implies that different filter protocols in analyzing WES data should be used giving rise to large numbers of candidate variants; 2) there is usually no DNA of other family members available to perform segregation or a trio analysis; therefore, a proper strategy such as pre-screening of a subset of genes relatively frequently involved in HI should be firstly considered. WES of isolated cases might follow when no potential variants are found. Although the availability of WES data of sporadic cases is definitely valuable *e.g.* to look for variants in candidate genes, when the budget is limited collection and WES of families with multiple affected individuals should be a priority.

In families with multiple affected individuals with suspected arNSHI, adNSHI or X-linked HI, WGS should be considered after targeted gene pre-screening and WES. WGS is the most comprehensive genetic test developed to date.[93] The two major advantages of WGS over WES are: 1) WGS can robustly cover the exome because an enrichment step is not required; 2) WGS can identify intronic variants and complex rearrangements such as inversions and translocations.[94] Therefore, in the near future, when the costs of WGS decrease, WGS will definitely substitute WES to explore the exome. Then the WES step in Figure 2 will disappear. WGS can generate more than three million variants per individual. Thus, the analysis and interpretation of how these variants can influence the disease manifestation, especially those in the non-coding sequences which account for 98% of the genome,[95] will require a multiple step strategy. A combined strategy of WGS of multiple affected individuals with other genetic approaches such as linkage analysis or/and homozygosity mapping will already narrow the genomic region(s) of interest. Besides, WGS combined with transcriptomics, specifically with RNA sequencing, can reveal new (intronic) mutations and thus new disease mechanisms. However, only a subset of genes involved in audition are expressed in blood or other accessible tissues *e.g. USH2A* in nasal epithelium or skin fibroblasts.[96,97] Therefore the generation of inner ear epithelium or inner ear hair-like cells from HI patient's skin or blood cells to perform RNA sequencing will be required (Figure 2).

ANIMAL MODELS FOR STUDYING THE DISEASE MECHANISM UNDERLYING HEARING IMPAIRMENT

During the course of this thesis project, several animal models have been employed in order to study the function of proteins of interest in the auditory system. Recapitulation of the human phenotype in these mutant organisms gave us crucial information about the disease mechanism. Although mouse models are most frequently used for studying HI, the generation and maintenance is both cost- and labour- intensive. Therefore the fruit fly and zebrafish are being increasingly used.

In chapter 2, downregulation of *otogl* in zebrafish was induced by using morpholinos. In chapters 3 and 5, evidence from mutant mouse models supported the involvement of *CLIC5* and *KITLG* in HI. In chapter 6, conditional gene ablation via RNAi of *Fitm* in *Drosophila melanogaster* could recapitulate the human phenotype.

Mus musculus - mouse model

The homology between the mouse and the human genome is about 80%.[98] Many HI genes were identified in mutant mice before mutations in those genes were detected in humans.[99] Many molecular pathways are conserved and a remarkable structural similarity between the human and mouse auditory systems has been reported.[99] The human inner ear is located in the temporal bone and is therefore highly inaccessible. Mouse models allow histopathological and ultrastructural analyses of the inner ear tissues as well as electrophysiological measurements that can give more insight into the nature of the HI. Different from *Danio rerio* and *Drosophila melanogaster*, which do not have a cochlea *per se*, mice preserve independent organs for hearing, the cochlea, and equilibrium, the vestibular system. This allows the molecular study of both organs separately and also the investigation of structures specific to mammals, *e.g.* the tectorial membrane.[100] The results of these studies also contribute to the knowledge of inner ear biology in mammals.

Danio rerio - zebrafish model

The zebrafish (*Danio rerio*) is an extensively used animal model in hearing research. Zebrafish do not have a cochlea as mammals do. In contrast, larval zebrafish have two otolith organs, the utricle and the saccule, that process both auditory and vestibular stimuli.[101] Behavioral studies in fish models lacking either otolith organ revealed that the saccule is important for sound perception

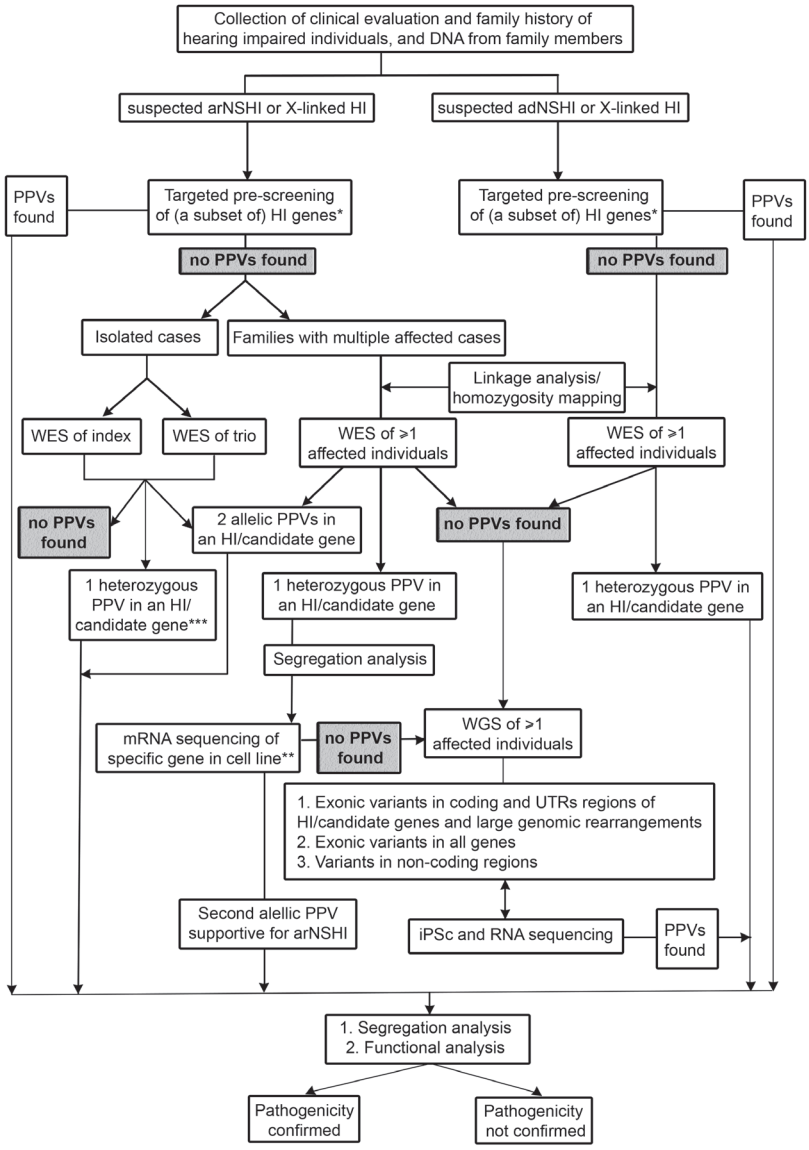

Figure 2. Flowchart of the proposed steps that could be taken in order to find the genetic causes underlying HI (keeping in mind that WGS is still developing and costly). PPV means potentially pathogenic variant. The * indicates that PPVs in a subset of genes, as suggested in chapter 7, should be excluded before WES is performed. The ** indicates that mRNA of the gene in which a heterozygous PPV was found should be isolated from a stable cell line derived from patient tissue in order to seek for the second PPV required in arHI. The *** indicates that when parents are available a trio analysis should be considered to look for heterozygous *de novo* PPVs.

and the utricle for the equilibrium (Figure 3).[102,103] Another macular organ, the lagena, is present in juvenile stage[104] (Figure 3). As it is shown in Figure 3, the otolith organs harbor hair cells, the ultimate sensory receptors with stereocilia on the apical surface which are embedded in a matrix, the otolith membrane.[105] After a sound or movement stimulus, the otolith organs are displaced relative to the hair cells due to the difference in inertia between them. This displacement evokes the opening of the mechanotranduction channels upon hair bundle deflection. The resulting depolarization of the hair cells initiates the release of neurotransmitters at the basal part of the cells.[34]

In addition to the two otolith organs, zebrafish also have a sensory system with hair cells on the surface called the lateral line. The lateral line organ consists of interconnected neuromasts and allows the detection of low frequency waves such as those made by water movements (Figure 3).[104]

Due to the evolutionary conservation of the auditory process from zebrafish to humans, zebrafish is a suitable model to study human genes involved in HI. The main advantages of using zebrafish in HI research are:

1. Adult zebrafish produce lots of offspring on a weekly basis, facilitating large scale experiments.
2. Eggs are fertilized *ex vivo* and therefore all embryonic developmental stages can be studied easily.
3. Embryos are optically transparent thus different embryonic stages can be followed *in vivo*.
4. Zebrafish can easily be manipulated genetically.

Of the human genes 71.4% have at least one zebrafish orthologue. Due to a genome duplication event, approximately 30% of these genes have two zebrafish orthologs and the function of their encoded protein have likely been evolved differently, as is seen for for Kitla and Kitlb.[106-108] Therefore, when zebrafish is used as a model, knockdown of the appropriate duplicate is essential in order to study the right molecular pathway.

Drosophila melanogaster – fruit fly model

Despite the evolutionary distance between *Drosophila* and humans, there are significant genetic and molecular similarities in the auditory system that make the fruit fly a good model organism for studying HI.[31,109] The *Drosophila* antenna consists of three segments: the a1 (antennal segment) or scape, a2 or pedicelus and the a3 or funiculus and a feathery hair-like extension of the a3 segment called arista. The role of the a1 segment in hearing is not well understood yet.

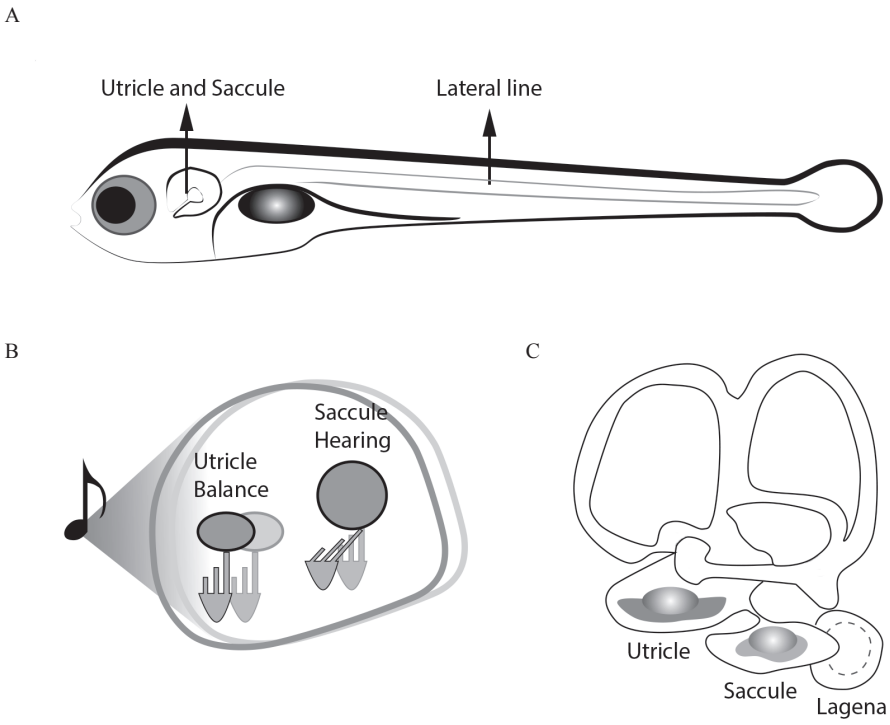

Figure 3. Organs of hearing and equilibrium in larval zebrafish. A. Drawing of a zebrafish larvae indicating the lateral line organ, the utricle and saccule. B. A schematic representation of the saccule and utricle in larval zebrafish. C. Diagram of the adult zebrafish ear in which the utricle, the saccule and the lagena are shown.

Segment a3 and the arista together form the sound receiver. Segment a2 contains the Johnston's organ that serves as a sensor of hearing and orientation. In the Johnston's organ an array of about 250 scolopale cells (also called "chordotonal sensillia") is present which are involved in signal transduction. Each scolopale cell is part of an entity called scalopidium. Each scolopidium is built up by a scolopale cell, a ligament and a cap cell which are in charge of the scolopidium basal and apical attachments, respectively (Figure 4). Besides the scolopidium also contains actin- and microtubule-rich scolopale rods (supporting cells) and ciliated sensory dendrites of two or three mechanosensory neurons (Figure 4).[110,111] A near-field sound causes the deflection of the arista and consequently the rotation of the a2-a3 joint occurs making the scolopidium in the Johnston's organ to stretch (Figure 4). Afterwards, an influx of potassium

occurs into the scolopidium triggering the depolarization of the mechanosensory neurons whose axons aggregate to form the antennal nerve to carry peripheral sound information to the auditory center of the brain (Figure 4).[110,111] The depolarisation of the scolopidium is thus dependent on the potassium ion-rich fluid, the counterpart of the endolymph in humans, that embeds these sensory cells.[112] The molecular details of the mechanotransduction channels involved in this process have not yet been fully elucidated.

Senthilan *et al.* (2012) employed an *ato*-based knockout strategy to compare gene expression profiles in the *Drosophila* Johnston's organ. The *ato* gene encodes the atonal transcription factor. In *Drosophila,* ato is involved in the development of mechanosensitive neurons. In contrast, in vertebrates the *Atoh1* signaling pathway is not involved in the development of sensory neurons but in the development of the inner ear hair cells, the lateral line and the touch-sensitive cells in the skin.[113] Senthilan *et al*. (2012) reported that 89 of the 274 genes expressed in the Johnston's organ genes have vertebrate homologs and some of them are found to be expressed in vertebrate inner ears.[31] Therefore, genes found to be relevant for the auditory function in *Drosophila* are to be considered good candidates for explaining HI in humans.

Finally, using *Drosophila* as a model organism has advantages such as fast generation time, low cost, high conservation of genes and pathways and an excellent genetic toolbox.

IMPACT OF MY RESEARCH ON SOCIETY

The primary aim of my PhD project was the identification of genes involved in HI and to provide insight into the molecular pathways and protein networks important in the process of hearing. The results obtained during my project have a significant impact on society both on the short and long terms. On the short term, the genes identified during my project were immediately translated into patient care in our DNA diagnostics division which is the main reference center for HI in the Netherlands. An enhanced knowledge on genetics, molecular mechanisms and phenotypes will allow a proper genetic diagnosis and subsequent counselling of the patients and their families.[114] In the long term, most of the genetic therapies that are currently being developed have the prerequisite to know the underlying genetic defect. To apply genetic therapies, the HI in the patients should be progressive and starting after birth and not congenital profound suggesting a developmental defect in the auditory system.

A

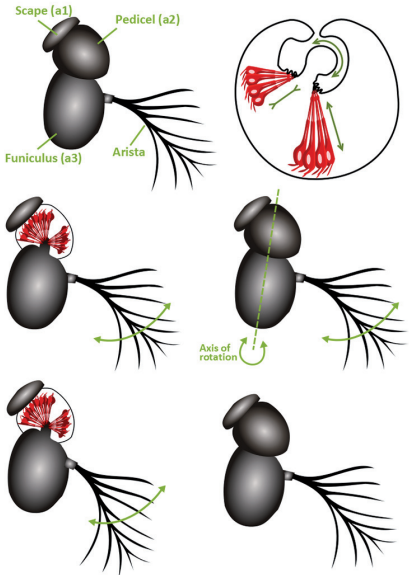

B

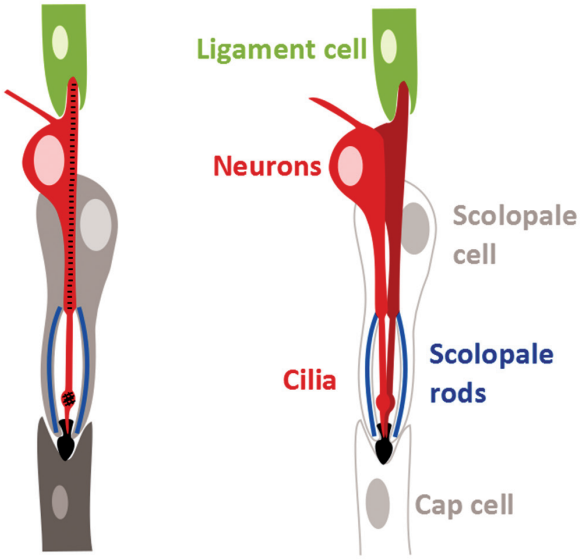

Figure 4. Organ of hearing of *Drosophila.* A. Sketch of the fly's antenna showing the three segments (a1, a2 and a3). The scalopidium in the Johnston's organ is shown in red B. Sketch of a scolopidium depicting the different cell types. (Figure derived from and published with permission of Seol-hee).

For the latter cases, cochlear implants and hearing aids are solutions that may improve the quality of life of the patients.[114,115] Regarding genetic therapies, several attempts aiming at preventing or reversing HI have been undertaken in mouse models.[116] Depending on both the type and the molecular mechanism of the mutated protein, the approaches are different: for loss of function (recessive) mutations, the genetic therapy should add a functional gene copy e.g. by viral delivery of the gene copy in the cochlea.[117,118] Akil *et al.* (2012) delivered a wild type copy of *Slc17a8* to the cochlea of knockout *Slc17a8* mice by using AAV1 and were able to restore the hearing in these mutant mice for more than a year.[117] In case of heterozygous (dominant) mutations the effect of which could also be gain of function or a dominant negative effect, the genetic therapy should aim at silencing the aberrant gene copy to enable the wild type allele to fulfil its function *e.g*. by silencing an allele by siRNA.[119,120] Maeda *et al.* (2005) reported a successful attempt of hearing restoration in mice carrying the dominant negative mutation p.Arg75Trp in *GJB2* by suppressing the expression of the mutant copy up to 70% by siRNA.[121] Besides genetic therapies, regenerative therapies targeting hair cells are also being explored with so far less promising results.[122] Most genes linked to HI are expressed in hair cells therefore these cells are the main target for regenerative therapies. One approach is to transplant embryonic stem cells or iPSCs into the inner ear to replace the lost hair cells; another approach is to express *ATOH1* in the cochlea in order to induce the formation of hair cells.

In summary, unravelling the genetic defects underlying HI in humans improves the genetic diagnostics of HI families. Besides, knowing the genetic defect has a positive impact on their quality of life because (genetic) therapy or treatment possibilities can be assessed in the future (personalized medicine).[123] Last but not least, genetic therapy attempts in mouse models are giving hope to prevent HI and restore hearing in humans in the near future.

REFERENCES

1. www.who.int
2. Yariz KO, Duman D, Seco CZ, et al.: Mutations in OTOGL, encoding the inner ear protein otogelin-like, cause moderate sensorineural hearing loss. Am J Hum Genet 2012; 91: 872-882.
3. Freeman DM, Masaki K, McAllister AR, Wei JL, Weiss TF: Static material properties of the tectorial membrane: a summary. Hear Res 2003; 180: 11-27.
4. Richardson GP, Lukashkin AN, Russell IJ: The tectorial membrane: one slice of a complex cochlear sandwich. Curr Opin Otolaryngol Head Neck Surg 2008; 16: 458-464.
5. Richardson GP, Russell IJ, Duance VC, Bailey AJ: Polypeptide composition of the mammalian tectorial membrane. Hear Res 1987; 25: 45-60.
6. Schraders M, Ruiz-Palmero L, Kalay E, et al.: Mutations of the gene encoding otogelin are a cause of autosomal-recessive nonsyndromic moderate hearing impairment. Am J Hum Genet 2012; 91: 883-889.
7. Kammerer R, Ruttiger L, Riesenberg R, et al.: Loss of mammal-specific tectorial membrane component carcinoembryonic antigen cell adhesion molecule 16 (CEACAM16) leads to hearing impairment at low and high frequencies. J Biol Chem 2012; 287: 21584-21598.
8. Cohen-Salmon M, El-Amraoui A, Leibovici M, Petit C: Otogelin: a glycoprotein specific to the acellular membranes of the inner ear. Proc Natl Acad Sci U S A 1997; 94: 14450-14455.
9. Hoefsloot LH, Feenstra I, Kunst HP, Kremer H: Genotype phenotype correlations for hearing impairment: approaches to management. Clin Genet 2014; 85: 514-523.
10. Jovine L, Qi H, Williams Z, Litscher E, Wassarman PM: The ZP domain is a conserved module for polymerization of extracellular proteins. Nat Cell Biol 2002; 4: 457-461.
11. Russell IJ, Legan PK, Lukashkina VA, et al.: Sharpened cochlear tuning in a mouse with a genetically modified tectorial membrane. Nat Neurosci 2007; 10: 215-223.
12. Zheng J, Miller KK, Yang T, et al.: Carcinoembryonic antigen-related cell adhesion molecule 16 interacts with alpha-tectorin and is mutated in autosomal dominant hearing loss (DFNA4). Proc Natl Acad Sci U S A 2011; 108: 4218-4223.
13. Gagnon LH, Longo-Guess CM, Berryman M, et al.: The chloride intracellular channel protein CLIC5 is expressed at high levels in hair cell stereocilia and is essential for normal inner ear function. J Neurosci 2006; 26: 10188-10198.
14. Pierchala BA, Munoz MR, Tsui CC: Proteomic analysis of the slit diaphragm complex: CLIC5 is a protein critical for podocyte morphology and function. Kidney Int 2010; 78: 868-882.
15. Seco CZ, Oonk AM, Dominguez-Ruiz M, et al.: Progressive hearing loss and vestibular dysfunction caused by a homozygous nonsense mutation in CLIC5. Eur J Hum Genet 2015; 23: 189-194.

16. Wegner B, Al-Momany A, Kulak SC, et al.: CLIC5A, a component of the ezrin-podocalyxin complex in glomeruli, is a determinant of podocyte integrity. Am J Physiol Renal Physiol 2010; 298: F1492-1503.
17. Riazuddin S, Belyantseva IA, Giese AP, et al.: Alterations of the CIB2 calcium- and integrin-binding protein cause Usher syndrome type 1J and nonsyndromic deafness DFNB48. Nat Genet 2012; 44: 1265-1271.
18. Ahmed ZM, Riazuddin S, Khan SN, et al.: USH1H, a novel locus for type I Usher syndrome, maps to chromosome 15q22-23. Clin Genet 2009; 75: 86-91.
19. Hartong DT, Berson EL, Dryja TP: Retinitis pigmentosa. Lancet 2006; 368: 1795-1809.
20. Wehrle-Haller B, Weston JA: Soluble and cell-bound forms of steel factor activity play distinct roles in melanocyte precursor dispersal and survival on the lateral neural crest migration pathway. Development 1995; 121: 731-742.
21. Cable J, Barkway C, Steel KP: Characteristics of stria vascularis melanocytes of viable dominant spotting (Wv/Wv) mouse mutants. Hear Res 1992; 64: 6-20.
22. Nin F, Hibino H, Doi K, et al.: The endocochlear potential depends on two K+ diffusion potentials and an electrical barrier in the stria vascularis of the inner ear. Proc Natl Acad Sci U S A 2008; 105: 1751-1756.
23. Hou L, Pavan WJ: Transcriptional and signaling regulation in neural crest stem cell-derived melanocyte development: do all roads lead to Mitf? Cell Res 2008; 18: 1163-1176.
24. Kadereit B, Kumar P, Wang WJ, et al.: Evolutionarily conserved gene family important for fat storage. Proc Natl Acad Sci U S A 2008; 105: 94-99.
25. Suter U, Scherer SS: Disease mechanisms in inherited neuropathies. Nat Rev Neurosci 2003; 4: 714-726.
26. Neveling K, Feenstra I, Gilissen C, et al.: A post-hoc comparison of the utility of sanger sequencing and exome sequencing for the diagnosis of heterogeneous diseases. Hum Mutat 2013; 34: 1721-1726.
27. http://www.acgs.uk.com/media/774853/evaluation_and_reporting_of_sequence_variants_bpgs_june_2013_-_finalpdf.pdf.
28. Ng PC, Henikoff S: SIFT: Predicting amino acid changes that affect protein function. Nucleic Acids Res 2003; 31: 3812-3814.
29. Adzhubei IA, Schmidt S, Peshkin L, et al.: A method and server for predicting damaging missense mutations. Nat Methods 2010; 7: 248-249.
30. Gonzalez-Perez A, Lopez-Bigas N: Improving the assessment of the outcome of nonsynonymous SNVs with a consensus deleteriousness score, Condel. Am J Hum Genet 2011; 88: 440-449.
31. Kircher M, Witten DM, Jain P, et al.: A general framework for estimating the relative pathogenicity of human genetic variants. Nat Genet 2014; 46: 310-315.
32. Krieger E, Koraimann G, Vriend G: Increasing the precision of comparative models with YASARA NOVA--a self-parameterizing force field. Proteins 2002; 47: 393-402.

33. Krieger E, Joo K, Lee J, et al.: Improving physical realism, stereochemistry, and side-chain accuracy in homology modeling: Four approaches that performed well in CASP8. Proteins 2009; 77 Suppl 9: 114-122.
34. den Hollander AI, Koenekoop RK, Yzer S, et al.: Mutations in the CEP290 (NPHP6) gene are a frequent cause of Leber congenital amaurosis. Am J Hum Genet 2006; 79: 556-561.
35. Garanto A, Duijkers L, Collin RW: Species-dependent splice recognition of a cryptic exon resulting from a recurrent intronic CEP290 mutation that causes congenital blindness. Int J Mol Sci 2015; 16: 5285-5298.
36. Xiong HY, Alipanahi B, Lee LJ, et al.: RNA splicing. The human splicing code reveals new insights into the genetic determinants of disease. Science 2015; 347: 1254806.
37. Littink KW, Pott JW, Collin RW, et al.: A novel nonsense mutation in CEP290 induces exon skipping and leads to a relatively mild retinal phenotype. Invest Ophthalmol Vis Sci 2010; 51: 3646-3652.
38. Lenassi E, Saihan Z, Bitner-Glindzicz M, Webster AR: The effect of the common c.2299delG mutation in USH2A on RNA splicing. Exp Eye Res 2014; 122: 9-12.
39. Arts HH, Bongers EM, Mans DA, et al.: C14ORF179 encoding IFT43 is mutated in Sensenbrenner syndrome. J Med Genet 2011; 48: 390-395.
40. Nishikawa T, Ota T, Isogai T: Prediction whether a human cDNA sequence contains initiation codon by combining statistical information and similarity with protein sequences. Bioinformatics 2000; 16: 960-967.
41. Nagy E, Maquat LE: A rule for termination-codon position within intron-containing genes: when nonsense affects RNA abundance. Trends Biochem Sci 1998; 23: 198-199.
42. Rivas MA, Pirinen M, Conrad DF, et al.: Human genomics. Effect of predicted protein-truncating genetic variants on the human transcriptome. Science 2015; 348: 666-669.
43. Shearer AE, Eppsteiner RW, Booth KT, et al.: Utilizing ethnic-specific differences in minor allele frequency to recategorize reported pathogenic deafness variants. Am J Hum Genet 2014; 95: 445-453.
44. MacArthur DG, Manolio TA, Dimmock DP, et al.: Guidelines for investigating causality of sequence variants in human disease. Nature 2014; 508: 469-476.
45. Donaudy F, Ferrara A, Esposito L, et al.: Multiple mutations of MYO1A, a cochlear-expressed gene, in sensorineural hearing loss. Am J Hum Genet 2003; 72: 1571-1577.
46. Eisenberger T, Di Donato N, Baig SM, et al.: Targeted and genomewide NGS data disqualify mutations in MYO1A, the “DFNA48 gene”, as a cause of deafness. Hum Mutat 2014; 35: 565-570.
47. Absalan F, Ronaghi M: Molecular inversion probe assay. Methods Mol Biol 2007; 396: 315-330.
48. O’Roak BJ, Vives L, Fu W, et al.: Multiplex targeted sequencing identifies recurrently mutated genes in autism spectrum disorders. Science 2012; 338: 1619-1622.

49. de Vree PJ, de Wit E, Yilmaz M, et al.: Targeted sequencing by proximity ligation for comprehensive variant detection and local haplotyping. Nat Biotechnol 2014; 32: 1019-1025.
50. Lupski JR, Reid JG, Gonzaga-Jauregui C, et al.: Whole-genome sequencing in a patient with Charcot-Marie-Tooth neuropathy. N Engl J Med 2010; 362: 1181-1191.
51. Gilissen C, Hehir-Kwa JY, Thung DT, et al.: Genome sequencing identifies major causes of severe intellectual disability. Nature 2014; 511: 344-347.
52. Mattick JS: Non-coding RNAs: the architects of eukaryotic complexity. EMBO Rep 2001; 2: 986-991.
53. Steele-Stallard HB, Le Quesne Stabej P, Lenassi E, et al.: Screening for duplications, deletions and a common intronic mutation detects 35% of second mutations in patients with USH2A monoallelic mutations on Sanger sequencing. Orphanet J Rare Dis 2013; 8: 122.
54. Vache C, Besnard T, Blanchet C, et al.: Nasal epithelial cells are a reliable source to study splicing variants in Usher syndrome. Hum Mutat 2010; 31: 734-741.
55. Pennacchio LA: Insights from human/mouse genome comparisons. Mamm Genome 2003; 14: 429-436.
56. Kikkawa Y, Seki Y, Okumura K, et al.: Advantages of a mouse model for human hearing impairment. Exp Anim 2012; 61: 85-98.
57. Legan PK, Lukashkina VA, Goodyear RJ, et al.: A deafness mutation isolates a second role for the tectorial membrane in hearing. Nat Neurosci 2005; 8: 1035-1042.
58. Popper AN, Fay RR: Rethinking sound detection by fishes. Hear Res 2011; 273: 25-36.
59. Riley BB, Moorman SJ: Development of utricular otoliths, but not saccular otoliths, is necessary for vestibular function and survival in zebrafish. J Neurobiol 2000; 43: 329-337.
60. Inoue M, Tanimoto M, Oda Y: The role of ear stone size in hair cell acoustic sensory transduction. Sci Rep 2013; 3: 2114.
61. Nicolson T: The genetics of hearing and balance in zebrafish. Annu Rev Genet 2005; 39: 9-22.
62. Stooke-Vaughan GA, Obholzer ND, Baxendale S, Megason SG, Whitfield TT: Otolith tethering in the zebrafish otic vesicle requires Otogelin and alpha-Tectorin. Development 2015; 142: 1137-1145.
63. Howe K, Clark MD, Torroja CF, et al.: The zebrafish reference genome sequence and its relationship to the human genome. Nature 2013; 496: 498-503.
64. Slijkerman RW, Song F, Astuti GD, et al.: The pros and cons of vertebrate animal models for functional and therapeutic research on inherited retinal dystrophies. Prog Retin Eye Res 2015.
65. Hultman KA, Bahary N, Zon LI, Johnson SL: Gene Duplication of the zebrafish kit ligand and partitioning of melanocyte development functions to kit ligand a. PLoS Genet 2007; 3: e17.
66. Fritzsch B, Beisel KW, Pauley S, Soukup G: Molecular evolution of the vertebrate mechanosensory cell and ear. Int J Dev Biol 2007; 51: 663-678.
67. Senthilan PR, Piepenbrock D, Ovezmyradov G, et al.: Drosophila auditory organ genes and genetic hearing defects. Cell 2012; 150: 1042-1054.

68. Todi SV, Sharma Y, Eberl DF: Anatomical and molecular design of the Drosophila antenna as a flagellar auditory organ. Microsc Res Tech 2004; 63: 388-399.
69. Cosetti M, Culang D, Kotla S, et al.: Unique transgenic animal model for hereditary hearing loss. Ann Otol Rhinol Laryngol 2008; 117: 827-833.
70. Eberl DF: Feeling the vibes: chordotonal mechanisms in insect hearing. Curr Opin Neurobiol 1999; 9: 389-393.
71. Jarman AP, Groves AK: The role of Atonal transcription factors in the development of mechanosensitive cells. Semin Cell Dev Biol 2013; 24: 438-447.
72. Parker M, Bitner-Glindzicz M: Republished: Genetic investigations in childhood deafness. Postgrad Med J 2015; 91: 395-402.
73. Ji F, Li J, Hong M, et al.: Determination of benefits of cochlear implantation in children with auditory neuropathy. PLoS One 2015; 10: e0127566.
74. Chien WW, Monzack EL, McDougald DS, Cunningham LL: Gene therapy for sensorineural hearing loss. Ear Hear 2015; 36: 1-7.
75. Akil O, Seal RP, Burke K, et al.: Restoration of hearing in the VGLUT3 knockout mouse using virally mediated gene therapy. Neuron 2012; 75: 283-293.
76. Askew C, Rochat C, Pan B, et al.: Tmc gene therapy restores auditory function in deaf mice. Sci Transl Med 2015; 7: 295ra108.
77. Lentz JJ, Jodelka FM, Hinrich AJ, et al.: Rescue of hearing and vestibular function by antisense oligonucleotides in a mouse model of human deafness. Nat Med 2013; 19: 345-350.
78. Yu Q, Wang Y, Chang Q, et al.: Virally expressed connexin26 restores gap junction function in the cochlea of conditional Gjb2 knockout mice. Gene Ther 2014; 21: 71-80.
79. Maeda Y, Fukushima K, Nishizaki K, Smith RJ: In vitro and in vivo suppression of GJB2 expression by RNA interference. Hum Mol Genet 2005; 14: 1641-1650.
80. Muller U, Barr-Gillespie PG: New treatment options for hearing loss. Nat Rev Drug Discov 2015; 14: 346-365.
81. Hamburg MA, Collins FS: The path to personalized medicine. N Engl J Med 2010; 363: 301-304.

Summary in English

Hearing impairment (HI) is the most common sensory disorder. In developed countries, approximately one in 750 newborns presents with HI at birth or develop HI shortly after birth. The factors that contribute to the development of HI are very diverse. Environmental factors such as viral infections during pregnancy, noise exposure and ototoxic medications, can explain about half of the cases. The other half can be explained by pathogenic genetic variants. Hereditary HI can be non-syndromic (NSHI) when only the hearing function is affected, occurring in 70% of the prelingual cases; or syndromic (SHI) when the HI is accompanied by other clinical phenotype(s) which occurs in the remaining 30%. The most prevalent syndromes with HI are Usher syndrome, which is characterized by HI and retinitis pigmentosa, and Waardenburg syndrome (WS) which is characterized by HI and pigmentation abnormalities. Besides these, there are over 400 syndromes known in which HI is associated with a broad range of other clinical features, *e.g.* sensory neuropathy and dystonia as shown in **chapter 6**.

To date, there are more than a hundred genes known to be involved in NSHI as presented in **chapter 1**. Despite this large genetic heterogeneity, in many of the patients the genetic defect underlying HI is still unknown. Therefore, during the course of this thesis project, we aimed at resolving the genetic etiology of HI to ultimately provide patients with an adequate genetic diagnosis and, in the long term, with an appropriate (genetic) therapy.

In **chapter 1**, a general introduction about the auditory system, the genetic heterogeneity of HI and the strategies for gene identification used in this thesis are described.

Autosomal recessively inherited NSHI (arNSHI) is the most common form accounting for about 77% of hereditary prelingual cases with HI. SNP genotyping is a robust method to identify homozygous (homozygosity mapping) and compound heterozygous alleles (shared genotyping) in inbred and outbred populations. This strategy in combination with Sanger sequencing of the most promising candidate genes resulted in the identification of mutations in two novel arNSHI genes, *OTOGL* (**chapter 2**) and *CLIC5* (**chapter 3**), and in mutations in a gene already known to be involved in arNSHI, *CIB2* (**chapter 4**).

In **chapter 2**, we described the identification of compound heterozygous mutations in *OTOGL*, c.547C>T (NM_173591.3; p.(Arg183Ter)) and c.5238+5G>A, in a Dutch family; and a homozygous truncating mutation,

c.1430delT (p.(Val477Glufs*25)), in a family of Turkish origin. These mutations were segregating with the congenital moderate mid-frequency HI present in each family. We demonstrate that Otogl was located in all the acellular membranes of the mouse inner ear and that knock down of *Otogl* expression in zebrafish resulted in reduced inner ear microphonic potentials, supporting the involvement of *OTOGL* mutations in the human phenotype.

Chapter 3 is about the identification of a homozygous truncating mutation, c.96T>A (NM_016929.3; p.(Cys32Ter)), in *CLIC5* underlying the progressive HI and vestibular areflexia in two sibs from Turkey. The orthologous mouse gene, *Clic5*, described to be mutated in the jitterbug (*jbg*) mouse, exhibited a similar phenotype as seen in the presented family: congenital progressive HI and vestibular dysfunction, due to progressive hair cell degeneration. One of the affected sibs also presented with very mild renal dysfunction. This might well be due to the *CLIC5* mutations since the *jbg* mice have abnormalities in kidney podocytes leading to proteinuria. Therefore, renal function of the affected sibs will be monitored in future.

In **chapter 4**, three different mutations in *CIB2* are described that are causative for severe to profound arNSHI: 1) a homozygous founder mutation, c.272T>C (NM_006383.3; p.(Phe91Ser)), in two Pakistani families; 2) a homozygous mutation, c.196C>T (p.(Arg66Trp)) in a Dutch family and 3) compound heterozygous mutations, c.97C>T (p.(Arg33Ter)) and c.196C>T (p.(Arg66Trp)), in another Dutch family. We demonstrated that the missense mutations do neither affect either the subcellular localization of Cib2 in mouse vestibular hair cells nor the ATP-induced calcium responses in COS-7 cells. Mutations in *CIB2* are also the underlying cause of Usher syndrome 1J, however, the patients described in **chapter 4** did not show any signs of retinitis pigmentosa or vestibular dysfunction. Our results contribute to the insight in genotype-phenotype correlations of *CIB2* mutations.

Autosomal dominantly inherited NSHI (adNSHI) accounts for about 22% of the hereditary prelingual cases with HI. In **chapter 5**, we described a large family from the Netherlands with autosomal dominant non-syndromic unilateral and asymmetric hearing impairment (NS-UHI/AHI). By performing linkage analysis and whole-exome sequencing (WES) we identified a heterozygous nonsense mutation, c.286_303delinsT (NM_000899.4; p.Ser96Ter), in KITLG that was segregating with the disease with reduced penetrance. *KITLG* encodes the ligand

of the KIT receptor. KIT-KITLG interaction triggers a pathway involved in the development of melanocytes which seems to be ultimately connected to MITF. Mutations in *MITF* are associated with Waardenburg syndrome type II (WS II). Therefore, we screened two different panels of probands with NS-UHI/AHI and WS II for mutations in *KITLG*. We found a heterozygous mutation, c.200_202del (p.His67_Cys68delinsArg), in *KITLG* to be causative of NS-UHI/AHI in a family of Spanish origin and a heterozygous c.310C>G (p.Leu104Val) mutation underlying WS II in a small family of Dutch origin. We evaluated the impact of these mutations on both protein isoforms of KITLG, the secreted soluble and the transmembrane isoforms. The p.His67_Cys68delinsArg transmembraneous KITLG could not reach the membrane as the wild type KITLG does and the secreted soluble p.His67_Cys68delinsArg KITLG could not be detected in culture medium of transfected cells. In contrast, the p.Leu104Val transmembraneous KITLG was incorporated into the membrane but reduced levels of the p.Leu104Val soluble KITLG were secreted into the culture medium as compared to wild type. These data suggest that the p.Ser96Ter and p.His67_Cys68delinsArg mutations underlying NS-UHI/AHI are loss-of-function mutations whereas the p.Leu104Val mutation possibly has a dominant negative or gain of function effect on KITLG. In conclusion, we demonstrated that *KITLG* is the first gene known to be mutated in NS-UHI/AHI and that allelic mutations in *KITLG* can also result in WS II adding *KITLG* to the group of genes associated with hypopigmentation-deafness disorders.

The auditory organ is very complex and many of the proteins encoded by HI genes also have a role in other organs. Therefore, it comes as no surprise that there are numerous syndromes with HI described to date. In **chapter 6**, we presented a novel syndrome characterized by a combination of HI, sensory neuropathy and dystonia. Homozygosity mapping and WES revealed a homozygous nonsense mutation, c.4G>T (NM_001080472.1; p.Glu2Ter), in *FITM2*, a member of a protein family involved in lipid storage and metabolism. By using conditional gene ablations by RNAi in *Drosophila melanogaster*, we demonstrated that the human phenotype is recapitulated in flies. By using the island test, it was demonstrated that locomotion of the flies was progressively impaired as it is in the patients. The sensory neural phenotype of the patients was recapitulated by the aberrant morphology of sensory type IV neurons in *Drosophila*. Moreover, we evaluated the hearing of flies upon RNAi which presented a loss of electrical responses and mechanical amplification in the Johnston's organ indicative of sensorineural HI. Furthermore, lipid storage seems to be disturbed which is in line with a function of the human ortholog in lipid storage.

In **chapter 7**, the efficacy of WES for the genetic diagnosis of 200 individuals with HI was investigated. The obtained diagnostic yield of WES was greater than that of predictive single gene testing based on the HI phenotype (29.5% vs 7.6%). In our cohort we found that mutations in G*JB2, STRC, USH2A, MYO15A* and *MYO6* underlined the HI in ~14% of the cases, therefore we suggested that it would be cost-effective, at least in our population, to pre-screen these genes by using novel cost-effective technologies, *e.g.* molecular inversion probes, before WES.

In **chapter 8**, the findings, challenges and implications on health care described within this thesis are discussed.

Samenvatting in het Nederlands

Gehoorverlies is de meest voorkomende sensorische beperking. In ontwikkelde landen heeft één op de 750 pasgeborenen gehoorverlies of ontwikkelt zij of hij dit kort na de geboorte. De factoren die bijdragen aan het ontstaan van gehoorverlies zijn erg divers. Omgevingsfactoren, zoals virale infecties gedurende de zwangerschap en ototoxische medicatie, kunnen de helft van de gevallen verklaren. De andere helft kan verklaard worden door pathogene genetische varianten. Erfelijk gehoorverlies is niet-syndromaal wanneer alleen het gehoor is aangedaan en dit komt voor bij 70% van de prelinguale gevallen. Gehoorverlies is syndromaal wanneer het gepaard gaat met andere klinische kenmerken, wat voorkomt in de overige 30% van de gevallen. Twee van de meest voorkomende syndromen met gehoorverlies zijn Usher syndroom, gekenmerkt door gehoorverlies en retinitis pigmentosa, en Waardenburg syndroom, gekenmerkt door gehoorverlies en pigmentatie-afwijkingen. Naast deze syndromen zijn er meer dan 400 syndromen bekend waarbij het gehoorverlies gepaard gaat met een breed scala aan andere klinische eigenschappen, zoals sensorische neuropathie en dystonie zoals beschreven in **hoofdstuk 6.**

Momenteel zijn er meer dan honderd genen bekend die betrokken zijn bij niet-syndromaal gehoorverlies, zoals beschreven in **hoofdstuk 1**. Ondanks deze grote genetische heterogeniteit is in veel van de patiënten het onderliggend genetische defect nog onbekend. Daarom was het doel van deze thesis het ontrafelen van de genetische etiologie van gehoorverlies om uiteindelijk te komen tot een adequate genetische diagnose voor de patiënten en, op lange termijn, een toepasbare (genetische) therapie.

Hoofdstuk 1 omvat een algemene inleiding van het auditieve systeem, de genetische heterogeniteit van gehoorverlies en de strategieën die zijn gebruikt voor genidentificatie in dit proefschrift.

Autosomaal recessief overervend niet-syndromaal gehoorverlies (arNSHI) is de meest voorkomende vorm van gehoorverlies en omvat ongeveer 77% van de erfelijke prelinguale gevallen van niet-syndromaal gehoorverlies. SNP-genotypering is een robuuste methode om homozygote en compound heterozygote allelen te identificeren in consanguine en niet-consanguine populaties. Deze strategie in combinatie met sequentie-analyse van de meest veelbelovende kandidaatgenen hebben geresulteerd in de identificatie van mutaties in twee nieuwe genen voor arNSHI, *OTOGL* (**hoofdstuk 2**) en *CLIC5* (**hoofdstuk 3**), en in mutaties in een gen dat al bekend was betrokken te zijn bij arNSHI, *CIB2* (**hoofdstuk 4**).

In **hoofdstuk 2** wordt de identificatie van compound heterozygote mutaties in *OTOGL* beschreven. De c.547C>T (NM_173591.3; p.(Arg183Ter)) en c.5238+5G>A mutaties werden gevonden in een Nederlandse familie en een homozygote truncerende mutatie, c.1430delT (p.(Val477Glufs*25)) werd geïdentificeerd in een familie van Turkse afkomst. Deze mutaties erfden over met het aangeboren matige mid-frequentie gehoorverlies in de families. We tonen aan dat Otogl aanwezig is in alle acellulaire membranen van het binnenoor in de muis en dat verminderde expressie van *Otogl* in de zebravis resulteert in een afname van elektrische potentialen in het binnenoor. Deze resultaten ondersteunen de bevinding dat mutaties in *OTOGL* betrokken zijn bij het humane fenotype.

Hoofdstuk 3 beschrijft de identificatie van een homozygote truncerende mutatie, c.96T>A (NM_016929.3; p.(Cys32Ter)), in *CLIC5* als oorzaak van progressief gehoorverlies en vestibulaire areflexie in een broer en zus van Turkse afkomst. Het orthologe gen in de muis, *Clic5*, is gemuteerd in de jitterbug (*jbg*) muis, die een vergelijkbaar fenotype vertoont als de beschreven familie: aangeboren progressief gehoorverlies en vestibulaire afwijkingen ten gevolge van progressief haarcelsterfte. Een van de aangedane personen had ook een zeer milde nierfunctiestoornis. Dit zou mogelijk veroorzaakt kunnen worden door de CLIC5 mutatie, omdat *jbg* muizen afwijkingen vertonen in de podocyten die leiden tot proteïnurie. Daarom zal in de toekomst de nierfunctie van de aangedane personen gevolgd worden.

In **hoofdstuk 4**, worden drie verschillende mutaties in *CIB2* beschreven die ernstig tot zeer ernstig autosomaal recessief overervend gehoorverlies veroorzaken: 1) een homozygote foundermutatie, c.272T>C (NM_006383.3; p.(Phe91Ser)), in twee Pakistaanse families; 2) een homozygote mutatie, c.196C>T (p.(Arg66Trp)), in een Nederlandse familie en 3) compound heterozygote mutaties, c.97C>T (p.(Arg33Ter)) en c.196C>T (p.(Arg66Trp)), in een tweede Nederlandse familie. We hebben aangetoond dat mutaties die leiden tot aminozuurveranderingen in CIB2 geen effect hebben op de cellulaire lokalisatie van het eiwit in vestibulaire haarcellen van de muis en ook niet op de door ATP geïnduceerde calciumreacties in COS-7 cellen. Mutaties in *CIB2* zijn ook beschreven als onderliggende oorzaak van Usher syndroom 1J, hoewel de patiënten beschreven in **hoofdstuk 4** geen tekenen hadden van retinitis pigmentosa of vestibulaire problemen. Onze resultaten dragen bij aan inzicht in genotype-fenotype correlaties van *CIB2* mutaties.

Autosomaal dominant overervende niet-syndromale slechthorendheid is goed voor ongeveer 22% van de gevallen met erfelijk prelinguaal gehoorverlies. In **hoofdstuk 5** is een grote Nederlandse familie beschreven met autosomaal dominant niet-syndromaal unilateraal en asymmetrisch gehoorverlies. Door linkage analyse te combineren met sequentie-analyse van het hele exoom (WES) hebben we een heterozygote truncerende mutatie, c.286_303delinsT (NM_000899.4; p.Ser96Ter), in *KITLG* gevonden die met een verminderde penetrantie segregeert met de ziekte binnen de familie. *KITLG* codeert voor de ligand van de KIT receptor. De interactie tussen KIT en KITLG activeert een cascade betrokken bij de ontwikkeling van melanocyten die uiteindelijk leidt naar MITF. Mutaties in *MITF* zijn geassocieerd met Waardenburg syndroom type II (WS II). Daarom, hebben we twee verschillende cohorten van indexpatiënten met niet-syndromaal unilateraal/asymmetrisch gehoorverlies en WS II onderzocht op mutaties in *KITLG*. We hebben hiermee een heterozygote mutatie, c.200_202del (p.His67_Cys68delinsArg), in *KITLG* geïdentificeerd als oorzaak van niet-syndromaal unilateraal/asymmetrisch gehoorverlies in een Spaanse familie en een heterozygote c.310C>G (p.Leu104Val) mutatie in een Nederlandse WS II familie. We hebben het effect onderzocht van deze mutaties op beide isovormen van KITLG, de uitgescheiden en oplosbare en de membraangebonden isovorm. Het membraangebonden p.His67_Cys68delinsArg KITLG kon, in tegenstelling tot het wildtype eiwit, het membraan niet bereiken en het uitgescheiden oplosbare p.His67_Cys68delinsArg KITLG kon niet worden gedetecteerd in het kweekmedium van getransfecteerde cellen. Het membraangebonden p.Leu104Val KITLG werd daarentegen wel aangetoond in het membraan, maar de concentratie van het p.Leu104Val oplosbare KITLG was lager in vergelijking met het wildtype eiwit in het kweekmedium. Resultaten laten zien dat de p.Ser96Ter en p.His67_Cys68delinsArg mutaties leiden tot een verlies van de normale functie van KITLG, terwijl de p.Leu104Val mutatie mogelijk een dominant negatief effect heeft op de werking van KITLG of leidt tot een anderszins veranderde functie van het eiwit. Concluderend kunnen we zeggen dat we hebben aangetoond dat *KITLG* het eerste gen is waarin mutaties leiden tot niet-syndromaal unilateraal/asymmetrisch gehoorverlies en dat mutaties in *KITLG* ook kunnen leiden tot WS II; dit voegt *KITLG* toe aan de groep genen geassocieerd met hypopigmentatie-doofheidsaandoeningen.

Het auditieve orgaan is zeer complex en veel van de eiwitten die gecodeerd worden door doofheidsgenen hebben ook een rol in andere organen. Daarom, is het geen verrassing dat er al talloze syndromen zijn beschreven met gehoorverlies

als een van de symptomen. In **hoofdstuk 6** presenteren we een nieuw syndroom dat gekenmerkt wordt door een combinatie van gehoorverlies, sensorische neuropathie en dystonie. Het bepalen van de homozygote regio's en WES toonden een homozygote mutatie aan, c.4G>T (NM_001080472.1; p.Glu2Ter), in *FITM2*, dat deel uitmaakt van een eiwitfamilie die betrokken is bij het opslaan van triacylglyceriden bij het lipidmetabolisme. Via RNAi in *Drosophila melanogaster*, hebben we aangetoond dat het humane fenotype en het fenotype van de fruitvlieg overlappen. Met behulp van de eilandtest werd aangetoond dat de motorische functie van de vliegen progressief vermindert zoals dit ook gezien wordt in de patiënten. Het sensorineurale fenotype van de patiënten zien we terug in de afwijkende morfologie van de type IV sensorische neuronen in *Drosophila*. Ook, hebben we het gehoor van de fruitvliegen onderzocht na RNAi waarbij een verlies van elektrische reacties en mechanische amplificatie in het Johnston's orgaan werd gevonden wat indicatief is voor sensorineuraal gehoorverlies. Verder, lijkt de opslag van triacylglyceriden verstoord wat in lijn is met de functie van het *FITM2* gen.

In **hoofdstuk 7** werd de doelmatigheid van WES voor genetische diagnostiek onderzocht voor een cohort van 200 personen met gehoorverlies. De behaalde diagnostische opbrengst van WES was groter dan die van het testen van enkele genen die geselecteerd zijn op basis van het type gehoorverlies (29% *versus* 7.6%). In het WES-cohort waren mutaties in *GJB2, STRC, USH2A, MYO15A* and *MYO6* de oorzaak van het gehoorverlies in ~14% van de gevallen. Daarom concluderen we dat het kostenbesparend zou zijn, tenminste in onze populatie, om deze genen te analyseren met nieuwe kosteneffectieve technieken, zoals 'molecular inversion probes', voordat wordt overgegaan tot WES.

In **hoofdstuk 8**, worden de resultaten van het onderzoek beschreven in deze thesis in een breder kader geplaatst en worden uitdagingen voor de toekomst en gevolgen voor de medische genetica besproken.

List of publications

Seco CZ*, Serrao de Castro LS*, van Nierop JW*, Morín M*, Jhangiani S, Verver EJJ, Schraders M, Maiwald N, Wesdorp M, Venselaar H, Spruijt L, Oostrik J, Schoots J, Baylor-Hopkins Center for Mendelian Genomics, van Reeuwijk J, Lelieveld L.H., Huygen PLM, Insenser M, Admiraal RJC, Pennings RJE, Hoefsloot L, Arias-Vásquez A, Helger Y, de Ligt J, Jansen JH, Muzny DM, Huls G, Van Rossum MM, Lupski, JR, Moreno-Pelayo MA[#], Kunst HP[#], Kremer H[#]. Allelic mutations of *KITLG*, encoding KIT ligand, cause asymmetric and unilateral hearing loss and Waardenburg syndrome type II. American journal of human genetics, in press.

Seco CZ*, Giese AP*, Shafique S*, Schraders M, Oonk AM, Grossheim M, Oostrik J, Strom T, Hegde R, van Wijk E, Frolenkov GI, Azam M, Riazuddin S, Admiraal RJ, Qamar R, Ahmed ZM[#], Kremer H[#]. Novel and recurrent *CIB2* variants, associated with non-syndromic deafness, do not affect calcium buffering and localization in hair cells. European journal of human genetics 2015 doi: 10.1038/ejhg.2015.157.

Shafique S*, Siddiqi S*, Schraders M, Oostrik J, Ayub H, Bilal A, Ajmal M, **Seco CZ**, Strom TM, Mansoor A, Mazhar K, Shah ST, Hussain A, Azam M, Kremer H, Qamar R. Genetic Spectrum of Autosomal Recessive Non-Syndromic Hearing Loss in Pakistani Families. PLos One, 9(6), 2014,e100146.

Seco CZ*, Oonk AM*, Domínguez-Ruiz M, Draaisma JM, Gandía M, Oostrik J, Neveling K, Kunst HP, Hoefsloot LH, Del Castillo I, Pennings RJ, Kremer H, Admiraal RJ, Schraders M. Progressive hearing loss and vestibular dysfunction caused by a homozygous nonsense mutation in *CLIC5*. European journal of human genetics, 23(2), 2014, 189-94.

Yariz KO*, Duman D*, **Seco CZ**, Dallman J, Huang M, Peters TA, Sirmaci A, Lu N, Schraders M, Skromne I, Oostrik J, Diaz-Horta O, Young JI, Tokgoz-Yilmaz S, Konukseven O, Shahin H, Hetterschijt L, Kanaan M, Oonk AM, Edwards YJ, Li H, Atalay S, Blanton S, Desmidt AA, Liu XZ, Pennings RJ, Lu Z, Chen ZY, Kremer H, Tekin M. Mutations in *OTOGL*, encoding the inner ear protein Otogelin-like, cause moderate sensorineural hearing loss. American journal of human genetics, 91(5), 2012, 2; 872-82.

Schraders M, Ruiz-Palmero L, Kalay E, Oostrik J, del Castillo FJ, Sezgin O, Beynon AJ, Strom TM, Pennings RJ, **Seco CZ**, Oonk AM, Kunst HP, Domínguez-Ruiz M, García-Arumi AM, del Campo M, Villamar M, Hoefsloot LH, Moreno F, Admiraal RJ, del Castillo I, Kremer H. Mutations of the gene encoding otogelin (*OTOG*) are a cause of autosomal recessive nonsyndromic moderate hearing impairment. American journal of human genetics, 91(5), 2012, 883-9.

Schrauwen I*, Helfmann S*, Inagaki A*, Predoehl F, Tabatabaiefar MA, Picher MM, Sommen M, **Seco CZ**, Oostrik J, Kremer H, Dheedene A, Claes C, Fransen E, Chaleshtori MH, Coucke P, Lee A[#], Moser T[#], Van Camp G[#].A mutation in *CABP2*, expressed in cochlear hair cells, causes autosomal-recessive hearing impairment. American journal of human genetics, 91(4), 2012, 636-45.

Perez-Nanclares G*, Romanelli V*, Mayo S*, Garin I, **Seco CZ**, Fernandez-Rebollo E, Martínez F, Lapunzina P, de Nanclares GP; Spanish PHP Group. Detection of Hypomethylation Syndrome among Patients with Epigenetic Alterations at the *GNAS* Locus. Journal of clinical endocrinology and metabolism, 97(6), 2012, E1060-7.

Mayo S, Garin I, Monfort S, Roselló M, Orellana C, Oltra S, **Seco CZ**, de Naclares GP, Martínez F. Hypomethylation of the *KCNQ1OT1* imprinting center of chromosome 11 associated to Sotos-like features. Journal of Human Genetics, 57, 2012, 153-156.

Seco CZ, Thiele S, Martín C, Fernandez-Rebollo E, Martinez-Indart L, Werner R, Garin I; Spanish PHP Group, Hiort O, Perez de Nanclares G. Gsα activity is reduced in erythrocyte membranes of patients with psedohypoparathyroidism due to epigenetic alterations at the *GNAS* locus. Journal of Bone and Mineral Research, 26(8), 2011, 1864-70.

[#,*] Authors contributed equally

Acknowledgements

This thesis is the result of the hard-work of many people to whom I would like to acknowledge.

Firstly, I would like to express my sincere gratitude to my supervisor Prof. dr. Hannie Kremer, for all the support and motivation. Her guidance helped me all the time of research and writing of this thesis. Besides my supervisor, I would like to thank my co-supervisors, Dr. Margit Schraders and Dr. Erwin van Wijk, for all the good discussions and support, especially appreciated in the end of the PhD.

Next, I would like to thank Jaap for his technical help and nice talks we have had during all these years.

It is a pleasure to thank my fellow group mates in the protein lab for the stimulating discussions and help when I needed.

I am especially grateful to the PhD roommates, to those that left and those who came in: Anna C., Maria Maleeha, Galuh, Evelyn, Anna S., Merel, Korinna, Zafar, Tom, Human, Bonnie, Susanne, Ilse, Minh and Brooke. For all the coffee breaks, personal and scientific discussions, cheerful spirit and laughs that have made P2 the best environment to do a PhD.

To Anna, I have no words to express how much I appreciate you. You have become one of the most important people of my life and I am going to miss you a lot in my new “home”.

To Sarah, thanks for all the support, endless laughs and love during all this time. I will miss you a lot, everyday, you are exceptional.

To the rest of the group: Sarah F., Sophie, Steve, Minh, Duy, Lluis, Will and Amrish with whom I have had the best time in Nijmegen.

To my students, I have learnt a lot from you. I am proud of the great job all you guys have done during your internships.

To all colleagues from Human Genetics who have made these years unforgettable for me.

To my colleagues from ENT department. I have learnt a lot from our Otogenetics discussions and collaborations.

To my colleagues from DNA diagnostics, especially to Helger Ijntema, it has been a pleasure to have worked with you.

I want to thank my collaborators for the great and fruitful contribution to this thesis.

To my Spanish friends in Nijmegen, I have had a great and endless fun time with you, you are all cheerful and special to me, thanks a lot!
To my Erasmus, Salamanca University and Cantalapiedra friends: thanks for following me around the world and visit me anywhere!

To Quique, everyday is special next to you, you are my life companion, thanks for all support during these years doing my PhD. A big thank to my family, especially to my parents and sister for supporting me spiritually throughout doing this thesis and my life in general.

PhD portfolio

Name PhD student: Celia Zazo Seco	PhD period: 17-01-2011 – 04-12-2015	
Department: Otorynolaringology	Promotor: Prof. dr. H. Kremer	
Research School: Radboud institute for Molecular Life Sciences	Co-promotor(s): Dr. Margit Schraders and Dr. E. van Wijk	
	Year(s)	ECTS
TRAINING ACTIVITIES		
a) Courses & Workshops		
- Graduate course	2011	2
- Bioinformatics summer school (Hinxton, UK)#	2011	2.25
- Poster presentation workshop	2011	0.25
- Presentations skills	2012	1.25
- Medical genetics course (Bologna, Italy)#	2012	1.50
- Academic writing	2013	1.25
- Inner ear biology workshop (Alcala de Henares, Spain)*	2013	2.25
b) Seminars & lectures^		
- RIMLS Seminar series	2011-2015	2
- RIMLS Technical forums		1
- RIMLS Symposia		4
- RIMLS PhD retreats*,#		4
c) (Inter)national Symposia & congresses		
- Molecular biology of hearing and deafness conference (Hinxton, UK)#	2011	1.25
- Molecular biology of hearing loss and deafness (San Francisco, USA)#	2013	1.25
- Inner ear biology workshop (Alcalá de Henares, Spain)#	2013	2
- American Society of Human Genetics (San Diego, USA)*	2014	1.75
d) Other		
- Literature discussion series*	2011-2015	
- Theme discussion series*		
- Sensory disease discussion series*		
- Oto-genetics discussion series*		
TEACHING ACTIVITIES		
e) Teaching activities		
- Supervision student internship projects (17 months)	2013	4.3
TOTAL		32.3

#poster presentation; *oral presentation

Curriculum Vitae

Celia Zazo Seco was born on the 13th of October in 1986 in Salamanca, Spain. In 2004, she finished secondary school at Senara highschool, in Babilafuente, Salamanca. In the same year, she started her university studies in Biotechnology at the University of Salamanca. In 2007 she spent an academic year at the University of Ghent, Ghent, Belgium, as an Erasmus student. She graduated from her master's in Biotechnology in 2009 and in that year, she started as a junior researcher in (epi)genetics at Txagorritxu hospital, Vitoria, Spain. In 2011 she entered the PhD program of the Radboud Institute for Molecular Life Sciences (RIMLS). She performed her research in the department of Otorhinolaryngology and the department of Human Genetics of the Radboud university medical center under the supervision of Prof. dr. Hannie Kremer, dr. Margit Schraders and dr. Erwin van Wijk.